

Towards a greater mechanistic understanding of reversible protein-protein interactions and irreversible aggregation of IgG1 monoclonal antibodies

By

[Copyright 2016]

Jayant Arora

Submitted to the graduate degree program in Pharmaceutical Chemistry and the Graduate Faculty of the University of Kansas in partial fulfillment of the requirements for the degree of Doctor of Philosophy.

Chairperson: Dr. David B. Volkin, Ph.D.

David D. Weis, Ph.D.

C. Russell Middaugh, Ph.D.

Teruna J. Siahaan, Ph.D.

Roberto N. De Guzman, Ph.D.

Date Defended: July 14, 2016

The Dissertation Committee for Jayant Arora
certifies that this is the approved version of the following dissertation:

Towards a greater mechanistic understanding of reversible protein-protein interactions and
irreversible aggregation of IgG1 monoclonal antibodies

Chairperson: Dr. David B. Volkin, Ph.D.

Date approved: July 14, 2016

ABSTRACT

Immunoglobulin G1 monoclonal antibodies (IgG1-mAbs) are one of the most important and fastest growing class of biotherapeutic agents. These mAbs are being used to treat a wide range of medical conditions such as cancer, macular degeneration, autoimmune diseases, rheumatoid arthritis, etc. Antibodies are dynamic molecules and their dynamic nature governs their physiological and biological functions. Antibodies are protein based drugs and are prone to both physical and chemical degradation *in vitro*. The biggest concerns related to IgGs mAb stability is their propensity to form protein aggregates (at low and high protein concentrations) and transient protein-protein interactions at high protein concentrations leading to dramatic increase in solution viscosity. Predicting protein stability and mapping protein interactions at high protein concentrations remains some of the most desirable long term goals of protein formulation development.

This dissertation's second chapter focused on exploring the utility of hydrogen exchange mass spectrometry (HX-MS) in predicting stability profile of an IgG1 mAb, mAb-4, upon addition of various destabilizing phenolic antimicrobial preservatives (APs). The trends in mAb-4's physical stability measurements using differential scanning calorimetry and extrinsic fluorescence spectroscopy (thermal stability) and size exclusion chromatography (aggregation propensity) showed correlations with significant increases in local flexibility of the aggregation hot-spot peptide segment in the C_{H2} domain of mAb-J (HC 237-254) upon addition of APs. Most hydrophobic AP (m-cresol) caused the greatest decrease in physical stability of mAb-4 and also the biggest increase in the local flexibility of C_{H2} domain peptide hot-spot of the antibody. Global deuterium uptake by mAb-4 was also highest in the presence of m-cresol, followed by phenol, phenoxyethanol and benzyl alcohol.

In the third and fourth chapter, the effect of different solution and environmental variables on viscoelastic behavior and propensity of concentration-dependent self-association of two IgG1 mAbs was tested. One of the IgG1 mAbs, mAb-C showed a primarily hydrophobic interaction driven protein association behavior, however, the other IgG1 mAb, mAb-J, showed a distinct association mechanism where the antibody monomers associated through electrostatic attractive interactions. A novel HX-MS methodology was developed to map protein-protein interaction interfaces of transient intermolecular antibody associations at high protein concentrations. Antibody solutions of low (non-associating) and high protein concentrations (associating) were lyophilized and reconstituted directly in D₂O solutions to initiate HX process directly at target concentrations.

Protein interface of mAb-C reversible self-association was confined in the relatively hydrophobic V_H and V_L domains of the antibody that spanned its CDR2H and CDR2L loops, indicating towards a Fab-Fab interaction drive association event. HX-MS also revealed distant dynamic coupling effects of mAb-C association in the form of significant increases in local flexibility of certain peptide segments in the V_H and C_H2 domains of the antibody. HX-MS analysis of mAb-J reversible self-association revealed one of the interfaces in the V_H and V_L domain (positively charged, spanning CDR3H and CDR2L) and other interface in the C_H3 domain of the antibody (negatively charged). Hence, HX-MS can provide a robust solution to protein physical stability prediction for rational design of protein formulation strategies and high-resolution protein-protein interaction interface mapping at high protein concentrations for engineering mutant antibody molecules with superior physicochemical properties and enhanced stability.

Dedicated to:

My parents

Virender Kumar and Rosy Arora,

my brother Hemant Arora

and especially my wife Yamini Mutreja

ACKNOWLEDGEMENTS

The work accomplished in this dissertation couldn't have come to fruition without tremendous guidance of a lot of individuals at the university of Kansas and MedImmune Inc. Firstly, I would like to express my sincere appreciation towards my Ph.D. thesis advisor, Dr. David Volkin. He has been a continuous source of inspiration, guidance and knowledge for me. I want to thank him for his patience towards me, his guidance and trust during the last four and half years. In addition to science, I have learnt a wide range of skills including organizational, leadership and mentorship from him. David always emphasized over the importance of scientific collaborations and effective communication. I am confident that his teachings will keep guiding me throughout my professional career. Working with him has been a great learning experience and I feel fortunate for having this opportunity.

I would like to thank my thesis co-advisor, Dr. David Weis for his support and scientific guidance. I always admired his work ethics, writing/presentation skills and attention to scientific details during data interpretation. I am grateful for getting a chance to train under him and learning many valuable skills from him that will be useful throughout my scientific career. I thank Dr. Teruna Siahaan, and Dr. Roberto N. De Guzman for agreeing to be a part of my thesis defense committee and making time to review my scientific research. I feel very fortunate to be a part of the department of pharmaceutical chemistry at KU, I appreciate all the professors for imparting their knowledge onto me through valuable coursework and meticulously designed curriculum.

I also thank Dr. Russ Middaugh, for being a vast source of scientific knowledge, I learnt a great deal about protein chemistry and biophysics from this coursework and during lab meetings. I particularly enjoyed our scientific talks and I greatly appreciate him for showing trust in my scientific abilities. I want to extend my sincere appreciation to the director of Macromolecular and

Vaccine Stabilization Center (MVSC), Dr. Sangeeta Joshi for providing me support both scientifically and personally throughout my stint at KU. Her passion towards science and research has always encouraged me to strive harder to achieve my goals. I thank her for her friendship, her patience towards me and her motivation every step of the way. I thank Dr. John Hickey and Dr. Cavan Kalonia (former MVSC member) for their friendship and countless hours of scientific discussions on a wide range of topics. I greatly appreciate their support through both ups and downs of my scientific journey in graduate school. I would also like to thank Dr. Ronald Toth, Dr. Yu Wang and Martin Hu for their various direct and indirect contributions to my research at KU. I thank all the present and past members of MVSC for their support and friendship. I acknowledge MedImmune Inc. and Kansas Bioscience Authority for providing financial support for the scientific research presented in this dissertation.

I would like to thank my parents and my brother for their unwavering trust and support. Their blessings, teachings and love have guided me throughout my life, I sincerely appreciate them for never losing faith in my abilities and supporting my decisions concerning my career. Lastly, I would like to extend my special thanks to my wife, Yamini. She has been a constant source of motivation, inspiration and support for me. Her love kept me resolute during some of the most difficult times and humble upon my accomplishments. She is a brilliant scientist and I truly value all the scientific discussions that I had with her over the years. She is the one who made science “fun” for me for the first time. I dedicate this thesis dissertation to my parents, my brother and especially my wife.

TABLES OF CONTENTS

Chapter 1. Introduction	1
1.1 Overview.....	2
1.2 Intermolecular Protein-Protein Interactions.....	3
1.2.1 Classification of Protein-Protein Interactions.....	4
1.2.1.1 Homo-Oligomers vs. Hetero-Oligomers.....	4
1.2.1.2 Transient vs. Permanent Associations.....	4
1.2.1.3 Native vs. Non-Native Associations.....	5
1.2.1.4 Covalent vs. Non-Covalent Associations.....	6
1.2.2 Types of Non-Covalent Interactions.....	7
1.2.2.1 Electrostatic Interactions.....	7
1.2.2.2 Dipolar Interactions.....	8
1.2.2.3 London Dispersion forces or van der Waals Interactions.....	9
1.2.2.4 Hydrogen Bonding.....	10
1.2.2.5 Hydrophobic Interactions/Apolar Interactions.....	11
1.3 Monoclonal Antibody Structure.....	12
1.4 Pharmaceutically Relevant Challenges Triggered by Colloidal and Conformational Destabilization of Monoclonal Antibodies.....	14
1.4.1 Protein Aggregation: Mechanisms, Challenges and Solutions.....	17
1.4.2 Concentration Dependent Reversible Self-Association of Proteins.....	21
1.5 Analytical and Biophysical Tools to Characterize Reversible Self-Association of Proteins....	28
1.5.1 Dynamic Light Scattering (DLS).....	28

1.5.2	Multi-Angle Light Scattering (MALS).....	30
1.5.3	Viscosity Measurements.....	32
1.5.4	Sedimentation Velocity Analytical Ultra-Centrifugation (SV-AUC).....	33
1.5.5	Affinity Capture Self-Interaction Nanoparticle Spectroscopy (AC-SINS).....	35
1.5.6	Hydrogen Exchange Mass Spectrometry (HX-MS).....	35
1.5.6.1	Basics of Hydrogen Exchange.....	36
1.6	References.....	43
Chapter 2. Correlating the effects of antimicrobial preservatives on conformational stability, aggregation propensity and local flexibility of an IgG1 monoclonal antibody.....		
59		
2.1	Introduction.....	60
2.2	Materials and Methods.....	63
2.2.1	Materials.....	63
2.2.2	Sample Preparation.....	63
2.2.3	Differential Scanning Calorimetry.....	64
2.2.4	8-Anilino-1-Napthalene Sulfonate (ANS) Extrinsic fluorescence.....	64
2.2.5	Accelerated Storage Stability Study.....	65
2.2.6	Size Exclusion High-Performance Liquid Chromatography.....	65
2.2.7	Hydrogen Exchange Mass Spectrometry.....	66
2.2.8	Mass Spectrometry data analysis.....	67
2.3	Results.....	68
2.3.1	Antimicrobial preservatives negatively impact the conformation stability of mAb-4.....	68
2.3.2	Antimicrobial preservatives decrease the accelerated stability of mAb-4.....	69
2.3.3	Backbone flexibility of mAb-4 in control buffer (No Preservatives).....	70

2.3.4	Antimicrobial preservatives affect the local backbone flexibility of mAb-4.....	71
2.4	Discussion.....	73
2.5	References.....	80
2.6	Tables and Figures.....	88
Chapter 3. Hydrogen exchange mass spectrometry reveals protein interfaces and distant dynamic coupling effects during the reversible self-association of an IgG1 monoclonal antibody.....		
		126
3.1	Introduction.....	127
3.2	Materials and Methods.....	130
3.2.1	Materials.....	130
3.2.2	Sample preparation.....	130
3.2.3	Dynamic Light Scattering.....	130
3.2.4	Chemical cross-linking and SDS-PAGE analysis.....	131
3.2.5	Viscosity Measurements.....	132
3.2.6	Lyophilization of mAb-C.....	132
3.2.7	Size Exclusion Chromatography (SEC).....	133
3.2.8	Circular Dichroism.....	134
3.2.9	Deuterated Reconstitution Buffer Preparation.....	134
3.2.10	Hydrogen Exchange Mass Spectrometry.....	135
3.2.11	HX-MS data processing and analysis.....	136
3.3	Results.....	137
3.3.1	Defining solution conditions that favor RSA.....	137

3.3.2 Solution viscosity as a function of protein concentration, temperature and salt concentration.....	139
3.3.3 Development of a freeze-dried formulation for HX-MS analysis of RSA.....	140
3.3.4 Effects of reversible self-association (RSA) on hydrogen exchange of mAb-C.....	141
3.4 Discussion.....	144
3.4.1 Effect of solution conditions on RSA of mAb-C.....	145
3.4.2 Development of an HX-MS method to examine RSA.....	147
3.4.3 HX-MS mapping of the protein interface of RSA of mAb-C.....	148
3.4.4 HX-MS mapping of distant dynamic effects on other regions of mAb-C upon RSA.....	151
3.5 References.....	153
3.6 Tables and Figures.....	164
Chapter 4. Charge-mediated Fab-Fc interactions in an IgG1 antibody induce reversible self-association, cluster formation, and elevated viscosity.....	203
4.1 Introduction.....	204
4.2 Materials and Methods.....	206
4.2.1 Sample preparation.....	206
4.2.2 Dynamic light scattering.....	207
4.2.3 Viscosity Measurements.....	207
4.2.4 Composition-gradient multi-angle light scattering.....	207
4.2.5 Lyophilization of mAb-J samples.....	209
4.2.6 Circular Dichroism.....	209
4.2.7 Size-Exclusion Chromatography.....	209

4.2.8 Deuteration of arginine.....	210
4.2.9 Hydrogen-Exchange Mass Spectrometry.....	210
4.2.10 Hydrogen Exchange Mass Spectrometry (HX-MS) with viscosity-decreasing solutes....	211
4.2.11 HX-MS data processing and analysis.....	212
4.3 Results.....	212
4.3.1 Increases in mAb hydrodynamic diameter suggests reversible self-association.....	212
4.3.2 Effects of solutes on the dynamic viscosity of mAb-J solutions.....	213
4.3.3 Reversible self-association of mAb-J involves a monomer-dimer-tetramer equilibrium....	214
4.3.4 Hydrogen exchange mass spectrometry reveals association between the Fc and Fab.....	215
4.4 Discussion.....	219
4.5 References.....	227
4.6 Tables and Figures.....	236
Chapter 5. Conclusions and Future Work.....	278
5.1 Overview.....	279
5.2 Chapter summaries and future work.....	280
5.2.1 Chapter 2.....	280
5.2.2 Chapter 3.....	282
5.2.3 Chapter 4.....	284
5.3 References.....	286

Chapter 1

Introduction

1.1 Overview

Intermolecular protein-protein interactions can play a key role in determining both the efficacy and safety of biopharmaceutical candidates. Reversible self-associations and irreversible aggregation of biotherapeutic agents can present serious challenges related to product formulation development, process control and regulatory concerns regarding safety and immunogenicity of the product^{1,2}. The work presented in this thesis will primarily focus on one subclass of biotherapeutic protein drugs, immunoglobulin G1 (IgG1) monoclonal antibodies (mAbs). Monoclonal antibodies are one of the fastest growing class of biotherapeutic drug products with the greatest number of potential candidates in a clinical phase³. Monoclonal antibodies are produced from the immortalized clones of single B plasma immune cells. Due to the nature of their origin, mAbs exhibit mono-specificity towards their targets and this property is exploited to develop highly potent and efficacious antibody based therapies for cancer, autoimmune, inflammatory and metabolic conditions.

The first segment of this introductory chapter will focus on the underlying mechanisms of protein-protein interactions and the fundamental physical underpinnings responsible for such phenomenon. Emphasis will be given to the effect of conformational dynamics, colloidal interactions, surface exposure and distribution of charged and apolar residues, protein concentration and solution environment on the nature and extent of protein-protein interactions. In the second section we will discuss the role of protein-protein interactions in governing protein stability from a pharmaceutical perspective. Particular emphasis will be given to high protein concentration solutions of mAbs and factors that negatively impact protein production and formulation development under crowded environments. Finally, traditional and novel/emerging analytical tools used for characterization of protein-protein interactions at high protein

concentrations will be discussed. In addition, basics of hydrogen exchange mass spectrometry (HX-MS) will be briefly explained with a focus on the utility of a novel lyo/recon HX-MS method in mapping interfaces of transient protein-protein interactions under crowded solution conditions (high protein concentration).

1.2 Intermolecular Protein-Protein Interactions

Protein-protein interactions are integral to many biochemical processes *in vivo*. Intra and extracellular functions are usually carried out by large molecular machineries composed of several protein partners organized through protein-protein interactions⁴. These interactions between proteins are usually specific in nature and culminate into a form exhibiting a specific biological function. Such contacts are also known as functional contacts^{5,6}. These intermolecular interactions however, are not always beneficial and productive for a biological system. Many protein-protein interaction events *in vivo* are deleterious and aberrant. Such abnormal intermolecular interactions are either a consequence of protein complex formation at an improper time and location or due to non-specific interactions between misfolded/conformationally distorted sub-fractions of functional proteins, invoking either an immune response from the body or discontinuing important biological processes like signal transduction⁷. Unwanted protein-protein interaction events are the basis of a multitude of diseases including but not limited to Alzheimer's disease, Huntington's disease and prion disease. Protein-protein interactions can follow multiple pathways and can be categorized based on their strength, nature of interaction partners and nature of non-covalent interactions between associating members⁸. A brief description of such classifications is given below.

1.2.1 Classification of Protein-Protein Interactions

1.2.1.1 Homo-Oligomers vs. Hetero-Oligomers

Protein complexes that involve only one type of monomeric unit are classified as homo-oligomers. Hetero-oligomers consist of non-identical members which can either be monomers or oligomers of a different protein molecule. Depending upon the nature of the protein interaction interface, homo-oligomers can be further sub-categorized into isologous oligomers and heterologous oligomers. Isologous homo-oligomers involve identical protein interfaces between every interacting partner. Isologous associations generally give rise to defined complexes of finite members. Heterologous associations although they involve the same class of protein monomers, do not share the same protein interface. Such associations, if lack cyclical symmetry, may give rise to isodesmic association.

1.2.1.2 Transient vs. Permanent Associations

Protein-protein interactions can also be categorized based on the time-scale of association. Permanent associations, as the name suggests, have very high binding affinities and appear to be irreversible over the entire experimental time-scale. Rate of association (k_{on}) for permanent interactions is significantly higher compared to rate of dissociation (k_{off}). Transient associations, however, are weaker and thus can dissociate at a much faster rate. The rate of association and dissociation can change upon application of an external stress (or other trigger) that affects association equilibrium⁷. Transient protein-protein interactions can further be subdivided into weak and strong interactions. Transient interactions, which are also the main focus of this thesis, exhibit dynamic equilibrium in solution. The direction of the equilibrium depends upon many factors including protein conformation, global/local dynamics, physiochemical properties of the

protein, as well as, solution variables such as pH, temperature and ionic strength. The interaction interface of weak transient protein-protein interactions tend to be smaller and have fewer contact points⁹⁻¹¹. Strong transient protein-protein interactions also are present in an equilibrated state, however, an external molecular trigger needs to be introduced to the system to shift the equilibrium towards the dissociated, monomeric state. Strong transient associations usually involve larger conformational changes in the protein structure and may elicit biological processes like signal transduction.

1.2.1.3 Native vs. Non-Native Associations

Protein conformation is a significant driver of protein-protein interactions. Proteins can associate in both native and non-native states. Amino acid content, chemical nature of surface exposed residues, solution properties and external stresses dictate the association route that the protein will undertake, especially for in vitro studies in various solutions¹². Both native and non-native associations can be reversible or irreversible in nature. Hemoglobin, a tetramer, is an example of native association of very high affinity, in which the protein remains in its complexed form under a wide range of solution conditions and effectively appears irreversible except at very low concentrations. Antibodies, on the other hand, can undergo reversible oligomerization in their native form, and such associations are weak and can disrupt upon changes in protein concentration and solution properties¹³⁻¹⁷.

Proteins are dynamic in nature undergoing continued breathing motions and global/local dynamic changes in flexibility. Due to sub-molecular dynamical motions, the solvent accessibility of apolar residues (which are primarily buried in the core of proteins) increases. The amount of time these apolar residues spend exposed to the solvent under native conditions is relatively slight, however,

under stressed conditions, this time-span can increase, leading to non-native contacts between protein molecules in solution¹⁸. Such complexes can be reversible or irreversible. Strong contacts between apolar residues between molecules can also lead to further distortion of the conformational integrity of the protein structure which leads to formation of nuclei and eventually to generation of extensive levels of non-native irreversible oligomerization¹⁸⁻²¹.

1.2.1.4 Covalent vs. Non-Covalent Associations

Protein intermolecular interactions can also be distinguished based on the nature of the interactions that exist at the interface of association. Native and non-native interactions between protein partners can be established by both covalent bonds and non-covalent interactions. Covalent interactions between protein molecules are rare in nature, except for disulfide bonds. They do however, play an important role in biological functions such as post-translational modifications (ubiquitination and SUMOylation etc.). Certain covalent bond formations can also lead to protein aggregation and degradation. Under alkaline conditions and reducing environments, disulfide bonds are labile and can degrade to give rise to deprotonated free thiols. Direct attack of hydroxyl anions on sulfur can degrade disulfide bonds to form thiolate anions which eventually attack another disulfide bond to form non-native thiolate dimers²². The presence of free thiols under native, oxidative environments can lead to the formation of non-native intermolecular disulfide bonds, causing covalent oligomerization of protein molecules, via mixed disulfide exchange reactions.²³

Non-covalent interactions between and within protein molecules (i.e., inter and intramolecular protein associations) are weak in nature (1-5 kcal/mol). They are widely prevalent in biology. For example, their formation assists in protein folding and function^{24,25}. Depending

upon amino acid variability, surface distribution, chemical nature of the amino-acids and solvent exposure, folded protein molecules can associate with each other through a number of different types of non-covalent interactions²⁶. Protein concentration also plays a significant role in determining the extent and kinetics of non-covalent associations. Protein-protein interactions initiated by non-covalent interactions are usually transient and are disrupted upon dilution or upon varying the solution conditions (depending upon the nature of non-covalent interactions)²⁷. In the subsequent section of this introduction, various type of non-covalent interactions that initiate and stabilize protein-protein interactions will be briefly discussed.

1.2.2 Types of Non-Covalent Interactions

1.2.2.1 Electrostatic Interactions

Electrostatic interactions exist between and among cations and anions which are species with integral charge. These type of forces can be attractive or repulsive depending upon the nature of the charge on the interacting partners. Electrostatic attractive interactions play an important role in protein folding and biochemical processes involving intermolecular protein associations where oppositely charged amino acid side chains form salt bridges.

Electrostatic potential or electrostatic force is formally given by Coulomb's law²⁸:

$$F_E = \frac{k_e q_1 q_2}{\epsilon r^2} \quad (1.1)$$

Where F_E is the electrostatic force, measured in Newtons, q_1 and q_2 are two formal point charges in solution, measured in Coulombs, k_e is the Coulomb's constant ($9.0 \times 10^9 \text{ N m}^2/\text{C}^2$), r is the distance between the charges in meters and ϵ is the dielectric constant of the solution in which the two charges are placed. F_E , electrostatic force is thus defined as an interaction between charges that are paired or pairwise interaction²⁹. Dielectric constant reflects the tendency of the solution to

reduce the coulombic force between the point charges relative to a vacuum. The dielectric constant of a vacuum is 1 and that of water is 78.3 at 25°C, measured in Farads per meter (F/m)³⁰. Compared to vacuum, water is very efficient at shielding and reducing the force between point charges. Since the interior of a protein is relatively apolar, the dielectric constant of the interior of a protein is relatively low compared to water and though to ranges from 1 to 20 F/m³¹. In biological systems where the proteins are present in crowded environments, it is extremely difficult to accurately determine the dielectric constant of the solution in the immediate vicinity or within a protein. Dielectric constants of micro-environments are variable and accurately modelling such values for molecular mechanics force fields is an active area of investigation³².

1.2.2.2 Dipolar Interactions

Dipole formation is based on the concept of separation of charge. Electronegativity is a measure of dipole strength which is simply defined as the tendency of an atom to attract electrons towards itself. In a molecule containing atoms of varying values of electronegativity, atoms with higher electronegativity carry a partial negative charge and other atoms of lower electronegativities carry a partial positive charge. This separation of charges within a molecule makes the bond between the atoms, polar. The magnitude of the polarity of a molecule is given by its dipole moment, which depends upon the distance of charge separation as well as the magnitude of the partial charges. The unit of dipole moment is Debye. The potential energy for dipolar interactions is given by equation 1.2²⁹.

$$V = -\frac{2\mu_1\mu_2}{4\pi\epsilon r^3} \quad (1.2)$$

Where V is the potential energy associated with a dipolar interaction, measure in Joules, μ_1 and μ_2 are the dipole moments of each interacting molecule, ϵ is the dielectric constant of the solution and r is the distance between the interacting partners separated by a straight line in space.

In proteins, oxygen is the most electronegative atom and carries a partially negative charge. High electronegativity of oxygen imparts a dipole moment to the amide bond (3.7 Debye). The large dipole moment of backbone amide bonds play an important role in protein folding (in the form of hydrogen bonding; see below) and maintaining the structural and conformational integrity of proteins. In addition to the attractive interactions between opposite poles of two dipoles (dipole-dipole interactions), they also exert potential over neighboring charges and partial charges. Attractive or repulsive interactions between dipoles and neighboring charged ions are called ion-dipole interactions. Since dipoles carry an electrostatic field around them, this electrostatic field interacts with electron clouds around neighboring molecules. This interaction shifts the electron cloud densities over molecules, thus inducing a dipole or polarization. Aromatic amino acids containing π electron clouds such as, phenylalanine, tyrosine and tryptophan are more polarizable than their aliphatic counterparts and interact with dipoles to a much greater extent. Such dipolar interactions are known as dipole-induced dipole interactions.

1.2.2.3 London Dispersion or van der Waals Interactions

Even neutral molecules attract each other. Electron densities of each atom fluctuate to some extent based on the natural resonant frequency of that atom³³. These short lived fluctuations or imbalance in electron density create a temporary dipole. To reduce charge-charge repulsions, this temporary dipole polarizes and thus induces an oppositely aligned dipole in the neighboring atom. This resulting interaction is called induced dipole-induced dipole attractive interaction, or London

dispersion forces³⁴. London dispersion forces are short range forces and can significantly affect protein-protein interactions in crowded solutions as well as within molecules.

1.2.2.4 Hydrogen Bonding

Hydrogen bonds are one of the most important determinants of protein folding and conformational stability³⁵. These bonds involve a Lewis base with lone pair of electrons (hydrogen bond acceptor), and an electronegative atom attached to the hydrogen (hydrogen bond donor). A strong electronegative donor pulls the electrons away from the hydrogen, thus imparting a partial positive charge on the hydrogen atom. Hydrogen atoms do not have non-bonding inner shell electrons that shield the nucleus, therefore its positively charged nucleus gets exposed which in turn attracts the hydrogen bond donor that carries a net negative charge due to the lone pair of electrons³⁶. Although hydrogen bond acceptor (Lewis base) attracts the hydrogen towards itself, the covalent bond between hydrogen and electronegative hydrogen bond donor never breaks and remains intact, therefore, hydrogen bonds can essentially be categorized as dipole-dipole interactions. Hydrogen bonds play an essential role in the formation of stabilizing secondary, tertiary, and if applicable, quaternary structures of proteins³⁶.

The strength of hydrogen bonds varies greatly depending upon the chemical nature of the donor and acceptor atoms. If the hydrogen bond forms between charged atoms, then the strength of such bonds ranges from 2-4 kcal/mol. The most common type of hydrogen bond is of moderate strength and are formed between neutral donors and acceptors. Strength of such bonds lies between 3-12 kcal/mol³⁷. Most of the intramolecular hydrogen bonds as well as hydrogen bonds between amino-acid side chains and water fall into the moderate strength category and as mentioned above play a key role in protein structure formation and stabilization. Hydrogen bonds also are a key

player in establishing intermolecular protein-protein interactions. Interactions between the oxygen of the carbonyl group and backbone amide hydrogens present at the protein interfaces often play a key role in establishing strong intermolecular associations.

1.2.2.5 Hydrophobic Interactions/Apolar Interactions

Hydrophobic or apolar interactions within biological systems such as proteins can be effectively explained with a thermodynamic basis. Protein molecules contain both hydrophilic and hydrophobic amino-acid residues. As the name suggests, hydrophobic residues do not interact favorably with water molecules. Due to this thermodynamically unfavorable interaction, water molecules arrange around the hydrophobic molecules creating an aqueous shell which causes disruption of hydrogen bonding network in the 3 dimensional space of the system. Creation of multiple aqueous shells around the hydrophobic residues produce a large entropic penalty in the system. To reduce this unfavorable entropic cost due to reduction in both rotational and translational entropy, the hydrophobic residues forced inside the protein core. This in turn lets the water molecules form favorable hydrogen bonds with each other, thus decreasing the free energy of the system.

The hydrophobic effect (in addition to hydrogen bonding) plays a crucial role in determining the folded native state and stability of a protein molecule. It also plays a significant role in protein-protein interactions. Partially disrupted protein conformers or highly dynamic local regions in a protein tend to occasionally expose the hydrophobic cores to their aqueous surroundings. Such partially distorted conformers and local fluctuations are short lived, and therefore, do not necessarily affect protein stability. Under stressed conditions, however, the life-span of such partially distorted conformers can increase causing water molecules to push exposed

hydrophobic patches on neighboring molecules together thus initiating protein associations. Interestingly, the nature of non-covalent interactions that promote protein folding within a protein molecule is same as those that promote non-native protein-protein interactions between protein molecules.

1.3 Monoclonal Antibody Structure

Monoclonal antibodies are one of the most important classes of biotherapeutic agents³. In this thesis, we specifically focus on the role of protein-protein interactions in governing the behavior of monoclonal antibodies in solution. The next section briefly describes the salient features of IgG1 antibody structure. Following this section, we will review impacts of protein-protein interactions on monoclonal antibody structure and stability and methods to qualitatively and quantitatively study such interacting systems.

Monoclonal antibodies (mAbs) are Y-shaped glycoproteins of the immunoglobulin class, where the Fab region (antigen binding domain) forms the “V” and Fc (crystallizable fragment) forms the stem of the molecule. Both of these fragments carry different biological functions. The Fab fragment is primarily responsible for antigen recognition, whereas, the Fc fragment binds to FcRn receptors (Figure 1.1).

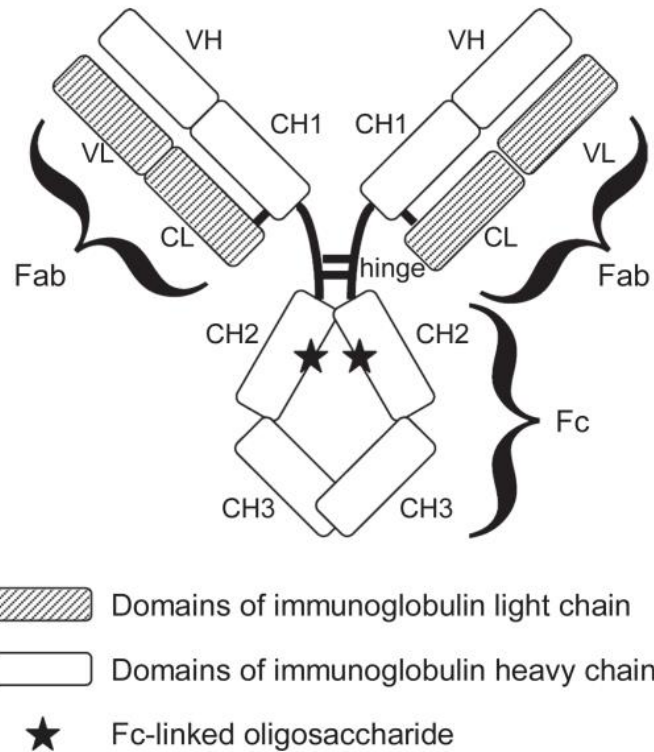


Figure 1.1: Structure of a human monoclonal IgG1 antibody³⁸. (Figure reproduced with permission from Dove Press).

The primary structure of mAbs can broadly be subdivided into two identical heavy and two identical light chains. Each heavy chain contains four domains and each light chain forms into two similar domains. These chains are held together by inter and intra-chain disulfide linkages and non-covalent interactions, therefore the antibody structure can also be called a “dimer of dimers” or homodimer. While each domain contains one intramolecular disulfide bond, the number of disulfide bonds linking the heavy chains (intermolecular disulfide bonds) varies between different classes and sub-classes of antibodies³⁹.

The first 100 to 110 amino-acids towards the N-terminus of the antibody constitute the variable domain (V region). This domain spans both the light chain and heavy chain (V_L and V_H). As the name suggests, the amino-acid makeup in this domain is variable and determines the specificity of

the antibody towards an antigen. These differences within the variable domain are found within areas called complementarity-determining regions (CDRs)³⁹. These CDRs (both in variable light and variable heavy chain) constitute the antigen binding interface of the antibody. The amino-acid content and sequence of rest of the antibody is relatively conserved and very few differences are seen in the rest of the molecule. Therefore, this region is called the “constant domain” (C_L and C_H). Antibodies can further be classified on the basis of various classes of light and heavy chains. Monoclonal antibodies have two variations of light chains, kappa (κ) and lambda (λ). In humans 60% of the antibodies have kappa light chains. In contrast, in mice 95% of the antibodies contain the kappa sub-type of light chain. The heavy chains also possess sub-types. Based on amino-acid sequence patterns the heavy chain can be subdivided into five different sub-types, μ, δ, γ, ε and α. Based on the subtype of heavy chain, immunoglobulins are classified as IgA (α), IgG (γ), IgM (μ), IgD (δ) and IgE (ε). Minor differences in the amino-acid sequences within IgA and IgG sub-types lead to further classifications into subisotypes. In humans, there are two subisotypes of IgA, IgA1 and IgA2, whereas, IgG has four subisotypes, IgG1, IgG2, IgG3 and IgG4. In this thesis we focus primarily on the IgG1 sub-class of an IgG monoclonal antibody³⁹. Immunoglobulin G1 (IgG1), is a ~150 kDa molecular weight protein with 4 inter and 12 intra-chain disulfide bonds. IgG1 antibodies, like other subclasses and subisotypes of mAbs, is variably glycosylated, with an N-linked glycosylation site at Asn 297 in the C_{H2} domain of the heavy chain⁴⁰⁻⁴².

1.4 Pharmaceutically Relevant Challenges Triggered by Colloidal and Conformational Destabilization of Monoclonal Antibodies

Both colloidal and conformational destabilization of antibodies can result in non-native, irreversible aggregation. Such an outcome is highly undesirable for antibodies since aggregation

impacts their developability, viability and safety as potential drug candidates^{43,44}. Both of these pathways of destabilization act together to cause increases in protein aggregation. Depending upon the environmental/solution variables (e.g. temperature, additives, ionic strength and pH) and physiochemical properties of protein molecules (morphology, chemical nature of exposed amino acids, isoelectric point, etc.), either conformational destabilization or colloidal destabilization can be the dominant form of the aggregation pathway.

Various formulation approaches can be used to address issues related to conformational and colloidal destabilization. Global and local charge on the surface of macromolecules including antibodies govern their colloidal stability. In a colloidally stable solution, individual molecules of proteins carry nearly equivalent net charge and thus experience an overall repulsive interaction from neighboring monomers. Any change in solution properties like pH relative to the isoelectric point of the protein molecules can affect the colloidal stability of proteins. At isoelectric point (pI), protein molecules carry a net zero charge. Under such conditions due to reduction in overall repulsive interactions, asymmetrically charged patches of amino-acids on the surface of proteins start reorienting the molecules to establish favorable long-range intermolecular electrostatic attractive interactions. In addition to charge heterogeneity, patches of exposed hydrophobic amino-acids can also initiate such protein-protein interactions. As mentioned above, exposed hydrophobic patches from the interior of a protein molecule are thermodynamically unfavorable. Therefore, water molecules under crowded conditions can be viewed as pushing the protein molecules together to exclude such amino acid side-chains from the surface, thus initiating non-native protein-protein interactions. Changing solution pH so that protein molecules carry a net negative or positive charge helps to increase the colloidal stability of the molecule. Site-specific mutagenesis can be used to target asymmetric charge patches on the surface of a protein. However,

this approach can also potentially effect protein potency and structural integrity. Addition of charged excipients (e.g., salts, charged amino acids) can break salt-bridges between protein molecules and can be used to increase the colloidal stability of proteins.

Conformational destabilization pertains to structural integrity and overall folding of the protein molecules. Proteins are dynamic entities with both large scale global and localized dynamic motions^{45,46}. As mentioned above, hydrophobic residues are buried inside the core of the natively folded protein. Due to such dynamic motions in protein structure, however, these hydrophobic patches are transiently exposed to the solution for a relatively very short time span⁴⁷. Such changes in protein dynamics can be reversible and might not affect the overall average folded state of the protein. Environmental and solution variables like pH, temperature and mechanical stresses affect the magnitude and kinetics of dynamic motions and in turn can affect the overall conformational integrity of the protein^{48,49}. Changes in protein conformation and generation of partially perturbed conformers with exposed hydrophobic aggregation prone amino acid sequences can lead to the formation of irreversibly associated oligomers of protein molecules. Several formulation strategies can be followed to minimize protein aggregation initiated by conformational distortion in solution. Various stabilizing excipients can be used to enhance the conformational stability of the proteins. Sucrose is one of such stabilizer. Due to its thermodynamically unfavorable interactions with the unfolded state of the protein, sucrose gets preferentially excluded from the protein surface leaving water molecules to populate around the proteins. This causes a thermodynamically unfavorable increase in the system's chemical potential. To minimize thermodynamically unfavorable interactions between water molecules and surface exposed apolar residues, preferential exclusion causes protein surface area to decrease which in turn favors the native fold (lowest surface area) and stabilizes the native protein conformation⁵⁰⁻⁵⁴. In addition to sucrose, other sugars and small

molecules can also be used to exhibit similar behavior. Kosmotropic salts like sodium sulfate have been shown to stabilize protein conformation through favorable interactions with positively charged amino-acids (stabilization of native-fold) and preferential exclusion mechanisms⁵⁵⁻⁵⁸.

In subsequent sections, we will discuss various protein association events with pharmaceutical implications such as protein aggregation, concentration dependent transient reversible self-association and phase separation of protein solutions. Mechanisms behind such phenomenon will be briefly discussed followed by approaches to minimize their occurrence in protein formulations.

1.4.1 Protein Aggregation: Mechanisms, Challenges and Solutions

Protein aggregation is one of the greatest pharmaceutical challenges faced by protein formulation development scientists. To mitigate protein aggregation, it is essential to understand the underlying mechanisms and variables that affect this process. This section will only briefly cover protein aggregation mechanisms and preventative measures. Protein aggregation is a complicated phenomenon and to discuss every aspect and mechanism leading to aggregation is beyond the scope of this chapter. Extensive reviews have appeared to provide more detailed information^{18,21,48}.

Protein aggregation has been classically explained using the Lumry-Eyring model of aggregation (Equation 1.03)^{21,59}. According to this scheme, proteins in their native state first form a reversible partially perturbed intermediate conformer “U”. As explained above this partially unfolded conformer can then undergo an irreversible step where these conformers come together to form an irreversible aggregate “A”.



where N is the natively folded monomer, U is the partially unfolded intermediate and A₂ represents an irreversible dimer. K_{unf} is the equilibrium constant of the change from N to U, whereas k_{agg} represents the kinetics of association of two molecules of partially unfolded conformer “U” to form an irreversible dimer “A₂”. Thermodynamic underpinnings of this aggregation model can be understood using a reaction energetics diagram (Figure 1.2). Protein aggregation can be modulated both by thermodynamic as well as kinetic controls. As mentioned above, one way to control protein aggregation is to increase the activation free energy of formation of the partially unfolded conformer “U”. Pharmaceutical excipients like sucrose and kosmotropic salts that directly affect the partially unfolded conformer can be used to stabilize the native conformer through the preferential exclusion principle.

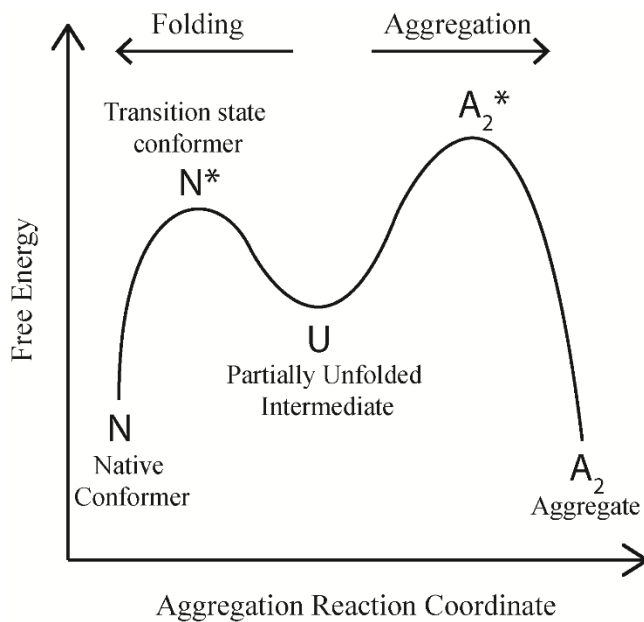


Figure 1.2: Schematic theoretical reaction coordinate diagram conceptualizing protein aggregation process as explained by Lumry-Eyring model¹⁸.

In addition to thermodynamic control of protein aggregation, kinetic stabilization can also be achieved by increasing the activation energy of the association step of the aggregation process. The theory of slow agglomeration explains in detail, how altering the potential of mean force (PMF) of protein solution perturbs the kinetics of protein aggregation⁶⁰⁻⁶².

The Lumry-Eyring model helps to lay the foundation for building a better understanding of protein aggregation. Protein aggregation is at times, however, not so straightforward. Protein aggregation in practice can be affected by a number of variables and the actual mechanisms of protein aggregation is a complex interplay between various different competing pathways like conformational distortion⁶³, chemical degradation⁶⁴, native transient associations^{65,66} and protein adsorption to various types of interfaces⁶⁷⁻⁷¹. Antibody aggregation in bulk solution is a complex process that includes many pathways and steps. A modification of the classical Lumry-Eyring model was proposed by Roberts et al⁷². Figure 1.3 shows various pathways and steps of antibody aggregation. As shown in the figure, antibody aggregation can be initiated by either protein oligomerization of native conformers or through partial disruption of protein structure leading to weak protein oligomerization of structurally disrupted sub-populations. Protein associations of native and distorted conformers are reversible in nature and under stabilizing solution conditions usually return back to their monomeric forms. However, under destabilizing solution conditions (exposed hydrophobic aggregation hot-spots) the transient oligomers could undergo an irreversible change to form nuclei. Nuclei are the smallest form of an irreversible aggregate. After generation of nuclei the protein molecules involved do not generally return to the original native conformation. Nuclei can grow through different pathways such as monomer-monomer addition, monomer-aggregate addition or aggregate-aggregate addition to form smaller or bigger aggregates

which eventually form particles, under certain conditions phase separation can also occur (Figure 1.3).

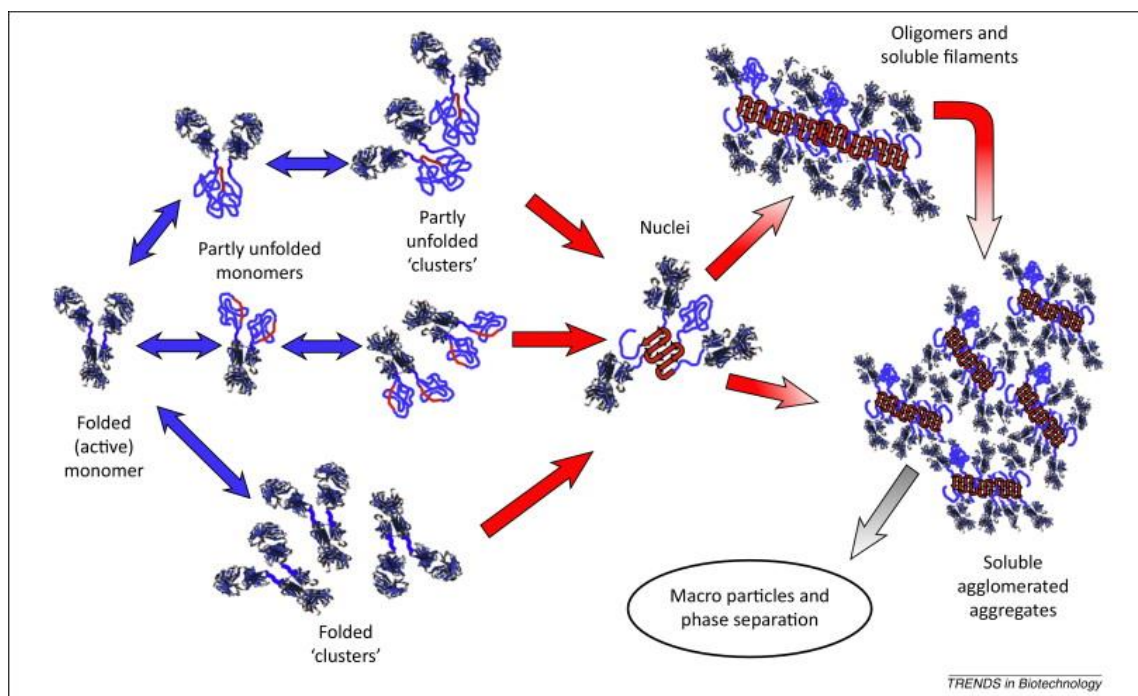


Figure 1.3: Schematic representation of monoclonal antibody multi-step non-native aggregation process in bulk solution⁷². (Image reproduced with permission from Elsevier).

If the net charge on the partially distorted conformer and nuclei is high (e.g., solution pH below or above the pI of the protein) and the charge screening length is short (low ionic strength solution conditions) then the nuclei undergo minimal growth and small aggregates are formed. However, if the net charge on the nuclei are low (e.g., solution pH approaching the pI of the protein) and charge screening length is long (high ionic strength solution conditions), then the nuclei experience either monomer-aggregate addition or aggregate-aggregate addition, both of which lead to formation of larger aggregates and particle formation (Figure 1.4).

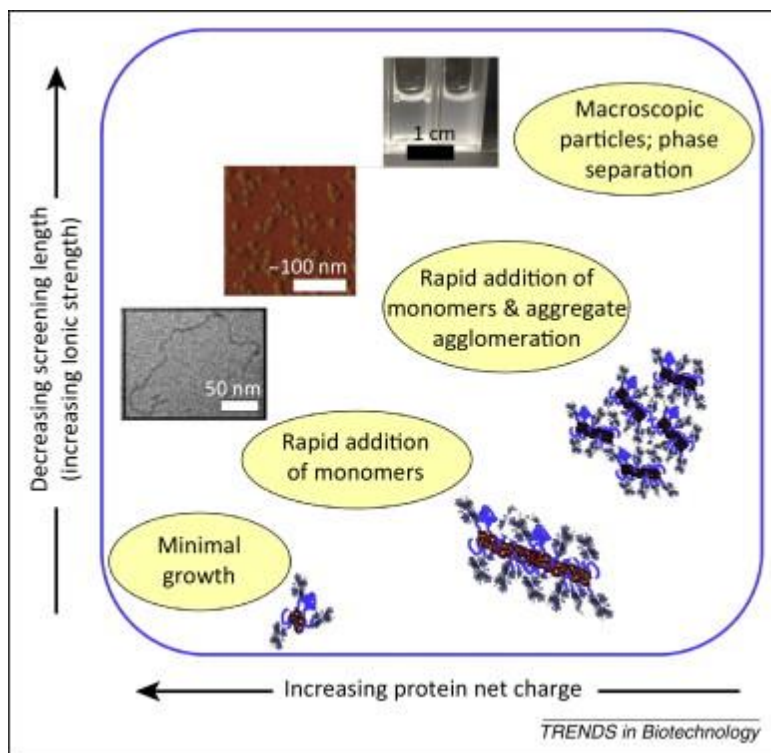


Figure 1.4: Effect of solution conditions and physicochemical nature of mAb molecule on the mechanism/pathway of protein aggregation⁷². (Image reproduced with permission from Elsevier).

1.4.2 Concentration Dependent Reversible Self-Association of Proteins

Reversible self-association (RSA) or reversible oligomerization is a concentration dependent process in which there exists an equilibrium between the native monomeric and oligomeric state. This type of association between protein molecules is ubiquitous in nature, especially intracellularly where protein concentrations can reach up to 300 mg/mL and intermolecular distances between protein molecules are very small⁷³⁻⁷⁶. The subcutaneous delivery of biopharmaceuticals is gaining interest over the past few years due to reasons related to patient compliance and self-administration of doses. The subcutaneous space, however, does not allow high volume injections and restricts pharmaceutical dosage forms to only 1-2 mL to deliver

relatively high doses of protein drugs. Due to this restriction, protein drugs for subcutaneous delivery are formulated at very high protein concentrations (above 100 mg/mL)^{77,78}. At such high concentrations, the intermolecular distances between protein monomers decrease significantly causing them to initiate specific and non-specific protein-protein interactions thus causing the solution to deviate from ideality⁷⁹⁻⁸². In this introduction we will focus on specific intermolecular interactions between protein partners at high protein concentrations.

Reversible self-association can be mathematically defined by the equations given below:



where n is the number of monomeric units involved in self-association and M is the native monomer. Equation 1.4⁸³, shows the interrelationship between critical parameters like the association rate constant, k_a and dissociation rate constant, k_d of protein association. One of the most important parameter by which the self-association process can be efficiently described is the association constant, K_a and dissociation constant, K_d which is reciprocal of K_a ($K_d = 1/K_a$). K_a can be calculated using the concentrations of the product and reactants of the association equilibrium (Eq. 1.5)⁸³

$$K_a = \frac{M_n}{[M]^n} \quad (1.5)$$

Reversible oligomerization of proteins at high protein concentrations depends on the amino acid makeup and surface exposure of electrostatic and hydrophobic amino acid residues. Structural morphology also plays a crucial role in determining the strength and stoichiometry of protein association process. This process can also involve multiple oligomerization equilibrium states such as monomer-dimer, monomer-trimer, monomer-trimer-hexamer, monomer-dimer-tetramer etc. Although rare, association of protein molecules at high protein concentrations can also follow an

isodesmic distribution or monomer addition mechanism. In this system a single molecule of native monomer associates through monomer addition to a growing oligomeric chain in every step⁸⁴⁻⁸⁶.

Various mechanisms of antibody self-associations have been studied and described previously. Two of the prevalent mechanisms are associations initiated by enthalpically driven electrostatic interactions and entropically driven hydrophobic interactions between native monomeric species of antibodies. Anisotropically distributed patches on an antibody surfaces initiate either long range electrostatic attractive interactions or hydrophobic interactions driven by the solvent. For both of these processes, overall electrostatic repulsive interactions between the mAb molecules should be at its minimum. At a solution pH where overall repulsive interactions between the protein molecules reach a minimum, self-association may be initiated. First, the monomeric molecules reorient themselves based on their reactive centers (electrostatic anisotropy or hydrophobic heterogeneity). Then, based on the nature of the non-covalent interactions and surface area of the interface of interactions, protein monomers undergo multiple collisions before a successful association event occurs. Although electrostatic attractive interactions and hydrophobic interactions appear to be the main drivers of self-association, a reversible oligomerization process is often the outcome of a balance between various types of non-covalent interactions including van der Waals, hydrophobic, dipolar, hydrogen bonding and electrostatic interactions⁸².

Reversible self-association of mAbs presents several challenges towards their pharmaceutical development. Protein-protein interactions directly affect solution dynamic viscosity. The modified Mooney's equation provides an expression for protein solution viscosity (Eq. 1.06)⁸⁰

$$\eta = \eta_o \exp \left[\frac{[\eta]c}{1 - \frac{k}{v}[\eta]c} \right] \quad (1.6)$$

where, η represents solution dynamic viscosity, η_0 represents solvent viscosity, C signifies protein concentration, $[\eta]$ is the intrinsic viscosity in mL/g and v is the Simha shape parameter (molecular orientation and morphology)⁸⁷. The modified Mooney's equation also takes into account the first order interaction parameter (κ) or the crowding factor at high protein concentrations. Protein solution viscosity, according to this equation, depends on the effective volume as well as shape/morphology of the protein species and crowding of the solution. However, contributions from specific (e.g., overall charge, electrostatics) and non-specific (e.g., ion-pairs, anisotropic charge distributions) effects should also be considered. The modified Mooney's equation does not consider contributions from such forces. Deviations from a purely excluded volume effect have been previously reported and can only be explained when contributions from the above mentioned forces are considered as significant⁸⁷. Therefore, it can be concluded that long and short ranged non-covalent interactions modulate protein-protein interactions and can impact protein solution viscosity.

Large protein complexes result in significant increases the shear modulus of the solution¹⁵. This increase in shear modulus or modulus of rigidity results in a dramatic increases in solution viscosity at higher concentration^{88,89}. Figure 1.5 and equation 1.7⁹⁰ show how protein-protein interactions affect shear modulus (G) by increasing the amount of displacement force (F) to maintain the same displacement (u) of the solution column of height (H). Shear modulus is directly proportional to the dynamic viscosity of the solution (η)

$$G = \frac{F}{A} \times \frac{H}{u} \quad (1.7)$$

“A” represents the cross-sectional area of the moving plate.

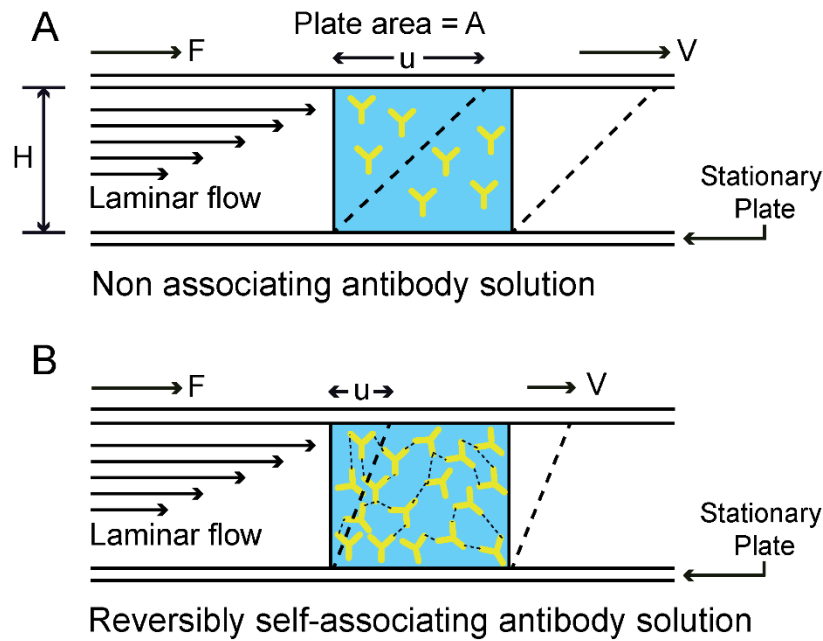


Figure 1.5: (A) Non-associating antibody solution displacement upon application of force, F . (B) Self-associating antibody slows down the displacement of the solution column upon application of the equivalent force applied in case (A) demonstrating greater viscosity in case (B).

Significant increases in solution viscosity imposes various pharmaceutical development and engineering challenges related to product filtration, pumping and syringeability. Due to high viscosity, a self-associating antibody solutions at high protein concentrations often cannot be delivered employing regularly used needles⁹¹. Due to high backpressure issues, wide gauge needles will need to be utilized that may cause painful injections. This effect decreases patient acceptability and compliance. Transient protein-protein interactions have also been shown to lead to irreversible aggregate formation which causes issues related to immunogenicity and loss of product viability and potency⁹². Depending upon the dissociation rate of oligomers, self-associated antibodies can exhibit aberrant pharmacokinetic profiles after subcutaneous injection⁹³. Extensive

self-association may also lead to phase separation and increases in solution turbidity causing protein destabilization and patient acceptance issues⁹⁴.

Reversible self-association, depending upon the nature of the non-covalent interactions, can be disrupted by addition of appropriate formulation excipients and/or by applying changes to the solution conditions. For systems that associate through either electrostatic or hydrophobic interactions, formulating antibodies at pH values below their pI value, where they carry a net positive charge, increases their colloidal stability by initiating overall electrostatic repulsive interactions between mAb monomers in bulk solution. In the case in which protein associations are primarily driven by electrostatic attractive interactions, addition of charged excipients such as salts and charged amino-acids can shield the surface exposed point charges on the antibody thereby disrupting any pairwise interactions between interacting partners. Apart from formulation strategies, high resolution analytical characterization and interfacial mapping of RSA in conjunction with site-specific mutagenesis at the interface has been successful in designing more stable mAb mutants with enhanced physiochemical properties and low viscosities at high protein concentrations^{17,95}. Figure 1.6 describes the antibody self-association phenomenon and factors that affect the extent of such processes.

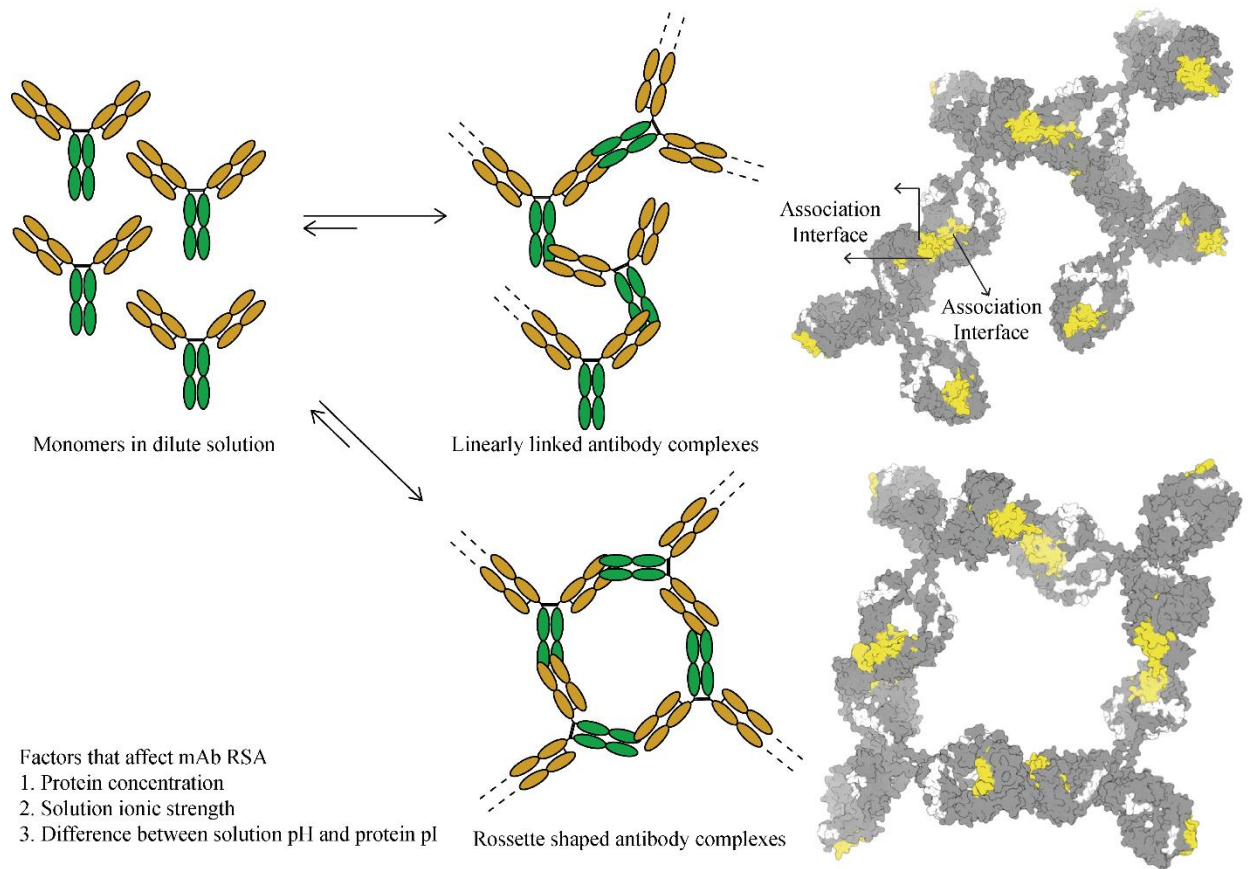


Figure 1.6: Pictorial representation of reversible self-association (RSA) of antibodies. Factors affecting the extent of reversible self-association are listed in the lower left corner of the figure.

Due to the inherent non-ideality in high protein concentration solutions, many analytical tools used to study protein-protein interactions in dilute solutions fail to produce reliable and reproducible data at high protein concentrations. Analytical characterization is of great importance and necessity to better understand protein self-association at high protein concentrations⁹⁶. In the subsequent section of the introduction we will briefly discuss various biophysical and analytical tools that can be used to study self-association of proteins at both lower and higher resolutions. We will also discuss a novel hydrogen exchange mass spectrometry method developed by our lab

as part of this thesis work to map protein interfaces of these transient associations at peptide level resolution, directly at high protein concentrations.

1.5 Analytical and Biophysical Tools to Characterize Reversible Self-Association of Proteins

1.5.1 Dynamic Light Scattering (DLS)

DLS is one of the most widely used analytical techniques to measure protein-protein interactions in solution. This technique can be used both in a batch mode and high throughput microplate format which makes it an important tool for early developability studies. DLS measurements are based on the fluctuations of intensity of the light scattered by the particles undergoing constant Brownian motions. In bulk solution, protein molecules are constantly bombarded by neighboring water molecules, due to the kinetic energy of the smaller water molecules. Transfer of kinetic energy from water molecules to protein molecules cause a randomness in motion of the protein molecules and the frequency of this randomness forms the basis of size determination by DLS. Particles of different sizes show either fast Brownian motions (smaller particle sizes) or slow motions (larger particle sizes). Based on the frequent change in Brownian motion, protein particles impart a randomness to the phase of the scattered light which in turn introduces intensity fluctuations that are time-dependent (fast vs. slow fluctuations) and can be tracked using a light scattering detector to determine the size of the particle. These fluctuations are a direct function of the diffusional property of the particle through which the hydrodynamic size of the particle is measured. Phase transitions in the scattered light are fitted to a second order intensity correlation function (Eq. 1.8)⁹⁷

$$g^2(\tau) = \frac{\langle I(t)I(t+\tau) \rangle}{\langle I(t) \rangle^2} = \frac{1}{2T\langle I \rangle^2} \int_{-T}^T I(t)I(t+\tau)dt \quad (1.8)$$

where $g^2(\tau)$ is the second order correlation function, $I(t)$ is the intensity of the scattered light at time t and $I(t+\tau)$ is the intensity of scattered light shifted in time by a small time interval τ and T is the infinite time limit. The correlation function correlates the intensity decay after time t to $t+\tau$. The diffusion coefficient is calculated from the correlation function fits. The Stokes-Einstein equation (Eq. 1.9)⁹⁷ describes the relationship between diffusion coefficient (D_t) and hydrodynamic radius (R_H) of particles undergoing Brownian motion in an ideal solution with no intermolecular interactions.

$$D_t = \frac{k_B T}{6\pi\eta R_H} \quad (1.9)$$

In equation 1.9⁹⁷ k_B is Boltzmann's constant, T is the temperature and η is the viscosity of the solution. Attractive intermolecular interactions such as reversible self-association between antibody monomers can lower the translational diffusion coefficient which is reflected by an increase in the average hydrodynamic diameter^{77,98}.

The mutual diffusion constant is measured as a function of protein concentration. A linear fit of mutual diffusion constant vs. concentration data to equation 1.10¹⁵ enables calculation of k_D .

$$D_m = D_o(1 + k_D C) \quad (1.10)$$

where, D_m represents the mutual diffusion coefficient, D_o is the self-diffusion coefficient, k_D is the diffusion interaction parameter and C is protein concentration. Value of k_D indirectly measures self-association phenomenon since it contains contributions from both hydrodynamic and thermodynamic processes^{15,99}. A positive value of k_D represent overall repulsive interactions between protein monomers and a negative value net attractive interactions in solution. Although k_D is not a direct measure of protein-protein interactions, several studies have shown good agreement between k_D and second virial coefficient values which is another measure of colloidal stability^{81,100,101}. Despite the ease of use and high throughput of the DLS platform, this technique

fails to provide reliable and reproducible data above a protein concentration of 20 mg/mL due to physical processes like multiple scattering and non-ideal behavior due to non-specific protein-protein interactions at high protein concentrations. However, DLS still remains one of the most utilized analytical technique to measure strong protein-protein interactions and aggregation in the dilute concentration regime with attempts to extrapolate the experimental results to high protein concentration solutions still under active investigation.

1.5.2 Multi-Angle Light Scattering (MALS)

As the name suggests, in MALS measurements light scattering from a particle is measured at multiple angles using multiple detectors. The fundamental quantity that is measured in these experiments is the excess Rayleigh ratio ($R(\theta, c)$) as a function of protein concentration and scattering angle. The measured quantity is related to the scattering angle and protein concentration (c), in addition or in excess of the scattering of the solvent devoid of any solute, i.e. scattering contributions from the pure solvent. The Zimm equation (Eq. 1.11)⁹⁷ describes the interplay between excess Rayleigh ratio, weight averaged molecular mass M , apparent second virial coefficient A_2 and the protein concentration, c , of the species present in the solution.

$$R(\theta, c) = K^*McP(\theta)[1 - 2A_2McP(\theta)] \quad (1.11)$$

where,

$$K^* = \frac{4\pi^2 n_0^2}{N_A \lambda_0^4} \times (dn/dc)^2 \quad (1.12)$$

where, n_0 represents the refractive index of the solvent, N_A is the Avogadro's number, $(dn/dc)^2$ is the incremental increase in refractive index with increasing protein concentration and λ_0 is the wavelength of the incidental wavelength in a vacuum. The apparent second virial coefficient A_2 , similar to the diffusion interaction parameter k_D discussed above, is a measure of the colloidal

stability of protein solutions. Positive value of A_2 represents an overall repulsive interactions between solute particles, whereas, negative values indicate a destabilizing solution condition with net attractive interactions between solute or protein monomers^{102,103}. Therefore, A_2 can be used to screen multiple solution conditions for their effect on the colloidal stability of a protein molecule, making MALS an extremely useful technique in formulation development for protein therapeutics¹⁰⁴⁻¹⁰⁶. Variations of classical multi-angle light scattering are also being used to qualitatively and quantitatively characterize transient protein-protein interactions in dilute to high protein concentration solution conditions.

Composition-gradient multi-angle light scattering (CG-MALS) involves stop-flow injections of a series of dilution/concentrations of an associating system that allows true equilibration at each step. To analyze specific, reversible self-association protein molecules in the ideal limit, a modification of the Zimm equation is used (Eq. 1.13) to measure the light scattering of two components A and B. Equations of mass action (Eq. 1.14) and conservation of mass (Eq. 1.15)⁹⁷ are used to estimate the stoichiometry of protein association along with mole fraction of each component¹⁰⁷.

$$\frac{R}{K^*} = \sum^{i,j} (iM_A + jM_B)^2 [A_i B_j] \quad (1.13)$$

with mass action

$$K_{ij} = \frac{[A_i B_j]}{[A]^i [B]^j} \quad (1.14)$$

and conservation of mass

$$[A]_{total} = \sum_{i,j} i [A_i B_j], \quad [B]_{total} = \sum_{i,j} j [A_i B_j] \quad (1.15)$$

M_a and M_b represent molar masses of system components A and B, i and j represent stoichiometric distribution of A and B in complex $A_i B_j$.

Although MALS provides a thorough characterization of reversible-self association and protein-protein interactions, experimental A_2 values are only reliable within the ideal limit (dilute solutions). CG-MALS equations (given above) can be used to fit the Rayleigh scattering data to various association models and through this fitted apparent second virial coefficients can be estimated at high protein concentrations. Another limitation of this technique is the experimental throughput. CG-MALS experiments can only be done in batch mode and pumps attached to the experimental system can only withstand low levels of backpressure. At high protein concentrations, where the extent of self-association is high, pumps installed in the CG-MALS setup may fail to inject, forcing the user to manually inject samples.

1.5.3 Viscosity Measurements

As mentioned above, transient protein-protein interactions can dramatically affect the viscosity of a protein solution. Associating systems show significantly higher viscosities when compared to non-associating systems at high protein concentrations. This outcome is exploited by formulation developmental scientists to characterize various solution conditions and excipient combinations while formulating proteins at high concentrations^{108,109}. Solution viscosity can be presented as a virial expansion of a polynomial (Eq. 1.16)⁸⁰

$$\eta = \eta_o(1 + k_1C + k_2C^2 + k_3C^3 + \dots) \quad (1.16)$$

where η is dynamic viscosity of the solution, η_o represents the viscosity of pure solvent, C is the protein concentration and k_1 , k_2 and k_3 are the first, second and third virial coefficients⁸⁰. Contributions from the second virial and third virial coefficients are negligible under dilute conditions which permits 1.16 to be simplified to equation 1.17⁹²:

$$\eta_{red} = \left(\frac{\eta - \eta_o}{C} \right) = k_1 + k_2C \quad (1.17)$$

where, η_{red} represents reduced solution viscosity which provides a measure of intrinsic viscosity (k_1) at infinite dilution. As the protein concentration is increased, contributions from the second and third virial coefficients (pair-wise interactions and higher-order intermolecular interactions) become significant and cause the solution behavior to deviate from Newtonian to non-Newtonian which can be qualitatively assessed by shear ramping experiments using viscometers¹¹⁰. While the above mentioned light scattering techniques struggle to provide reliable screening data of protein solutions at high protein concentrations, rheometers or viscometers provide an excellent opportunity to screen various formulation combinations at high protein concentrations in a relatively high throughput manner.

1.5.4 Sedimentation Velocity Analytical Ultra-Centrifugation (SV-AUC)

Sedimentation velocity analytical ultra-centrifugation (SV-AUC) is a classic technique used to characterize reversible as well as irreversible protein oligomerization. Samples containing protein oligomers are subjected to very high centrifugal force. This causes the individual constituents of the sample to sediment to the bottom of the cell over time. The sedimentation rate of these constituents and factors that affect this sedimentation rate are given by equation 1.18¹¹¹:

$$s = \frac{u}{\omega^2 r} = \frac{M(1-v\rho)}{N_A f} = \frac{MD(1-v\rho)}{RT} \quad (1.18)$$

where s is the sedimentation coefficient, u is the radial velocity, ω represents the angular velocity of the rotor and r is the radial position. The product of the square of angular velocity and radial position $\omega^2 r$ is the angular momentum. M represents the molar mass of the species, v is the partial specific volume and ρ represents the density of the solvent, N_A is the Avogadro's number and f is the frictional coefficient. The diffusional coefficient is represented by D and R is the gas constant. Sedimentation coefficient values are reported in Svedberg units (S) which equal 10^{-13} seconds¹¹¹.

The Stoke's equation can be used to calculate frictional coefficient for a uniform sphere (Eq. 1.19)¹¹¹

$$f_o = 6\pi\eta R_o \quad (1.19)$$

where f_o represents the frictional coefficient of a regular sphere and R_o is the radius of that sphere. η represents the dynamic viscosity of the solution. A combination of equation 1.17 and 1.18 gives equation 1.20, i.e., the sedimentation coefficient of a sphere.

$$S_{\text{sphere}} = \frac{M(1-v\rho)}{N_A 6\pi\eta \times \left(\frac{3Mv}{4\pi N_A}\right)^{1/3}} \quad (1.20)$$

Some of the values in equation 1.20 are known constants and can be replaced by their values at 20°C. This provides a simpler, modified equation 1.21¹¹¹:

$$S_{\text{sphere}} = 0.012 \frac{M^{2/3}(1-v\rho)}{v^{-1/3}} \quad (1.21)$$

Equation 1.19 represents the sedimentation coefficient in terms of M , v and ρ and can be used to calculate sedimentation coefficients for a spherical protein in water at 20°C¹¹¹.

SV-AUC utilizes two different types of optics to measure the radial concentration distributions, absorbance and interference optics. This technique can be used to measure the size and obtain information on the shape of the molecule with little to no restrictions on the nature of the solvent that can be used¹¹². The sample for analysis should have some distinguishing optical property (should be compatible with either of the two optical systems) and should be highly purified with only a few distinct components. Purity of the sample can affect the reliability of the measurements. SV-AUC is considered as an orthogonal technique to size exclusion chromatography (SEC), but in some ways is superior because the samples do not interact with any external matrix and the dynamic range of SV-AUC is much larger than SEC¹¹³. SV-AUC's biggest drawback is its low throughput and limitation on protein concentration. Since the most widely used

optical property is absorbance, this limits protein concentration between absorbance values of 0.2-1.0 OD at the chosen wavelength. The protein concentration limit can be pushed slightly using narrower path length cells and the interference optical system, however, it still does not allow protein concentrations to exceed ~10 mg/mL. This limitation restricts SV-AUC's ability to use for analysis of high protein concentration systems.

1.5.5 Affinity Capture Self-Interaction Nanoparticle Spectroscopy (AC-SINS)

AC-SINS is a promising and novel technique in the field of protein-protein interaction assessment^{114,115}. This technique involves decorating the surfaces of gold-nanoparticles with varying ratios of capture antibodies (e.g., specific polyclonal, goat anti-human) and non-capture antibodies (e.g., non-specific polyclonal). These gold-nanoparticles are then introduced in dilute solutions (0.001-0.05 mg/mL) of the antibody of interest. Capture antibodies on the surface of the nanoparticles immobilize the antibody of interest on the surface of the nanoparticles. Agglomeration/colloidal stability of gold-nanoparticles after their introduction in the mAb solution is governed by the immobilized mAb's self-association potential. Reduction in the inter-particle distance between the nanoparticles or their aggregation causes a red-shift in the wavelength of the absorbance maximum. AC-SINS holds promise because of its ability to quantitatively assess protein self-association in very dilute solutions. This technique can also analyze impure solutions of antibodies because the capture antibodies have specific affinities.

1.5.6 Hydrogen Exchange Mass Spectrometry (HX-MS)

Hydrogen exchange (HX) is a classic tool to study protein backbone dynamics and protein-protein interactions. HX coupled to mass spectrometry (HX-MS) provides an excellent opportunity

to extend its utility to larger, more complex macromolecules such as monoclonal antibodies. HX-MS has a rich experimental history and a wide spectrum of applicability. The subsequent section briefly explains the basics of hydrogen exchange process and how it can be used to measure backbone amide flexibility of macromolecules. More detailed descriptions of various aspects of this technique have been published recently¹¹⁶.

Protein molecules are dynamic entities with motions ranging from femtoseconds to seconds time-scale¹¹⁷. Various techniques can be utilized to capture protein dynamics corresponding to various time-scales. Motions ranging from picoseconds to seconds can be tracked using nuclear magnetic resonance (NMR), whereas X-ray diffraction cannot be used to track protein motions. Although these two techniques are the well-established and widely employed to study protein structure and protein-protein interactions at very high resolution¹¹⁸⁻¹²¹, they find relatively little applicability in pharmaceutical development of formulated protein drugs, especially analysis of local dynamics or protein-protein interactions of entire monoclonal antibody molecules. On the contrary, HX-MS has recently found utility in measuring local flexibility and probing protein-protein interactions of large multi-domain macromolecules such as antibodies.

1.5.6.1 Basics of Hydrogen Exchange

Labile hydrogens in the amino-acids when introduced in an aqueous environment constantly exchange with the hydrogens in the solvent. Not all hydrogens in protein structure are labile, hydrogens attached to the electronegative heteroatoms (oxygen, nitrogen and sulfur) exchange at a measurable time-scale. Hydrogens attached to the carbon atoms do not exchange with the solvent. When solvent is changed from H₂O to D₂O, labile hydrogens attached to the above-mentioned heteroatoms start exchanging with deuterium atoms in the solvent. Hydrogens bonded

to heteroatoms in the side-chains of amino-acids undergo essentially instantaneous exchange with the solvent, and due to the reversible nature of the process, revert back to hydrogen once exposed to H₂O during liquid chromatography (LC) step of the experiment. Therefore, such hydrogens cannot be utilized for any practical purposes.

In contrast, the exchange rate of hydrogens bonded to the backbone amide depends upon the folded state of the protein and stability of intramolecular hydrogen bonding¹²²⁻¹²⁵. Backbone hydrogens that are involved in secondary structure of the protein (i.e., α -helices and β -sheets) are significantly shielded from the solvent and form stable hydrogen bonds with neighboring H-bond acceptors (e.g., carbonyl group of amide bonds). Therefore, these hydrogens exchange at a much slower rate compared to hydrogens from a region of the protein that are solvent exposed and form weak intramolecular H-bonds (e.g., unstructured loops, CDRs of mAbs). Kinetics of deuterium uptake correspond to the stability of hydrogen bonding between backbone amide hydrogens in any particular location. Regions of proteins that are well structured, stable and solvent protected like the β -sandwich domains of the antibody, show very slow backbone exchange kinetics (from hours to months), however, unstructured and solvent exposed regions of the protein exchange very quickly (within milliseconds of initial exposure to D₂O)¹²⁶.

By tracking and comparing the kinetics of deuterium uptake of different locations of the protein between various solution conditions, one can retrieve useful information concerning the local flexibility of the protein molecule and external factors that affect the local flexibility. The same fundamentals can be applied while mapping the interface of protein-protein interactions. Various non-covalent interactions specifically or non-specifically initiate intermolecular associations, these associations in addition to other non-covalent interactions also form as a consequence of intermolecular H-bonding between interacting protein partners. When kinetics of

deuterium in associating and non-associating conditions are compared, valuable information about the protein interface of protein-protein interactions can be retrieved using hydrogen exchange methodology^{17,127}. However, one should be cautious while interpreting results of such HX-MS experiments as changes in HX kinetics due to allosteric effects of protein-protein interactions can make data interpretation challenging.

Amide backbone hydrogen exchange rate in a protein is a combination of two factors, chemistry and structure. Peptide segments even in an unstructured state (i.e., devoid of any higher order structure) exchange at a kinetic rate. This exchange rate of unstructured peptide is referred to as chemical exchange. This chemical exchange process includes contributions from acid catalysis, base catalysis and a minor contribution from water catalysis (Eq. 1.22)^{116,128}

$$k_{ch} = k_{int,H}[H^+] + k_{int,OH}[OH^-] + k_{int,water}[H_2O] \quad (1.22)$$

where $k_{int,H}$, $k_{int,OH}$ and $k_{int,water}$ represent rate constants of acid catalysis, base catalysis and water catalysis of HX process. HX kinetic rate shows a strong dependence on pH. Figure 1.7 shows the pH rate profile for the chemical exchange process.

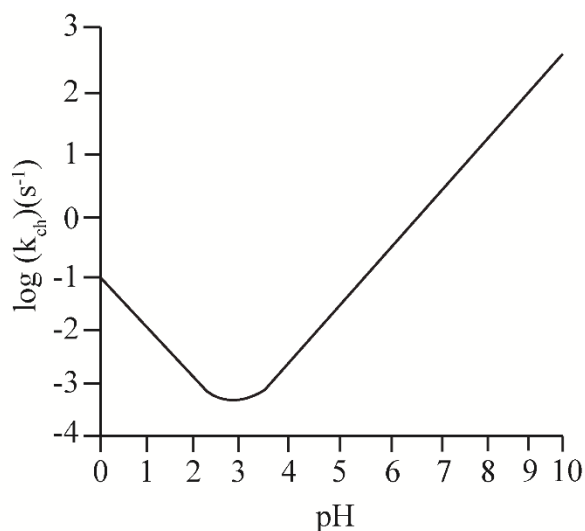
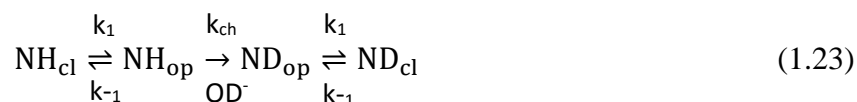


Figure 1.7: pH rate profile showing dependence of HX chemical exchange rate (k_{ch}) on solution pH of an amide hydrogen in a random coil poly-DL-alanine peptide at 20°C. Adapted from Ref. [31]

Above pH 3, the HX process is primarily catalyzed through base catalysis. The rate of the reaction reaches at its minimum around pH 2.5, and below pH 2.5, the rate of HX primarily is driven by acid catalysis. Above pH 4, the rate of chemical exchange shows a 10-fold increase in rate with every pH unit increase. Other solution variables such as ionic strength and temperature and neighboring amino acids also modulate chemical exchange rate^{126,129}.

Proteins in their native state remain as an ensemble of various different conformers of nearly similar ground state free energy. Native state conformation is an average structure of all the different ground state conformers. However, protein does not stay in one conformation and spans different native conformations at any given time. This behavior is translated as global and local dynamics and proteins appear to be in a constant state of flux^{117,130,131}. Due to the inherent fluidity of protein structures, the H-bonds that hold them together also break and reform. The kinetics of H-bond breaking and reforming depends upon the local dynamics of the region of interest in a protein structure. HX process in folded, dynamic proteins can be explained using the Linderstrom-Lang model of exchange¹³². Based on the location of the backbone amide, high energy local fluctuations that are part of the transition states between natively folded structures can temporarily disrupt intramolecular H-bond network, thus enabling the backbone amide to engage in H-bonding with the solvent instead. The Linderstrom-Lang model conceptualizes exchange process from folded and unfolded intermediates of the protein is given in equation 1.23¹¹⁶.



where NH_{cl} represent natively folded conformation of the protein also called the exchange incompetent state. As the protein undergoes local fluctuations, NH_{cl} changes to NH_{op} which is the locally perturbed, exchange competent state with a disrupted intermolecular H-bond. k_1 and k_{-1} represent rates of opening and closing of intermolecular backbone amide H-bonds.

In an exchange competent state, if the protein is introduced into D_2O , the backbone amides start forming H bonds with the deuterium atoms in the solution. Protein molecules in their ground state are present both in exchange competent and incompetent states, these forms are interchangeable and protein spends time in both the states. Depending upon external stress conditions, the time spent in one particular state can change in relation to other, which reflects the change in local flexibility. Therefore, the HX process depends upon the structural flexibility of the protein molecule as well as the chemical exchange rate (k_{ch}). From equation 1.21, expression for HX rate can be derived (Eq. 1.24)¹¹⁶

$$k_{\text{HX}} = \frac{k_{\text{op}} \times k_{\text{ch}}}{k_{\text{op}} + k_{\text{cl}} + k_{\text{ch}}} \quad (1.24)$$

k_{HX} is the rate of hydrogen exchange or isotopic exchange rate. Normally, protein conformation does not deviate too far from the average conformer and under native state proteins return to their folded state very rapidly. Therefore, it can be safely assumed that rate of H-bond closing is much greater than their opening rates under native state conditions ($k_{\text{cl}} \gg k_{\text{op}}$). This assumption modifies equation 1.24 to equation 1.25¹¹⁶.

$$k_{\text{HX}} = \frac{k_{\text{op}} \times k_{\text{ch}}}{k_{\text{cl}} + k_{\text{ch}}} \quad (1.25)$$

Depending upon the rate of closing and opening of hydrogen bonds, two extreme conditions can be envisioned. The unfolded intermediates that populate the transition states are usually short lived.

However, due to external stress and other environmental variables the life-span of such local unfolded intermediates can lengthen, allowing enough time for HX process to finish at all possible positions in that particular peptide segment. Under such conditions where k_{cl} is much slower than the chemical exchange, k_{ch} of the peptide segment, chemical exchange rate becomes the rate limiting step and equation 1.25 gets modified to equation 1.26¹¹⁶:

$$k_{HX,obs} = k_{op} \quad (1.26)$$

This mechanism is known as EX1 limit where the observed rate constant for HX is equal to the rate of opening of backbone amide H-bonds. EX1 limit is often regarded as evidence for the presence of global unfolding or large domain unfolding events that drive the exchange process. EX1 mechanism of HX is rarely seen in folded proteins under native conditions.

Most of the proteins under stable native conditions follow EX2 kinetics of HX. In this case with most folded proteins, the rate of refolding is much greater than the chemical exchange rate k_{ch} ($k_{cl} \gg k_{ch}$) and the probability of a successful exchange event is low, which means that the hydrogen bond opening and closing occur multiple times before a successful HX event. In EX2 limit rate of HX can be redefined as equation 1.27:

$$k_{HX,obs} = \frac{k_{op}}{k_{cl}} \times k_{ch} = K_{op} \times k_{ch} \quad (1.27)$$

As mentioned above HX coupled to MS has recently found applicability in protein formulation development and early stage developability efforts for pharmaceutically relevant proteins like antibodies¹³³⁻¹³⁵. Past studies have shown correlations between HX data and long term stability of monoclonal antibodies¹³⁶⁻¹³⁹. In another study (also discussed here in later chapters), practical limits of HX-MS methodology was stretched to include high protein concentration

regime. Transient protein-protein interactions were studied and mapped using a novel HX-MS methodology.

In this thesis, at first we will present applicability of HX-MS in identifying local perturbations in antibody structure upon introduction of various antimicrobial preservatives (conformational destabilizers) to the antibody solutions. Correlation between the degree of local fluctuations in flexibility with global, low resolution measures of physical stability such as thermal melting temperatures and protein aggregation propensity of an IgG1 monoclonal antibody will be presented. In later chapters, we will present a novel HX-MS methodology developed in our lab which is geared towards identifying and mapping protein-protein interaction interfaces of transient RSA of monoclonal antibodies at high protein concentrations. This work involved examining two different mAbs that undergo RSA by two different mechanisms.

1.6 References

1. Shire SJ, Shahrokh Z, Liu J 2004. Challenges in the development of high protein concentration formulations. *Journal of pharmaceutical sciences* 93(6):1390-1402.
2. Joubert MK, Hokom M, Eakin C, Zhou L, Deshpande M, Baker MP, Goletz TJ, Kerwin BA, Chirmule N, Narhi LO 2012. Highly aggregated antibody therapeutics can enhance the in vitro innate and late-stage T-cell immune responses. *Journal of Biological Chemistry* 287(30):25266-25279.
3. Wang W, Singh S, Zeng DL, King K, Nema S 2007. Antibody structure, instability, and formulation. *Journal of pharmaceutical sciences* 96(1):1-26.
4. De Las Rivas J, Fontanillo C 2010. Protein–protein interactions essentials: key concepts to building and analyzing interactome networks. *PLoS Comput Biol* 6(6):e1000807.
5. Mackay JP, Sunde M, Lowry JA, Crossley M, Matthews JM 2007. Protein interactions: is seeing believing? *Trends in biochemical sciences* 32(12):530-531.
6. Chatr-aryamontri A, Ceol A, Licata L, Cesareni G. Protein interactions: integration leads to belief. *Trends in biochemical sciences* 2008; 33:241-2
7. Ryan DP, Matthews JM 2005. Protein–protein interactions in human disease. *Curr Opin Struct Biol* 15(4):441-446.
8. Jones S, Thornton JM 1996. Principles of protein-protein interactions. *Proceedings of the National Academy of Sciences* 93(1):13-20.
9. Nooren IM, Thornton JM 2003. Structural characterisation and functional significance of transient protein–protein interactions. *Journal of molecular biology* 325(5):991-1018.

10. Mintseris J, Weng Z 2005. Structure, function, and evolution of transient and obligate protein–protein interactions. *Proceedings of the National Academy of Sciences of the United States of America* 102(31):10930-10935.
11. Jones S, Thornton JM 1997. Analysis of protein-protein interaction sites using surface patches. *Journal of molecular biology* 272(1):121-132.
12. O'Brien C, Blanco M, Costanzo J, Enterline M, Fernandez E, Robinson A, Roberts C 2016. Modulating non-native aggregation and electrostatic protein–protein interactions with computationally designed single-point mutations. *Protein Engineering Design and Selection* 29(6):231-243.
13. Liu J, Nguyen MD, Andya JD, Shire SJ 2005. Reversible self-association increases the viscosity of a concentrated monoclonal antibody in aqueous solution. *Journal of pharmaceutical sciences* 94(9):1928-1940.
14. Kanai S, Liu J, Patapoff TW, Shire SJ 2008. Reversible self-association of a concentrated monoclonal antibody solution mediated by Fab–Fab interaction that impacts solution viscosity. *Journal of pharmaceutical sciences* 97(10):4219-4227.
15. Yadav S, Liu J, Shire SJ, Kalonia DS 2010. Specific interactions in high concentration antibody solutions resulting in high viscosity. *Journal of pharmaceutical sciences* 99(3):1152-1168.
16. Yadav S, Sreedhara A, Kanai S, Liu J, Lien S, Lowman H, Kalonia DS, Shire SJ 2011. Establishing a link between amino acid sequences and self-associating and viscoelastic behavior of two closely related monoclonal antibodies. *Pharmaceutical research* 28(7):1750-1764.
17. Arora J, Hickey JM, Majumdar R, Esfandiary R, Bishop SM, Samra HS, Middaugh CR, Weis DD, Volkin DB 2015. Hydrogen exchange mass spectrometry reveals protein interfaces and

distant dynamic coupling effects during the reversible self-association of an IgG1 monoclonal antibody. *mAbs* 7(3):525-539.

18. Roberts CJ. 2006. Nonnative protein aggregation. *Misbehaving Proteins*, ed.: Springer. p 17-46.

19. Roberts CJ 2007. Non-native protein aggregation kinetics. *Biotechnology and bioengineering* 98(5):927-938.

20. Weiss WF, Young TM, Roberts CJ 2009. Principles, approaches, and challenges for predicting protein aggregation rates and shelf life. *Journal of pharmaceutical sciences* 98(4):1246-1277.

21. Andrews JM, Roberts CJ 2007. A Lumry-Eyring nucleated polymerization model of protein aggregation kinetics: 1. Aggregation with pre-equilibrated unfolding. *The Journal of Physical Chemistry B* 111(27):7897-7913.

22. Florence TM 1980. Degradation of protein disulphide bonds in dilute alkali. *Biochem J* 189(3):507-520.

23. Trivedi MV, Laurence JS, Siahaan TJ 2009. The role of thiols and disulfides in protein chemical and physical stability. *Curr Protein Peptide Sci* 10(6):614-625.

24. Privalov PL, Makhatadze GI 1992. Contribution of hydration and non-covalent interactions to the heat capacity effect on protein unfolding. *Journal of molecular biology* 224(3):715-723.

25. McClements DJ 2006. Non-covalent interactions between proteins and polysaccharides. *Biotechnol Adv* 24(6):621-625.

26. Frieden E 1975. Non-covalent interactions: key to biological flexibility and specificity. *J Chem Educ* 52(12):754.

27. Whitesides GM, Grzybowski B 2002. Self-assembly at all scales. *Science* 295(5564):2418-2421.
28. Atkins P, De Paula J. 2006. *Atkins' physical chemistry*. ed.: Oxford University Press, Oxford, New York.
29. Van Holde KE, Johnson WC, Ho PS 2006. *Principles of physical biochemistry*.
30. Malmberg C, Maryott A 1956. Dielectric constant of water from 00 to 1000 C. *J Res Nat Bureau Stand* 56:1-8.
31. Schutz CN, Warshel A 2001. What are the dielectric “constants” of proteins and how to validate electrostatic models? *Proteins: Structure, Function, and Bioinformatics* 44(4):400-417.
32. Ross PD, Subramanian S 1981. Thermodynamics of protein association reactions: forces contributing to stability. *Biochemistry* 20(11):3096-3102.
33. Nick Pace C, Scholtz JM, Grimsley GR 2014. Forces stabilizing proteins. *FEBS Lett* 588(14):2177-2184.
34. Jeffrey GA, Saenger W. 2012. *Hydrogen bonding in biological structures*. ed.: Springer Science & Business Media.
35. Schulz GE, Schirmer RH. 2013. *Principles of protein structure*. ed.: Springer Science & Business Media.
36. Hubbard RE, Kamran Haider M 2010. Hydrogen bonds in proteins: role and strength. eLS.
37. Natsume A, Niwa R, Satoh M 2009. Improving effector functions of antibodies for cancer treatment: Enhancing ADCC and CDC. *Drug Des Devel Ther* 3:7-16.
38. Kindt TJ, Goldsby RA, Osborne BA, Kuby J. 2007. *Kuby immunology*. ed.: Macmillan.
39. Wright A, Morrison SL 1997. Effect of glycosylation on antibody function: implications for genetic engineering. *Trends in biotechnology* 15(1):26-32.

40. Sheeley DM, Merrill BM, Taylor LC 1997. Characterization of monoclonal antibody glycosylation: comparison of expression systems and identification of terminal α -linked galactose. *Analytical biochemistry* 247(1):102-110.
41. Shade K-TC, Anthony RM 2013. Antibody glycosylation and inflammation. *Antibodies* 2(3):392-414.
42. Amin S, Barnett GV, Pathak JA, Roberts CJ, Sarangapani PS 2014. Protein aggregation, particle formation, characterization & rheology. *Current Opinion in Colloid & Interface Science* 19(5):438-449.
43. Kamerzell TJ, Esfandiary R, Joshi SB, Middaugh CR, Volkin DB 2011. Protein–excipient interactions: Mechanisms and biophysical characterization applied to protein formulation development. *Adv Drug Del Rev* 63(13):1118-1159.
44. Teague SJ 2003. Implications of protein flexibility for drug discovery. *Nature reviews Drug discovery* 2(7):527-541.
45. Carlson HA, McCammon JA 2000. Accommodating protein flexibility in computational drug design. *Mol Pharmacol* 57(2):213-218.
46. Chi EY, Krishnan S, Randolph TW, Carpenter JF 2003. Physical stability of proteins in aqueous solution: mechanism and driving forces in nonnative protein aggregation. *Pharmaceutical research* 20(9):1325-1336.
47. Philo JS, Arakawa T 2009. Mechanisms of protein aggregation. *Curr Pharm Biotechnol* 10(4):348-351.
48. Perchiacca JM, Tessier PM 2012. Engineering aggregation-resistant antibodies. *Annual review of chemical and biomolecular engineering* 3:263-286.

49. Kendrick BS, Chang BS, Arakawa T, Peterson B, Randolph TW, Manning MC, Carpenter JF 1997. Preferential exclusion of sucrose from recombinant interleukin-1 receptor antagonist: Role in restricted conformational mobility and compaction of native state. *Proceedings of the National Academy of Sciences* 94(22):11917-11922.
50. Lee JC, Timasheff SN 1981. The stabilization of proteins by sucrose. *Journal of Biological Chemistry* 256(14):7193-7201.
51. Baier S, McClements DJ 2001. Impact of preferential interactions on thermal stability and gelation of bovine serum albumin in aqueous sucrose solutions. *J Agric Food Chem* 49(5):2600-2608.
52. Timasheff SN 1993. The control of protein stability and association by weak interactions with water: how do solvents affect these processes? *Annu Rev Biophys Biomol Struct* 22(1):67-97.
53. Kerwin BA, Heller MC, Levin SH, Randolph TW 1998. Effects of Tween 80 and sucrose on acute short-term stability and long-term storage at -20° C of a recombinant hemoglobin. *Journal of pharmaceutical sciences* 87(9):1062-1068.
54. Moelbert S, Normand B, De Los Rios P 2004. Kosmotropes and chaotropes: modelling preferential exclusion, binding and aggregate stability. *Biophysical chemistry* 112(1):45-57.
55. Arakawa T, Prestrelski SJ, Kenney WC, Carpenter JF 2001. Factors affecting short-term and long-term stabilities of proteins. *Adv Drug Del Rev* 46(1):307-326.
56. Roettger BF, Myers JA, Ladisch MR, Regnier FE 1989. Adsorption phenomena in hydrophobic interaction chromatography. *Biotechnol Prog* 5(3):79-88.

57. Perkins TW, Mak DS, Root TW, Lightfoot EN 1997. Protein retention in hydrophobic interaction chromatography: modeling variation with buffer ionic strength and column hydrophobicity. *J Chromatogr* 766(1):1-14.
58. Li Y, Roberts CJ 2009. Lumry– Eyring nucleated-polymerization model of protein aggregation kinetics. 2. Competing growth via condensation and chain polymerization. *The Journal of Physical Chemistry B* 113(19):7020-7032.
59. Bajaj H, Sharma VK, Badkar A, Zeng D, Nema S, Kalonia DS 2006. Protein structural conformation and not second virial coefficient relates to long-term irreversible aggregation of a monoclonal antibody and ovalbumin in solution. *Pharmaceutical research* 23(6):1382-1394.
60. Sahin E, Grillo AO, Perkins MD, Roberts CJ 2010. Comparative effects of pH and ionic strength on protein–protein interactions, unfolding, and aggregation for IgG1 antibodies. *Journal of pharmaceutical sciences* 99(12):4830-4848.
61. Mehta SB, Bee JS, Randolph TW, Carpenter JF 2014. Partial unfolding of a monoclonal antibody: role of a single domain in driving protein aggregation. *Biochemistry* 53(20):3367-3377.
62. Sanchez-Ruiz JM 1992. Theoretical analysis of Lumry-Eyring models in differential scanning calorimetry. *Biophysical Journal* 61(4):921.
63. Mozziconacci O, Arora J, Toth IV RT, Joshi SB, Zhou S, Volkin DB, Schoneich C 2016. Site-Specific Hydrolysis Reaction C-Terminal of Methionine in Met-His during Metal-Catalyzed Oxidation of IgG-1. *Molecular pharmaceuticals* 13(4):1317-1328.
64. Banks DD, Latypov RF, Ketchem RR, Woodard J, Scavezze JL, Siska CC, Razinkov VI 2012. Native-state solubility and transfer free energy as predictive tools for selecting excipients to include in protein formulation development studies. *Journal of pharmaceutical sciences* 101(8):2720-2732.

65. Banks DD, Zhang J, Siska CC 2014. Relationship between native-state solubility and non-native aggregation of recombinant human granulocyte colony stimulating factor: Practical implications for protein therapeutic development. *Molecular pharmaceutics* 11(10):3431-3442.
66. Bee JS, Davis M, Freund E, Carpenter JF, Randolph TW 2010. Aggregation of a monoclonal antibody induced by adsorption to stainless steel. *Biotechnology and bioengineering* 105(1):121-129.
67. Bee JS, Schwartz DK, Trabelsi S, Freund E, Stevenson JL, Carpenter JF, Randolph TW 2012. Production of particles of therapeutic proteins at the air–water interface during compression/dilation cycles. *Soft Matter* 8(40):10329-10335.
68. Bee JS, Chiu D, Sawicki S, Stevenson JL, Chatterjee K, Freund E, Carpenter JF, Randolph TW 2009. Monoclonal antibody interactions with micro-and nanoparticles: Adsorption, aggregation, and accelerated stress studies. *Journal of pharmaceutical sciences* 98(9):3218-3238.
69. Gerhardt A, Bonam K, Bee JS, Carpenter JF, Randolph TW 2013. Ionic strength affects tertiary structure and aggregation propensity of a monoclonal antibody adsorbed to silicone oil–water interfaces. *Journal of pharmaceutical sciences* 102(2):429-440.
70. Mehta SB, Lewus R, Bee JS, Randolph TW, Carpenter JF 2015. Gelation of a monoclonal antibody at the silicone oil–water interface and subsequent rupture of the interfacial gel results in aggregation and particle formation. *Journal of pharmaceutical sciences* 104(4):1282-1290.
71. Roberts CJ 2014. Therapeutic protein aggregation: mechanisms, design, and control. *Trends in biotechnology* 32(7):372-380.
72. Weiss A, Schlessinger J 1998. Switching signals on or off by receptor dimerization. *Cell* 94(3):277-280.
73. McNally F 2000. Capturing a ring of samurai. *Nat Cell Biol* 2(1):E4-E7.

74. Bouvier M 2001. Oligomerization of G-protein-coupled transmitter receptors. *Nature Reviews Neuroscience* 2(4):274-286.
75. Marianayagam NJ, Sunde M, Matthews JM 2004. The power of two: protein dimerization in biology. *Trends in biochemical sciences* 29(11):618-625.
76. Esfandiary R, Hayes DB, Parupudi A, Casas-Finet J, Bai S, Samra HS, Shah AU, Sathish HA 2013. A systematic multitechnique approach for detection and characterization of reversible self-association during formulation development of therapeutic antibodies. *Journal of pharmaceutical sciences* 102(9):3089-3099.
77. Sukumar M, Doyle BL, Combs JL, Pekar AH 2004. Opalescent appearance of an IgG1 antibody at high concentrations and its relationship to noncovalent association. *Pharmaceutical research* 21(7):1087-1093.
78. Yadav S, Laue TM, Kalonia DS, Singh SN, Shire SJ 2012. The influence of charge distribution on self-association and viscosity behavior of monoclonal antibody solutions. *Molecular pharmaceutics* 9(4):791-802.
79. Yadav S, Shire SJ, Kalonia DS 2010. Factors affecting the viscosity in high concentration solutions of different monoclonal antibodies. *Journal of pharmaceutical sciences* 99(12):4812-4829.
80. Connolly BD, Petry C, Yadav S, Demeule B, Ciaccio N, Moore JM, Shire SJ, Gokarn YR 2012. Weak interactions govern the viscosity of concentrated antibody solutions: high-throughput analysis using the diffusion interaction parameter. *Biophysical journal* 103(1):69-78.
81. Lilyestrom WG, Yadav S, Shire SJ, Scherer TM 2013. Monoclonal antibody self-association, cluster formation, and rheology at high concentrations. *The Journal of Physical Chemistry B* 117(21):6373-6384.

82. Sharma VK, Bajaj H, Kalonia DS 2010. Reversible self-association of pharmaceutical proteins: characterization and case studies. *Formulation and Process Development Strategies for Manufacturing Biopharmaceuticals*:429.
83. Romberg L, Simon M, Erickson HP 2001. Polymerization of ftsz, a bacterial homolog of tubulin is assembly cooperative? *Journal of Biological Chemistry* 276(15):11743-11753.
84. Kameyama K, Minton AP 2006. Rapid quantitative characterization of protein interactions by composition gradient static light scattering. *Biophysical journal* 90(6):2164-2169.
85. Melki R, Carlier MF 1993. Thermodynamics of tubulin polymerization into zinc sheets: assembly is not regulated by GTP hydrolysis. *Biochemistry* 32(13):3405-3413.
86. Mehl J, Oncley J, Simha R 1940. Viscosity and the shape of protein molecules. *Science (New York, NY)* 92(2380):132-133.
87. Graessley WW. 1974. The entanglement concept in polymer rheology. *The Entanglement Concept in Polymer Rheology*, ed., Berlin, Heidelberg: Springer Berlin Heidelberg. p 1-179.
88. Buscall R, Goodwin JW, Hawkins MW, Ottewill RH 1982. Viscoelastic properties of concentrated latices. Part 1.—Methods of examination. *Journal of the Chemical Society, Faraday Transactions 1: Physical Chemistry in Condensed Phases* 78(10):2873-2887.
89. Benjamins J, van Voorst Vader F 1992. The determination of the surface shear properties of adsorbed protein layers. *Colloids and surfaces* 65(2):161-174.
90. Esfandiary R, Parupudi A, Casas-Finet J, Gadre D, Sathish H 2015. Mechanism of Reversible Self-Association of a Monoclonal Antibody: Role of Electrostatic and Hydrophobic Interactions. *Journal of pharmaceutical sciences* 104(2):577-586.
91. Li L, Kumar S, Buck PM, Burns C, Lavoie J, Singh SK, Warne NW, Nichols P, Luksha N, Boardman D 2014. Concentration dependent viscosity of monoclonal antibody solutions:

explaining experimental behavior in terms of molecular properties. *Pharmaceutical research* 31(11):3161-3178.

92. Clodfelter DK, Pekar AH, Rebhun DM, Destrampe KA, Havel HA, Myers SR, Brader ML 1998. Effects of non-covalent self-association on the subcutaneous absorption of a therapeutic peptide. *Pharmaceutical research* 15(2):254-262.

93. Mason BD, Zhang L, Remmele RL, Zhang J 2011. Opalescence of an IgG2 monoclonal antibody solution as it relates to liquid–liquid phase separation. *Journal of pharmaceutical sciences* 100(11):4587-4596.

94. Geoghegan JC, Fleming R, Damschroder M, Bishop SM, Sathish HA, Esfandiary R 2016. Mitigation of reversible self-association and viscosity in a human IgG1 monoclonal antibody by rational, structure-guided Fv engineering. *mAbs*:00-00.

95. Geng SB, Cheung JK, Narasimhan C, Shameem M, Tessier PM 2014. Improving monoclonal antibody selection and engineering using measurements of colloidal protein interactions. *Journal of pharmaceutical sciences* 103(11):3356-3363.

96. Some D 2013. Light-scattering-based analysis of biomolecular interactions. *Biophysical reviews* 5(2):147-158.

97. Bloomfield VA 2000. Static and dynamic light scattering from aggregating particles. *Biopolymers* 54(3):168-172.

98. Salinas BA, Sathish HA, Bishop SM, Harn N, Carpenter JF, Randolph TW 2010. Understanding and modulating opalescence and viscosity in a monoclonal antibody formulation. *Journal of pharmaceutical sciences* 99(1):82-93.

99. Lehermayr C, Mahler HC, Mäder K, Fischer S 2011. Assessment of net charge and protein–protein interactions of different monoclonal antibodies. *Journal of pharmaceutical sciences* 100(7):2551-2562.
100. Saito S, Hasegawa J, Kobayashi N, Kishi N, Uchiyama S, Fukui K 2012. Behavior of monoclonal antibodies: relation between the second virial coefficient (B_2) at low concentrations and aggregation propensity and viscosity at high concentrations. *Pharmaceutical research* 29(2):397-410.
101. Asthagiri D, Paliwal A, Abras D, Lenhoff A, Paulaitis M 2005. A consistent experimental and modeling approach to light-scattering studies of protein-protein interactions in solution. *Biophysical journal* 88(5):3300-3309.
102. Wyatt PJ 1993. Light scattering and the absolute characterization of macromolecules. *Anal Chim Acta* 272(1):1-40.
103. Blanco MA, Sahin E, Li Y, Roberts CJ 2011. Reexamining protein–protein and protein–solvent interactions from Kirkwood-Buff analysis of light scattering in multi-component solutions. *The Journal of chemical physics* 134(22):225103.
104. Blanco MA, Perevozchikova T, Martorana V, Manno M, Roberts CJ 2014. Protein–protein interactions in dilute to concentrated solutions: α -chymotrypsinogen in acidic conditions. *The Journal of Physical Chemistry B* 118(22):5817-5831.
105. Barnett GV, Razinkov VI, Kerwin BA, Laue TM, Woodka AH, Butler PD, Perevozchikova T, Roberts CJ 2015. Specific-ion effects on the aggregation mechanisms and protein–protein interactions for anti-streptavidin immunoglobulin gamma-1. *The Journal of Physical Chemistry B* 119(18):5793-5804.

106. Attri AK, Minton AP 2005. Composition gradient static light scattering: A new technique for rapid detection and quantitative characterization of reversible macromolecular hetero-associations in solution. *Analytical Biochemistry* 346(1):132-138.
107. Saluja A, Badkar AV, Zeng DL, Kalonia DS 2007. Ultrasonic rheology of a monoclonal antibody (IgG2) solution: implications for physical stability of proteins in high concentration formulations. *Journal of pharmaceutical sciences* 96(12):3181-3195.
108. Alford JR, Kendrick BS, Carpenter JF, Randolph TW 2008. High concentration formulations of recombinant human interleukin-1 receptor antagonist: II. aggregation kinetics. *Journal of pharmaceutical sciences* 97(8):3005-3021.
109. Eric D. 1992. *An Introduction to Food Colloids*. ed.: Oxford University Press: Oxford, UK.
110. Lebowitz J, Lewis MS, Schuck P 2002. Modern analytical ultracentrifugation in protein science: a tutorial review. *Protein Science* 11(9):2067-2079.
111. Laue T, Stafford III W 1999. Modern applications of analytical ultracentrifugation. *Annu Rev Biophys Biomol Struct* 28(1):75-100.
112. Carpenter JF, Randolph TW, Jiskoot W, Crommelin DJ, Middaugh CR, Winter G 2010. Potential inaccurate quantitation and sizing of protein aggregates by size exclusion chromatography: essential need to use orthogonal methods to assure the quality of therapeutic protein products. *Journal of pharmaceutical sciences* 99(5):2200-2208.
113. Sule SV, Dickinson CD, Lu J, Chow C-K, Tessier PM 2013. Rapid analysis of antibody self-association in complex mixtures using immunogold conjugates. *Molecular pharmaceutics* 10(4):1322-1331.
114. Liu Y, Caffry I, Wu J, Geng SB, Jain T, Sun T, Reid F, Cao Y, Estep P, Yu Y. *MAbs*, 2014, pp 483-492.

115. Jensen PF, Rand KD 2016. Hydrogen Exchange: A Sensitive Analytical Window into Protein Conformation and Dynamics. *Hydrogen Exchange Mass Spectrometry of Proteins: Fundamentals, Methods, and Applications*: p 1-15..
116. Henzler-Wildman K, Kern D 2007. Dynamic personalities of proteins. *Nature* 450(7172):964-972.
117. Panjwani N, Hodgson DJ, Sauvé S, Aubin Y 2010. Assessment of the effects of pH, formulation and deformulation on the conformation of interferon alpha-2 by NMR. *Journal of pharmaceutical sciences* 99(8):3334-3342.
118. Fávero-Retto MP, Palmieri LC, Souza TA, Almeida FC, Lima LMT 2013. Structural meta-analysis of regular human insulin in pharmaceutical formulations. *European Journal of Pharmaceutics and Biopharmaceutics* 85(3):1112-1121.
119. Norrman M, Schluckebier G 2007. Crystallographic characterization of two novel crystal forms of human insulin induced by chaotropic agents and a shift in pH. *BMC Struct Biol* 7(1):1.
120. Amezcua CA, Szabo CM 2013. Assessment of higher order structure comparability in therapeutic proteins using nuclear magnetic resonance spectroscopy. *Journal of pharmaceutical sciences* 102(6):1724-1733.
121. Hvidt A, Linderstrøm-Lang K 1954. Exchange of hydrogen atoms in insulin with deuterium atoms in aqueous solutions. *Biochimica et biophysica acta* 14:574-575.
122. Englander SW, Kallenbach NR 1983. Hydrogen exchange and structural dynamics of proteins and nucleic acids. *Quarterly reviews of biophysics* 16(04):521-655.
123. Skinner JJ, Lim WK, Bédard S, Black BE, Englander SW 2012. Protein dynamics viewed by hydrogen exchange. *Protein Science* 21(7):996-1005.

124. Skinner JJ, Lim WK, Bédard S, Black BE, Englander SW 2012. Protein hydrogen exchange: Testing current models. *Protein Science* 21(7):987-995.
125. Bai Y, Milne JS, Mayne L, Englander SW 1993. Primary structure effects on peptide group hydrogen exchange. *Proteins: Structure, Function, and Bioinformatics* 17(1):75-86.
126. Chalmers MJ, Busby SA, Pascal BD, He Y, Hendrickson CL, Marshall AG, Griffin PR 2006. Probing protein ligand interactions by automated hydrogen/deuterium exchange mass spectrometry. *Analytical chemistry* 78(4):1005-1014.
127. Majumdar R, Middaugh CR, Weis DD, Volkin DB 2015. Hydrogen–deuterium exchange mass spectrometry as an emerging analytical tool for stabilization and formulation development of therapeutic monoclonal antibodies. *Journal of pharmaceutical sciences* 104(2):327-345.
128. Gregory RB, Crabo L, Percy AJ, Rosenberg A 1983. Water catalysis of peptide hydrogen isotope exchange. *Biochemistry* 22(4):910-917.
129. Tokuriki N, Tawfik DS 2009. Protein dynamism and evolvability. *Science* 324(5924):203-207.
130. Bryan PN, Orban J 2010. Proteins that switch folds. *Curr Opin Struct Biol* 20(4):482-488.
131. Englander SW 2006. Hydrogen exchange and mass spectrometry: A historical perspective. *Journal of the American Society for Mass Spectrometry* 17(11):1481-1489.
132. Houde D, Berkowitz SA, Engen JR 2011. The utility of hydrogen/deuterium exchange mass spectrometry in biopharmaceutical comparability studies. *Journal of pharmaceutical sciences* 100(6):2071-2086.
133. Zhang J, Banks DD, He F, Treuheit MJ, Becker GW 2015. Effects of Sucrose and Benzyl Alcohol on GCSF Conformational Dynamics Revealed by Hydrogen Deuterium Exchange Mass Spectrometry. *Journal of pharmaceutical sciences* 104(5):1592-1600.

134. Zhang A, Singh SK, Shirts MR, Kumar S, Fernandez EJ 2012. Distinct aggregation mechanisms of monoclonal antibody under thermal and freeze-thaw stresses revealed by hydrogen exchange. *Pharmaceutical research* 29(1):236-250.
135. Houde D, Arndt J, Domeier W, Berkowitz S, Engen JR 2009. Characterization of IgG1 conformation and conformational dynamics by hydrogen/deuterium exchange mass spectrometry. *Analytical chemistry* 81(7):2644-2651.
136. Majumdar R, Manikwar P, Hickey JM, Arora J, Middaugh CR, Volkin DB, Weis DD 2012. Minimizing carry-over in an online pepsin digestion system used for the H/D exchange mass spectrometric analysis of an IgG1 monoclonal antibody. *Journal of the American Society for Mass Spectrometry* 23(12):2140-2148.
137. Majumdar R, Manikwar P, Hickey JM, Samra HS, Sathish HA, Bishop SM, Middaugh CR, Volkin DB, Weis DD 2013. Effects of salts from the Hofmeister series on the conformational stability, aggregation propensity, and local flexibility of an IgG1 monoclonal antibody. *Biochemistry* 52(19):3376-3389.
138. Manikwar P, Majumdar R, Hickey JM, Thakkar SV, Samra HS, Sathish HA, Bishop SM, Middaugh CR, Weis DD, Volkin DB 2013. Correlating excipient effects on conformational and storage stability of an IgG1 monoclonal antibody with local dynamics as measured by hydrogen/deuterium-exchange mass spectrometry. *Journal of pharmaceutical sciences* 102(7):2136-2151.

Chapter 2

Correlating the effects of antimicrobial preservatives on conformational stability, aggregation propensity and local flexibility of an IgG1 monoclonal antibody

2.1 Introduction

Multi-dose formulations constitute approximately one-third of all parenteral formulations¹. Multi-dose formulations offer multiple advantages over single use formulations, including: (1) product wastage is minimized, since different sized doses can be drawn overtime from the same container, (2) product efficacy and safety is maintained in an opened container over a longer period of time due to inhibition of microbial growth, and (3) product packaging is minimized which is beneficial from economic and patient compliance perspective¹. One challenge in the development of multi-dose injectable formulations is to inhibit microbial growth unintentionally introduced into the containers during multiple drawings. For this reason, antimicrobial preservatives (APs) are added to multi-dose formulations to inhibit microbial growth during storage and administration². Despite the benefit that APs offer, they have been shown to cause physical instability when added to formulations of protein-based drugs via protein structural alterations and aggregation³⁻⁷. Heljo et al linked peptide-preservative interactions to a decrease in the antimicrobial efficacy of APs and an increase in peptide self-interactions. Using NMR, they determined that the extent to which phenolic APs bind/interact to the peptides follows the order of their cLogP (calculated value of the octanol-water partition coefficient) values (more hydrophobic APs bound more strongly showed greater binding)⁸. To better understand how APs interact with, and potentially destabilize, more complex proteins such as mAbs, we have examined the effects of four different commonly-used pharmaceutical phenolic APs, m-cresol, phenol, phenoxyethanol and benzyl alcohol, with different hydrophobicities on an immunoglobulin G1 (IgG1) monoclonal antibody (mAb) as a model multi-domain therapeutic protein.

IgG1 mAbs are one the most important and successful classes of biotherapeutic agents. Due to their specificity, affinity and avidity, ~40 monoclonal antibodies have now been approved

by regulatory agencies and scores of mAbs are currently being researched for treatment of a wide spectrum of human diseases⁹. IgG1 antibodies are multi-domain, glycosylated proteins containing four polypeptide chains (two heavy and two light chains) connected by inter and intramolecular disulfide bond linkages. The structure of IgG1 mAbs can further be classified into Fab (antigen binding fragment) and Fc (crystallizable fragment). These two fragments (Fab and Fc) contain constant (C_L and C_{H1}) and variable domains (V_L and V_H) in the Fab and constant domains in the Fc fragment (C_{H2} and C_{H3})¹⁰. The Fab and Fc fragments are joined by a proline-rich, unstructured and highly dynamic hinge^{11,12}. The hinge region imparts structural independence to the Fab and Fc fragments, enabling the antibody domains to exhibit a wide-range of global and local dynamical motions relative to each other¹³.

Similar to other protein-based therapeutics, antibodies are susceptible to structural destabilization and aggregation upon exposure to external environmental stresses during manufacturing, product storage, and administration^{9,14,15}. Covalent and non-covalent protein-protein interactions that lead to irreversible protein aggregation can be triggered by changes in solution conditions (e.g., pH and addition of cosolutes) or external stresses (e.g., agitation, temperature, freeze-thaw, interface exposure, etc.). Conformational integrity of protein molecules and colloidal stability of their interactions both can play a role in the protein aggregation potential of proteins. For example, antibodies can undergo significant conformation changes that cause hydrophobic patches from the core of the antibody structure to become solvent exposed. These surface exposed patches of hydrophobic residues can then initiate intermolecular contacts, or in contrast, the nature of charge-charge interactions can alter causing a decrease in antibody colloidal stability¹⁶. protein aggregation induced by Conformational perturbation occurs through generation of a partially unfolded conformer of the monomeric species¹⁶. The population of the partially

perturbed conformer dictates the extent of protein aggregation and subsequent generation of protein particles. Previous studies have emphasized the importance of the stability of the protein aggregation hotspots (aggregation-prone motifs) in governing protein aggregation and physical stability^{17,18}. Previously, we have highlighted the utility of studying changes in local flexibility of protein aggregation hotspots in response to external stresses and solution conditions using hydrogen exchange-mass spectrometry (HX-MS)^{19,20}. Developing a deeper understanding of protein aggregation pathways and particle formation is of great importance as protein aggregates can illicit unwanted immune responses in patients that may reduce the efficacy and safety of antibody therapy²¹.

Protein flexibility has a complex relationship with the overall physical stability of proteins, especially from a pharmaceutical point of view²². Lower-resolution biophysical techniques like red-edge excitation shift fluorescence and ultrasonic spectroscopy that measure global dynamics of proteins were used by Thakkar et al to imply a direct relationship between mAb global dynamics and physical stability²³. In the present study, in addition to developing a better understanding of how APs affect mAb conformational stability and aggregation profiles, we also expand on our previous research to draw correlations between mAb local backbone flexibility, conformational stability (DSC and extrinsic fluorescence) and aggregation propensity (SEC). Interestingly, the phenolic APs tested in this study affect local flexibility of the same protein aggregation hot-spot in the C_{H2} domain of this IgG1 mAb (mAb-4) that was strongly correlated with physical stability profiles of other mAbs^{19,20,24,25}. We also determined that the extent of change in the local flexibility of the C_{H2} protein aggregation hot-spot, conformational instability and increased aggregation propensity of mAb-4 correlate well with the hydrophobicity of the phenolic APs. based on the

calculated log of the octanol-water partition coefficient (cLogP, see Table 1), an established measure of its hydrophobicity. Higher values of cLogP indicate higher hydrophobicity.

2.2 Materials and Methods

2.2.1 Materials

A highly purified IgG1 monoclonal antibody, mAb-4, was obtained from Janssen Biotech Inc. (Horsham, PA) at a stock concentration of approximately 40 mg/mL. LC-MS grade water, 2-propanol, LC-MS grade water containing 0.1% formic acid, citric acid monohydrate, dibasic anhydrous sodium phosphate and sodium chloride were obtained from Fisher Scientific (Fair Lawn, NJ). Liquid chromatography grade acetic acid and phosphoric acid were obtained from Fluka (Saint Louis, MO). LC-MS grade acetonitrile containing 0.1% formic acid was purchased from Honeywell (Morristown, NJ). Porcine pepsin, tris (2-carboxyethyl) phosphine hydrochloride (TCEP), guanidine hydrochloride, deuterium oxide (99.9% D), m-cresol (99%), GC grade phenol ($\geq 99.5\%$), 2-phenoxyethanol ($\geq 99\%$) and benzyl alcohol ($\geq 99\%$) were purchased from Sigma-Aldrich (Saint Louis, MO)

2.2.2 Sample Preparation

All samples of mAb-4 were prepared by dialyzing the mAb stock solution against the indicated corresponding buffer using 3500 kDa molecular-weight cutoff membranes (Slide-A-Lyzer, Thermo Scientific, Rockford, IL) for 24 hours at 4°C.

2.2.3 Differential Scanning Calorimetry

Differential scanning calorimetry (DSC) thermograms were obtained on a Microcal VP-Capillary DSC with autosampler (MicroCal, Northampton, MA), over a temperature range of 10 - 90°C at a scan rate of 60°C/hour. All samples of mAb-4, at a concentration of 1 mg/mL, were prepared in 20 mM citrate-phosphate buffer (pH 6.0) containing 100 mM NaCl with or without 53 mM m-cresol, phenol, phenoxyethanol or benzyl alcohol (mAb-4 to AP ratio was kept at 1:8000, therefore, 53 mM AP was added to a solution of 1 mg/mL mAb-4). Thermograms of mAb-4 at a concentration of 1 mg/mL in the presence of 100 mM NaCl alone (control) or containing 53 mM APs were compared to the reference thermograms of corresponding buffers containing no protein. Data were analyzed using Origin 7.0 software package with MicroCal LLC DSC plug-in. Thermal melting (T_m) values were obtained by iteratively fitting the thermograms to a non-two-state model for unfolding. Onset temperature for unfolding (T_{onset}) values were determined using a procedure described by Manikwar et al ²⁰.

2.2.4 8-Anilino-1-Naphthalene Sulfonate (ANS) Extrinsic fluorescence

Unfolding of mAb-4 with increase in temperature in the presence of preservatives was also monitored by measuring fluorescence emission of 8-anilino-1-naphthalene sulfonate (ANS) using a QM-40 spectrofluorometer (Photon Technology International (PTI), Inc., Birmingham, NJ) equipped with a four position cell holder and Peltier temperature control device (Quantum Northwest). ANS was added to the protein solution at a 20-fold molar excess and excited at 375 nm. Excitation and emission slits were set at 4 nm. Emission spectra were collected from 400 to

600 nm (step size 1 nm) at an interval of 2.5°C, over a temperature range of 10-87.5°C. Emission peak intensity was monitored at 475 nm.

2.2.5 Accelerated Storage Stability Study

Samples of mAb-4 in 20 mM citrate-phosphate buffer (pH 6.0), containing 100 mM NaCl in the absence of preservatives (control), or containing 53 mM of m-cresol, phenol, phenoxyethanol or benzyl alcohol were prepared at a protein concentration of 1 mg/mL. These samples were sterile filtered through a 0.22 µm filter (Millipore, Billerica, MA) and 1 mL aliquots were dispensed into 2 mL borosilicate glass type I vials (West Pharmaceutical Services, Exton, PA). Vials containing mAb-4 samples were then stored in triplicate at 50°C for 2, 4, 14 and 28 days.

2.2.6 Size Exclusion High-Performance Liquid Chromatography

To analyze mAb-4 samples, a Shimadzu high performance liquid-chromatography system equipped with a photodiode array detector. A 7.8 mm × 30 cm Tosoh TSK-Gel BioAssist G3SW_{xL} (TOSOH Biosciences, King of Prussia, PA) and a corresponding guard column were preconditioned and calibrated using gel-filtration molecular weight standards (Bio-Rad, Hercules, CA). All samples of mAb-4 control and with preservatives, were centrifuged at 14000×g for 5 minutes to remove any insoluble aggregates. a mobile phase containing 0.2 M sodium phosphate, pH 6.8 at a flowrate of 0.7 mL min⁻¹ was used to separate mAb-4 species based on their hydrodynamic size. A dual wavelength quantification method described by Bond et al²⁶ was used to quantify the amounts of various species (soluble aggregates, monomer and fragments) of mAb-4. To quantify the amount of insoluble aggregates, the total area (sum of all SEC peaks) of mAb-

4 chromatogram at each time point was subtracted from its corresponding time zero sample. This difference was defined as the total amount of insoluble aggregates present in than sample. The percentage of insoluble aggregates, soluble aggregates and monomer loss in mAb-4 samples are reported as described in Manikwar et al²⁰.

2.2.7 Hydrogen Exchange-Mass Spectrometry

The stock solution of mAb-4 was diluted to a final concentration of 20 mg/mL using 20 mM citrate-phosphate buffer containing 100 mM NaCl at pH 6.0. For sample handling, preparation and injection an H/DX PAL robot (LEAP Technologies, Carrboro, NC) was used. To initiate the hydrogen exchange process, 2 μ L of protein stock (at 20 mg/mL) was diluted in a 1:20 ratio with 38 μ L of labelling buffers (20 mM citrate-phosphate containing 100 mM NaCl at pH 6.0) containing either no preservatives (control) or 53 mM of m-cresol, phenol, phenoxyethanol or benzyl alcohol prepared in deuterium oxide. Thereafter, the reaction mixture was incubated at 25°C for four exchange time-points, 30, 150, 1000 and 10000 seconds prepared in triplicate. Hydrogen exchange was quenched by 1:1 dilution with 0.2 M phosphate buffer at pH 2.5 containing 0.5 M TCEP and 4 M guanidine HCl in H₂O to stop the hydrogen exchange process. During the deuterium labeling and quenching steps, labeling buffers and quench buffer were maintained at 25°C and 1°C respectively using temperature controlled drawers of the H/DX PAL robot. Subsequent to the quench step, samples were loaded into the sample loop of the refrigerated column compartment containing connected to an Agilent 1260 infinity series LC (Agilent Technologies, Santa Clara, CA), an immobilized pepsin column, a peptide desalting trap and a C18 column. The temperature of the refrigerated LC compartment was maintained at 1°C to reduce the extent of back-exchange. Mobile phase A containing 0.1% formic acid was used to for protein

digestion and desalting. A combination of mobile phase A and mobile phase B (90% acetonitrile + 10% water and 0.1% formic acid) was used to elute the peptides^{19,27}. To minimize the carry-over of peptides from the previous runs, immobilized pepsin column was washed between each HX run using a procedure described previously^{22,27}. The level of deuteration in each peptide was measured using an Agilent 6530 quadrupole-time of flight mass spectrometer (Agilent Technologies, Santa Clara, CA), equipped with a standard electrospray ionization source operated in positive mode.

2.2.8 Mass Spectrometry data analysis

Accurate mass measurements in combination with collision induced dissociation with tandem MS on an Agilent 6530 quadrupole-time of flight mass spectrometer was used to identify mAb-4 peptides. A total of 140 unique mAb-4 peptides covering approximately 92% of the primary sequence were identified and utilized for subsequent hydrogen exchange (HX) analysis. HDExaminer 2.0 software package (Sierra Analytics, Modesto, CA) was used to analyze the HX data and an R-script developed in-house was used to generate deuterium uptake plots with average deuterium uptake values and standard deviations for triplicate HX runs for each peptide of mAb-4. To identify statistically significant differences between mAb-4 control sample (no preservatives) and samples containing preservatives, a 99% confidence interval value for the entire dataset was calculated and established as ± 0.18 Da using a method described by Houde et al²⁴. Differences in HX crossing the 99% confidence limit were deemed significant and were displayed on the homology model of mAb-4 based on crystal structure of an isolated Fc fragment²⁸ and the Fab fragment structure was adopted from an in-silico created KOL/Padlan structure²⁹.

2.3 Results

2.3.1 Antimicrobial preservatives decrease the thermal stability of mAb-4

A combination of differential scanning calorimetry (DSC) and extrinsic fluorescence spectroscopy was utilized to probe the effects of antimicrobial preservatives (APs) on the overall thermal stability of mAb-4. Four different APs commonly used as pharmaceutical agents were chosen in this study based on differences in their physical properties such as cLogP values (see Table 1). Figure 1a-d shows representative DSC thermograms of mAb-4 in the presence of each of the four APs while Table 2 summarizes the T_{onset} and the two T_m values from triplicate runs. Two distinct thermal unfolding events were observed in the thermograms of mAb-4 at pH 6.0. Based on previously reported DSC analyses with other of IgG1 mAbs,^{30,31} the first thermal transition likely represents unfolding of the C_{H2} and Fab domains (labeled T_{m1}/T_{m2}) while the second transition is the unfolding of Fc domain (labeled T_{m3}). Each of the APs destabilized mAb-4 indicated by decreases in the thermal transition values (T_{onset} and T_m) compared to the mAb in the absence of APs. Interestingly, the ranking of decreased thermal stability is the same as the ranking of cLogP, with the most hydrophobic AP causing the greatest destabilization as represented by ΔT_{onset} and ΔT_m values (Table 2).

To further assess the destabilizing effect of APs on mAb-4 conformational stability, extrinsic fluorescence spectroscopy experiments using ANS as an extrinsic probe were conducted. Figure 2 shows the change in ANS emission peak intensity (wavelength 475 nm) of mAb-4 samples with increasing temperature in the presence of the various APs tested. Onset temperature for unfolding of mAb-4 in the presence of APs was measured and compared to the control as shown in Table 3. The magnitude of destabilization of mAb-4 conformational integrity in the presence of the various APs followed the same trend seen in DSC experiments. In summary, both

DSC and extrinsic fluorescence spectroscopy analyses demonstrated that antimicrobial preservatives cause a decrease in mAb-4 overall conformational stability where the most hydrophobic AP caused the biggest destabilization followed by APs with decreasing cLogP values (table 2 and 3).

2.3.2 Antimicrobial preservatives decrease the stability of mAb-4 under accelerated conditions

To assess the effect of APs on accelerated storage stability profiles, mAb-4 samples were stored at 50°C for up to 28 days. Size exclusion chromatography (SEC) was utilized to compare the monomer, aggregate and fragment content in mAb-4 samples in the presence of selected APs compared to the control (no preservatives) at day zero and over time. Overlaid SEC chromatographic profiles of these samples are shown in dotted lines in Supplemental Figure S1. No noticeable change was observed between chromatographic profiles of mAb-4 samples at time zero. Supplemental Figure S1 also shows overlaid chromatographic profiles of mAb-4 samples with preservatives after 28 days of storage at 50°C in which significant increases in the peak areas of multimeric protein complexes and fragments (solid lines, peak assignments based on comparison to molecular weight standards) were observed. The effects of the preservatives on mAb-4 stability in terms of percent loss in monomer content and percent increase in soluble and insoluble aggregates during accelerated storage are summarized in Figure 3 (monomer loss in Fig 3A, and increase in soluble aggregates and insoluble aggregates in Figs 3B and Fig3C, respectively). Samples of mAb-4 containing APs showed elevated soluble (dimers and multimers) and insoluble aggregates at during storage at 50°C. Moreover, as shown in Figure 3D, m-cresol caused largest increase in total aggregates after 28 days (14.5%) followed by the addition of phenol

(9%), phenoxyethanol (5.5%) and benzyl alcohol (4.3%). In summary, the trend in the increase in aggregation propensity of mAb-4 in the presence of APs follows the rank order of AP hydrophobicity, where the most hydrophobic AP caused the greatest increase in mAb-4 aggregation.

2.3.3 Backbone flexibility of mAb-4 in control buffer (No Preservatives)

Interrelationship between intrinsic protein dynamics and aggregation propensity has been a continuous topic of interest^{32,33}. Here, hydrogen exchange mass spectrometry was utilized to measure relative backbone flexibility of mAb-4 in control buffer conditions (20 mM citrate-phosphate, 100 mM NaCl, pH 6.0). A total of 140 mAb-4 peptides covering 90% of the primary sequence were identified. Deuterium uptake at 30 seconds for all mAb-4 peptides in the presence of 100 mM NaCl was measured and used to calculate percent flexibility as described by Majumdar et al¹⁹ using equation 1:

$$\text{Flexibility (\%)} = \frac{\Delta m_{30s}}{Nf} \times 100\% \quad (1)$$

where Δm_{30s} denotes the mass increase after 30 seconds of exchange, N is the number of exchangeable backbone protons conditions (all non-proline residues starting from position 3 of every peptide segment³⁴) and f denotes the mole fraction of deuterium available for exchange under chosen labeling ($f = 0.99$). The distribution of percent flexibility for every mAb-4 segment is given in Supplemental Figure S2A. Peptide segments of mAb-4 that are in the lowest quartile of flexibility are classified as rigid, while the peptides in the top quartile are classified as flexible and segments in the middle 50% as intermediate. Regions where overlapping peptides showed conflicting results, flexible or rigid categories took priority over intermediate category and rigid

category took priority over flexible category. Figure S2B shows the flexibility categories mapped onto a homology model of mAb-4 (Supplemental Figure S2B). Several surface exposed secondary structural elements within mAb-4 (loops and β -strands in the Fab and CH₃ domains), were highly flexible (colored in yellow) while most of CH₂ domain and buried β -strands and loops in other domains of mAb-4 had lower flexibility (lowest quartile, colored in blue). No apparent correlation between mAb-4 flexibilities and segment-averaged B factor values obtained from the crystal structure of the antibody for peptides with identical sequences from the constant domains of the two mAbs (data not shown)²⁸. The effect of APs on the relative local flexibility these domain regions in mAb-4 are addressed in the following section.

2.3.4 Antimicrobial preservatives affect the local backbone flexibility of mAb-4

To measure the effect of antimicrobial preservatives on mAb-4 local backbone flexibility, mAb samples were labeled by hydrogen exchange in deuterated solutions containing 20 mM citrate phosphate buffer (pH 6.0) containing 100 mM NaCl and 53 mM of each antimicrobial preservatives, m-cresol, phenol, phenoxyethanol and benzyl alcohol at 25°C. To identify localized effects of APs on mAb-4's backbone flexibility, hydrogen exchange profiles of each of the 140 peptide segments from mAb-4 was measured for up to 10000 seconds) in the presence of each of the APs and compared to the mAb-4 control (no APs). Figure 4 shows hydrogen exchange kinetics of six representative peptides from mAb-4 for the antibody in control buffer and in the presence of each of the four APs. Local flexibility of several regions within mAb-4 did not change upon addition of APs, while for other for other regions changed significantly (99% confidence interval, 0.18 Da). For example, local flexibility of peptide region HC 237-254 in the CH₂ domain of the antibody increased upon addition of all APs tested (two representative peptides from this region

shown in Figure 4), and these trends in the increase in local flexibility of this peptide segment, primarily at 1000 and 10000 seconds, correlates with the decrease in mAb-4 conformational stability and protein aggregation induced by APs described above.

Difference plots for all the 140 peptides within mAb-4 present a global comparison of their deuterium uptake values between mAb-4 in control buffer containing APs vs. mAb-4 in the control buffer alone (Figure 5). Relative mass differences (Δm , equation 2) for mAb-4 peptides are plotted on the vertical axis and peptide number is plotted on the horizontal of the plot.

$$\Delta m = m_{\text{AP}} - m_{\text{control}} \quad (2)$$

A positive value for Δm signifies an increase in the HX rate of the mAb segment in the presence of APs implying an increase in flexibility while a negative value indicates that the rate of HX is slower implying that APs decrease the flexibility of that peptide segment.

A nearly global increase in mAb-4 backbone flexibility was observed in the presence of APs (majority of individual changes were not significant at the 99% confidence limit of the dataset). The values for backbone flexibility for peptide segments were added together and subtracted from the control (no AP) to get a value for global flexibility change (Δm_{global} , table 4). Increase in global flexibility in the presence of APs followed their hydrophobicity rank order, where the most hydrophobic AP (m-cresol) showed the biggest increase in global flexibility. Local flexibility of peptides covering HC 182-254 (peptides 42 to 57) spanning parts of both CH1 and CH2 domains of mAb-4 increased significantly at 150 second time-point upon addition of m-cresol and phenol. Although this increase was significant, its magnitude of increase over the significance limit was small. For the later time points, 1000 and 10000 seconds, local flexibility of peptides covering segment HC 237-254 (peptides 50 to 57) increased significantly upon addition of all APs,

however, the magnitude of this increase was much greater in comparison to 150 second time-point and also correlated with physical stability measurements. Backbone flexibility of overlapping peptides covering LC 183-215 (peptides 131 to 140) significantly increased (150, 1000 and 10000 second time-points) upon addition of phenoxyethanol and benzyl alcohol and to a lesser extent in m-cresol and phenol, however, no direct correlation was apparent between flexibility increase in this segment and mAb-4 physical stability trends.

Not all peptides became more flexible in the presence of APs. Segment HC 50-59 (peptide 12) in the V_H domain became significantly more rigid in the presence of m-cresol and phenoxyethanol at 10000 second time-point. Backbone flexibility of HC 147-160 (C_{H1} domain, peptide 32) significantly decreased at 150 and 1000 second time-points upon addition of phenol. All the significant changes in local backbone flexibility (increases or decreases) observed above were mapped onto the homology model of mAb-4 (Figure 6). Regions (peptide segments) with increased or decreased local flexibility are colored in magenta and blue, respectively. In addition, peptide region HC 237-254 (peptides 50 to 57) in the C_{H2} domain of the antibody, where strong correlations between changes in local flexibility and mAb-4 physical stability were observed, is colored yellow in Figure 6 and labelled as the “primary effect”.

2.4 Discussion

Antimicrobial preservatives are used in multi-dose parenteral formulations to inhibit and prevent inadvertent microbial growth during repeated drawing of drug dosage over time^{1,35}. In addition to APs desirable inhibitory effect on microbial growth, however, APs have been shown to decrease physical stability and promote protein aggregation^{4,36,37}. In the present work we use an

IgG1 monoclonal antibody to elucidate mechanistic insights into the destabilizing effects of four phenolic APs commonly used in pharmaceutical formulations. HX-MS is utilized to probe the effect of APs on the local flexibility of various peptide segments across the twelve Ig domains of the IgG1 mAb, and the findings are examined in comparison to the conformational stability and accelerated storage stability of the antibody in the presence of APs. This result demonstrates correlations between high resolution HX-MS characterization of mAb local flexibility in the presence of destabilizing APs and protein conformational stability/aggregation propensity. Several studies have identified such correlations between the local flexibility of C_{H2} domain peptide segments covering the region HC 237-254 and changes in the conformational stability and aggregation propensity of antibodies^{19,20,25,38,39}. The present study provides additional data in support of HX-MS as a useful analytical tool for reliable monitoring of altered HX of aggregation hot-spots in the presence excipients thus, can be utilized for formulation development of mAbs.

Four APs that are commonly used in multi-dose formulations of protein therapeutics were chosen for this study, m-cresol, phenol, phenoxyethanol and benzyl alcohol. These APs are phenolic compounds and span a wide range of hydrophobicity (cLogP). The decrease in mAb conformational stability and increase in its aggregation propensity in the presence of APs followed their hydrophobicity rank ordering (table 1). The most hydrophobic AP of the four, m-cresol, caused the biggest conformational destabilization (measured by DSC and extrinsic fluorescence) and increase in aggregation propensity/kinetics (measured by SEC), followed by phenol, then phenoxyethanol and the least destabilizing benzyl alcohol (rank ordered in table 2 and 3). Several studies probed the effect of phenolic APs on smaller proteins and had similar observations. Maa and Hsu tested the effects of several phenolic APs (including m-cresol, phenol and benzyl alcohol) on physical stability and aggregation propensity of human growth hormone. They found that

among the three overlapping APs tested, m-cresol was the most destabilizing followed by phenol and then the least destabilizing, benzyl alcohol³⁶. Gupta and Kaisheva probed the effect of these APs on aggregation propensity of an antibody under isothermal incubation conditions, they reached similar conclusions where more hydrophobic APs, m-cresol followed by phenol caused more aggregation when compared to less hydrophobic benzyl alcohol³. Decrease in conformational stability and increase in aggregation propensity of interleukin-1 receptor in the presence m-cresol, phenol and benzyl alcohol also correlated with their hydrophobicity rank ordering⁴⁰. Heljo et al extended this research to peptides and probed the effect of APs on peptide stability, reaching the same conclusion where more hydrophobic m-cresol caused greater peptide destabilization followed by phenol which was followed by benzyl alcohol⁸. However, in another study, Bis et al and Hutchings et al probed the effect of phenolic APs on the physical stability and aggregation propensity of cytochrome c and interferon- α -2a. For both of these proteins, they demonstrated that although m-cresol was the most destabilizing AP followed by phenol, benzyl alcohol caused more protein aggregation than phenoxyethanol^{2,37}. This behavior is opposite to what we have reported in this study: phenoxyethanol is more destabilizing than benzyl alcohol for mAb-4 which can be attributed to the differences in the proteins and/or possibly solution conditions.

Hydrogen exchange mass spectrometry was used in this study to probe the effects of the four phenolic APs on the local flexibility of mAb-4. HX-MS provides an excellent opportunity to examine changes in local flexibility of proteins upon changes in external environment or solution conditions. Correlation between changes in local flexibility in protein segments and global stability is of great interest to pharmaceutical scientists as it can shed light on to the mechanisms by which protein structure gets destabilized which eventually leads to protein aggregation. Two notable

effects were noted in this study in terms effects of phenolic APs on local flexibility of mAb-4. First, a nearly global increase in local flexibility was observed for mAb-4 peptides in the presence of all APs at 1000 and 10000 second time-point, although most of these differences were not statistically significant ($\Delta m < 0.18$ Da). This observation correlates very well with the DSC data (figure 1, table 2) that showed a decrease in all thermal transitions (T_{m1}/T_{m2} and T_{m3}) corresponding to C_{H2} , Fab and C_{H3} domains of mAb-4 in the presence of APs. Second, local flexibility of peptide segments in region HC 237-254 in the C_{H2} domain increased significantly upon addition of APs to mAb-4, and this increase was more pronounced than changes in local flexibility of other peptide segments. This trend follows the rank ordering of hydrophobicity values of the APs which correlates well with the trends observed for physical stability and aggregation propensity of mAb-4 in the presence of APs (table 2 and 3).

Phenolic compounds have been previously used as solution additives to screen various physical properties of solvents that affect protein stability^{41,42}. Addition of phenolic compounds can affect local hydrophobic contacts within the protein structure causing local unfolding/increased flexibility events as seen in the C_{H2} domain segment of mAb-4^{41,43}. Thirumangalathu et al hypothesized that phenolic compounds increase the amount of aggregation-prone protein molecules with partially perturbed tertiary structure/ increased local flexibility in solution thereby increasing the extent of overall non-native aggregation⁶. It has been found in previous studies that cosolvents that enhance the aggregation potential of proteins, do so by shifting the equilibrium towards the partially unfolded conformation of the protein structure. For example, aggregation potential of IgG light chain variable domains increase upon addition of Congo red that shifts the equilibrium towards the partially unfolded conformer of the protein⁴⁴. This behavior can potentially be explained by the Wyman Linkage function⁴⁵. According to this

mechanism, aggregation-inducing ligands such as phenolic APs stabilize the aggregation-prone partially unfolded form of the protein, thereby, stabilizing these species through hydrophobic interactions and pairwise π - π and cation- π interactions that result in increase in the amount of partially perturbed conformers⁵. The difference in destabilization potential of the APs tested can potentially be explained by the differences in the extent of stabilization of aggregation-prone partially unfolded conformers (i.e., the primary effect in the C_H2 domain) of mAb-4. This is further supported by both extrinsic fluorescence spectroscopy and HX-MS results. Lower onset temperature for tertiary structure unfolding measured by extrinsic fluorescence signifies loosely packed structure of mAb-4 in the presence of APs, where m-cresol being the most hydrophobic AP results in greater stabilization of partially perturbed conformers of mAb-4 followed by phenol, phenoxyethanol and benzyl alcohol.

Excellent correlation was observed between preservative-induced physical destabilization of mAb-4 and increase in local flexibility of HC 237-254 in the mAb C_H2 domain. Both of these observations further correlated with the rank ordering of APs based on their hydrophobicity values. Previous studies conducted in our laboratories examined the effect of stabilizing and destabilizing excipients (chaotropic and kosmotropic salts, arginine and sucrose) on mAb physical stability, aggregation propensity and local flexibility of a different IgG1 mAb. A substantial increase in flexibility of two regions in the C_H2 domain of the antibody was observed in the presence of arginine and chaotropic salts. This increase in local flexibility was then associated with decrease in conformational stability and increase in aggregation propensity of mAb in the presence of those cosolvents. No such effect was observed in the presence of sucrose and kosmotropic salts^{19,20}. In a follow up study, the authors probed the effect of distal, destabilizing mutations on the local flexibility of mAb domains. The same region in the C_H2 domain of the antibody showed significant

increase in local flexibility in destabilized mutant mAb molecule⁴⁶. Two other studies also reported this peptide segment in the C_{H2} domain of mAbs to be the least stable and most aggregation prone region of the protein^{25,47}. One study found this C_{H2} peptide segment (HC 243-247) to be more flexible in both oxidized and deglycosylated IgG molecules which also had lower physical stability²⁵. In the other study, insertion of an engineered disulfide bond in the same peptide segment of the C_{H2} domain increased the thermal stability of the isolated C_{H2} domain of an antibody by about 20°C⁴⁸. One of the two cysteines in the engineered antibody was inserted at (L242C), which lies in the same C_{H2} domain aggregation hot-spot peptide segment. Engineered disulfides have been known to decrease local flexibility of the molecules through direct and allosteric effects^{49,50}. All these studies together support the assertion that the changes in the local flexibility of peptide segment HC 237-254 in the C_{H2} domain of the IgG1 antibody strongly correlate with the changes in global physical stability and aggregation propensity of the same antibody molecule.

Peptide segment HC 237-254 in the CH₂ domain contains two phenylalanine residues and several aliphatic residues that pack next to the glycans⁵¹. Phenolic APs may have direct or allosteric interactions with the mAb structure which can cause an increase in the local flexibility of the hydrophobic aggregation “hot-spot” region. This increased local flexibility could further cause increase in surface exposure of apolar residues ultimately resulting in intermolecular interactions with neighboring antibody molecules and formation of seed nuclei for future aggregation^{52,53}. WaterLOGSY NMR and other binding studies between mAb and APs can help fully elucidating the actual mechanism of AP induced mAb destabilization (direct binding or indirect interactions). Such experiments are currently underway in our laboratories. The results in this study with a series of antimicrobial agents and an IgG1 mAb provide another example that demonstrates the utility of

HX-MS as an important analytical tool to identify stabilizing and destabilizing excipients for mAb formulation development.

2.5 References

1. Meyer BK, Ni A, Hu B, Shi L 2007. Antimicrobial preservative use in parenteral products: past and present. *Journal of pharmaceutical sciences* 96(12):3155-3167.
2. Bis RL, Mallela KM 2014. Antimicrobial preservatives induce aggregation of interferon alpha-2a: The order in which preservatives induce protein aggregation is independent of the protein. *Int J Pharm* 472(1):356-361.
3. Gupta S, Kaisheva E 2003. Development of a multidose formulation for a humanized monoclonal antibody using experimental design techniques. *AAPS PharmSci* 5(2):1-9.
4. Tobler SA, Holmes BW, Cromwell ME, Fernandez EJ 2004. Benzyl alcohol-induced destabilization of interferon- γ : A study by hydrogen-deuterium isotope exchange. *Journal of pharmaceutical sciences* 93(6):1605-1617.
5. Zhang Y, Roy S, Jones LS, Krishnan S, Kerwin BA, Chang BS, Manning MC, Randolph TW, Carpenter JF 2004. Mechanism for benzyl alcohol-induced aggregation of recombinant human interleukin-1 receptor antagonist in aqueous solution. *Journal of pharmaceutical sciences* 93(12):3076-3089.
6. Thirumangalathu R, Krishnan S, Brems DN, Randolph TW, Carpenter JF 2006. Effects of pH, temperature, and sucrose on benzyl alcohol-induced aggregation of recombinant human granulocyte colony stimulating factor. *Journal of pharmaceutical sciences* 95(7):1480-1497.
7. Singh SM, Cabello-Villegas J, Hutchings RL, Mallela KM 2010. Role of partial protein unfolding in alcohol-induced protein aggregation. *Proteins: Structure, Function, and Bioinformatics* 78(12):2625-2637.

8. Heljo P, Ross A, Zarraga I, Pappenberger A, Mahler H 2015. Interactions Between Peptide and Preservatives: Effects on Peptide Self-Interactions and Antimicrobial Efficiency In Aqueous Multi-Dose Formulations. *Pharmaceutical research* 32(10):3201-3212.
9. Wang W, Singh S, Zeng DL, King K, Nema S 2007. Antibody structure, instability, and formulation. *Journal of pharmaceutical sciences* 96(1):1-26.
10. Kuby J, Kindt TJ, Goldsby RA, Osborne BA. 2000. *Kuby immunology*. ed.: WH Freeman.
11. Kessler H, Mronga S, Müller G, Moroder L, Huber R 1991. Conformational analysis of a IgG1 hinge peptide derivative in solution determined by NMR spectroscopy and refined by restrained molecular dynamics simulations. *Biopolymers* 31(10):1189-1204.
12. Hanson DC, Yguerabide J, Schumaker VN 1981. Segmental flexibility of immunoglobulin G antibody molecules in solution: a new interpretation. *Biochemistry* 20(24):6842-6852.
13. Boehm MK, Woof JM, Kerr MA, Perkins SJ 1999. The Fab and Fc fragments of IgA1 exhibit a different arrangement from that in IgG: a study by X-ray and neutron solution scattering and homology modelling. *Journal of molecular biology* 286(5):1421-1447.
14. Amin S, Barnett GV, Pathak JA, Roberts CJ, Sarangapani PS 2014. Protein aggregation, particle formation, characterization & rheology. *Current Opinion in Colloid & Interface Science* 19(5):438-449.
15. Wang W, Roberts CJ 2013. Non-Arrhenius protein aggregation. *The AAPS journal* 15(3):840-851.
16. Roberts CJ, Das TK, Sahin E 2011. Predicting solution aggregation rates for therapeutic proteins: approaches and challenges. *Int J Pharm* 418(2):318-333.

17. Chennamsetty N, Helk B, Voynov V, Kayser V, Trout BL 2009. Aggregation-prone motifs in human immunoglobulin G. *Journal of molecular biology* 391(2):404-413.
18. Wang X, Das TK, Singh SK, Kumar S 2009. Potential aggregation prone regions in biotherapeutics. *mAbs* 1(3):254-267.
19. Majumdar R, Manikwar P, Hickey JM, Samra HS, Sathish HA, Bishop SM, Middaugh CR, Volkin DB, Weis DD 2013. Effects of salts from the Hofmeister series on the conformational stability, aggregation propensity, and local flexibility of an IgG1 monoclonal antibody. *Biochemistry* 52(19):3376-3389.
20. Manikwar P, Majumdar R, Hickey JM, Thakkar SV, Samra HS, Sathish HA, Bishop SM, Middaugh CR, Weis DD, Volkin DB 2013. Correlating excipient effects on conformational and storage stability of an IgG1 monoclonal antibody with local dynamics as measured by hydrogen/deuterium-exchange mass spectrometry. *Journal of pharmaceutical sciences* 102(7):2136-2151.
21. Rosenberg AS 2006. Effects of protein aggregates: an immunologic perspective. *The AAPS journal* 8(3):E501-E507.
22. Majumdar R, Manikwar P, Hickey JM, Arora J, Middaugh CR, Volkin DB, Weis DD 2012. Minimizing carry-over in an online pepsin digestion system used for the H/D exchange mass spectrometric analysis of an IgG1 monoclonal antibody. *Journal of the American Society for Mass Spectrometry* 23(12):2140-2148.
23. Thakkar SV, Joshi SB, Jones ME, Sathish HA, Bishop SM, Volkin DB, Middaugh CR 2012. Excipients differentially influence the conformational stability and pretransition dynamics of two IgG1 monoclonal antibodies. *Journal of pharmaceutical sciences* 101(9):3062-3077.

24. Houde D, Berkowitz SA, Engen JR 2011. The utility of hydrogen/deuterium exchange mass spectrometry in biopharmaceutical comparability studies. *Journal of pharmaceutical sciences* 100(6):2071-2086.
25. Houde D, Peng Y, Berkowitz SA, Engen JR 2010. Post-translational modifications differentially affect IgG1 conformation and receptor binding. *Molecular & Cellular Proteomics* 9(8):1716-1728.
26. Bond MD, Panek ME, Zhang Z, Wang D, Mehndiratta P, Zhao H, Gunton K, Ni A, Nedved ML, Burman S 2010. Evaluation of a dual-wavelength size exclusion HPLC method with improved sensitivity to detect protein aggregates and its use to better characterize degradation pathways of an IgG1 monoclonal antibody. *Journal of pharmaceutical sciences* 99(6):2582-2597.
27. Arora J, Hickey JM, Majumdar R, Esfandiary R, Bishop SM, Samra HS, Middaugh CR, Weis DD, Volkin DB 2015. Hydrogen exchange mass spectrometry reveals protein interfaces and distant dynamic coupling effects during the reversible self-association of an IgG1 monoclonal antibody. *mAbs* 7(3):525-539.
28. Matsumiya S, Yamaguchi Y, Saito J-i, Nagano M, Sasakawa H, Otaki S, Satoh M, Shitara K, Kato K 2007. Structural comparison of fucosylated and nonfucosylated Fc fragments of human immunoglobulin G1. *Journal of molecular biology* 368(3):767-779.
29. Padlan EA 1994. Anatomy of the antibody molecule. *Molecular immunology* 31(3):169-217.
30. Vermeer AW, Norde W 2000. The thermal stability of immunoglobulin: unfolding and aggregation of a multi-domain protein. *Biophysical journal* 78(1):394-404.

31. Vermeer AW, Norde W, van Amerongen A 2000. The Unfolding/Denaturation of Immunoglobulin of Isotype 2b and its F_{ab} and F_c Fragments. *Biophysical journal* 79(4):2150-2154.
32. Lebendiker M, Danieli T 2014. Production of prone-to-aggregate proteins. *FEBS Lett* 588(2):236-246.
33. Silva JL, Foguel D, Royer CA 2001. Pressure provides new insights into protein folding, dynamics and structure. *Trends in biochemical sciences* 26(10):612-618.
34. Bai Y, Milne JS, Mayne L, Englander SW 1993. Primary structure effects on peptide group hydrogen exchange. *Proteins: Structure, Function, and Bioinformatics* 17(1):75-86.
35. Akers MJ, Vasudevan V, Stickelmeyer M. 2002. Formulation development of protein dosage forms. *Development and manufacture of protein pharmaceuticals*, ed.: Springer. p 47-127.
36. Maa Y-F, Hsu CC 1996. Aggregation of recombinant human growth hormone induced by phenolic compounds. *Int J Pharm* 140(2):155-168.
37. Hutchings RL, M Singh S, Cabello-Villegas J, Mallela KM 2013. Effect of antimicrobial preservatives on partial protein unfolding and aggregation. *Journal of pharmaceutical sciences* 102(2):365-376.
38. Houde D, Arndt J, Domeier W, Berkowitz S, Engen JR 2009. Characterization of IgG1 conformation and conformational dynamics by hydrogen/deuterium exchange mass spectrometry. *Analytical chemistry* 81(7):2644-2651.

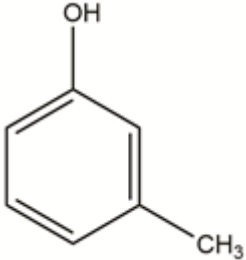
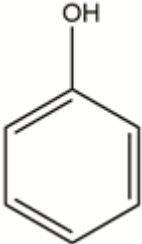
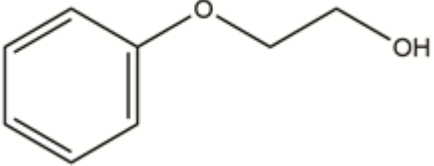
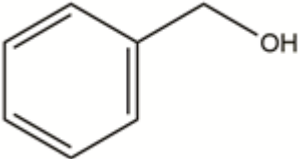
39. Burkitt W, Domann P, O'Connor G 2010. Conformational changes in oxidatively stressed monoclonal antibodies studied by hydrogen exchange mass spectrometry. *Protein Science* 19(4):826-835.
40. Remmele Jr RL, Nightlinger NS, Srinivasan S, Gombotz WR 1998. Interleukin-1 receptor (IL-1R) liquid formulation development using differential scanning calorimetry. *Pharmaceutical research* 15(2):200-208.
41. Thomas PD, Dill KA 1993. Local and nonlocal interactions in globular proteins and mechanisms of alcohol denaturation. *Protein Science* 2(12):2050-2065.
42. Buck M 1998. Trifluoroethanol and colleagues: cosolvents come of age. *Recent studies with peptides and proteins. Quarterly reviews of biophysics* 31(03):297-355.
43. Kamatari YO, Konno T, Kataoka M, Akasaka K 1996. The methanol-induced globular and expanded denatured states of cytochrome c: A study by CD fluorescence, NMR and small-angle X-ray scattering. *Journal of molecular biology* 259(3):512-523.
44. Kim Y-S, Randolph TW, Manning MC, Stevens FJ, Carpenter JF 2003. Congo red populates partially unfolded states of an amyloidogenic protein to enhance aggregation and amyloid fibril formation. *Journal of Biological Chemistry* 278(12):10842-10850.
45. Timasheff SN 1993. The control of protein stability and association by weak interactions with water: how do solvents affect these processes? *Annu Rev Biophys Biomol Struct* 22(1):67-97.

46. Majumdar R, Esfandiary R, Bishop SM, Samra HS, Middaugh CR, Volkin DB, Weis DD 2015. Correlations between changes in conformational dynamics and physical stability in a mutant IgG1 mAb engineered for extended serum half-life. *mAbs* 7(1):84-95.
47. Zhang J, Topp EM 2012. Protein G, protein A and protein A-derived peptides inhibit the agitation induced aggregation of IgG. *Molecular pharmaceuticals* 9(3):622-628.
48. Gong R, Vu BK, Feng Y, Prieto DA, Dyba MA, Walsh JD, Prabakaran P, Veenstra TD, Tarasov SG, Ishima R 2009. Engineered human antibody constant domains with increased stability. *Journal of Biological Chemistry* 284(21):14203-14210.
49. Gasymov OK, Abduragimov AR, Glasgow BJ 2011. The conserved disulfide bond of human tear lipocalin modulates conformation and lipid binding in a ligand selective manner. *Biochimica et Biophysica Acta (BBA)-Proteins and Proteomics* 1814(5):671-683.
50. Yu X-W, Tan N-J, Xiao R, Xu Y 2012. Engineering a disulfide bond in the lid hinge region of *Rhizopus chinensis* lipase: increased thermostability and altered acyl chain length specificity. *Plos one* 7(10):e46388.
51. Woof JM, Burton DR 2004. Human antibody–Fc receptor interactions illuminated by crystal structures. *Nature Reviews Immunology* 4(2):89-99.
52. Roberts CJ 2007. Non-native protein aggregation kinetics. *Biotechnology and bioengineering* 98(5):927-938.
53. Weiss WF, Young TM, Roberts CJ 2009. Principles, approaches, and challenges for predicting protein aggregation rates and shelf life. *Journal of pharmaceutical sciences* 98(4):1246-1277.

54. Kavan D, Man P 2011. MSTools—Web based application for visualization and presentation of HX-MS data. *International journal of mass spectrometry* 302(1):53-58.

2.6 Tables and Figures

Table 2.1

Name	Structure	cLogP (Hydrophobicity)
m-Cresol		1.98
Phenol		1.48
Phenoxyethanol		1.2
Benzyl Alcohol		1.05

Structure and clogP (calculated log of partition coefficient, a measure of hydrophobicity of a molecule) values of Antimicrobial Preservatives (APs) utilized in this study.

Table 2.2

T_m and T_{onset} for mAb4 in presence of different preservatives as measured by DSC

mAb-4 in 20 mM citrate-phosphate, 100 mM, NaCl, pH 6.0 containing	cLogP	T_{onset} (°C)		$T_{m1/2}$ (°C)		T_{m3} (°C)	
		Mean	ΔT_{onset}	Mean	$\Delta T_{m1/2}$	Mean	ΔT_{m3}
m-Cresol	1.98	52.6	-7.7	66.4	-5.6	78.1	-5.3
Phenol	1.48	55.7	-4.6	68.4	-3.5	79.8	-3.6
Phenoxyethanol	1.2	57.1	-3.3	68.4	-3.5	79.9	-3.5
Benzyl alcohol	1.05	57.6	-2.8	69.4	-2.5	80.8	-2.7
No Preservatives (Control)	-	60.3	-	71.9	-	83.4	-

n=3, Standard Deviation = $\geq 0.1, \leq 0.8$

Effects of antimicrobial preservatives on thermal melting temperature (T_m) and thermal onset temperature (T_{onset}) values for mAb-4 as measured by DSC. All mAb samples were prepared in 20 mM citrate-phosphate buffer (6.0) containing 100 mM NaCl with or without 53 mM APs. Range of standard deviation from three independent experimental runs is given at the bottom of the table.

Table 2.3

T_{onset} for mAb4 in presence of different preservatives as measured by DSC

mAb-4 in 20 mM citrate-phosphate, 100 mM, NaCl, pH 6.0 containing	cLogP	T_{onset} (°C)	
		Mean	ΔT_{m1}
m-Cresol	1.98	56.0	-7.9
Phenol	1.48	58.4	-5.5
Phenoxyethanol	1.2	59.8	-4.1
Benzyl alcohol	1.05	61.1	-2.8
No Preservatives (Control)	-	63.9	-

n=3, Standard Deviation = $\geq 0.1, \leq 0.4$

Thermal onset temperature (T_{onset}) values for mAb-4 unfolding in the presence of antimicrobial preservatives as measured by extrinsic fluorescence. All samples of mAb-4 were prepared in 20 mM citrate-phosphate buffer (pH 6.0) containing 100 mM NaCl with or without 53 mM APs. Standard deviation values from three independent measurements are given in the footnote of the table.

Table 2.4

Δm_{global} for mAb4 in presence of different preservatives as measured by HX-MS

mAb-4 in 20 mM citrate-phosphate, 100 mM, NaCl, pH 6.0 containing	LogP	Δm_{global}
m-Cresol	1.98	37.5
Phenol	1.48	33.2
Phenoxyethanol	1.2	27.9
Benzyl alcohol	1.05	19.7

n=3, Standard Deviation ≤ 0.7

Global flexibility change (Δm_{global}) of mAb-4 in the presence of APs as measured by HX-MS. All samples of mAb-4 were prepared in deuterated solution of 20 mM citrate-phosphate buffer (pH 6.0) containing 100 mM NaCl with or without 53 mM APs.

Table 2.S1

Peptide number	Peptide ID
1	Heavy 4-22 (VH)
2	Heavy 4-23 (VH)
3	Heavy 5-26 (VH)
4	Heavy 27-34 (VH)
5	Heavy 27-36 (VH)
6	Heavy 28-34 (VH)
7	Heavy 30-34 (VH)
8	Heavy 35-46 (VH)
9	Heavy 35-49 (VH)
10	Heavy 35-50 (VH)
11	Heavy 37-50 (VH)
12	Heavy 50-59 (VH)
13	Heavy 51-59 (VH)
14	Heavy 60-68 (VH)
15	Heavy 69-78 (VH)
16	Heavy 69-79 (VH)
17	Heavy 69-80 (VH)
18	Heavy 69-81 (VH)
19	Heavy 80-86 (VH)
20	Heavy 81-86 (VH)
21	Heavy 84-93 (VH)
22	Heavy 87-93 (VH)
23	Heavy 91-126 (VH)
24	Heavy 105-114 (VH)
25	Heavy 106-114 (VH)
26	Heavy 106-116 (VH)
27	Heavy 107-114 (VH)
28	Heavy 115-128 (VH)
29	Heavy 115-134 (VH)
30	Heavy 117-128 (VH)
31	Heavy 147-160 (CH1)
32	Heavy 147-176 (CH1)
33	Heavy 148-160 (CH1)
34	Heavy 148-176 (CH1)
35	Heavy 158-165 (CH1)
36	Heavy 158-176 (CH1)
37	Heavy 161-176 (CH1)
38	Heavy 165-176 (CH1)

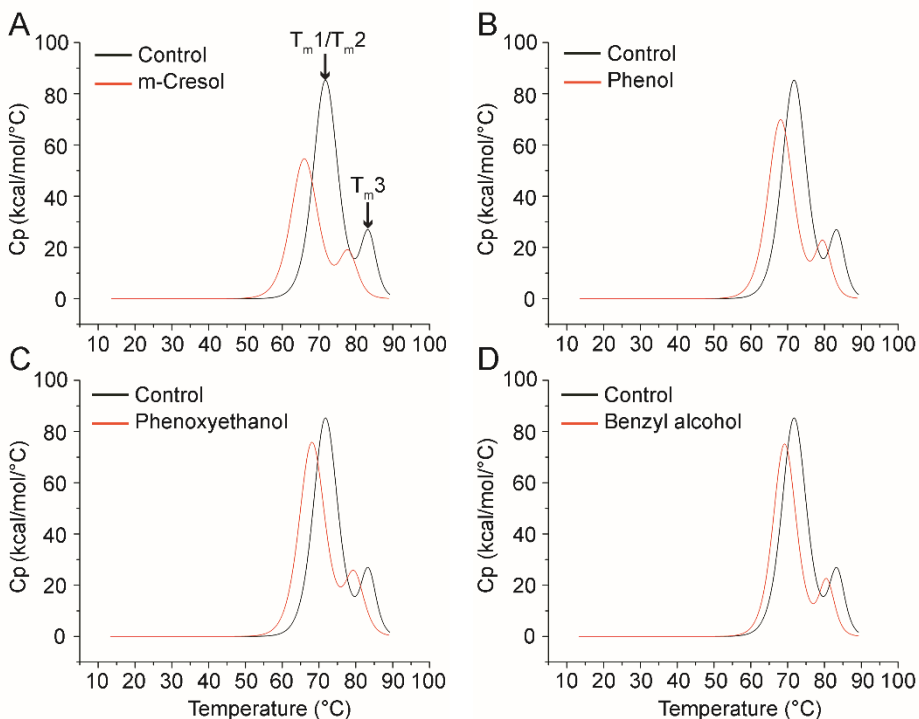
39	Heavy 166-176 (CH1)
40	Heavy 169-176 (CH1)
41	Heavy 170-176 (CH1)
42	Heavy 182-187 (CH1)
43	Heavy 182-199 (CH1)
44	Heavy 185-199 (CH1)
45	Heavy 186-199 (CH1)
46	Heavy 187-195 (CH1)
47	Heavy 187-199 (CH1)
48	Heavy 188-199 (CH1)
49	Heavy 207-234 (CH1)
50	Heavy 237-243 (CH2)
51	Heavy 237-253 (CH2)
52	Heavy 237-254 (CH2)
53	Heavy 243-253 (CH2)
54	Heavy 243-254 (CH2)
55	Heavy 244-253 (CH2)
56	Heavy 244-254 (CH2)
57	Heavy 255-263 (CH2)
58	Heavy 264-279 (CH2)
59	Heavy 265-279 (CH2)
60	Heavy 268-277 (CH2)
61	Heavy 268-279 (CH2)
62	Heavy 280-295 (CH2)
63	Heavy 302-308 (CH2)
64	Heavy 303-308 (CH2)
65	Heavy 309-315 (CH2)
66	Heavy 309-316 (CH2)
67	Heavy 309-320 (CH2)
68	Heavy 321-350 (CH2)
69	Heavy 328-335 (CH3)
70	Heavy 336-350 (CH3)
71	Heavy 338-350 (CH3)
72	Heavy 351-358 (CH3)
73	Heavy 351-360 (CH3)
74	Heavy 359-367 (CH3)
75	Heavy 361-367 (CH3)
76	Heavy 368-378 (CH3)
77	Heavy 371-378 (CH3)
78	Heavy 371-380 (CH3)
79	Heavy 371-381 (CH3)

80	Heavy 371-382 (CH3)
81	Heavy 379-392 (CH3)
82	Heavy 379-400 (CH3)
83	Heavy 381-400 (CH3)
84	Heavy 382-400 (CH3)
85	Heavy 383-392 (CH3)
86	Heavy 383-400 (CH3)
87	Heavy 392-400 (CH3)
88	Heavy 393-400 (CH3)
89	Heavy 394-400 (CH3)
90	Heavy 407-412 (CH3)
91	Heavy 408-412 (CH3)
92	Heavy 413-425 (CH3)
93	Heavy 429-448 (CH3)
94	Heavy 431-448 (CH3)
95	Heavy 433-448 (CH3)
96	Heavy 435-448 (CH3)
97	Heavy 435-449 (CH3)
98	Heavy 443-449 (CH3)
99	Light 1-10 (VL)
100	Light 5-10 (VL)
101	Light 12-19 (VL)
102	Light 12-21 (VL)
103	Light 19-30 (VL)
104	Light 32-46 (VL)
105	Light 33-46 (VL)
106	Light 33-48 (VL)
107	Light 36-46 (VL)
108	Light 47-53 (VL)
109	Light 47-70 (VL)
110	Light 47-71 (VL)
111	Light 54-62 (VL)
112	Light 54-70 (VL)
113	Light 71-82 (VL)
114	Light 71-83 (VL)
115	Light 75-82 (VL)
116	Light 83-92 (VL)
117	Light 97-104 (VL)
118	Light 117-123 (CL)
119	Light 117-126 (CL)
120	Light 117-132 (CL)

121	Light 118-123 (CL)
122	Light 118-126 (CL)
123	Light 118-131 (CL)
124	Light 118-133 (CL)
125	Light 127-144 (CL)
126	Light 137-144 (CL)
127	Light 145-149 (CL)
128	Light 154-162 (CL)
129	Light 156-173 (CL)
130	Light 161-173 (CL)
131	Light 163-173 (CL)
132	Light 163-174 (CL)
133	Light 163-176 (CL)
134	Light 163-180 (CL)
135	Light 163-182 (CL)
136	Light 174-182 (CL)
137	Light 181-193 (CL)
138	Light 183-196 (CL)
139	Light 197-207 (CL)
140	Light 197-215 (CL)

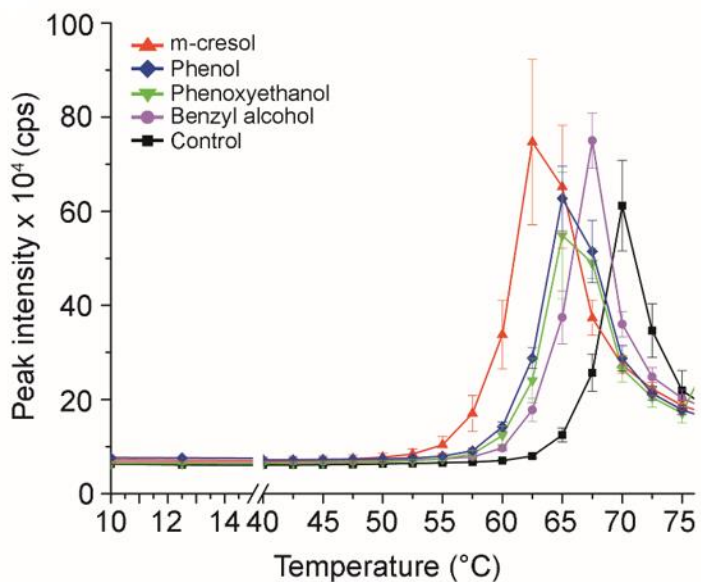
Peptic peptides of mAb-4 with their location on the primary structure and sequential peptide numbers used for HX-MS data analysis

Figure 2.1



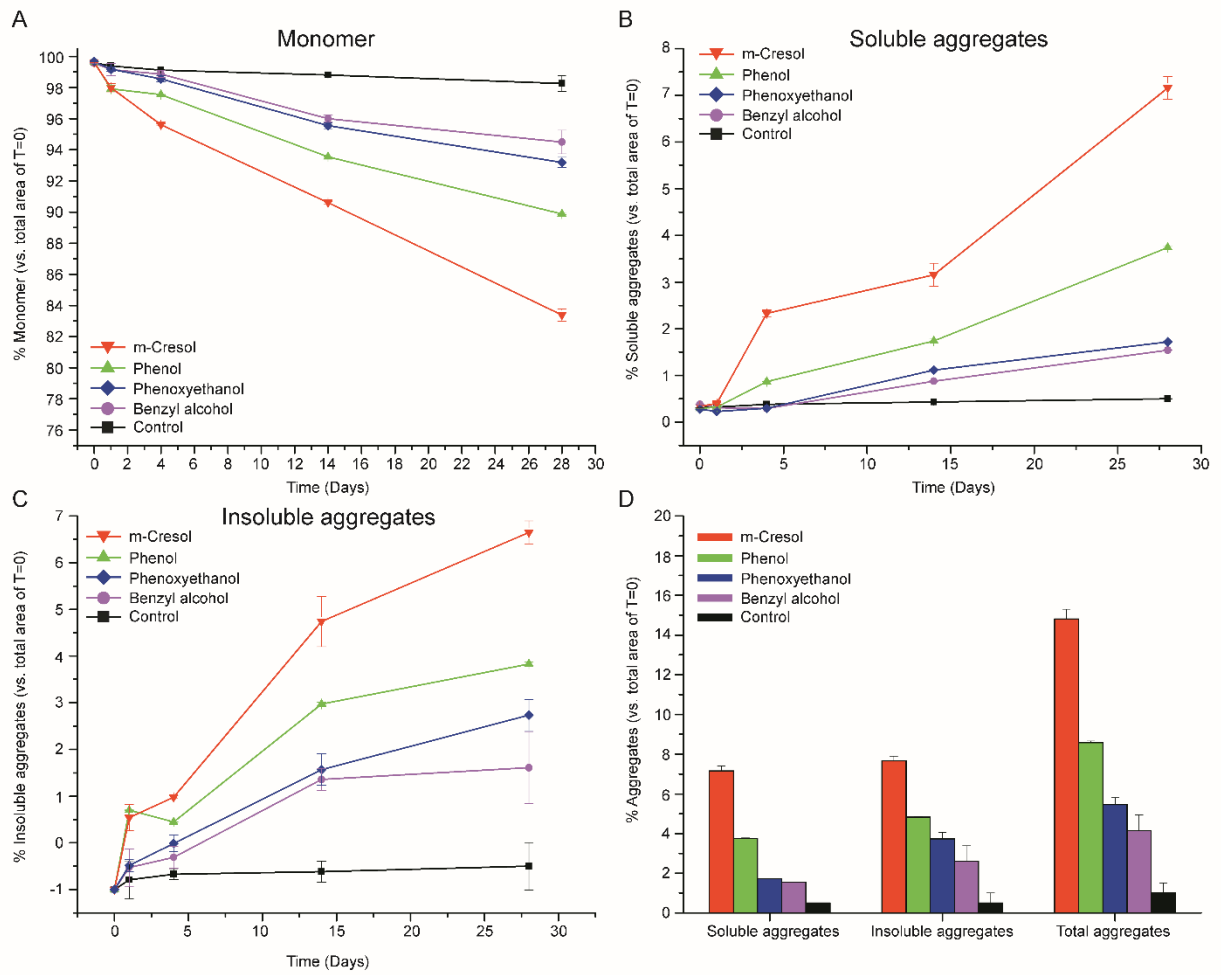
Representative DSC thermograms of mAb-4 in the presence and absence (control) of antimicrobial preservatives (APs). Samples contained 1 mg/mL protein in 20 mM citrate-phosphate buffer (pH 6.0) containing 100 mM NaCl with and without 53 mM of indicated antimicrobial preservative. Thermograms show the effect of buffer containing (A) m-Cresol, (B) Phenol, (C) Phenoxyethanol and (D) Benzyl alcohol vs. buffer alone (control) on conformational stability of mAb-4. Thermal melting temperature (T_m) and thermal onset temperature (T_{onset}) values from triplicate experiments are provided in Table 2.2

Figure 2.2



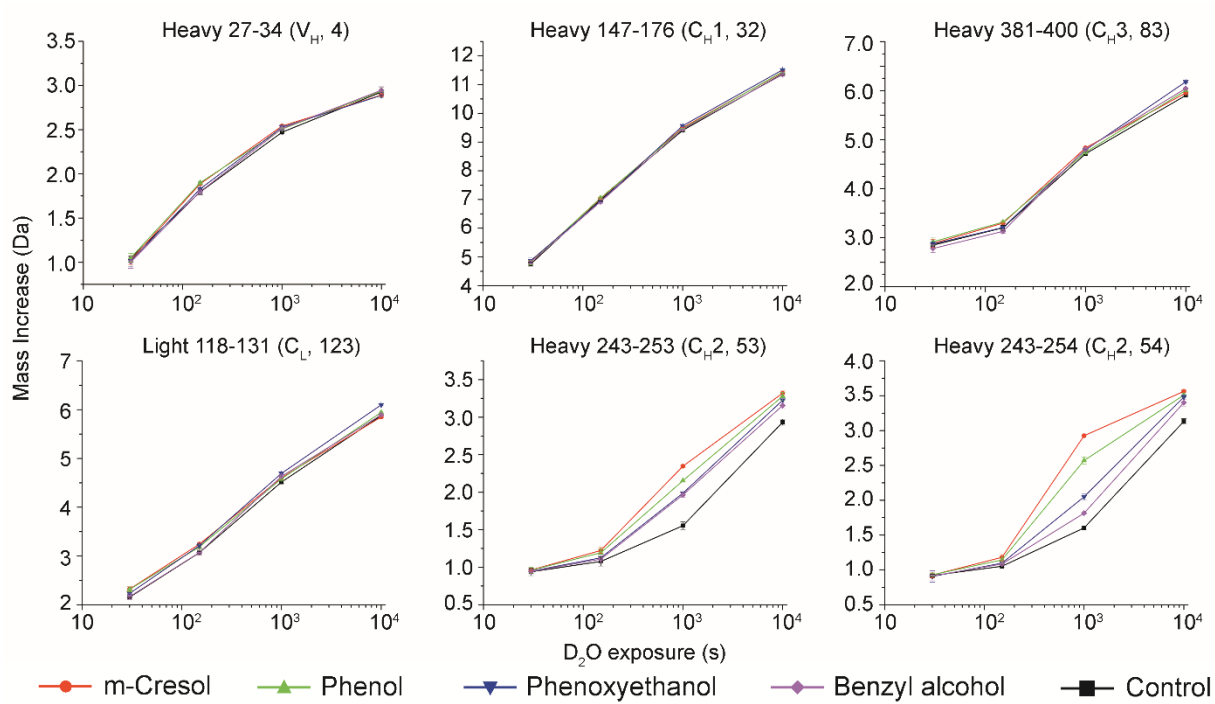
Extrinsic fluorescence spectroscopy analysis of mAb-4 conformational stability in the presence and absence (control) of antimicrobial preservatives. ANS extrinsic fluorescence temperature melts of mAb-4 in 20 mM citrate-phosphate buffer (pH 6.0) containing 100 mM NaCl with and without 53 mM of indicated antimicrobial preservative. Error bars represent one standard deviation from three independent measurements. Thermal onset temperature (T_{onset}) values from triplicate experiments are provided in Table 2.3

Figure 2.3



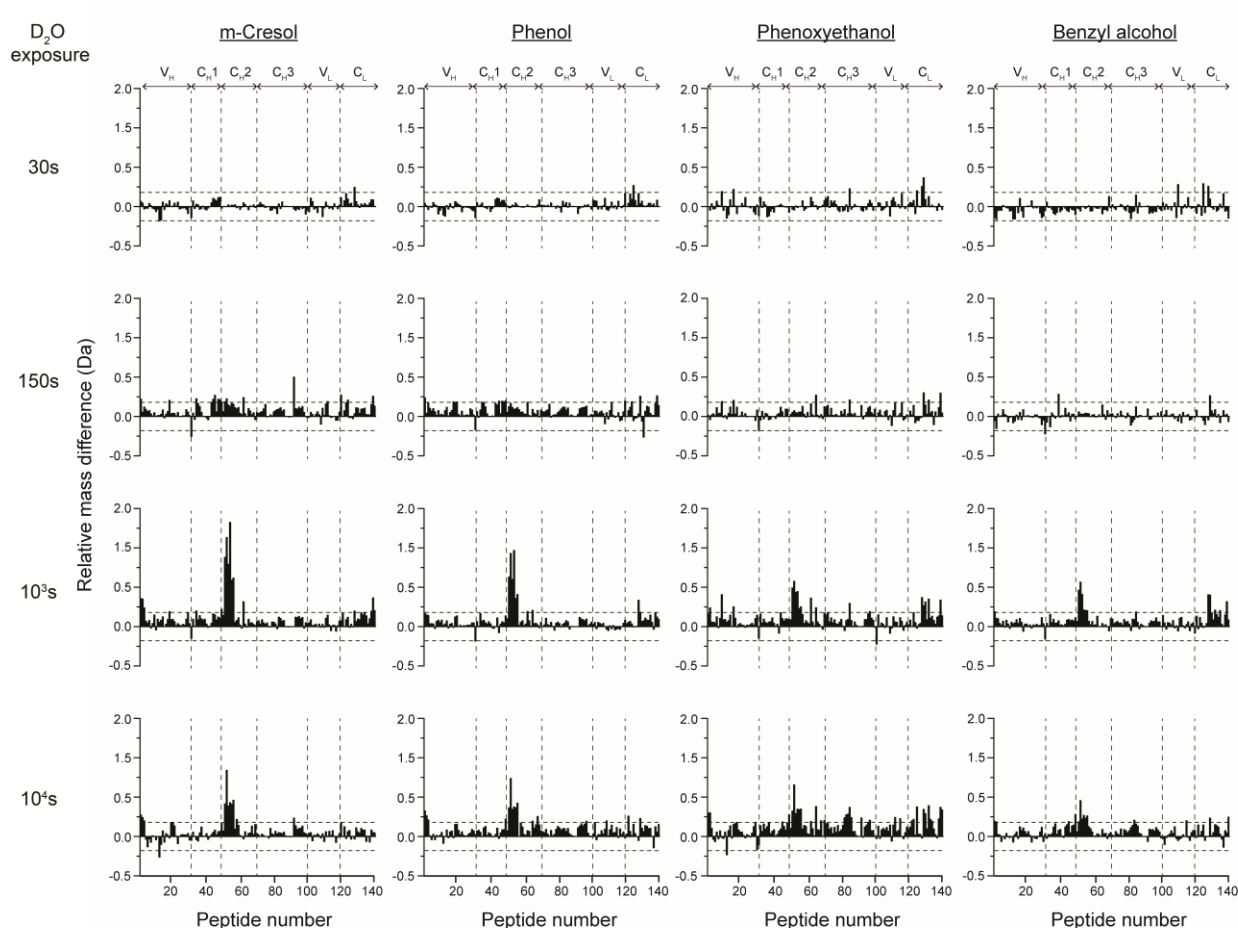
Time course of mAb-4 aggregation during storage at 50°C as monitored by SE-HPLC. Effect of different antimicrobial preservatives on mAb-4 is shown as (A) percent monomer loss, (B) increase in percent soluble aggregates, (C) increase in percent insoluble aggregates (loss of total area), and (D) total aggregates (soluble + insoluble). Samples are in 20 mM citrate-phosphate buffer (pH 6.0) containing 100 mM NaCl with and without 53 mM of indicated antimicrobial preservative. Error bars represent one standard deviation from three independent measurements.

Figure 2.4



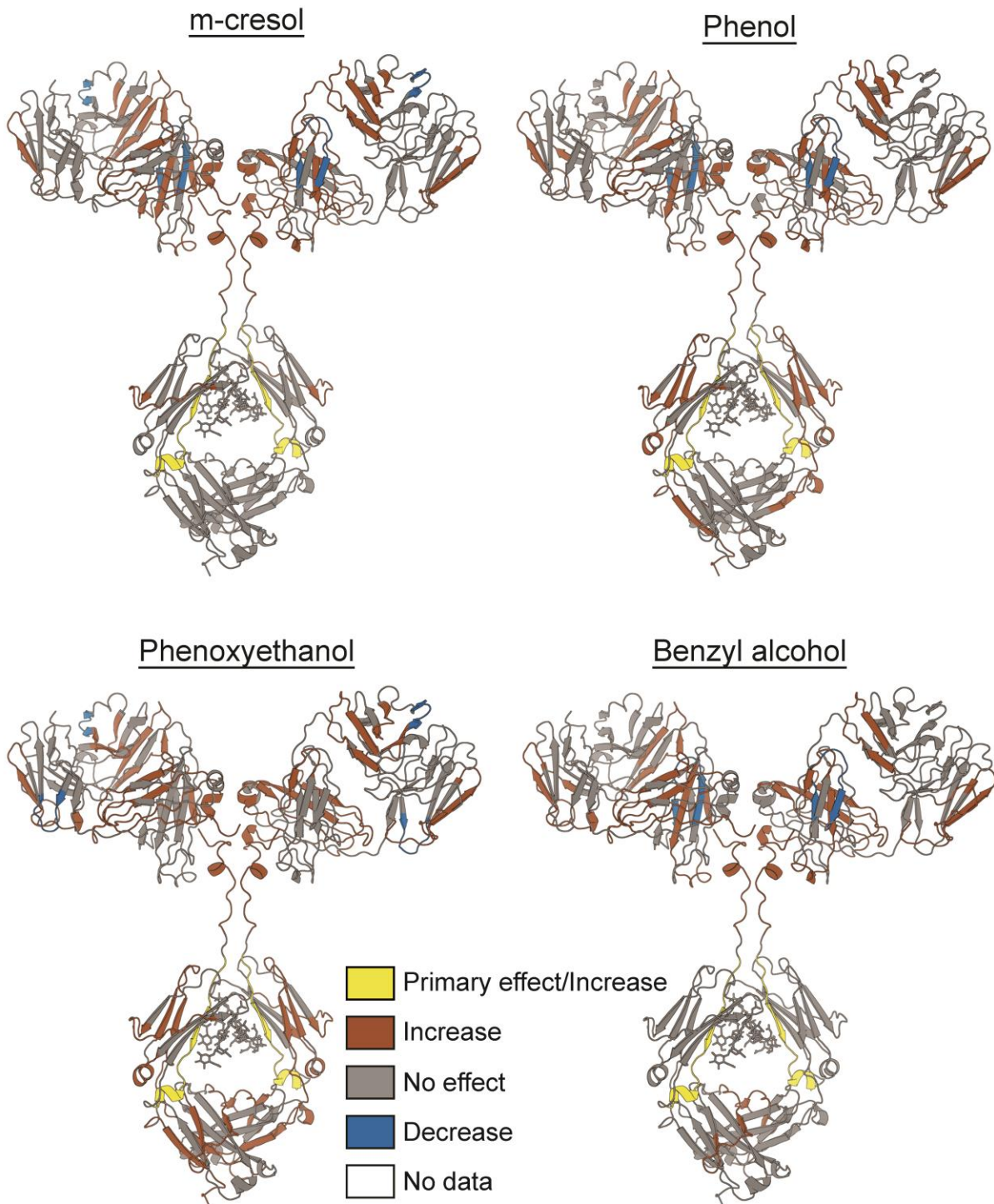
Effect of antimicrobial preservatives on the deuterium uptake kinetics of six representative peptide segments of mAb-4 as measured by HX-MS. Error bars denote one standard deviation from three independent measurements. Samples are in 20 mM citrate-phosphate buffer (pH 6.0) containing 100 mM NaCl with and without 53 mM of indicated antimicrobial preservative in D_2O .

Figure 2.5



Relative mass differences for all 140 peptide segments of mAb-4 in the presence of antimicrobial preservatives compared to the control (no preservatives) as measured by HX-MS. Dotted horizontal line represents 99% confidence limit for mass difference values for the whole dataset (± 0.18 Da). The horizontal axis denotes the ordinal peptide numbers, sorted in ascending order starting from the N-terminus of the heavy chain of the antibody. Positive bars represent increased local flexibility in the peptide segments in the presence of antimicrobial preservatives. Negative values represent peptides with decreased local flexibility. Location of individual peptide segments is shown on the top of the figure. Each value of relative mass difference is an average of three independent HX measurements for that particular peptide.

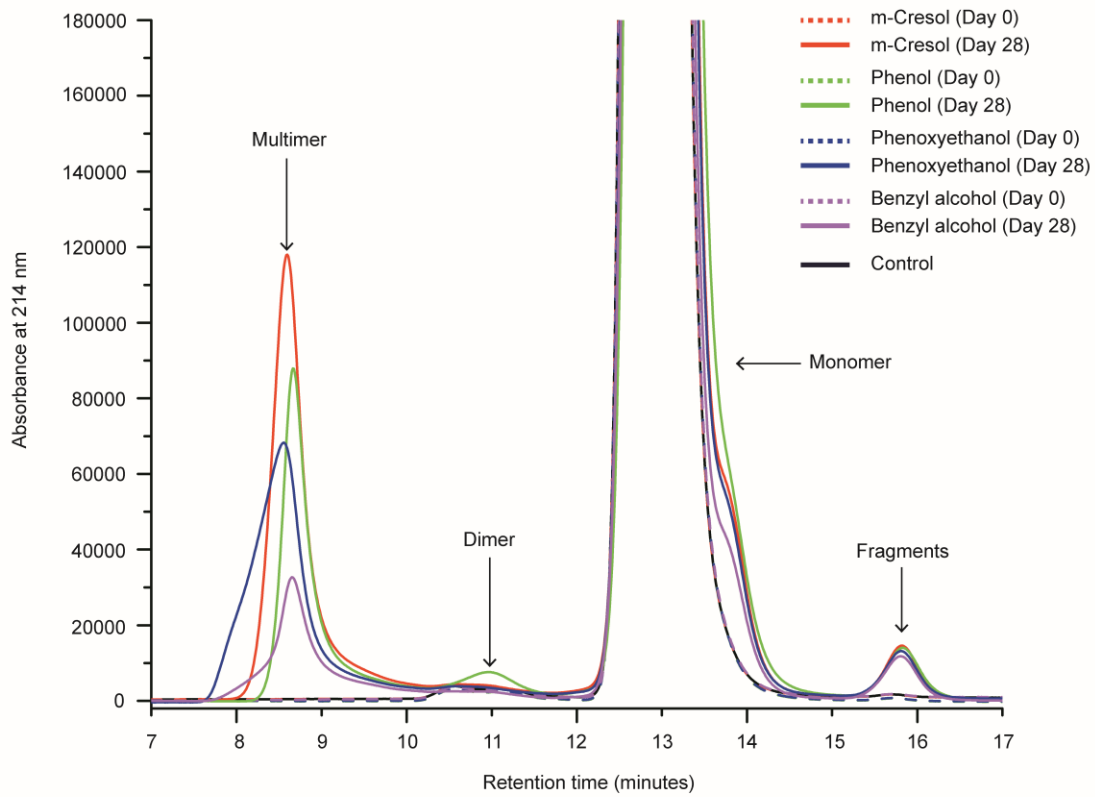
Figure 2.6



Homology model of mAb-4 representing the effects of antimicrobial preservatives on local flexibility of the antibody relative to the control (no preservatives), as measured by HX-MS. On

right. Changes in the backbone flexibility of peptide segments from the CH2 domain “aggregation hotspot” are labelled as “primary effect” of preservatives as they show excellent correlation between mAb-4 local flexibility.

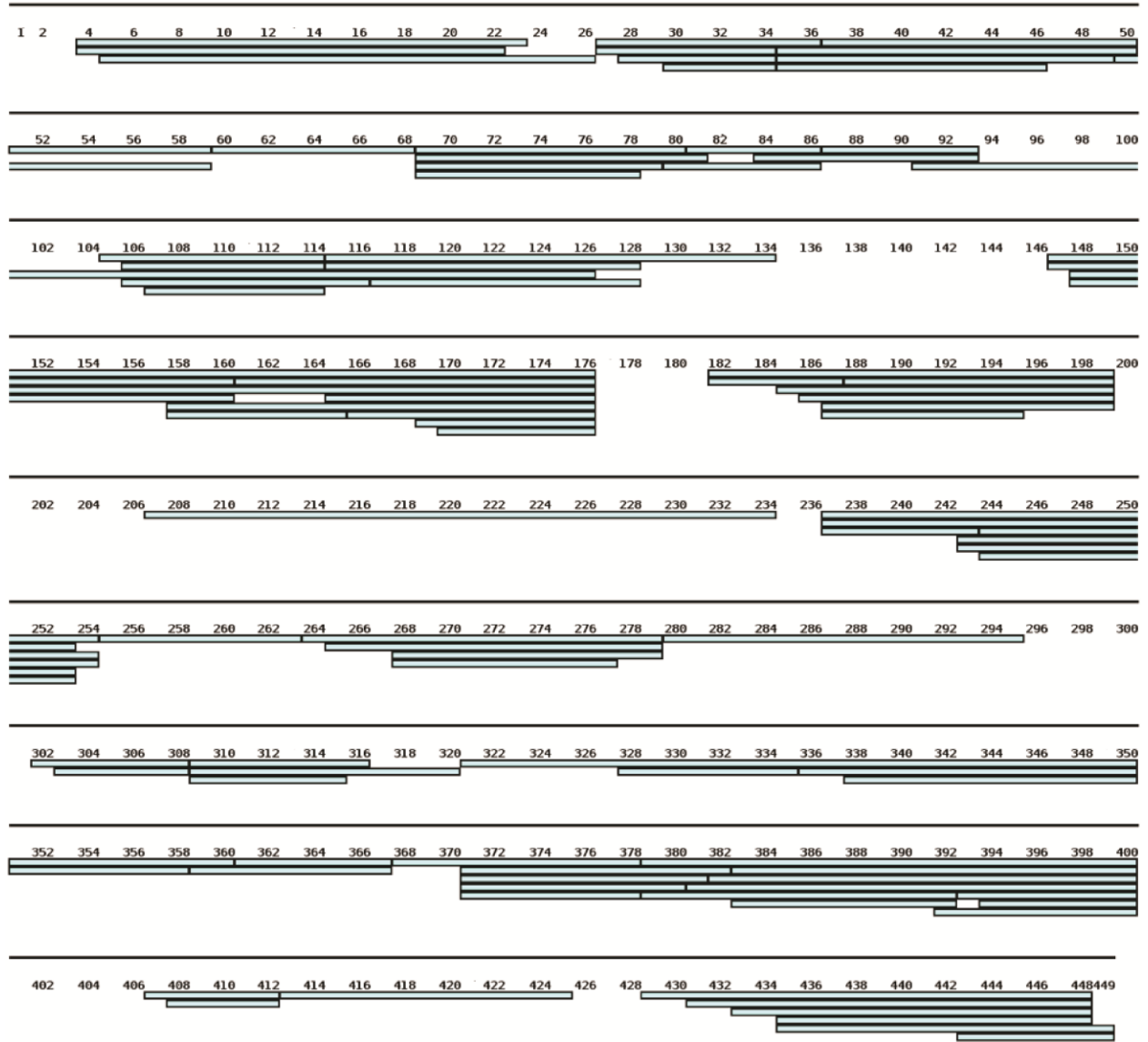
Figure 2.S1



Overlay of SEC chromatograms of mAb-4 comparing pre and post thermal stress. Dotted lines represent mAb-4 samples at day 0 and solid lines represent day 28 (stored at 50°C).

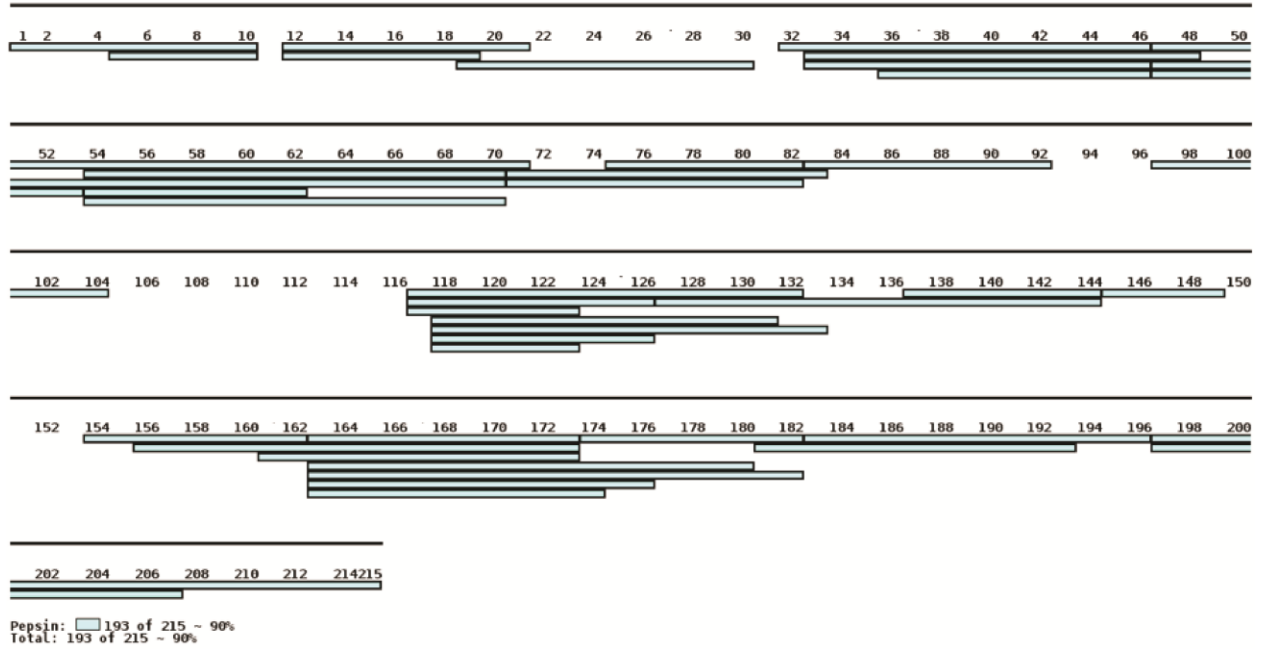
Figure 2.S2

A



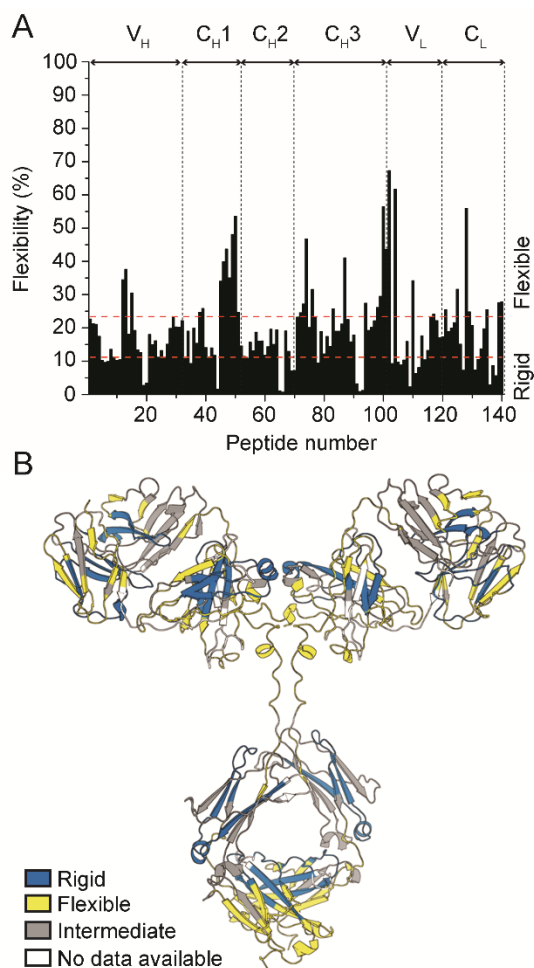
Pepsin: 405 of 449 ~ 90%
Total: 405 of 449 ~ 90%

B



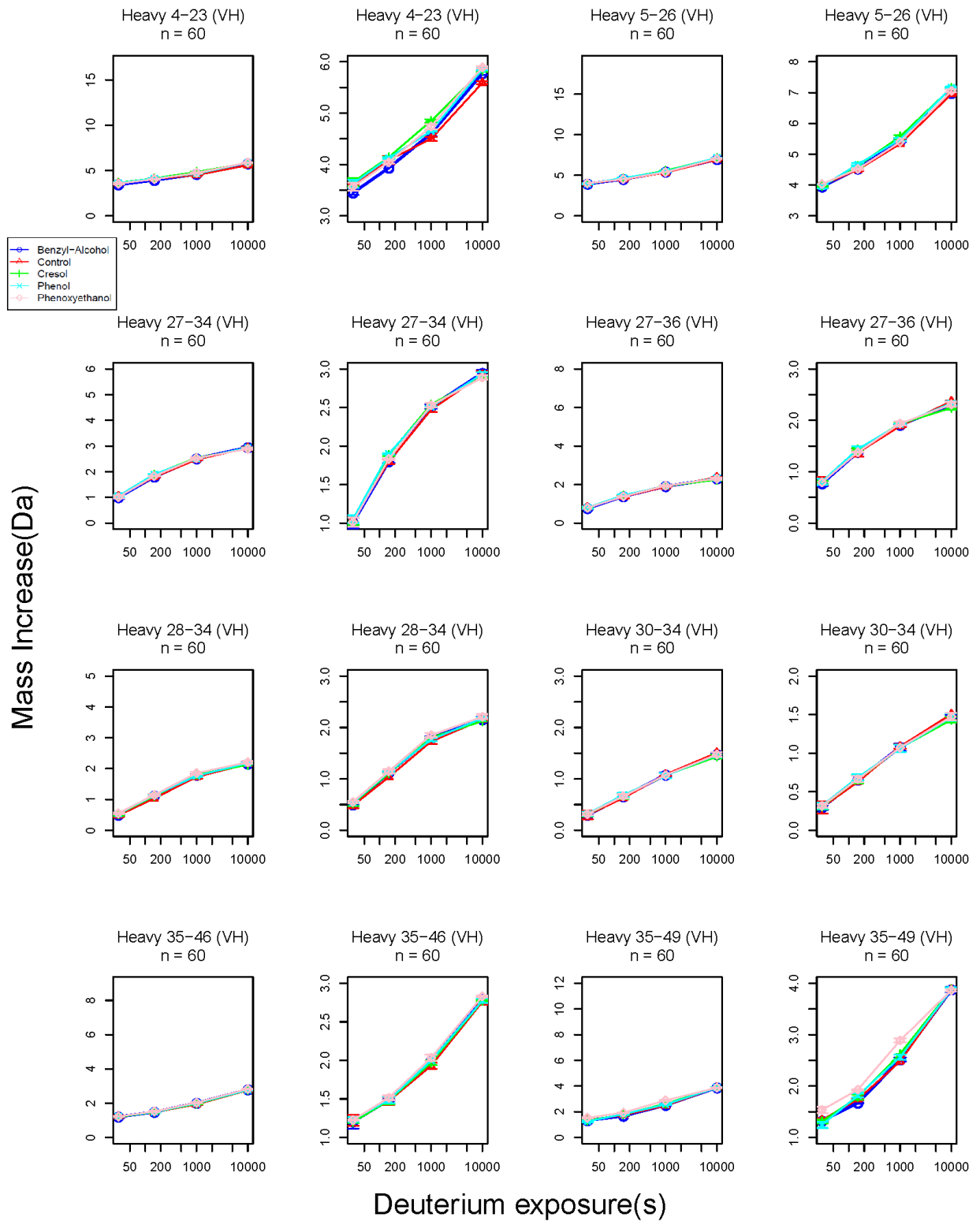
Peptide coverage map of mAb-4 (A) heavy chain and (B) light chain. 140 peptide segments of mAb-4 covered 90% of heavy chain and light chain primary sequence

Figure 2.S3

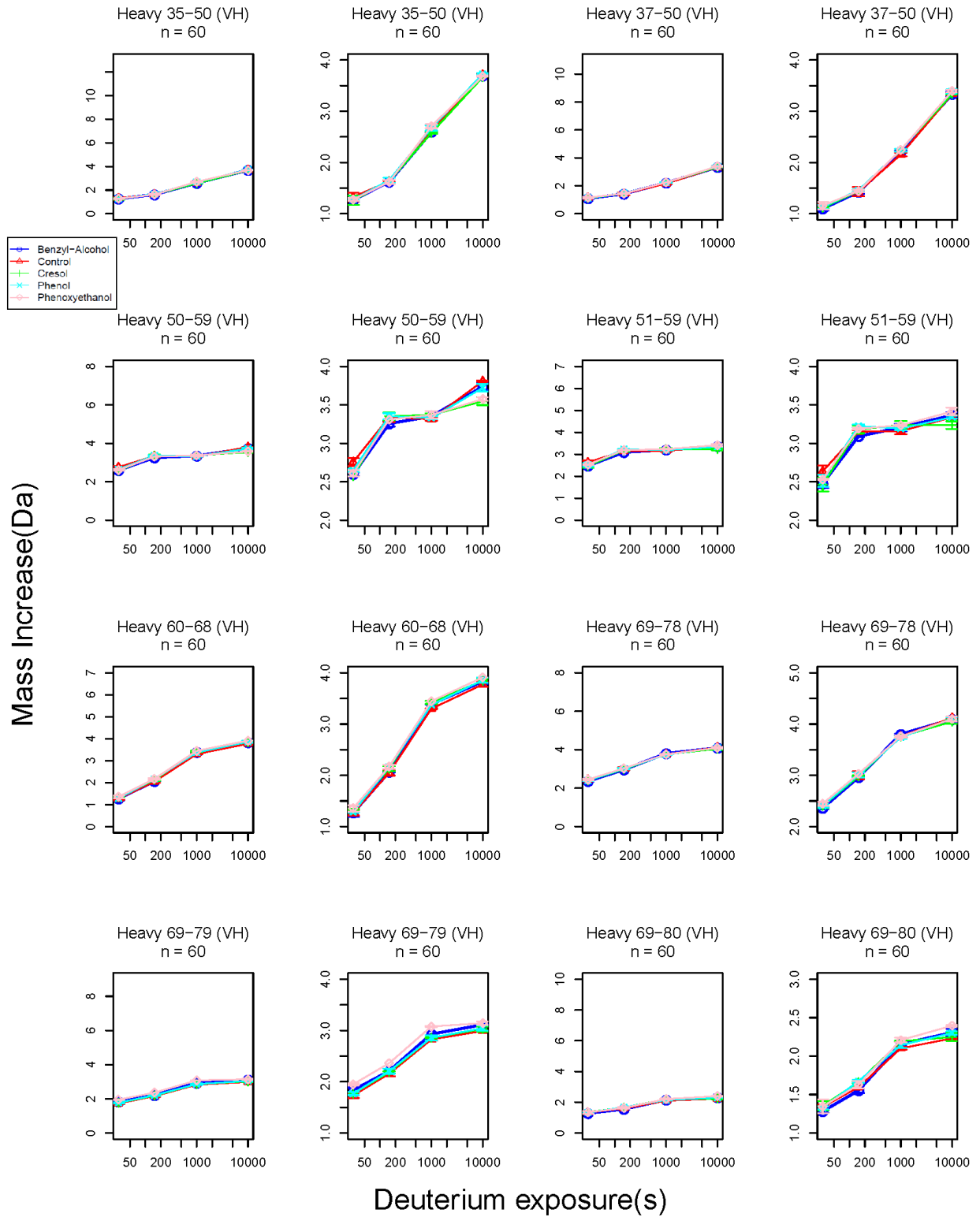


Relative local flexibility of mAb-4 in 20 mM citrate-phosphate buffer (pH 6.0) containing 100 mM NaCl prepared in deuterium. (A) Percent flexibility of all 140 peptide segments of mAb-4 obtained from the ratio of deuterium uptake at 30 second relative to the theoretical exchange for each peptide. (B) Percent flexibility plotted on to the homology model of mAb-4.

Figure 2.S3

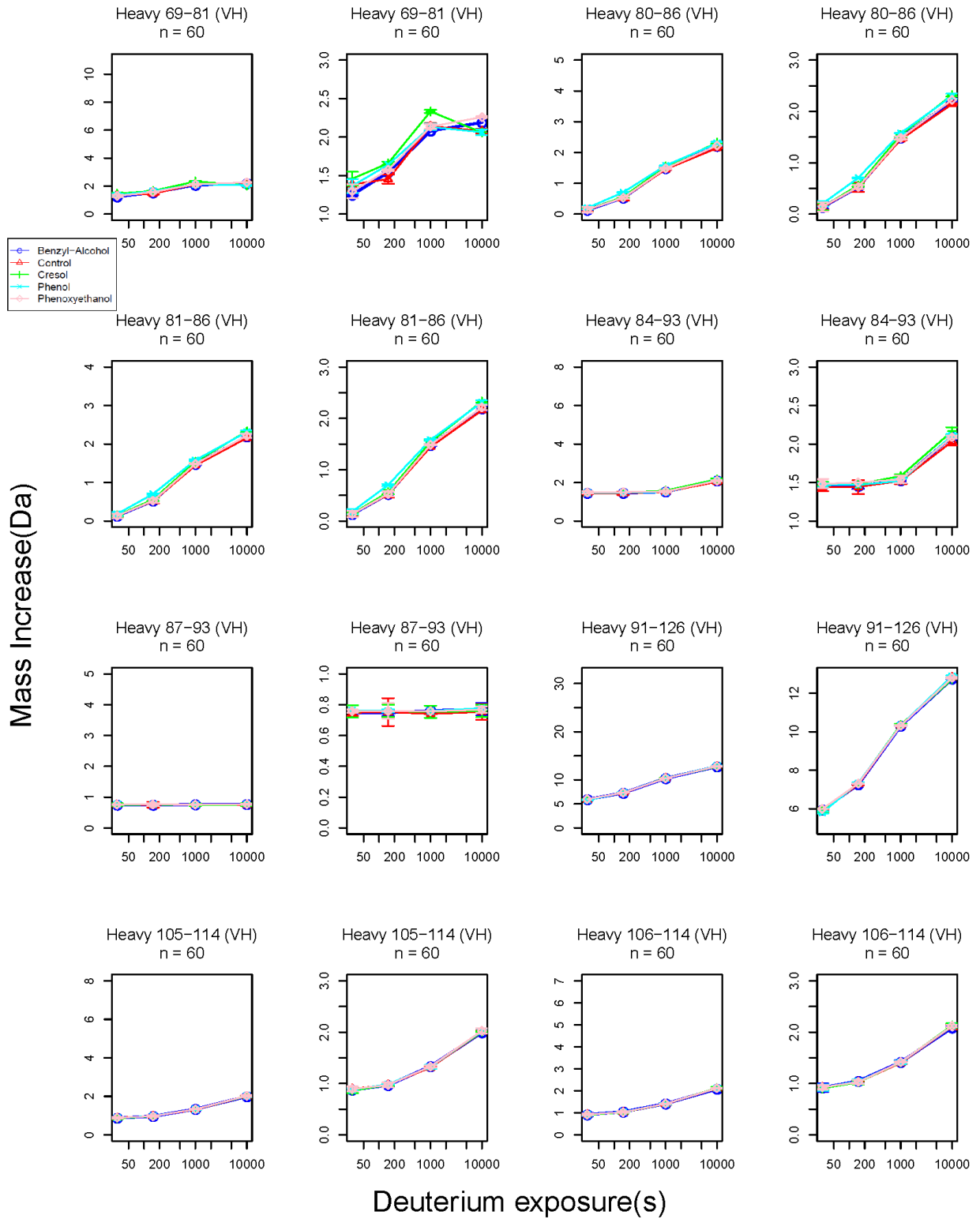


Mass Increase(Da)

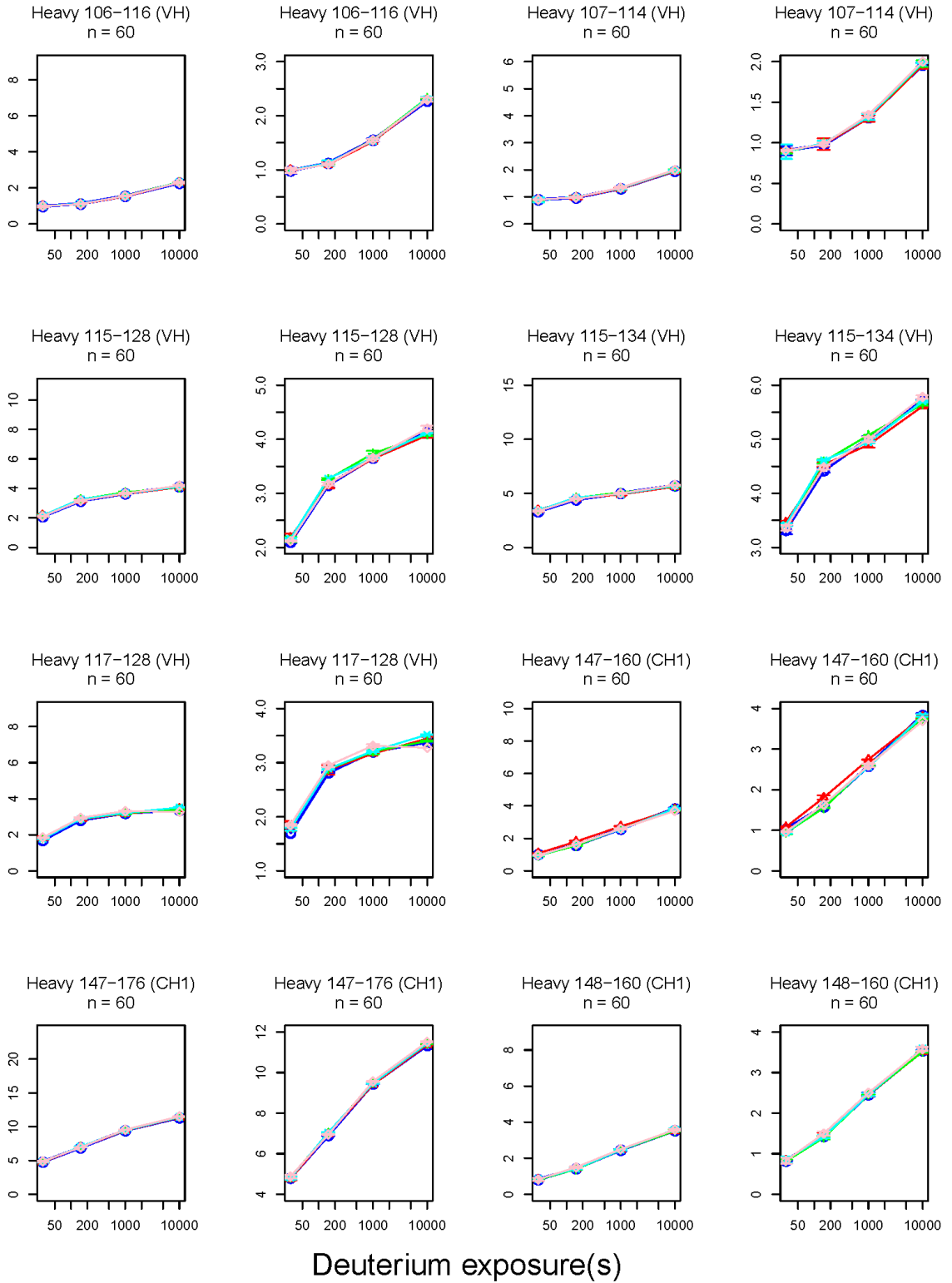


Deuterium exposure(s)

Mass Increase(Da)

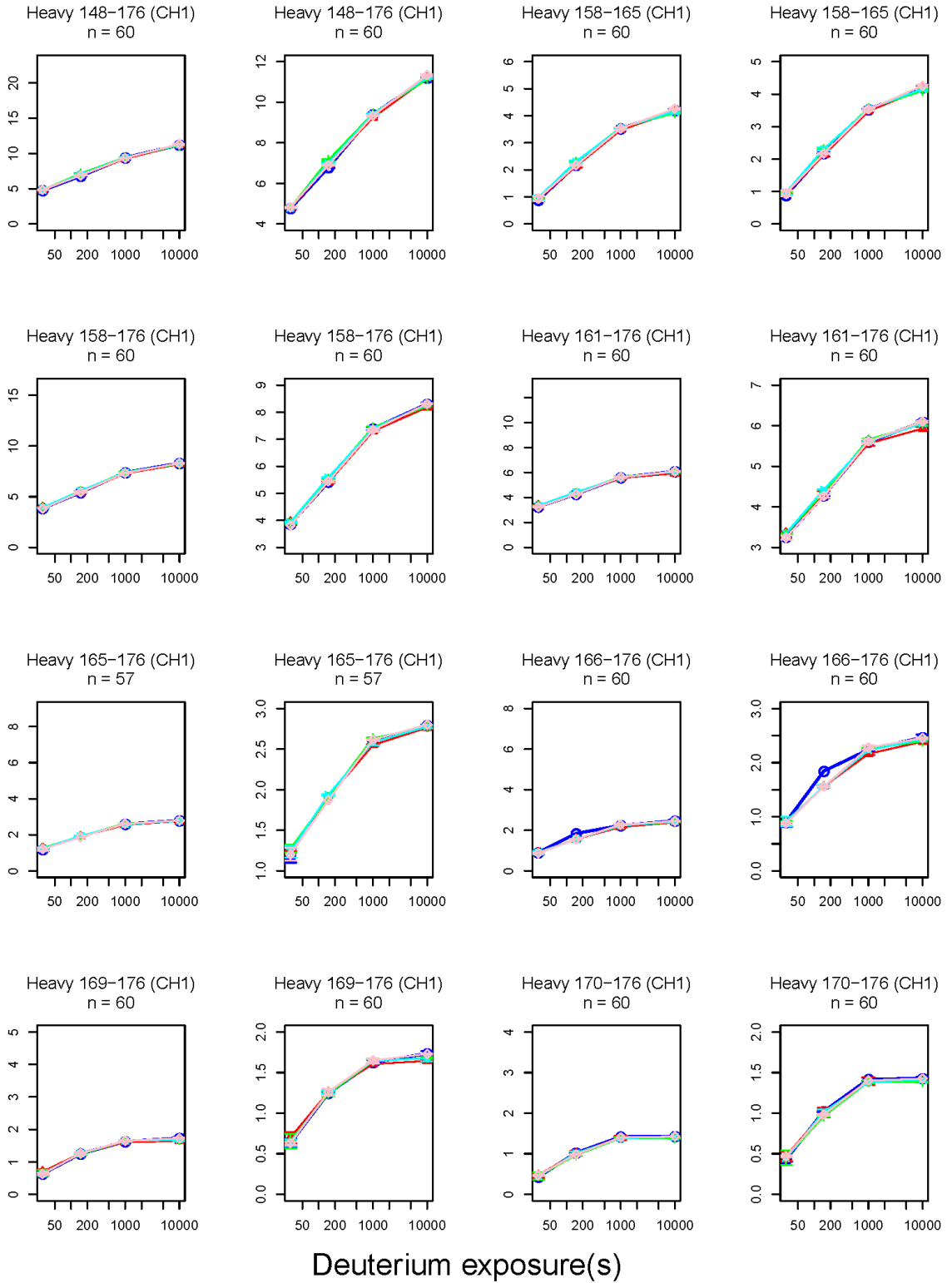


Mass Increase(Da)

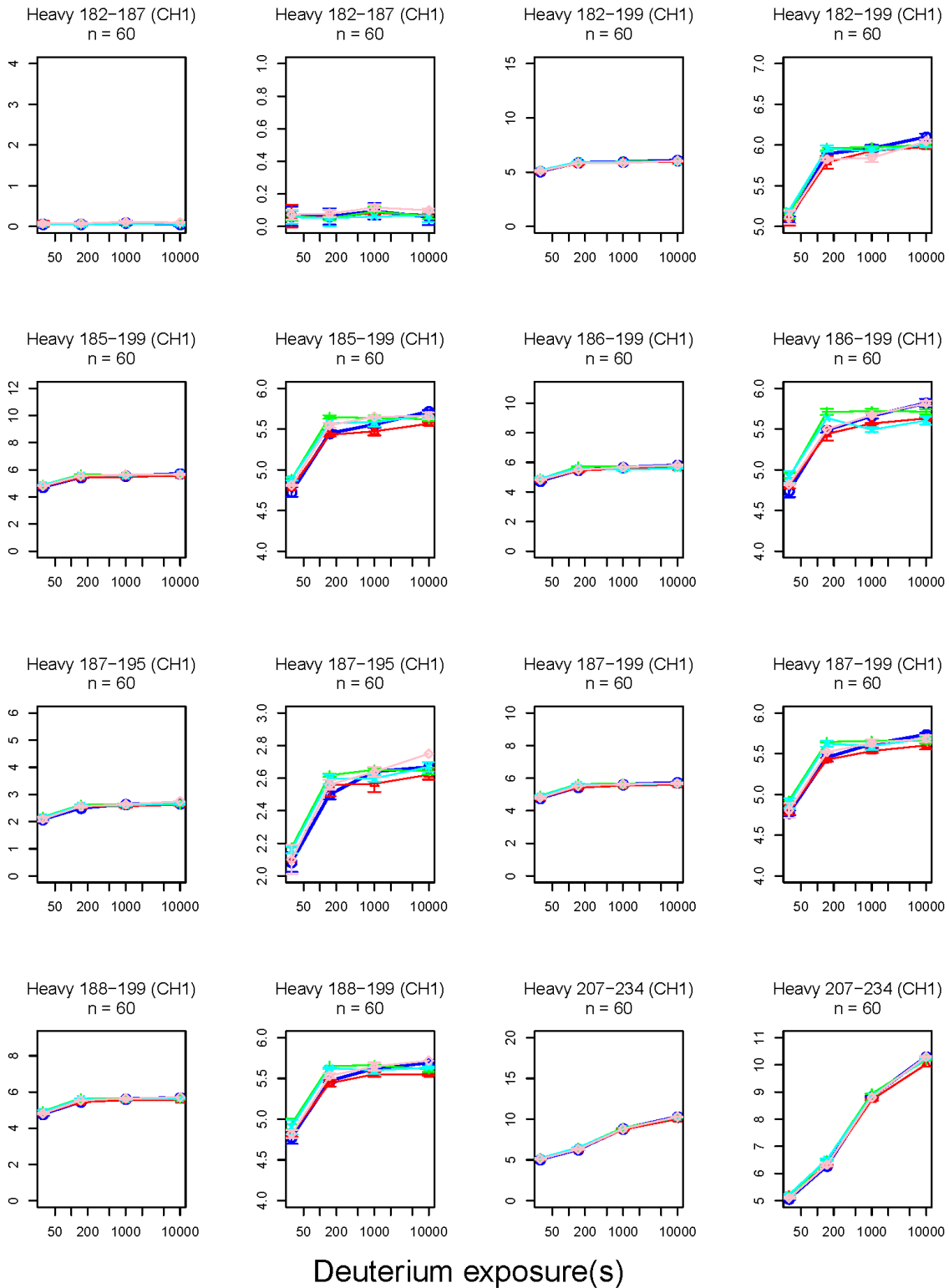


Deuterium exposure(s)

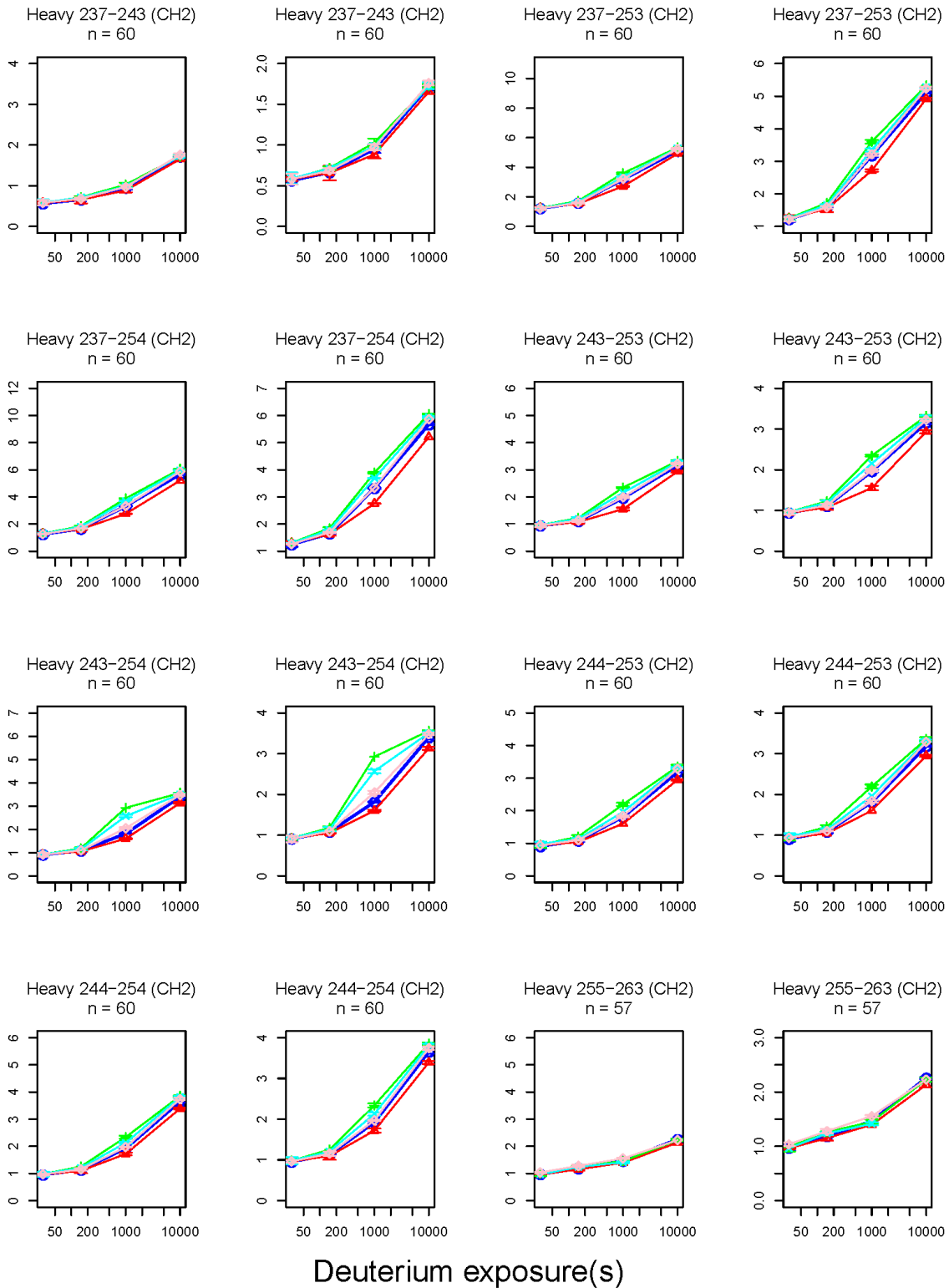
Mass Increase(Da)



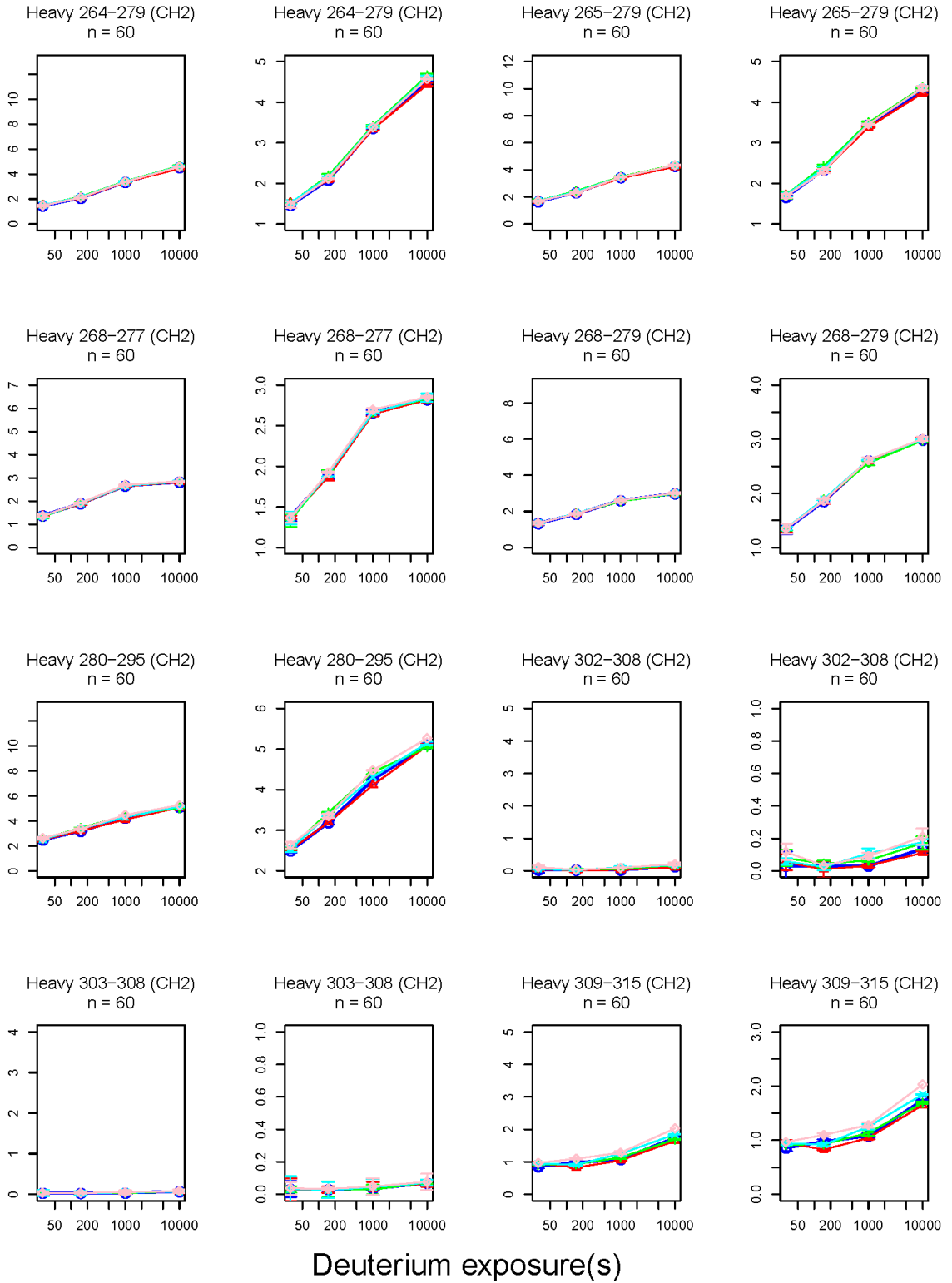
Mass Increase(Da)



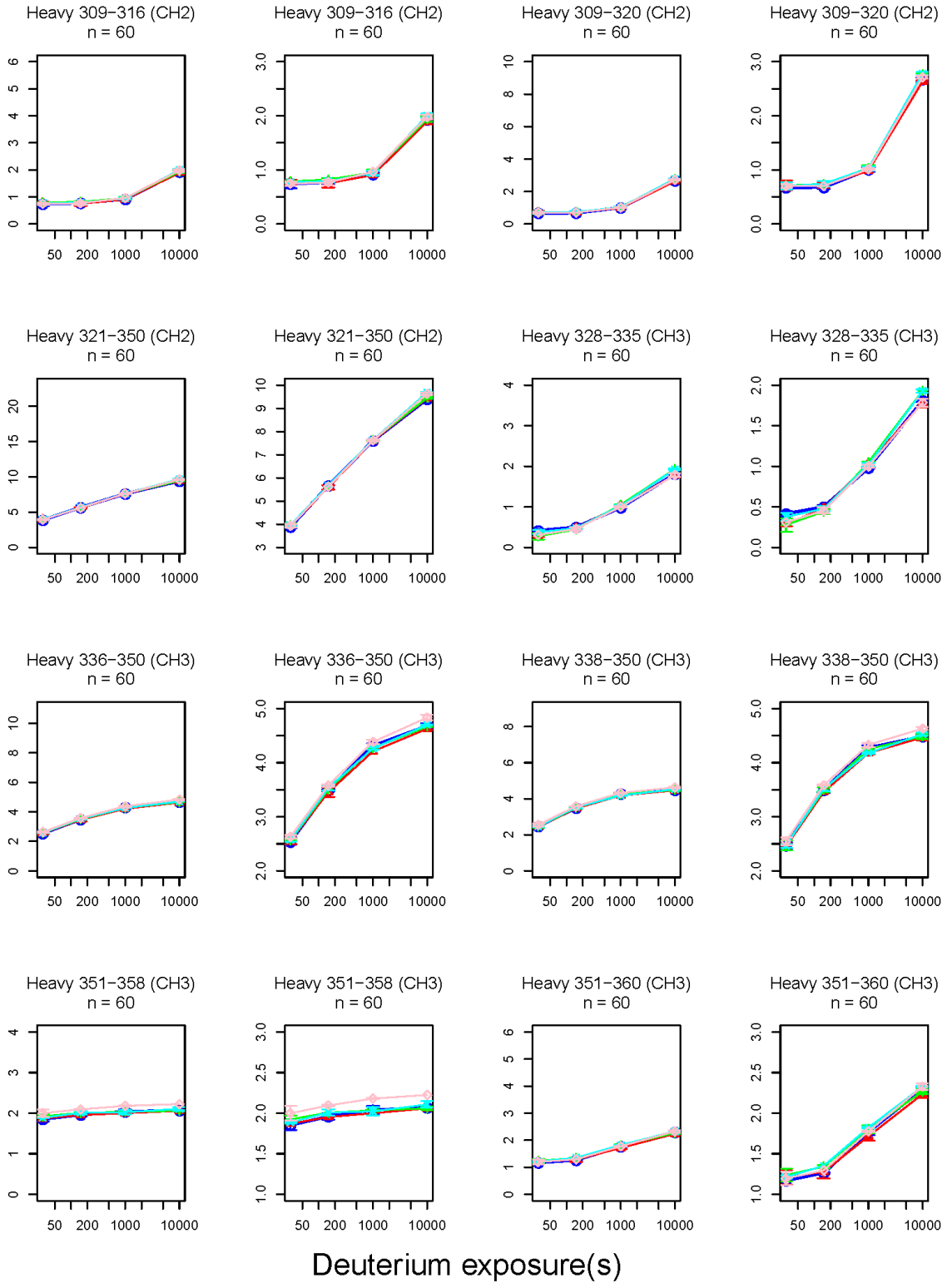
Mass Increase(Da)



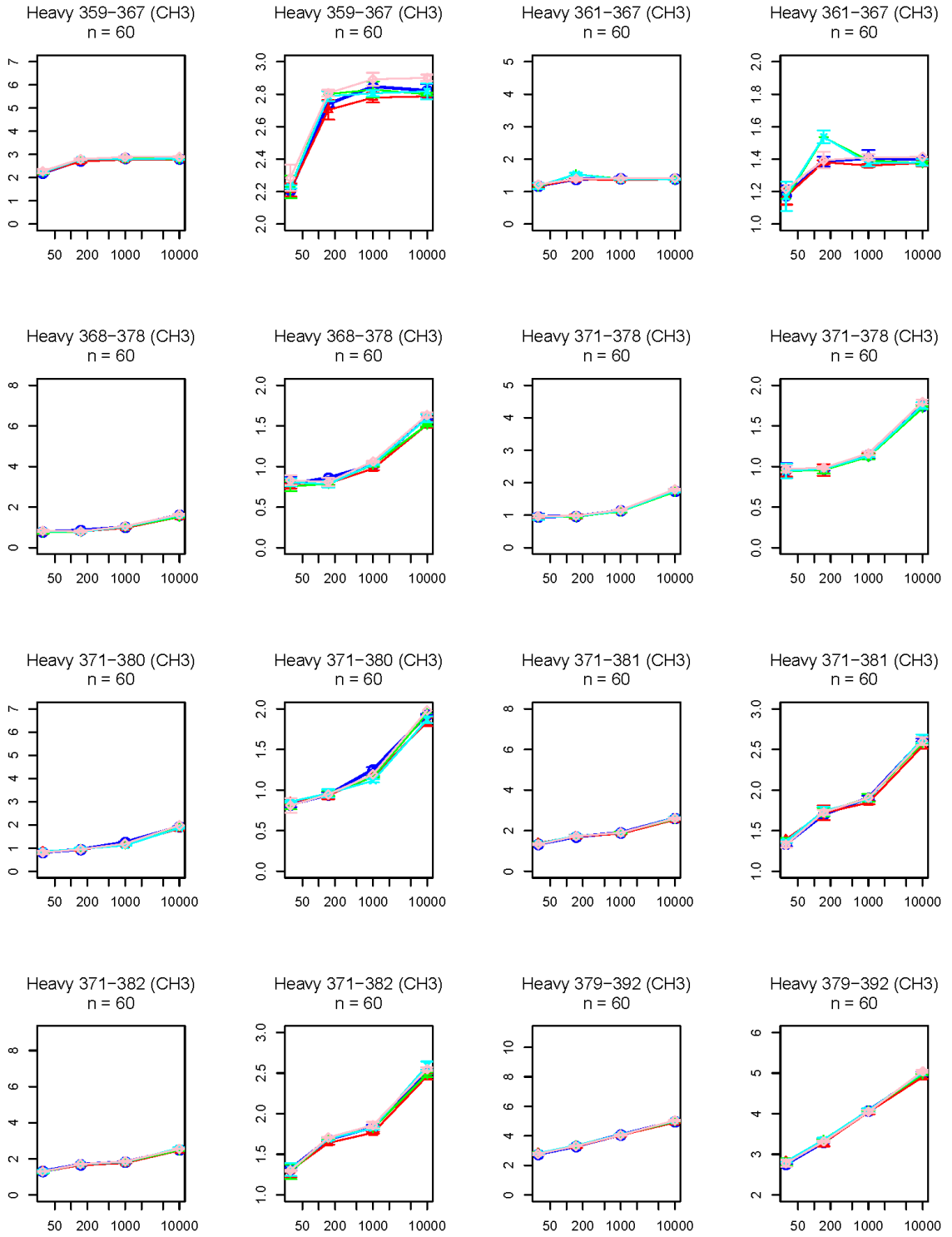
Mass Increase(Da)



Mass Increase(Da)

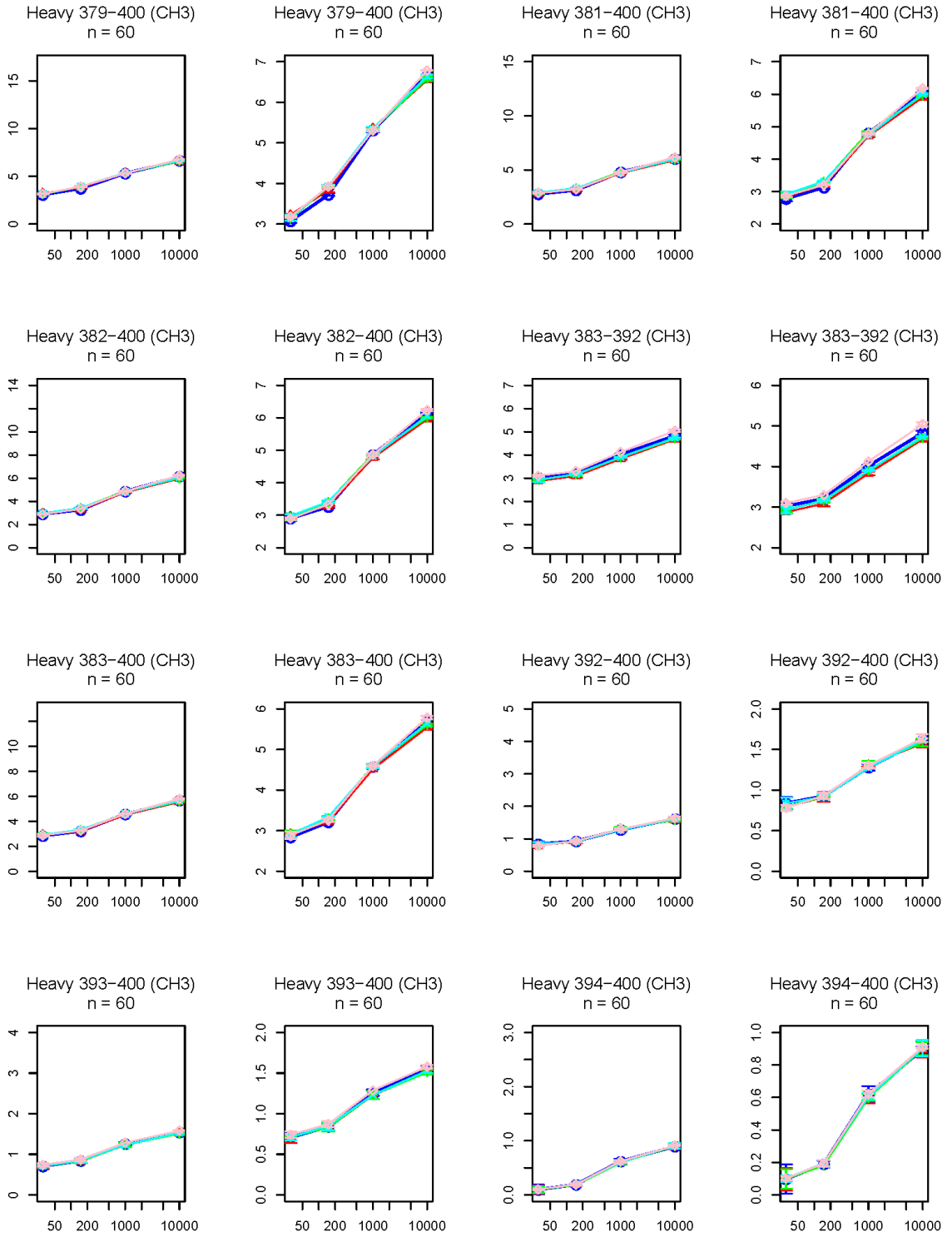


Mass Increase(Da)



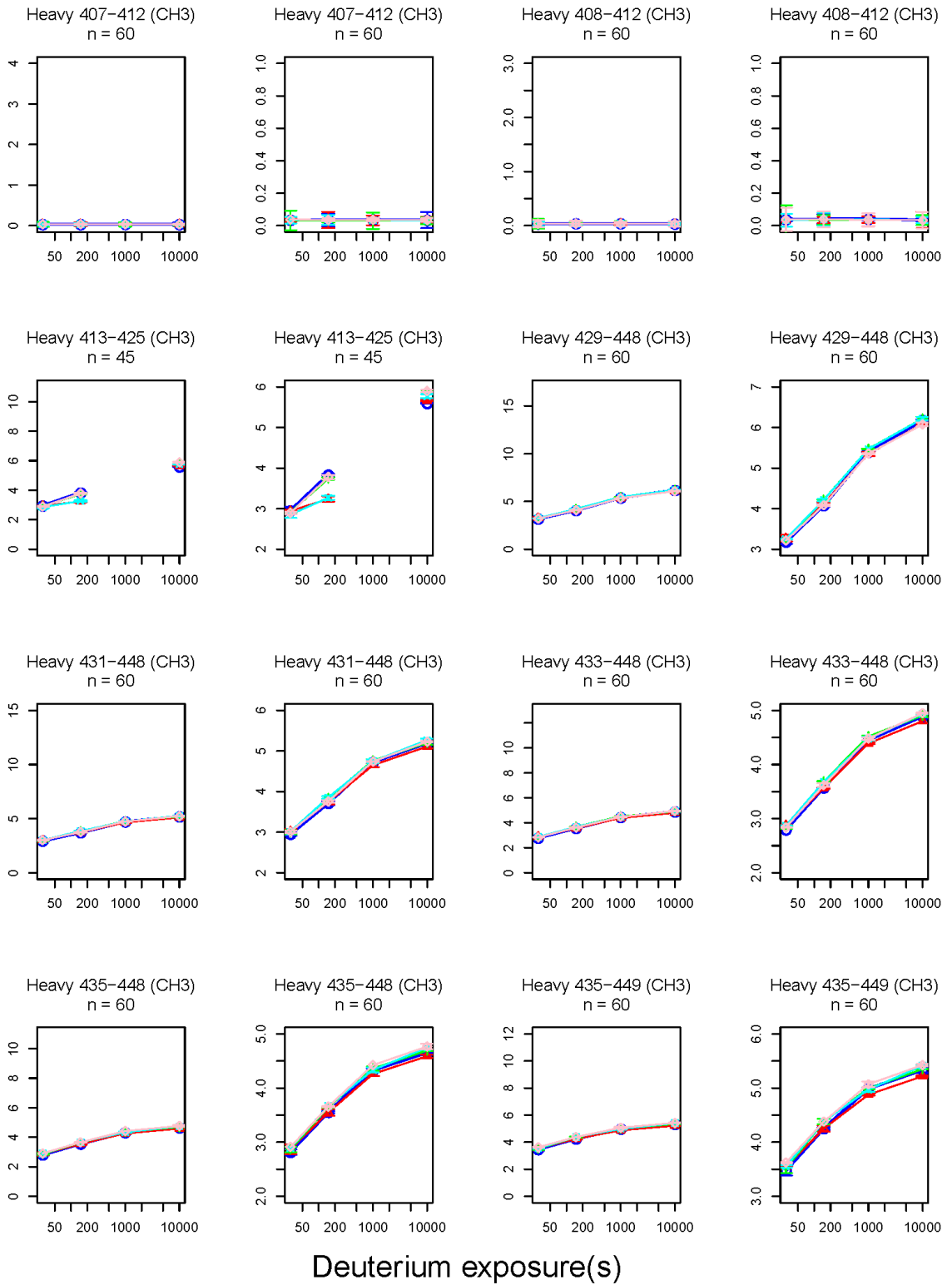
Deuterium exposure(s)

Mass Increase(Da)

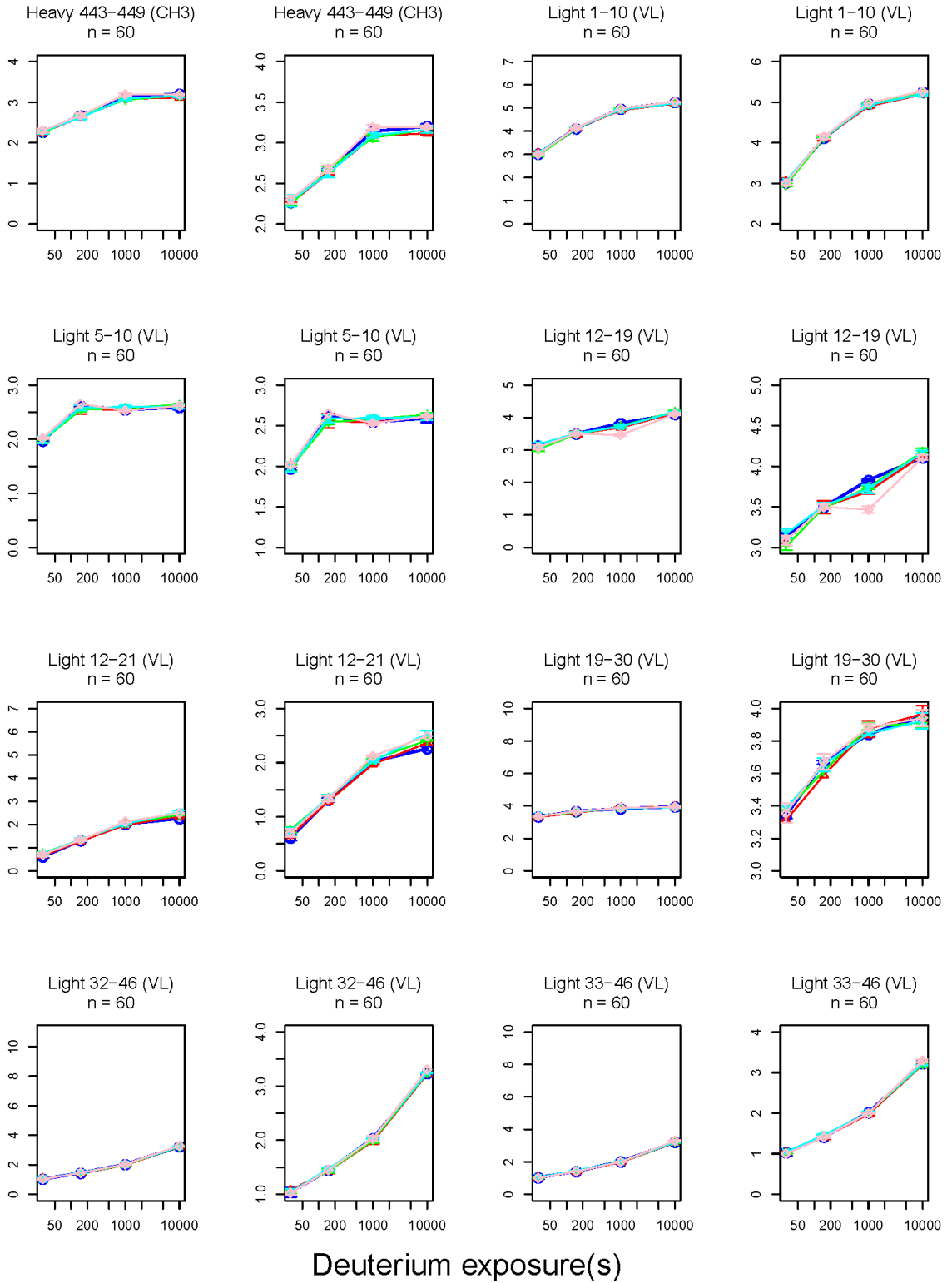


Deuterium exposure(s)

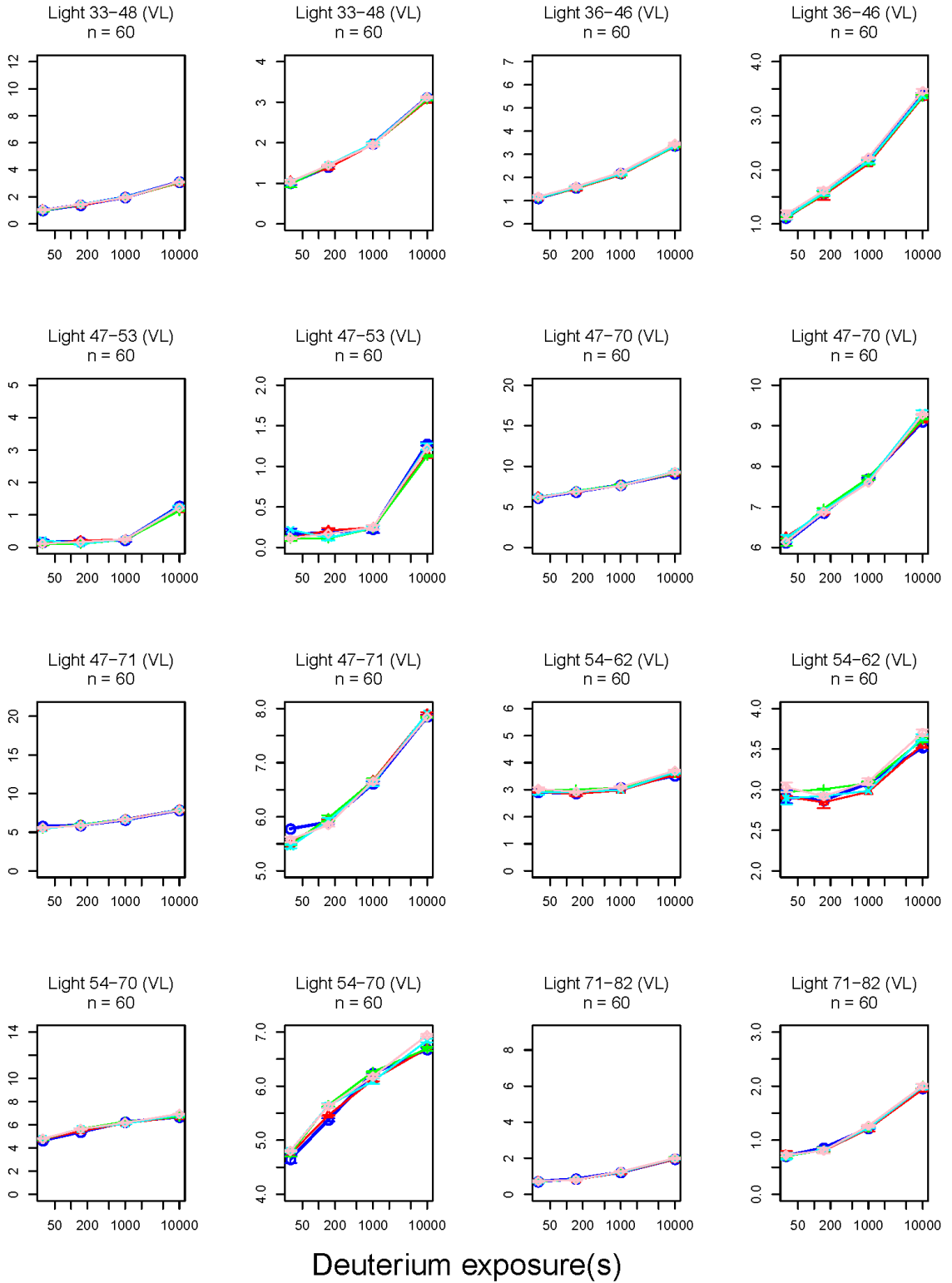
Mass Increase(Da)



Mass Increase(Da)

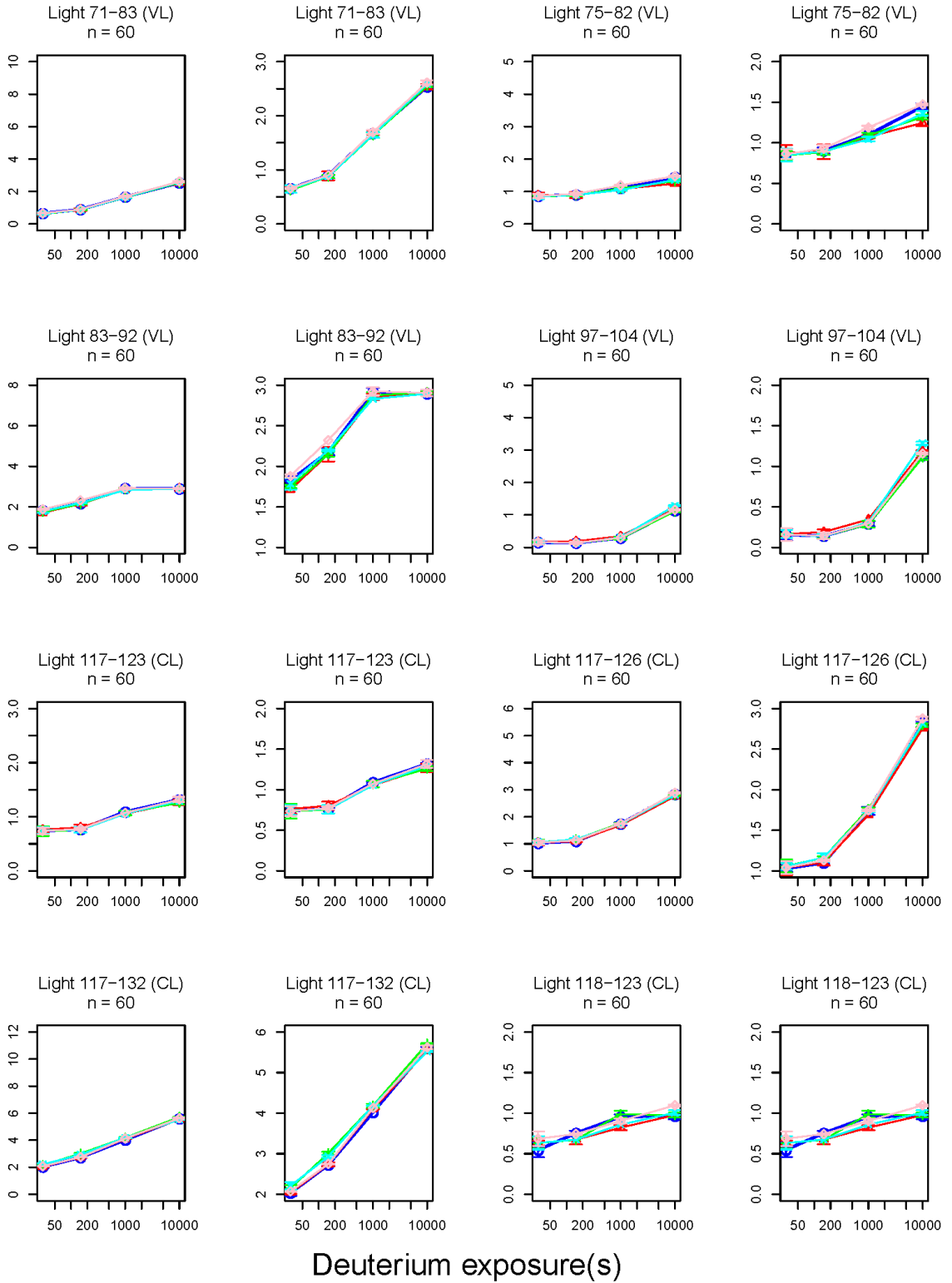


Mass Increase(Da)

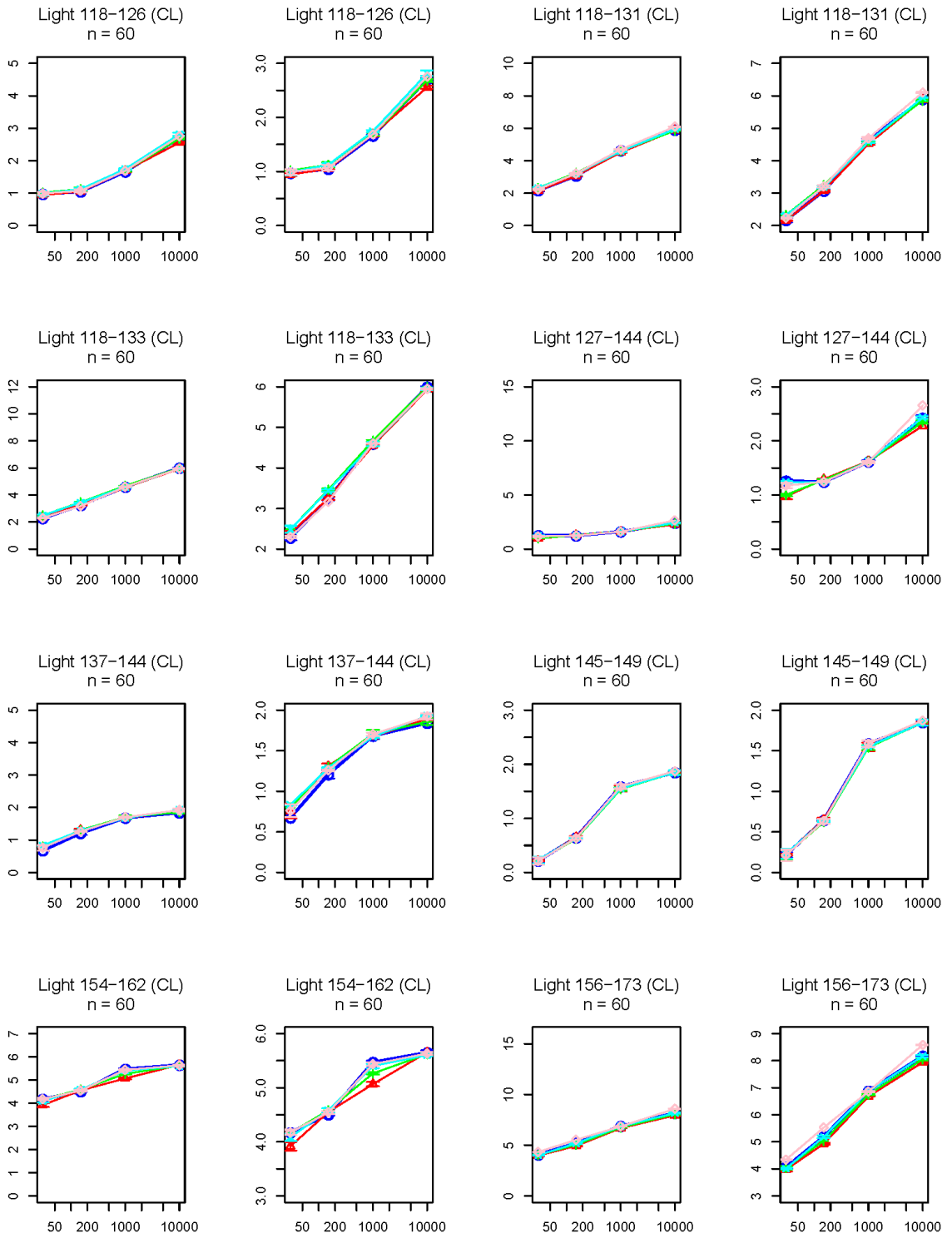


Deuterium exposure(s)

Mass Increase(Da)

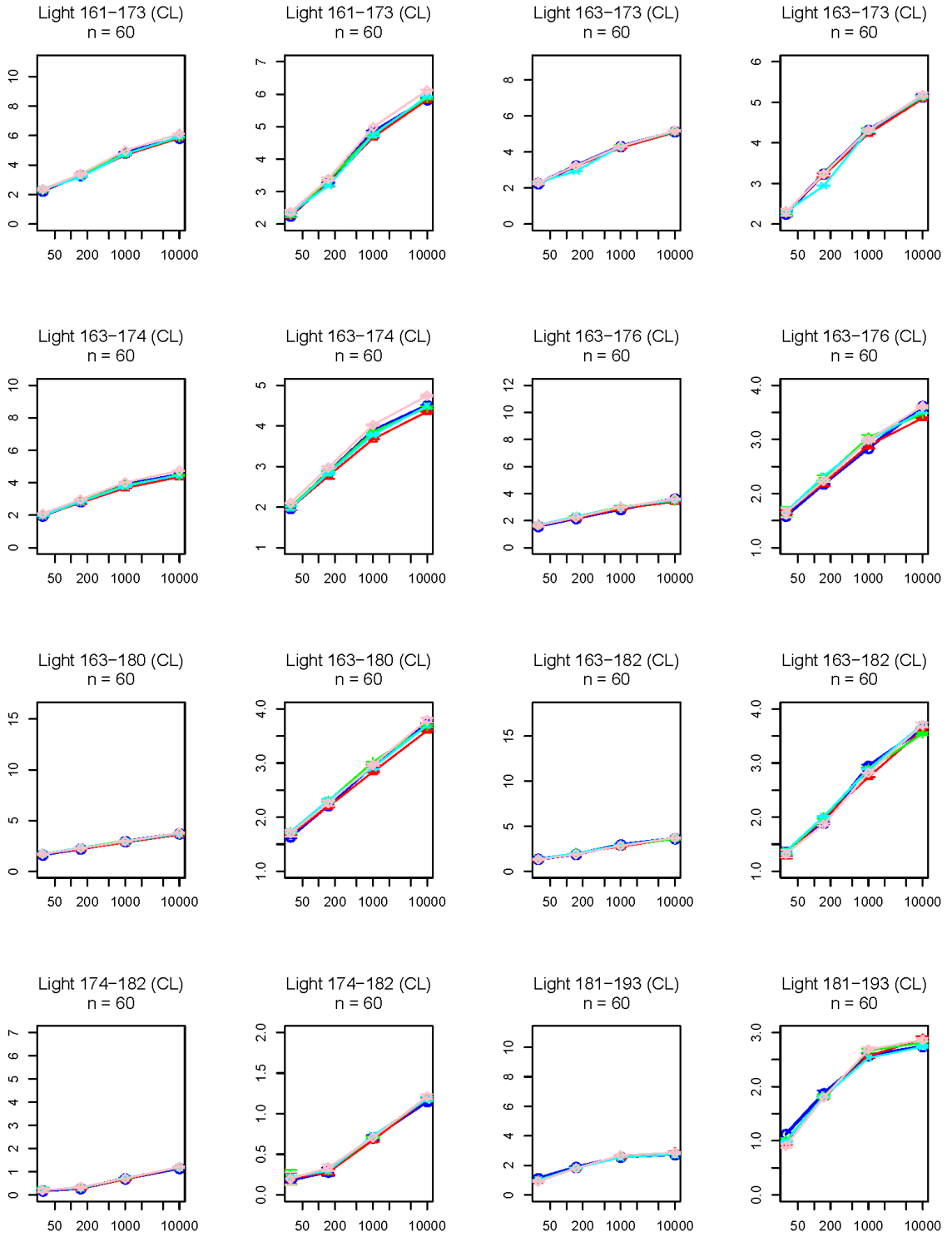


Mass Increase(Da)



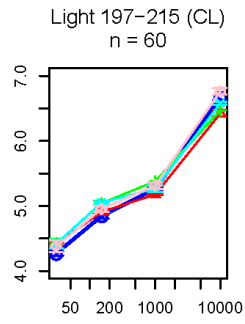
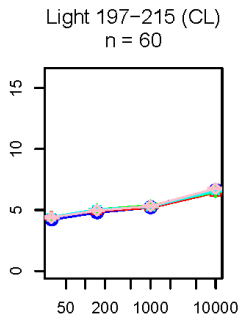
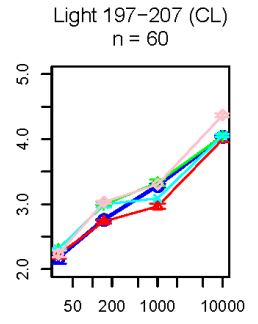
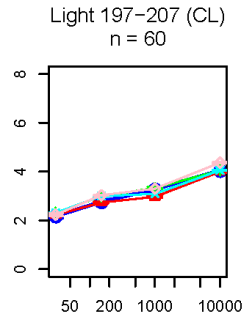
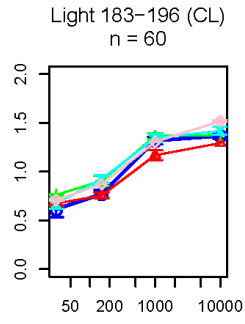
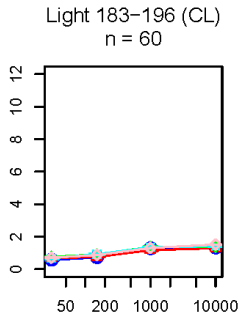
Deuterium exposure(s)

Mass Increase(Da)



Deuterium exposure(s)

Mass Increase(Da)



Deuterium exposure(s)

Deuterium uptake curves for all 142 peptide segments of mAb-4 comparing HX kinetics in the presence of APs to control. Domain location and peptide number of the segment are shown in parentheses. The error bars represent one standard deviation from three independent experiments.

Chapter 3

Hydrogen exchange mass spectrometry reveals protein interfaces and distant dynamic coupling effects during the reversible self-association of an IgG1 monoclonal antibody

3.1 Introduction:

Monoclonal antibodies (mAbs) and mAb derivatives are currently the fastest growing segment of the biopharmaceutical drug market.¹⁷⁶ Antibody therapy often requires relatively high dosing (>1 mg/kg) that can be administered either by intravenous (IV) or subcutaneous (SC) injection. Due to higher costs, lower patient compliance, and longer administration times associated with IV drug delivery by medical professionals, the self-administration of mAb drugs by patients at home via SC administration is being extensively investigated.¹ The formulation development challenges for SC administration of mAbs at high concentrations (~100-150 mg/mL), for use in prefilled syringes and auto-injectors, include protein instability as well as injection volume limitations (less than 2 mL) due to high tissue backpressure or injection pain.¹

Molecular interactions that occur in high concentration formulations can also introduce challenges to the development and manufacturing of mAbs. As the intermolecular distance between individual molecules decreases at higher protein concentrations, the extent of non-ideal behavior increases due to intermolecular interactions between the mAbs.^{177,178} Such intermolecular interactions increase the propensity of antibody molecules to undergo reversible self-association (RSA) where non-covalent multimers can form at high protein concentrations and then dissociate upon dilution.^{13,14,16} The RSA of mAbs presents various pharmaceutical challenges, including the formation of protein aggregation precursors that can lead to the irreversible formation of oligomers.^{47,179} In addition, the RSA of mAbs gives rise to a network of associated higher order species that can affect the viscoelastic properties of the solution,⁸⁰ resulting in increased viscosity,^{13,14,16,76} solution turbidity,⁹³ and, under certain conditions, even phase transitions.¹⁸⁰ The increase in solution viscosity also imposes manufacturing challenges including high back-pressure and clogging of membranes,¹ as well as elevated levels of shear stress during pumping.¹⁸¹

Reversible-self association of mAbs is generally attributed to weak and transient non-covalent interactions (e.g., hydrogen bonding, electrostatic, hydrophobic, π - π , and van der Waals interactions) between antibody molecules. As the protein concentration increases and the intermolecular distances decrease, the extent of non-covalent interactions between molecules rises.^{177,178} Not only have certain regions in the antibody structure (i.e., fragment antigen-binding region (Fab) and fragment crystallizable region, Fc) been shown to interact at high protein concentrations,^{182,183} such transient interactions have been shown to involve specific amino acid residues and sequences within mAbs.^{182,184} In addition, varying solution conditions (e.g., ionic strength, pH, temperature, salt type, etc.) can either increase or decrease the extent of RSA of mAbs, depending on the distinct nature of the non-covalent interactions for an individual mAb formulated under specific conditions.^{79,185}

A variety of analytical tools have been used to characterize the RSA of proteins, and related effects on solution properties, including dynamic light scattering (DLS),²¹ composition-gradient multi-angle static light scattering,^{95,106} isothermal titration calorimetry,¹⁸² surface plasmon resonance,¹⁸⁶ proton magnetic relaxation dispersion,¹⁸⁷ nuclear magnetic resonance,¹⁸⁸ fluorescence resonance energy transfer,¹⁸⁹ mass spectrometry (MS),¹⁹⁰ self-interaction nanoparticle spectroscopy,¹⁹¹ size-exclusion chromatography,¹⁹² analytical ultracentrifugation,¹⁹³ small angle X-ray scattering,⁸¹ and atomic force microscopy.¹⁹⁴ Most of these measurements provide reliable data only at low-to-moderate protein concentrations (~1-20 mg/mL). With further increases in protein concentration, the non-ideality of the solution, along with technical problems such as multiple scattering effects, compromises data reliability.^{195,196} NMR can provide higher resolution information about the site-specific nature of protein self-association, but the large size of antibody molecules and their complexes and the need for isotopic labeling limit the applicability

of NMR to examine the RSA of antibodies. Such limitations have led to the widespread use of solution viscosity to indirectly monitor RSA of mAbs at high protein concentrations (~20-200 mg/mL).^{13,14,184} Although viscosity measurements provide an experimentally convenient method to monitor RSA behavior of mAbs, they do not provide site-specific information about protein-protein interfaces.

Hydrogen exchange mass spectrometry (HX-MS) provides an exciting opportunity to obtain high-resolution information about higher-order structure in antibodies.¹⁹⁷⁻¹⁹⁹ For example, HX-MS has been recently applied to examine the effect of various solution factors and physicochemical structural changes on the local flexibility of mAbs, including salts from Hofmeister series,¹³⁷ pharmaceutical excipients,¹³⁸ freeze-thaw cycles,²⁰⁰ methionine oxidation,¹⁶⁵ asparagine deamidation,²⁰¹ antibody-drug conjugation,²⁰² and deglycosylation and glycan modifications,¹⁵⁷ and engineered point mutations.²⁰³

In this study, antibody clusters were characterized by a combination of DLS and chemical cross-linking experiments to determine the effect of solution conditions on the extent of RSA for an IgG1 mAb (referred to as “mAb-C”) as a function of mAb-C protein concentration (1-10 mg/mL). Solution viscosity measurements were then utilized to indirectly monitor the increase of RSA at higher mAb-C concentrations (up to 60 mg/mL protein). We then applied a novel HX-MS methodology, using a stable, lyophilized formulation followed by reconstitution in D₂O solutions that promote RSA, to map RSA-induced changes in hydrogen exchange by mAb-C (i.e., comparing relatively low vs. high levels of RSA at 5 vs 60 mg/mL). This HX-MS analysis revealed specific peptide segments at the protein interface leading to RSA of mAb-C and also identified regions of mAb-C distant from the protein-protein interface with increased backbone flexibility.

3.2 Materials and Methods:

3.2.1 Materials:

A highly purified IgG1 mAb at 10 mg/mL, referred to as “mAb-C”, was produced by MedImmune LLC, Gaithersburg, MD. The antibody stock solution was dialyzed into various buffers as indicated below. LC-MS grade water, 2-propanol and dibasic anhydrous potassium phosphate (>99.0%) and sodium chloride were obtained from Fisher Scientific (Fair Lawn, NJ). LC-MS grade acetonitrile was purchased from Honeywell (Morristown, NJ). Formic acid ($\geq 99.0\%$ LC-MS-grade) was purchased from Thermo Scientific (Rockford, IL). Monobasic anhydrous potassium phosphate (99.5%), sodium sulfate (>99.0%), porcine pepsin, tris (2-carboxyethyl) phosphine hydrochloride (TCEP), guanidine hydrochloride, deuterium oxide (99.9% D) and tris (hydroxymethyl) aminomethane hydrochloride ($\geq 99.0\%$) were purchased from Sigma-Aldrich (St. Louis, MO). The reagent bis-(sulfosuccinimidyl) 2,2,4,4, glutarate-d₀ (BS²G-d₀) was obtained from Pierce Biotechnology (Rockford, IL). The disaccharide α,α -trehalose dihydrate was obtained from Ferro Pfanstiehl laboratories (Waukegan, IL).

3.2.2 Sample preparation

As needed, mAb-C samples were dialyzed using 3.5 kDa molecular-weight-cutoff membranes (Slide-A-Lyzer, Thermo Scientific, Rockford, IL). mAb-C samples were concentrated using Vivaspin-20 (10 kDa molecular weight cutoff) ultrafiltration columns (Sartorius Stedim, Gottingen, Germany).

3.2.3 Dynamic Light Scattering

Stock samples of mAb-C were dialyzed against 40 mM potassium phosphate buffer (pH 6-8) containing either NaCl or Na₂SO₄ at concentrations ranging from 0.15 to 0.5M overnight at 4°C. Dialyzed samples were then diluted to 1, 2.5, 5 and 10 mg/mL using the dialysis buffer. The concentration of mAb-C was determined using ultraviolet absorption spectroscopy ($A_{280\text{ nm}}$) using $E_{1\text{ cm}} 0.1\%$ of $1.54\text{ mL mg}^{-1}\text{ cm}^{-1}$.²⁰⁴ DLS experiments were performed in triplicate at 25°C using the DynaPro Plate Reader (Wyatt Technology, Santa Barbara, CA). Scattered light was analyzed using a backscatter detector fixed at an angle of 173°. An autocorrelation function was calculated using a built-in digital autocorrelator. 20µL of sample was added to each well of a 384-well plate, and 10µL of paraffin oil was added on top of each sample to inhibit sample loss by evaporation. The 384-well plate was centrifuged at 2000 rpm for 2 minutes to remove any air bubbles. All mAb-C samples were kept at the temperature of interest for 10 minutes for temperature equilibration and then fifteen 5 second acquisitions were collected for each sample. Dynamics 7.1.7 software was used to calculate the hydrodynamic diameter of the mAb-C samples. The solution viscosity of each buffer alone (placebo) was measured using an m-VROC viscometer (Rheosence, San Ramon, CA) at 25°C and buffer viscosity correction was implemented in instrument software for calculation of the hydrodynamic diameter of mAb-C samples.

3.2.4 Chemical cross-linking and SDS-PAGE analysis

An amine-reactive cross-linker, bis (sulfosuccinimidyl) 2,2,4,4, glutarate (BS²G), with a spacer arm length of 7.7 Å, was used to study reversible-self association of mAb-C. mAb-C was concentrated to 10 mg/mL and then dialyzed against 40 mM potassium phosphate buffer (pH 7.0) with and without 300 mM sodium sulfate, for 24 hours at 4°C. For the chemical cross-linking reaction, 10 mg/mL mAb-C in the presence and absence of sodium sulfate was incubated with

increasing concentrations of BS²G ranging from 5- to 40-fold molar excess to mAb-C. The reaction mixtures were incubated at 4°C for 5 minutes and quenched by addition of 1 M tris hydrochloride. mAb-C from the reaction mixtures was combined with 4X lauryl dodecyl sulfate (LDS) buffer, iodoacetamide, and filtered deionized water to obtain a final sample volume of 20 µL containing eight micrograms of protein, 50 mM iodoacetamide, and 1X LDS buffer. For reducing conditions, 100 mM DTT was added to the mAb-C-LDS solution. All samples were heated at 75°C for 5 minutes and then analyzed using a 3%-8% tris-acetate SDS-PAGE gel (Life Technologies, Grand Island, NY).

3.2.5 Viscosity Measurements

Prior to solution viscosity measurements, mAb-C stock was dialyzed against 40 mM potassium phosphate buffer (pH 7) containing either 300 mM NaCl or Na₂SO₄. Dialyzed samples were concentrated to 60 mg/mL and then diluted with dialysis buffer to make protein concentrations ranging from 5 – 60 mg/mL. Solution viscosities were measured at 4°C and 25°C with an m-VROC viscometer (Rheosence, San Ramon, CA). Samples at different concentrations of mAb-C were injected at a rate of 100 µL/min at a shear rate of 1420 1/s using a 1 mL glass syringe (Hamilton Co, Reno, NV). Triplicate viscosity measurements were recorded over duration of 100 seconds. Viscosity values were obtained in the units of dynamic viscosity: mPa s.

3.2.6 Lyophilization of mAb-C

Prior to freeze-drying, mAb-C samples were dialyzed against 20 mM potassium phosphate buffer (pH 7) with 10% (W/V) trehalose for 24 hours and then concentrated to 60 mg/mL. Half of the mAb-C samples were diluted in the same buffer to 5 mg/mL. The mAb-C samples at 5 and 60

mg/mL were filled into 3 mL FIOLEX[®] clear Type 1 glass vials (Schott North America, Elmsford, NY) with a fill volume of 500 μ L. All the vials were partially stoppered by 2-leg, 13 mm siliconized rubber stoppers (Wheaton Industries Inc., Millville, NJ) The samples were then lyophilized using a LyoStar II lyophilizer (SP Scientific, Warminster, PA). Vials were subjected to an initial hold step at 5°C and then a freezing hold step at -40°C. During primary drying, the shelf temperature was maintained at -30°C for 400 minutes and then at -35°C for 800 minutes with the chamber pressure maintained at 100 mTorr. Secondary drying was done by ramping the shelf temperature at 0.1°C/min until reaching a final shelf temperature of 25°C for 60 minutes. Residual moisture levels of ~0.5% (v/v) in the lyophilized mAb-C samples were determined using a Karl-Fischer titration unit according to vendor instructions (Mettler Toledo. LLC, Columbus, OH)

3.2.7 Size Exclusion Chromatography (SEC)

Lyophilized mAb-C samples were reconstituted and diluted to 0.5 mg/mL with D₂O-based 40 mM potassium phosphate buffer containing 300 mM sodium sulfate and 10% (w/v) trehalose. All mAb-C samples were centrifuged at 14000g for 5 minutes prior to SEC analysis. For SEC experiments, a 7.8 cm \times 30 cm TSK-Gel BioAssist G3SW_{xL} column (TOSOH Biosciences, King of Prussia, PA) column was used. Samples were injected onto the column at a flow rate of 0.7 mL/min with a Shimadzu high-performance liquid chromatography (HPLC) system equipped with a diode array detector using a 200 mM phosphate buffer (pH 6.8) as the mobile phase. The performance of the column and the HPLC system was monitored using gel filtration standards (Bio-Rad, Hercules, CA) at the beginning and end of the experiment. The chromatograms were analyzed by integrating the monomer peak area detected at 214 nm. Percent aggregation in post-lyophilization samples

was measured relative to the total area of control samples (no lyophilization) at each protein concentration. To calculate the amount of insoluble aggregates, the total area of all the species (soluble aggregates, monomer, and fragment) in the chromatogram was calculated. The difference between the total peak areas of the sample and the control was used to quantify insoluble aggregates.

3.2.8 Circular Dichroism

Lyophilized mAb-C samples at 5 and 60 mg/mL were reconstituted to a concentration of 0.3 mg/mL with a D₂O-based 40 mM potassium phosphate buffer containing 300 mM sodium sulfate and 10% (w/v) trehalose at pH 7.0. The protein concentration of each sample was measured by absorbance at 280 nm using a previously reported value of $E_{1\text{ cm } 0.1\%}$ of $1.54\text{ mL mg}^{-1}\text{ cm}^{-1}$.⁷⁶ Circular dichroism (CD) experiments were conducted on a Chirascan Plus Circular Dichroism Spectrometer (Applied Photophysics Ltd., Leatherhead, UK) equipped with a Peltier temperature controller and a four-position cuvette holder. Far-ultraviolet (UV) CD spectra of control (no lyophilization) and freeze-dried mAbC samples (0.3 mg/mL) were collected from 200 nm to 260 nm using 0.1 cm path length quartz cuvettes. Control mAb-C samples were prepared in H₂O-based 40 mM potassium phosphate buffer containing 300 mM sodium sulfate and 10% (w/v) trehalose at pH 7.0. CD scans were collected at 10°C using a sampling time of 1 second and a bandwidth of 1 nm. Ellipticity values obtained from the instrument were then converted to molar ellipticity by dividing ellipticity by protein concentration (M) and cuvette path length (m).

3.2.9 Deuterated Reconstitution Buffer Preparation

Deuterium-based reconstitution/labeling buffer contained 20 mM potassium phosphate, 300 mM

sodium sulfate and 10% (w/v) trehalose at pH 7. The amount of D₂O in the reconstitution/labeling buffer was adjusted to 90 atom % by addition of H₂O as described previously.¹³⁸ The pH of the buffer was then adjusted to 7.0. The pH value of the solution was directly reported from the pH meter readout and does not include any correction for the deuterium isotope effect.²⁰⁵

3.2.10 Hydrogen Exchange Mass Spectrometry

Lyophilized vials containing 5 and 60 mg/mL mAb-C in 20 mM potassium phosphate and 10% (w/v) trehalose at pH 7.0, along with vials of the deuterium reconstitution/labeling buffer, were each equilibrated to 25°C on an Echotherm chilling/heating plate (Torrey Pines Scientific, Inc. Carlsbad, CA). A quench buffer containing 0.5 M tris(2-carboxyethyl) phosphine hydrochloride (TCEP), 4 M guanidine hydrochloride and 0.2 M sodium phosphate at pH 2.5 was equilibrated at 1°C. Deuterated reconstitution buffer (500 µL) was added to the lyophilized samples to yield a final protein concentration of 5 and 60 mg/mL and a final formulation composition of 40 mM potassium phosphate, 300 mM sodium sulfate, 10% (w/v) trehalose at pH 7.0 in D₂O. After addition of deuterated reconstitution buffer to the vials containing lyophilized protein, the vials were gently swirled for ~10 s until the freeze-dried cakes were reconstituted. The vials were held for an additional 60 s to allow foam to dissipate. The reconstituted mAb-C samples were then transferred to 2 mL microcentrifuge tubes and centrifuged at 14000g for 1 minute to remove small amounts of insoluble aggregates present in the sample (see Table 1). Reconstituted, centrifuged samples of mAb-C were then incubated for four labeling times: 120, 1620, 10⁴ and 10⁵ s; the labeling period was started at the end of the dissolution step. After labeling, the exchange reaction was quenched by adding 20 µL of the exchange reaction mixture to 180 µL of quench buffer equilibrated at 1°C. Dilution with quench buffer was maintained for both protein concentration

samples to keep the extent of back-exchange equal in the samples.

A LEAP HD/X PAL (LEAP Technologies, Carrboro, NC) was used to load quenched samples into the sample loop of the refrigerated column compartment containing two valves attached to the LC (Agilent 1200 series, Santa Clara, CA), an immobilized pepsin column, a peptide desalting trap, and a C18 column as described previously.^{137,138} Formic acid (0.1% v/v) was used for digestion and desalting. A mobile phase composed of water and acetonitrile, both containing 0.1% (v/v) formic acid, was used to elute the peptides. The temperature of the refrigerated compartment was maintained at 1°C during the course of the experiments. Different volumes of sample, 90 µL for the low, and 15 µL for the high concentrations were used so that the total amount of protein injected into the LC was similar: 45 µg for the low, and 90 µg for the high concentration samples. Three independent replicates for both protein concentrations were prepared and analyzed. To minimize peptide carryover in the immobilized pepsin column, the column was washed between samples following a cleaning procedure described previously¹³⁶ except that two cycles of pepsin column wash were used after each injection. Deuteration was measured using a time-of-flight mass spectrometer (Agilent 6220, Santa Clara, CA) equipped with a standard electrospray ionization source operated in positive mode.

3.2.11 HX-MS data processing and analysis

A combination of accurate mass measurements from time-of-flight MS and data obtained from collision induced dissociation with tandem MS on a linear quadrupole ion trap (LTQ-XL, Thermo-Scientific) was used to identify a total of 130 peptides. Identified peptides covered 94% of the primary sequence of the heavy and 93% of the light chain of mAb-C.

HDExaminer (Sierra Analytics, Modesto, CA) was used to analyze the hydrogen exchange

data. Peptide mass spectra from all three replicates of both protein concentrations were manually curated after initial processing. Deuterium uptake plots with average deuterium uptake values and standard deviations for each peptide were generated by using an R script program, written in-house.

Statistical significance was determined following the method described by Houde et al. for replicate differential hydrogen exchange data. For our triplicate measurements, the 99th percentile of the standard deviations ($s_{99\%}$) was 0.28. For differential measurements, i.e., Δm , the 99% confidence interval becomes $99\% \text{ CI} = \sqrt{s_{99\%}^2 + s_{99\%}^2}$, establishing a 99% confidence limit of ± 0.4 Da for our dataset (see supplemental Figure S3).¹³²

Hydrogen exchange data for each peptide was mapped onto a homology model of mAb-C based on human IgG b12 (PDB ID: 1HZH)²⁰⁶ developed as described previously.²⁰⁴ In some cases, peptides spanning the same region showed contradictory results: some indicated significant differences while others did not. At 99% confidence, false negatives are much more likely than false positives, peptides with significant differences “overruled” those that did not show significant differences. There were no cases where overlapping peptides indicated contradictory results (i.e. one peptide with $\Delta m > 0.4$ and an overlapping peptide with $\Delta m < -0.4$). Pymol (Schrödinger LLC, Portland, OR) was used to display the HX-MS data.

3.3 Results:

3.3.1 Defining solution conditions that favor RSA

DLS was used to measure the hydrodynamic diameter of mAb-C species under various solution conditions. Figure 1 shows the effect of protein concentration (1-10 mg/mL), pH, salt concentration, and salt type on the size of mAb-C complexes. A solution of primarily monomeric

mAb had a hydrodynamic diameter of ~9-12 nm. The hydrodynamic diameter increased with increasing protein concentration, increased solution pH (Figure 1a), and increased ionic strength (Figure 1b). In addition, mAb-C formulated in a solution containing sodium sulfate showed increased hydrodynamic diameter compared to sodium chloride (Figure 1b). These DLS results are consistent with those reported previously by Esfandiary et al. for the same antibody molecule formulated under similar solution conditions.^{76,204}

To further assess the effect of salt on reversible self-association (RSA) of mAb-C, we used chemical cross-linking to measure the effect of sulfate on the extent of RSA at pH 7. In the presence of 300 mM sodium sulfate, higher molecular weight bands at ~300 kDa and ~450 kDa were observed (Figure 2, top panels). The intensity of these bands increased as the concentration of the cross-linker was increased from 5 to 40 molar excess over mAb-C. In the absence of sodium sulfate, only a very faint band appeared at ~300 kDa and no band was observed at ~450 kDa. Similar results were obtained from reduced samples of mAb-C (Figure 2, bottom panels), where several higher molecular weight bands were observed above the heavy chain band (~50 kDa).

The DLS and cross-linking results (Figures 1 and 2) were limited to mAb-C protein concentrations of ~1-10 mg/mL because higher concentrations led to experimental variability, non-ideal behavior or experimental artifacts (data not shown). The inability of such techniques to provide reliable sizing data at higher protein concentrations is consistent with previous reports.^{1,207,208} Despite analytical limitations of DLS at higher protein concentrations, the RSA-promoting conditions identified with DLS were selected for RSA studies at high protein concentrations. In order to characterize RSA at higher mAb-C concentrations (10-60 mg/mL), we turned to a combination of solution viscosity and HX-MS measurements, as described in the following sections.

3.3.2 Solution viscosity as a function of protein concentration, temperature and salt concentration

We used solution viscosity measurements to determine the effects of sulfate concentration, and temperature on RSA of mAb-C at higher protein concentrations. The solution viscosity of mAb-C samples increased with protein concentration and was further elevated in the presence of sodium sulfate and at lower temperature (Figure 3a). For example, the solution viscosity of mAb-C at protein concentrations ranging from 5 mg/mL to 60 mg/mL at 4°C varied from 1 mPa·s to ~75 mPa·s in the presence of 300 mM sodium sulfate, and from 1 mPa·s to ~20 mPa·s in the presence of 300 mM sodium chloride. The same trends were also present at 25°C, but at lower viscosity values (Figure 3a).

Based on the combined results from the DLS, chemical-crosslinking and solution viscosity experiments, the subsequent evaluation of the effects of RSA on the local flexibility of mAb-C (as measured by HX-MS analysis) was performed under the following conditions: two protein concentrations (i.e., 5 and 60 mg/mL) were prepared in a deuterated phosphate buffer at pH 7 containing 300 mM sodium sulfate and 10% trehalose. Elevated solution pH and salt levels (and salt type) amplified the propensity of mAb-C to reversibly self-associate (as shown above) while the sugar was needed as a lyoprotectant (see below). The 5 mg/mL mAb-C was selected as a control with relatively limited RSA, whereas the 60 mg/mL mAb-C sample was chosen as a sample displaying more extensive RSA. Esfandiary et al. have recently shown that the same mAb can form a monomer-trimer-hexamer equilibrium under similar solution conditions (at 1-10 mg/mL at room temperature).²⁰⁴ Nonetheless, as shown in this work, notable differences in the extent of RSA are observed by solution viscosity and HX-MS measurements at 5 vs. 60 mg/mL of mAb-C.

3.3.3 Development of a freeze-dried formulation for HX-MS analysis of RSA

A conventional hydrogen exchange experiment typically begins with a five- to twenty-fold dilution of the protein with D₂O, but in our case, such a dilution would alter the reversible self-association of mAb-C. To maintain high protein concentration during hydrogen exchange, we developed an approach based on reconstitution of lyophilized protein with D₂O. To evaluate the effects of lyophilization and reconstitution on mAb-C we used viscosity measurements, CD, and SEC. mAb-C was prepared at concentrations between 5 and 60 mg/mL in phosphate buffer (pH 7.0) containing 10% trehalose (w/v). Samples were then freeze-dried and reconstituted and compared with samples that had not been freeze-dried.

A comparison of the solution viscosity of the reconstituted mAb-C samples with control mAb-C samples that were not lyophilized is shown in Figure 3b. There was no difference between the viscosity of the control (no freeze-drying) and lyophilized/reconstituted mAb-C samples, and no difference in the viscosity between samples reconstituted with either H₂O or D₂O at both temperatures (4°C and 25°C). These results show that the lyophilization/reconstitution of mAb-C at different protein concentrations, in either H₂O or D₂O buffers, had no significant effect on the extent of RSA of mAb-C, as measured by solution viscosity. This experimental approach thus affords the opportunity to prepare low and high protein concentration solutions of mAb-C in D₂O-containing buffers for HX-MS analysis.

To further ensure that freeze-drying had no notable effects on the overall structural integrity of mAb-C, lyophilized mAb-C samples were reconstituted with D₂O-based reconstitution buffer and analyzed by both circular dichroism (CD) and size-exclusion chromatography (SEC). Far-UV CD spectra of control and lyophilized mAb-C samples are indistinguishable with minima at 217

nm (Figure 4), characteristic of the high beta sheet content of IgG domains. This result indicates that lyophilization followed by reconstitution did not induce any changes in the overall secondary structure content of mAb-C.

The aggregate content of the same samples was measured by SEC (Table 1). The amount of soluble aggregates and fragments present in the mAb-C samples did not change after lyophilization, but the amount of insoluble aggregates (loss of total area by SEC) after reconstitution was somewhat higher (2.1-2.7%) compared to control samples. Based on these results, the small amount of aggregate was removed by centrifugation prior to HX-MS experiments (see Methods). In addition, the overall structural integrity of mAb-C before and after lyophilization and reconstitution was further confirmed by HX-MS analysis as described below. These results indicate that lyophilization followed by reconstitution did not induce significant aggregation.

3.3.4 Effects of reversible self-association (RSA) on hydrogen exchange of mAb-C

The RSA of mAb-C was analyzed by HX-MS by reconstituting 5 and 60 mg/mL lyophilized mAb-C preparations with a D₂O-based reconstitution/labeling buffer. Samples were incubated in D₂O for varying periods of time, quenched, digested with pepsin, and the deuterium uptake in pepsin-generated peptides of mAb-C was measured by MS (see Methods). A total of 130 mAb-C peptides were reproducibly generated by pepsin digestion, resulting in sequence coverage of 94% for the heavy chain and 93% for the light chain of mAb-C (see Supplemental Figure S1). Figure 5 shows representative deuterium uptake results for several different peptides as a function of hydrogen exchange labeling time. Figure 5A presents results from some representative mAb-C peptides that show no significant differences in hydrogen exchange kinetics between RSA and non-RSA mAb-C. In contrast, Figure 5B contains examples where RSA induced significant

differences in hydrogen exchange kinetics: RSA caused both faster and slower hydrogen exchange in different regions of mAb-C. As discussed in more detail below, for approximately 90% of the peptides, however, there were no significant differences in deuterium uptake between RSA and non-RSA mAb-C based on our significance criteria (see Methods).

Figure 6 presents a global view of these data by presenting the hydrogen exchange differences across the 130 peptides generated in a single plot. The differences in hydrogen exchange between mAb-C samples at 60 mg/mL and 5 mg/mL [$\Delta m(t) = m_{60}(t) - m_5(t)$] are plotted on the vertical axis. The individual peptides are arranged on the horizontal axis starting from the N-terminal of the heavy chain and ending at the C-terminal of the light chain. The peptides are numbered sequentially based on the locations of their middle residues (see Supplemental Table S1 for the identities and locations of the peptides). The domain locations are indicated by labels and alternate shading in white and grey. These plots efficiently display the trends in local flexibility changes between the RSA and non-RSA mAb-C. The direction of the bar indicates whether an individual peptide becomes more flexible ($\Delta m(t) > 0$ Da) or less flexible ($\Delta m(t) < 0$ Da) upon RSA. The dashed lines in figure 6 indicate $\Delta m(t)$ values that exceed the 99% confidence limit of ± 0.4 Da for statistically significant changes induced by RSA (see Methods).

The results in Figure 6 reveal differences in hydrogen exchange in mAb-C at high vs. low concentrations of mAb-C, conditions shown to affect the RSA of the antibody. Most of the mAb-C peptides (>90%) show no significant differences in hydrogen exchange. The specific peptides of mAb-C that display significant decreases in hydrogen exchange ($\Delta m(t) < 0.4$ Da) at high vs. low concentrations of mAb-C are located in V_H and V_L domains, primarily in sequences that

include the CDR2H and CDR2L. For example, in the V_H domain, there is a 26 amino acid sequence (HWVRQAPGQGLEWMGWINPHSGGTNY) that spans the CDR2H sequence of mAb-C and is covered by three V_H domain peptides (peptide numbers 10, 13 and 18 corresponding to HC 35-59, HC 45-59 and HC 50-60, respectively). These three peptides display significant decreases in hydrogen exchange at the 120 s time point. The magnitude of these effects is small, $|\Delta m| < 0.5$ Da. In the V_L domain, there is a 36 amino acid sequence covering LC 36-71 (YQQKPGKAPKLLIYVASSLQSGVPSRFSGSGSGTDF), corresponding to peptide numbers 100, 101, 102, 103, 104, 105 and 106, where significant decreases in hydrogen exchange in high vs. low concentrations of mAb-C were also observed. These seven peptides showed differences across all of the deuterium exposure time points. In the light chain, the magnitudes of the effects, $|\Delta m| > 0.7$ Da, are much larger than the effects in the heavy chain. The LC 36-71 sequence in the V_L domain spans the CDR2L sequence of mAb-C. In summary, significant decreases in hydrogen exchange (i.e., increased protection against deuterium uptake) were observed upon RSA of mAb-C in two of the six CDR regions in the mAb (i.e., the CDR2 region of the heavy and light chain).

Interestingly, several other peptide segments from mAb-C concomitantly displayed the opposite effect: increased local flexibility ($\Delta m(t) > 0.4$ Da) at the higher (vs. lower) mAb-C concentration (Figure 6). For example, two peptides in the V_H domain covering HC 4-29 (GAEVKKPGASVKVSCASGYTF, corresponding to peptide number 3 and 4) showed this trend. In addition, in comparing the 60 mg/mL vs. 5 mg/mL samples of mAb-C, two peptide segments located in the interface of C_{H1} and C_{H2} domains covering HC 229-252 (DKTHTCPPCPAPPELLGGPSVFLFPPK, corresponding to peptide number 48 and 49) as well as one C_{H2} domain peptide covering HC 311-325 (VSVLTVLHQDWLNGK, corresponding to peptide 64) also showed significant increases in deuterium uptake at one or more time points.

Figure 7 further summarizes these HX-MS results as mapped onto a homology model of mAb-C (Figure 7a shows the entire mAb-C molecule and Figure 7b displays a close-up view of the CDR2 regions within the Fab domain). The peptide segments in mAb-C where RSA caused significant decreases in hydrogen exchange ($\Delta m(t) < -0.4$ Da) are colored blue, while regions that exhibited significant increases ($\Delta m(t) > 0.4$ Da) are colored yellow. The regions of mAb-C without significant effects ($|\Delta m(t)| \leq 0.4$ Da) are colored in grey and regions of mAb-C lacking hydrogen exchange data are shown in white. The peptides that exhibited decreased hydrogen exchange at high vs. low mAb-C concentration constitute the primary protein-protein interface for RSA of mAb-C. The peptide segments showing increased local flexibility may indicate long-range dynamic coupling effects of RSA in mAb-C (see Discussion).

Finally, to further confirm that the lyophilization/reconstitution method did not adversely affect the structural integrity of mAb-C, we measured hydrogen exchange kinetics before and after lyophilization at two protein concentrations (6 and 60 mg/mL) in a subset of 35 peptides covering all domains of mAb-C and including all peptides that had significant differences in local flexibility caused by RSA (Figure 6). There were no significant differences in hydrogen exchange kinetics between lyophilized and control mAb-C samples at either protein concentration (see Supplemental Figures S4 and S5).

3.4 Discussion

The main aim of this study was to develop an HX-MS method to characterize the protein interfaces involved with the reversible self-association (RSA) of mAb-C directly at high protein concentrations (i.e., 60 mg/mL). Commonly available biophysical measurements used to monitor

RSA not only lack such local sequence information, but can only be performed at lower protein concentrations (~10 mg/ml) due to solution non-ideality (see Introduction). These analytical limitations were encountered with DLS and SV-AUC measurements of mAb-C under different solution conditions as described in this work and as reported previously.^{76,204} In the present study, we correlate solution effects on the RSA of mAb-C, as determined by DLS and chemical crosslinking at lower mAb-C concentrations, to solution viscosity measurements at higher protein concentrations. We then directly mapped the local regions of mAb-C involved at the interface of RSA at the higher protein concentration using HX-MS, an analytical tool that has been widely used to map interfaces of protein-protein interactions.²⁰⁹⁻²¹¹

3.4.1 Effect of solution conditions on RSA of mAb-C

As an initial evaluation of the RSA of mAb-C, we employed DLS and chemical crosslinking. There was a measurable increase in the RSA of mAb-C with increasing protein concentration, solution pH, and ionic strength (Figures 1 and 2). These results are consistent with trends previously reported for the RSA of mAb-C at low protein concentrations by DLS, SV-AUC and CG-MALS.⁷⁶ Many of these same trends were apparent at higher protein concentrations, as revealed by changes in viscosity, where an exponential increase in viscosity was observed ranging from ~1 to ~75 mPa·s depending on the protein concentration and solution conditions (Figure 3). Increases in intermolecular associations between antibody molecules at high protein concentrations have been previously correlated to elevated solution viscosity values.^{13,212} This effect can be attributed to the antibody network formation at high protein concentration, which affects the packing volume fraction of the antibody and ultimately results in an increase in solution viscosity.⁸⁰ For example, Pathak et al. demonstrated that the presence of reversibly associated

clusters at high protein concentrations contributed to an increase in solution viscosity.²¹³

Similar trends in viscosity in response to changes in solution conditions that we describe here for mAb-C have been reported for other IgG1 mAbs, where the extent of viscosity increased in a concentration-dependent manner with increasing ionic strength^{76,79,81,214,215} and solution pH,^{60,76} related to elevated levels of protein RSA due to charge shielding effects.^{99,216,217} The isoelectric point (pI) range of mAb-C is basic (pI~9.1-9.4),²⁰⁴ and therefore, the overall surface charge of mAb-C is expected to be positive at neutral pH. As the pH was changed from 6 to 8, the tendency of mAb-C to self-associate increased possibly due to overall decrease in electrostatic repulsive interactions. In addition, more specific charge effects are possible, including protonation/deprotonation of histidine (His) residues upon a change in solution pH in the range of the pKa (~ pH 6). From our present work, there are two histidine residues in the 26 amino acid sequence covering the CDR2H region (HWVRQAPGQGLEWMGWINPHSGGTNY) that showed significantly decreased hydrogen exchange upon RSA of mAb-C. The probable involvement of His side chain residues in the RSA of this mAb was demonstrated indirectly by DLS studies (vs. solution pH and composition) as reported recently.^{76,204} The homology model indicates that one of these histidines is highly solvent exposed (see Figure 7c).

As electrostatic repulsive interactions decrease when solution pH approaches pI, other non-covalent attractive interactions such as hydrophobic and van der Waals interactions are expected to become more dominant allowing mAb-C monomers to self-associate to a greater extent. To further explore the effects of two anions, sulfate and chloride, on the extent of RSA of mAb-C, both hydrodynamic diameter and solution viscosity of mAb-C samples were measured in the presence of both the anions. Sulfate had a bigger effect on the extent of RSA of mAb-C than chloride (Figures 1b and 3a). In terms of ranking in the Hofmeister series of anions, divalent sulfate

anions have a stronger kosmotropic effect on proteins than monovalent chloride ions.²¹⁸ Sulfate ions interact more strongly with the positively charged amino acid side chains on a protein surface than chloride ions,^{219,220} presumably resulting in enhanced charge shielding effects. Sulfate ions can also desolvate polar and non-polar regions of the protein surface, thus aggravating hydrophobic interactions by decreasing protein solubility, an effect commonly known as “salting out”.^{221,222} These ion-protein interactions correlate well with our observations of enhanced RSA of mAb-C in the presence of sulfate anions. Esfandiary et al. demonstrated by modeling of light scattering data that mAb-C formulated in the presence of 150 mM sodium sulfate at room temperature can assemble into monomer-trimer-hexamer mixtures, ranging from 100% monomer to ~ 75%-20%-5% molar ratios, as the protein concentration increases from 1 to 10 mg/mL.^{76,204}

3.4.2 Development of an HX-MS method to examine RSA

In most HX-MS studies on protein-protein interactions, the interactions are typically non-reversible or have relatively high affinity; therefore, HX-MS experiments can easily be carried out at low protein concentrations after dilution of protein stock solutions with deuterium containing buffers. In contrast, RSA is a concentration-driven phenomenon. In order to study RSA of mAbs, HX-MS experiments need to be performed at high protein concentrations requiring a novel methodology to prepare high protein concentrations in deuterium containing buffers. To this end, antibody solutions under RSA-promoting solution conditions at high and low protein concentration were lyophilized and reconstituted with a D₂O based labeling/ reconstitution buffer.

Lyophilization of proteins can cause detrimental effects on physical stability through ice crystal-water interfaces, cold-denaturation, solution pH change during lyophilization, and dehydration stress.^{223,224} We used a combination of CD and SEC analysis to demonstrate that the

lyophilization process itself did not lead to structural alterations or aggregation of mAb-C (Figure 4 and Table 1). In addition, based on hydrogen exchange measurements of 35 key peptides from mAb-C (Supplemental Figure S4 and S5), we can conclude that lyophilization followed by reconstitution did not cause any significant changes in the local flexibility across the mAb-C molecule (Supplemental Figure S3). These results illustrate a potential new pharmaceutical application of HX-MS: evaluations of the structural integrity of protein samples before and after lyophilization and reconstitution. These results also demonstrate the reproducibility achievable with this lyophilization/reconstitution HX-MS approach.

3.4.3 HX-MS mapping of the protein interface of RSA of mAb-C

From the HX-MS analysis of mAb-C at low and high protein concentrations (Figures 5 and 6), peptides with increased protection against deuterium uptake (i.e., slowed hydrogen exchange) at high mAb-C concentration are assigned as the primary interface for RSA of mAb-C. Two regions in V_L and V_H (LC 36-71 and HC 35-60) showed a significant decrease in hydrogen exchange at high mAb-C concentration. Both of these regions cover the CDR2 region in the heavy and light chain of mAb-C, respectively, which demonstrates two of the six CDRs in mAb-C are involved with RSA. The involvement of CDR regions, including specific aromatic/hydrophobic residues, in RSA of antibodies has been reported in previous studies with other antibodies.^{183,225,226}

More specifically with mAb-C, LC 36-71 and HC 35-60, which span CDR2L and CDR2H, respectively, showed significant decreases in hydrogen exchange under RSA-promoting conditions (Figure 7). This result indicates that the amino acid residues encompassing the CDR2 sequence within the Fab region of mAb-C provide an interface for RSA at high protein concentrations. More specifically, protection in the light chain was detected in seven overlapping

peptides spanning CDR2L in the V_L domain of mAb-C, LC 36-71 (YQQKPGKAPKLLIYVASSLQSGVPSRFSGSGSGTDF). In the heavy chain, protection was detected in two peptides spanning CDR2H in the V_H domain, for HC 35-60 (HWVRQAPGQGLEWMGWINPHSGGTNY). CDR loops are naturally hypervariable, provide a unique identity to each mAb, and are solvent exposed for high affinity binding to the antigen. The sequences that became significantly protected at 60 mg/mL (i.e., upon more extensive RSA of mAb-C) contain numerous aromatic/hydrophobic residues. The LC36-71 sequence contains four aromatic residues (Y and F) and six aliphatic residues (I, L, V) and the HC 35-60 sequence has four aromatic (Y and W) and three aliphatic residues (I, L, V). In addition, some of the peptide segments covering these sequences also contain histidine as well as charged amino acid residues at pH 7. Since the addition of 300 mM sodium sulfate promotes the RSA of mAb-C, the charged residues may become more shielded or charge-neutralized by sulfate binding. Upon such reduced electrostatic repulsive interactions, the presence of aromatic and hydrophobic residues can potentially facilitate RSA of mAb-C at high protein concentrations. Protection from hydrogen exchange in the V_L segment is stronger than in the V_H segment suggesting that there is higher affinity in the V_L segment.

To the best of our knowledge, this is the first study that utilizes HX-MS to characterize RSA of antibodies at peptide-level resolution directly at high protein concentrations. Several research groups have made observations using lower resolution biophysical tools to identify specific regions in an antibody associated with RSA. For example, Kanai et al. measured solution viscosity of purified $F(ab')_2$ and Fab fragments of a self-associating IgG1 mAb and concluded that the interface of RSA for an IgG1 mAb was in the Fab region.¹⁴ Yadav et al. swapped charged residues in the CDR region of a self-associating IgG1 mAb with those of a non-self-associating

antibody and observed a significant decrease in solution viscosity and weight average molecular weight (M_{wc}).¹⁶ Using these same mutants, the authors of a separate study used coarse-grain modeling to link domain-level charge distribution in the Fab region of the antibody to RSA.²²⁷ In another study, substitution of aromatic residues with non-aromatic amino acids (F99A, W100A) in the CDR3H region of the antibody caused a considerable decrease in RSA and an increase in protein solubility.^{183,226} However, Fab-Fab interactions are not necessarily always responsible for such interactions between antibody molecules. For example, Nishi et al. reported that the Fc-mediated RSA of an antibody under low ionic strength solution conditions.¹⁸²

Several groups have examined protein-protein interfaces of irreversible antibody aggregates (i.e., dimers and oligomers) by HX-MS. For example, Zhang et al. used HX-MS analysis of purified mAb aggregates to show that Fab-Fab interactions in the CDR region were generated as part of *irreversible* aggregate formation caused by heat exposure.²⁰⁰ In addition to HX-MS, antibody aggregates have been characterized using other higher resolution techniques. For example, Deperalta et al. used hydroxyl radical footprinting to map the interface region of an antibody dimer. This work demonstrated that the protein-protein interface lies in the Fab domain of the antibody.²²⁸ Using alternative approaches, Paul et al. used transmission electron microscopy to visualize purified antibody dimers and suggested Fab-Fab interactions were responsible for association.²²⁹ Wang et al. used computational predictive tools to delineate aggregation-prone regions in variable domains of an antibody are located in or around the CDR region.¹⁵² A recent study by Iacob et al. showed that irreversible antibody aggregation can affect the flexibility of the mAb's hinge loop region. They demonstrated decreased local backbone flexibility in the hinge region upon formation of a disulfide cross-linked mAb dimer.²³⁰ Interestingly, as discussed below,

the opposite effect (i.e., increased backbone flexibility in several regions including the hinge loop) was observed in our present work upon RSA of mAb-C.

3.4.4 HX-MS mapping of distant dynamic effects on other regions of mAb-C upon RSA

We also observed a significant increase in hydrogen exchange in regions in mAb-C that are distant from the RSA protein-protein interaction site described above (see Figure 6 and 7). These changes were observed in regions covering HC 4-29 (V_H domain, peptide number 2 and 3), HC 229-252 (C_{H1} - C_{H2} interface, peptide number 48 and 49) and HC 311-325 (C_{H2} domain, peptide number 64). Among these changes, an increase in local flexibility at the hinge region (C_{H1} - C_{H2} interface) of the antibody had the largest magnitude. One way to explain this significant increase in local backbone flexibility in the hinge region is through long-range, distant dynamic coupling effects that may occur upon protein-protein interactions.

In biological systems, protein allosteric effects play a major role in cellular regulation. The classical model of allosteric conformational effects constitute binding of a ligand to a region or domain of a protein and its effect on conformation of a distal, functional region of the protein.^{231,232} An emerging view of protein allostery includes a dynamic continuum in which protein-protein or protein-ligand interactions result in propagation of a signal through changes in protein dynamics, either with or without large scale conformational changes.^{231,232} Such alterations in protein dynamics as part of allosteric regulation of proteins are sometimes referred to as propagation of an “allosteric wave”.²³³ Examples of such flexibility shifts within single protein molecule upon ligand binding or protein-protein interaction have been reported.^{234,235} Such changes in protein dynamic allostery can also occur upon post-translational modifications, or upon changes in solution pH or protein concentration.²³³

Although the distant dynamic coupling effects we observed within the mAb-C upon extensive RSA may lack any biological consequences, the molecular mechanism of alterations in local backbone flexibility upon protein-protein interactions are “allosteric-like” in that they resemble the molecular mechanisms of protein dynamic allostery.^{231,232,236} The observed localized changes in backbone dynamics upon RSA may potentially have important implications in terms of pharmaceutical properties of a mAb including storage stability, manufacturability, and syringeability. Since HX-MS provides increased resolution for characterizing RSA directly at high protein concentrations, this information could be used to design superior next-generation mAb molecules with lower propensity for RSA. In terms of future work, further establishing the universality of such behavior among self-associating mAbs is being evaluated in our laboratories with a series of mAbs that reversibly self-associate to varying extents.

3.5 References:

1. Scolnik PA. mAbs: a business perspective. *MAbs*: Landes Bioscience, 2009:179.
2. Shire SJ, Shahrokh Z, Liu J. Challenges in the development of high protein concentration formulations. *Journal of pharmaceutical sciences* 2004; 93:1390-402.
3. Minton AP. The influence of macromolecular crowding and macromolecular confinement on biochemical reactions in physiological media. *Journal of biological chemistry* 2001; 276:10577-80.
4. Minton AP. Implications of macromolecular crowding for protein assembly. *Current opinion in structural biology* 2000; 10:34-9.
5. Liu J, Nguyen MD, Andya JD, Shire SJ. Reversible self-association increases the viscosity of a concentrated monoclonal antibody in aqueous solution. *Journal of pharmaceutical sciences* 2005; 94:1928-40.
6. Kanai S, Liu J, Patapoff TW, Shire SJ. Reversible self-association of a concentrated monoclonal antibody solution mediated by Fab–Fab interaction that impacts solution viscosity. *Journal of pharmaceutical sciences* 2008; 97:4219-27.
7. Yadav S, Sreedhara A, Kanai S, Liu J, Lien S, Lowman H, Kalonia DS, Shire SJ. Establishing a link between amino acid sequences and self-associating and viscoelastic behavior of two closely related monoclonal antibodies. *Pharmaceutical research* 2011; 28:1750-64.
8. Philo JS, Arakawa T. Mechanisms of protein aggregation. *Current pharmaceutical biotechnology* 2009; 10:348-51.
9. Saluja A, Kalonia DS. Nature and consequences of protein–protein interactions in high protein concentration solutions. *International journal of pharmaceutics* 2008; 358:1-15.

10. Connolly BD, Petry C, Yadav S, Demeule B, Ciaccio N, Moore JM, Shire SJ, Gokarn YR. Weak interactions govern the viscosity of concentrated antibody solutions: high-throughput analysis using the diffusion interaction parameter. *Biophysical journal* 2012; 103:69-78.
11. Esfandiary R, Hayes DB, Parupudi A, Casas-Finet J, Bai S, Samra HS, Shah AU, Sathish HA. A systematic multitechnique approach for detection and characterization of reversible self-association during formulation development of therapeutic antibodies. *Journal of pharmaceutical sciences* 2013; 102:3089-99.
12. Mason BD, Zhang L, Remmele RL, Zhang J. Opalescence of an IgG2 monoclonal antibody solution as it relates to liquid–liquid phase separation. *Journal of pharmaceutical sciences* 2011; 100:4587-96.
13. Nishi H, Miyajima M, Nakagami H, Noda M, Uchiyama S, Fukui K. Phase separation of an IgG1 antibody solution under a low ionic strength condition. *Pharmaceutical research* 2010; 27:1348-60.
14. Thomas C, Nienow A, Dunnill P. Action of shear on enzymes: studies with alcohol dehydrogenase. *Biotechnology and bioengineering* 1979; 21:2263-78.
15. Nishi H, Miyajima M, Wakiyama N, Kubota K, Hasegawa J, Uchiyama S, Fukui K. Fc domain mediated self-association of an IgG1 monoclonal antibody under a low ionic strength condition. *Journal of bioscience and bioengineering* 2011; 112:326-32.
16. Bethea D, Wu S-J, Luo J, Hyun L, Lacy ER, Teplyakov A, Jacobs SA, O'Neil KT, Gilliland GL, Feng Y. Mechanisms of self-association of a human monoclonal antibody CNTO607. *Protein Engineering Design and Selection* 2012:gzs047.

17. Li L, Kumar S, Buck PM, Burns C, Lavoie J, Singh SK, Warne NW, Nichols P, Luksha N, Boardman D. Concentration Dependent Viscosity of Monoclonal Antibody Solutions: Explaining Experimental Behavior in Terms of Molecular Properties. *Pharmaceutical Research* 2014;1-18.
18. Yadav S, Shire SJ, Kalonia DS. Factors affecting the viscosity in high concentration solutions of different monoclonal antibodies. *Journal of pharmaceutical sciences* 2010; 99:4812-29.
19. Sule SV, Cheung JK, Antochshuk V, Bhalla AS, Narasimhan C, Blaisdell S, Shameem M, Tessier PM. Solution pH that minimizes self-association of three monoclonal antibodies is strongly dependent on ionic strength. *Molecular pharmaceutics* 2012; 9:744-51.
20. Attri AK, Minton AP. Composition gradient static light scattering: a new technique for rapid detection and quantitative characterization of reversible macromolecular hetero-associations in solution. *Analytical biochemistry* 2005; 346:132-8.
21. Geng SB, Cheung JK, Narasimhan C, Shameem M, Tessier PM. Improving Monoclonal Antibody Selection and Engineering using Measurements of Colloidal Protein Interactions. *Journal of pharmaceutical sciences* 2014; 103:3356-63.
22. Ney A, Booms P, Epple G, Mörgelin M, Guo G, Kettelgerdes G, Geßner R, Robinson PN. Calcium-dependent self-association of the C-type lectin domain of versican. *The international journal of biochemistry & cell biology* 2006; 38:23-9.
23. Snoussi K, Halle B. Protein self-association induced by macromolecular crowding: a quantitative analysis by magnetic relaxation dispersion. *Biophysical journal* 2005; 88:2855-66.
24. Gottschalk M, Venu K, Halle B. Protein self-association in solution: the bovine pancreatic trypsin inhibitor decamer. *Biophysical journal* 2003; 84:3941-58.

25. Hassiepen U, Federwisch M, Mülders T, Lenz VJ, Gattner HG, Krüger P, Wollmer A. Analysis of protein self-association at constant concentration by fluorescence-energy transfer. *European Journal of Biochemistry* 1998; 255:580-7.
26. Chitta RK, Gross ML. Electrospray ionization-mass spectrometry and tandem mass spectrometry reveal self-association and metal-ion binding of hydrophobic peptides: a study of the gramicidin dimer. *Biophysical journal* 2004; 86:473-9.
27. Sule SV, Sukumar M, Weiss IV WF, Marcelino-Cruz AM, Sample T, Tessier PM. High-throughput analysis of concentration-dependent antibody self-association. *Biophysical journal* 2011; 101:1749-57.
28. Bajaj H, Sharma VK, Kalonia DS. A high-throughput method for detection of protein self-association and second virial coefficient using size-exclusion chromatography through simultaneous measurement of concentration and scattered light intensity. *Pharmaceutical research* 2007; 24:2071-83.
29. Howlett GJ, Minton AP, Rivas G. Analytical ultracentrifugation for the study of protein association and assembly. *Current opinion in chemical biology* 2006; 10:430-6.
30. Lilyestrom WG, Yadav S, Shire SJ, Scherer TM. Monoclonal antibody self-association, cluster formation, and rheology at high concentrations. *The Journal of Physical Chemistry B* 2013; 117:6373-84.
31. Ido S, Kimiya H, Kobayashi K, Kominami H, Matsushige K, Yamada H. Immunoactive two-dimensional self-assembly of monoclonal antibodies in aqueous solution revealed by atomic force microscopy. *Nat Mater* 2014; 13:264-70.
32. Pine D, Weitz D, Zhu J, Herbolzheimer E. Diffusing-wave spectroscopy: dynamic light scattering in the multiple scattering limit. *Journal de Physique* 1990; 51:2101-27.

33. Ross PD, Minton AP. Analysis of non-ideal behavior in concentrated hemoglobin solutions. *Journal of molecular biology* 1977; 112:437-52.
34. Engen JR. Analysis of protein conformation and dynamics by hydrogen/deuterium exchange MS. *Analytical chemistry* 2009; 81:7870-5.
35. Percy AJ, Rey M, Burns KM, Schriemer DC. Probing protein interactions with hydrogen/deuterium exchange and mass spectrometry—a review. *Analytica chimica acta* 2012; 721:7-21.
36. Majumdar R, Middaugh CR, Weis DD, Volkin DB. Hydrogen–Deuterium Exchange Mass Spectrometry as an Emerging Analytical Tool for Stabilization and Formulation Development of Therapeutic Monoclonal Antibodies. *Journal of pharmaceutical sciences* 2014.
37. Majumdar R, Manikwar P, Hickey JM, Samra HS, Sathish HA, Bishop SM, Middaugh CR, Volkin DB, Weis DD. Effects of salts from the Hofmeister series on the conformational stability, aggregation propensity, and local flexibility of an IgG1 monoclonal antibody. *Biochemistry* 2013; 52:3376-89.
38. Manikwar P, Majumdar R, Hickey JM, Thakkar SV, Samra HS, Sathish HA, Bishop SM, Middaugh CR, Weis DD, Volkin DB. Correlating excipient effects on conformational and storage stability of an IgG1 monoclonal antibody with local dynamics as measured by hydrogen/deuterium-exchange mass spectrometry. *Journal of pharmaceutical sciences* 2013; 102:2136-51.
39. Zhang A, Qi W, Singh SK, Fernandez EJ. A new approach to explore the impact of freeze-thaw cycling on protein structure: hydrogen/deuterium exchange mass spectrometry (HX-MS). *Pharmaceutical research* 2011; 28:1179-93.

40. Burkitt W, Domann P, O'Connor G. Conformational changes in oxidatively stressed monoclonal antibodies studied by hydrogen exchange mass spectrometry. *Protein Science* 2010; 19:826-35.
41. Hsieh M-C. Conformational characterization of the charge variants of a human IgG1 monoclonal antibody using H/D exchange mass spectrometry. 2012.
42. Pan LY, Salas-Solano O, Valliere-Douglass JF. Conformation and Dynamics of Interchain Cysteine-Linked Antibody-Drug Conjugates as Revealed by Hydrogen/Deuterium Exchange Mass Spectrometry. *Analytical chemistry* 2014; 86:2657-64.
43. Houde D, Peng Y, Berkowitz SA, Engen JR. Post-translational modifications differentially affect IgG1 conformation and receptor binding. *Molecular & Cellular Proteomics* 2010; 9:1716-28.
44. Majumdar R, Esfandiary R, Bishop SM, Samra HS, Middaugh CR, Volkin DB, Weis DD. Correlations between changes in conformational dynamics and physical stability in a mutant IgG1 mAb engineered for extended serum half-life. *mAbs* in press.
45. Esfandiary R, Parupudi A, Casas-Finet J, Gadre D, Sathish H. Mechanism of Reversible Self-Association of a Monoclonal Antibody: Role of Electrostatic and Hydrophobic Interactions. *J Pharm Sci* 2014.
46. Cromwell ME, Felten C, Flores H, Liu J, Shire SJ. Self-association of therapeutic proteins. *Misbehaving Proteins: Springer*, 2006:313-30.
47. Saluja A, Badkar AV, Zeng DL, Nema S, Kalonia DS. Ultrasonic storage modulus as a novel parameter for analyzing protein-protein interactions in high protein concentration solutions: correlation with static and dynamic light scattering measurements. *Biophysical journal* 2007; 92:234-44.

48. Mandell JG, Falick AM, Komives EA. Identification of protein–protein interfaces by decreased amide proton solvent accessibility. *Proceedings of the National Academy of Sciences* 1998; 95:14705-10.
49. Hamuro Y, Anand GS, Kim JS, Juliano C, Stranz DD, Taylor SS, Woods Jr VL. Mapping intersubunit interactions of the regulatory subunit (RI α) in the type I holoenzyme of protein kinase A by amide hydrogen/deuterium exchange mass spectrometry (DXMS). *Journal of molecular biology* 2004; 340:1185-96.
50. Robinson CV, Chung EW, Kragelund BB, Knudsen J, Aplin RT, Poulsen FM, Dobson CM. Probing the nature of noncovalent interactions by mass spectrometry. A study of protein-CoA ligand binding and assembly. *Journal of the American Chemical Society* 1996; 118:8646-53.
51. Yadav S, Laue TM, Kalonia DS, Singh SN, Shire SJ. The influence of charge distribution on self-association and viscosity behavior of monoclonal antibody solutions. *Mol Pharm* 2012; 9:791-802.
52. Pathak JA, Sologuren RR, Narwal R. Do clustering monoclonal antibody solutions really have a concentration dependence of viscosity? *Biophysical journal* 2013; 104:913-23.
53. Velev O, Kaler E, Lenhoff A. Protein interactions in solution characterized by light and neutron scattering: comparison of lysozyme and chymotrypsinogen. *Biophysical journal* 1998; 75:2682-97.
54. Rosenbaum D, Zukoski C. Protein interactions and crystallization. *Journal of crystal growth* 1996; 169:752-8.
55. Sahin E, Grillo AO, Perkins MD, Roberts CJ. Comparative effects of pH and ionic strength on protein–protein interactions, unfolding, and aggregation for IgG1 antibodies. *Journal of pharmaceutical sciences* 2010; 99:4830-48.

56. Lehermayr C, Mahler HC, Mäder K, Fischer S. Assessment of net charge and protein–protein interactions of different monoclonal antibodies. *Journal of pharmaceutical sciences* 2011; 100:2551-62.
57. Chari R, Jerath K, Badkar AV, Kalonia DS. Long-and short-range electrostatic interactions affect the rheology of highly concentrated antibody solutions. *Pharmaceutical research* 2009; 26:2607-18.
58. Zhang F, Skoda MW, Jacobs RM, Martin RA, Martin CM, Schreiber F. Protein interactions studied by SAXS: effect of ionic strength and protein concentration for BSA in aqueous solutions. *The Journal of Physical Chemistry B* 2007; 111:251-9.
59. Cacace MG, Landau EM, Ramsden JJ. The Hofmeister series: salt and solvent effects on interfacial phenomena. *Quarterly reviews of biophysics* 1997; 30:241-77.
60. Wernersson E, Heyda J, Kubíčková A, Křížek Ts, Coufal P, Jungwirth P. Effect of association with sulfate on the electrophoretic mobility of polyarginine and polylysine. *The Journal of Physical Chemistry B* 2010; 114:11934-41.
61. Zhang L, Zhang J. Specific Ion–Protein Interactions Dictate Solubility Behavior of a Monoclonal Antibody at Low Salt Concentrations. *Molecular pharmaceutics* 2012; 9:2582-90.
62. Baldwin RL. How Hofmeister ion interactions affect protein stability. *Biophysical Journal* 1996; 71:2056-63.
63. Von Hippel PH, Schleich T. Ion effects on the solution structure of biological macromolecules. *Accounts of Chemical Research* 1969; 2:257-65.
64. Carpenter J, Arakawa T, Crowe J. Interactions of stabilizing additives with proteins during freeze-thawing and freeze-drying. *Developments in biological standardization* 1991; 74:225-38; discussion 38-9.

65. Tang XC, Pikal MJ. The effect of stabilizers and denaturants on the cold denaturation temperatures of proteins and implications for freeze-drying. *Pharmaceutical research* 2005; 22:1167-75.
66. Perchiacca JM, Ladiwala ARA, Bhattacharya M, Tessier PM. Aggregation-resistant domain antibodies engineered with charged mutations near the edges of the complementarity-determining regions. *Protein Engineering Design and Selection* 2012; 25:591-602.
67. Wu S-J, Luo J, O'Neil KT, Kang J, Lacy ER, Canziani G, Baker A, Huang M, Tang QM, Raju TS. Structure-based engineering of a monoclonal antibody for improved solubility. *Protein Engineering Design and Selection* 2010; 23:643-51.
68. Chaudhri A, Zarraga IE, Yadav S, Patapoff TW, Shire SJ, Voth GA. The role of amino acid sequence in the self-association of therapeutic monoclonal antibodies: insights from coarse-grained modeling. *The Journal of Physical Chemistry B* 2013; 117:1269-79.
69. Deperalta G, Alvarez M, Bechtel C, Dong K, McDonald R, Ling V. Structural analysis of a therapeutic monoclonal antibody dimer by hydroxyl radical footprinting. *MAbs*, 2013:86-101.
70. Paul R, Graff-Meyer A, Stahlberg H, Lauer ME, Rufer AC, Beck H, Briguet A, Schnaible V, Buckel T, Boeckle S. Structure and function of purified monoclonal antibody dimers induced by different stress conditions. *Pharmaceutical research* 2012; 29:2047-59.
71. Wang X, Das TK, Singh SK, Kumar S. Potential aggregation prone regions in biotherapeutics: A survey of commercial monoclonal antibodies. *MAbs: Landes Bioscience*, 2009:254.
72. Iacob RE, Bou-Assaf GM, Makowski L, Engen JR, Berkowitz SA, Houde D. Investigating Monoclonal Antibody Aggregation Using a Combination of H/DX-MS and Other Biophysical Measurements. *Journal of pharmaceutical sciences* 2013; 102:4315-29.

73. Motlagh HN, Wrabl JO, Li J, Hilser VJ. The ensemble nature of allostery. *Nature* 2014; 508:331-9.
74. Tsai C-J, Nussinov R. A Unified View of “How Allostery Works”. *PLoS computational biology* 2014; 10:e1003394.
75. Nussinov R, Tsai C-J. Allostery in disease and in drug discovery. *Cell* 2013; 153:293-305.
76. Bennett MJ, Barakat K, Huzil JT, Tuszynski J, Schriemer DC. Discovery and characterization of the laulimalide-microtubule binding mode by mass shift perturbation mapping. *Chemistry & biology* 2010; 17:725-34.
77. Shi J, Koeppe JR, Komives EA, Taylor P. Ligand-induced conformational changes in the acetylcholine-binding protein analyzed by hydrogen-deuterium exchange mass spectrometry. *The Journal of biological chemistry* 2006; 281:12170-7.
78. Tompa P. Multiteric regulation by structural disorder in modular signaling proteins: an extension of the concept of allostery. *Chemical reviews* 2014.
79. Glasoe PK, Long FA. Use of glass electrodes to measure acidities in deuterium oxide. *Journal of Physical Chemistry* 1960; 64:188-90.
80. Majumdar R, Manikwar P, Hickey JM, Arora J, Middaugh CR, Volkin DB, Weis DD. Minimizing carry-over in an online pepsin digestion system used for the H/D exchange mass spectrometric analysis of an IgG1 monoclonal antibody. *Journal of the American Society for Mass Spectrometry* 2012; 23:2140-8.
81. Houde D, Berkowitz SA, Engen JR. The utility of hydrogen/deuterium exchange mass spectrometry in biopharmaceutical comparability studies. *Journal of pharmaceutical sciences* 2011; 100:2071-86.

82. Saphire EO, Parren PWHI, Pantophlet R, Zwick MB, Morris GM, Rudd PM, Dwek RA, Stanfield RL, Burton DR, Wilson IA. Crystal Structure of a Neutralizing Human IgG Against HIV-1: A Template for Vaccine Design. *Science* 2001; 293:1155-9.

3.6 Tables and Figures

Table 3.1

mAb-C Sample	% Insoluble aggregates	% Monomer	% Soluble aggregates	% Fragments
5 mg/mL, pre-lyophilization	0.0 ± 0.1	99.4 ± 0.1	0.5 ± 0.1	0.1 ± 0.1
5 mg/mL, post-lyophilization	2.1 ± 0.9	97.3 ± 0.9	0.5 ± 0.1	0.1 ± 0.1
60 mg/mL, pre-lyophilization	0.0 ± 0.1	99.4 ± 0.1	0.5 ± 0.1	0.1 ± 0.1
60 mg/mL, post-lyophilization	2.7 ± 0.2	96.7 ± 0.3	0.5 ± 0.1	0.1 ± 0.1

Effect of lyophilization and reconstitution on the aggregation profile of mAb-C as measured by size-exclusion chromatography (SEC). Samples of mAb-C were prepared at 5 and 60 mg/mL in 20 mM potassium phosphate buffer (pH 7.0) with 10% (w/v) trehalose (Pre-lyophilization samples). After lyophilization, mAb-C samples were reconstituted with D₂O-based 20 mM potassium phosphate buffer (pH 7.0) with 300 mM salt Na₂SO₄ (Post-lyophilization samples). The experimental data are mean and standard deviation calculated from three independent measurements on three separate lyophilized vials.

Table 3.S1

Peptide Number	Location
1	mAb-C Heavy 4-10 (VH)
2	mAb-C Heavy 4-17 (VH)
3	mAb-C Heavy 8-29 (VH)
4	mAb-C Heavy 11-22 (VH)
5	mAb-C Heavy 11-26 (VH)
6	mAb-C Heavy 27-35 (VH)
7	mAb-C Heavy 33-43 (VH)
8	mAb-C Heavy 33-44 (VH)
9	mAb-C Heavy 35-45 (VH)
10	mAb-C Heavy 35-59 (VH)
11	mAb-C Heavy 37-45 (VH)
12	mAb-C Heavy 37-48 (VH)
13	mAb-C Heavy 45-59 (VH)
14	mAb-C Heavy 46-59 (VH)
15	mAb-C Heavy 47-59 (VH)
16	mAb-C Heavy 49-60 (VH)
17	mAb-C Heavy 50-59 (VH)
18	mAb-C Heavy 50-60 (VH)
19	mAb-C Heavy 60-70 (VH)
20	mAb-C Heavy 60-71 (VH)
21	mAb-C Heavy 63-69 (VH)
22	mAb-C Heavy 71-78 (VH)
23	mAb-C Heavy 71-80 (VH)
24	mAb-C Heavy 81-86 (VH)
25	mAb-C Heavy 84-93 (VH)
26	mAb-C Heavy 87-94 (VH)
27	mAb-C Heavy 100-112 (VH)
28	mAb-C Heavy 101-112 (VH)
29	mAb-C Heavy 102-112 (VH)
30	mAb-C Heavy 113-122 (VH)
31	mAb-C Heavy 121-130 (CH1)
32	mAb-C Heavy 121-140 (CH1)
33	mAb-C Heavy 135-140 (CH1)
34	mAb-C Heavy 135-150 (CH1)
35	mAb-C Heavy 141-152 (CH1)
36	mAb-C Heavy 145-174 (CH1)
37	mAb-C Heavy 152-162 (CH1)

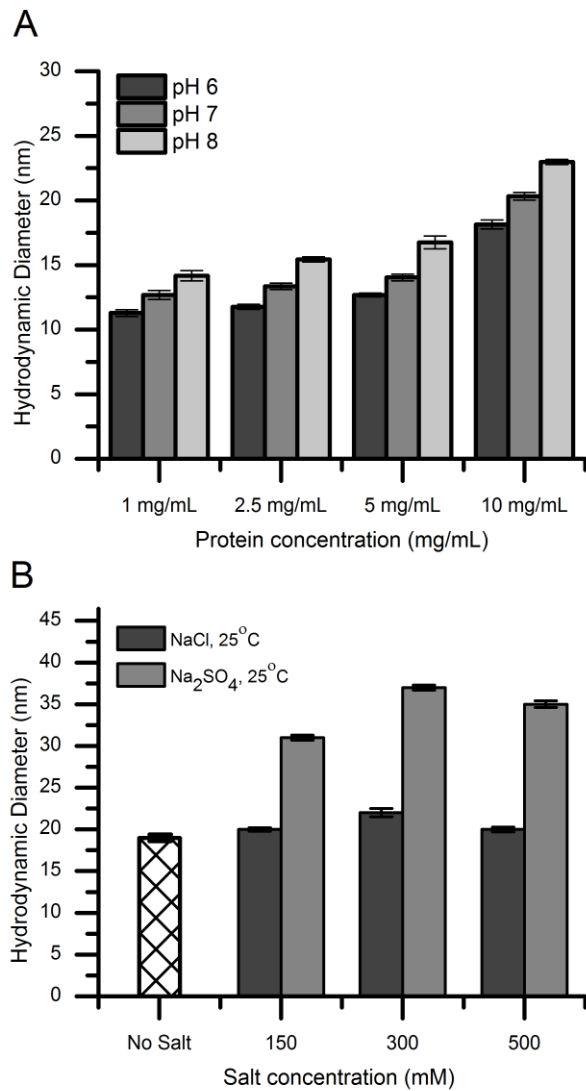
38	mAb-C Heavy 155-165 (CH1)
39	mAb-C Heavy 164-187 (CH1)
40	mAb-C Heavy 167-182 (CH1)
41	mAb-C Heavy 171-182 (CH1)
42	mAb-C Heavy 176-182 (CH1)
43	mAb-C Heavy 188-193 (CH1)
44	mAb-C Heavy 193-205 (CH1)
45	mAb-C Heavy 194-201 (CH1)
46	mAb-C Heavy 199-211 (CH1)
47	mAb-C Heavy 219-227 (CH1)
48	mAb-C Heavy 229-254 (CH2)
49	mAb-C Heavy 233-252 (CH2)
50	mAb-C Heavy 243-248 (CH2)
51	mAb-C Heavy 246-256 (CH2)
52	mAb-C Heavy 249-260 (CH2)
53	mAb-C Heavy 251-260 (CH2)
54	mAb-C Heavy 252-259 (CH2)
55	mAb-C Heavy 261-268 (CH2)
56	mAb-C Heavy 261-269 (CH2)
57	mAb-C Heavy 261-271 (CH2)
58	mAb-C Heavy 270-285 (CH2)
59	mAb-C Heavy 271-285 (CH2)
60	mAb-C Heavy 273-285 (CH2)
61	mAb-C Heavy 282-284 (CH2)
62	mAb-C Heavy 285-298 (CH2)
63	mAb-C Heavy 308-314 (CH2)
64	mAb-C Heavy 311-325 (CH2)
65	mAb-C Heavy 315-341 (CH2)
66	mAb-C Heavy 320-334 (CH2)
67	mAb-C Heavy 342-356 (CH2)
68	mAb-C Heavy 344-356 (CH3)
69	mAb-C Heavy 357-366 (CH3)
70	mAb-C Heavy 365-372 (CH3)
71	mAb-C Heavy 365-374 (CH3)
72	mAb-C Heavy 377-388 (CH3)
73	mAb-C Heavy 385-398 (CH3)
74	mAb-C Heavy 385-406 (CH3)
75	mAb-C Heavy 385-412 (CH3)
76	mAb-C Heavy 389-398 (CH3)
77	mAb-C Heavy 389-406 (CH3)
78	mAb-C Heavy 389-412 (CH3)

79	mAb-C Heavy 390-406 (CH3)
80	mAb-C Heavy 399-406 (CH3)
81	mAb-C Heavy 399-412 (CH3)
82	mAb-C Heavy 407-412 (CH3)
83	mAb-C Heavy 413-418 (CH3)
84	mAb-C Heavy 417-428 (CH3)
85	mAb-C Heavy 419-431 (CH3)
86	mAb-C Heavy 420-436 (CH3)
87	mAb-C Heavy 431-454 (CH3)
88	mAb-C Heavy 432-438 (CH3)
89	mAb-C Heavy 432-454 (CH3)
90	mAb-C Heavy 434-454 (CH3)
91	mAb-C Heavy 436-454 (CH3)
92	mAb-C Heavy 437-454 (CH3)
93	mAb-C Light 1-10 (VL)
94	mAb-C Light 1-12 (VL)
95	mAb-C Light 4-10 (VL)
96	mAb-C Light 11-22 (VL)
97	mAb-C Light 13-32 (VL)
98	mAb-C Light 33-49 (VL)
99	mAb-C Light 35-48 (VL)
100	mAb-C Light 36-54 (VL)
101	mAb-C Light 47-62 (VL)
102	mAb-C Light 48-70 (VL)
103	mAb-C Light 49-70 (VL)
104	mAb-C Light 49-71 (VL)
105	mAb-C Light 50-71 (VL)
106	mAb-C Light 55-71 (VL)
107	mAb-C Light 72-82 (VL)
108	mAb-C Light 74-82 (VL)
109	mAb-C Light 75-82 (VL)
110	mAb-C Light 80-83 (VL)
111	mAb-C Light 88-104 (VL)
112	mAb-C Light 102-115 (VL)
113	mAb-C Light 105-116 (VL)
114	mAb-C Light 106-115 (VL)
115	mAb-C Light 116-131 (VL)
116	mAb-C Light 117-130 (CL)
117	mAb-C Light 117-133 (CL)
118	mAb-C Light 123-133 (CL)
119	mAb-C Light 124-133 (CL)

120	mAb-C Light 132-146 (CL)
121	mAb-C Light 136-143 (CL)
122	mAb-C Light 149-172 (CL)
123	mAb-C Light 155-172 (CL)
124	mAb-C Light 160-172 (CL)
125	mAb-C Light 162-172 (CL)
126	mAb-C Light 162-178 (CL)
127	mAb-C Light 173-179 (CL)
128	mAb-C Light 179-184 (CL)
129	mAb-C Light 180-194 (CL)
130	mAb-C Light 203-214 (CL)

Location of pepsin generated peptide segments (from HX-MS analysis of mAb-C) in the mAb-C primary sequence and their corresponding unique peptide numbers.

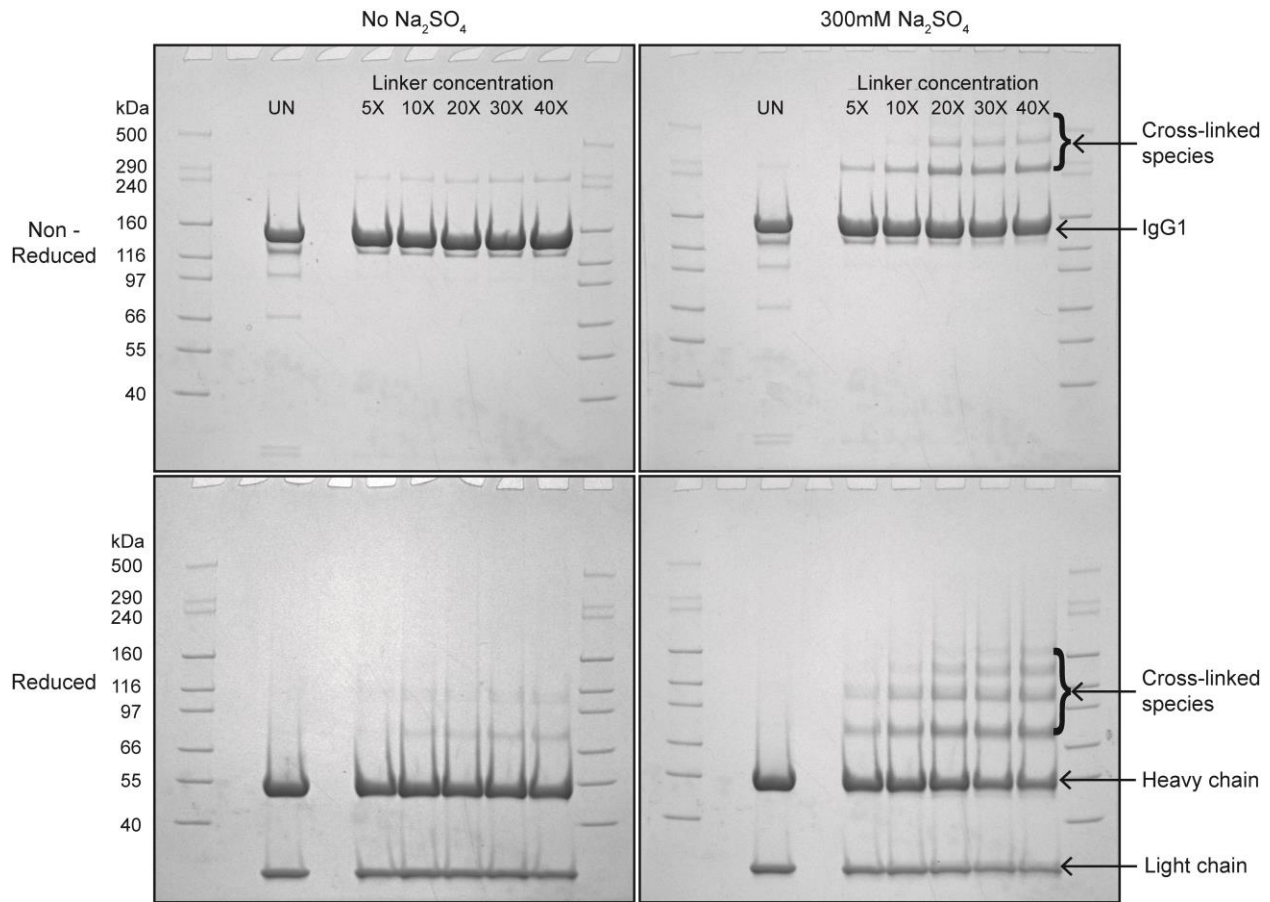
Figure 3.1



Hydrodynamic diameter of mAb-C under various solution conditions as measured by dynamic light scattering. (A) Effect of pH as a function of protein concentration. (B) Effect of salt type (NaCl and Na₂SO₄) and ionic strength. Experiments were conducted at 25°C with mAb-C samples prepared in 40 mM potassium phosphate buffer (pH 7), containing either NaCl or Na₂SO₄ at 0, 0.15, 0.3 and 0.5 M. The mAb-C samples were prepared in 40 mM potassium phosphate buffer (pH 6, 7 and 8)

containing 0.3 M NaCl. The error bars represent one standard deviation from three independent measurements.

Figure 3.2

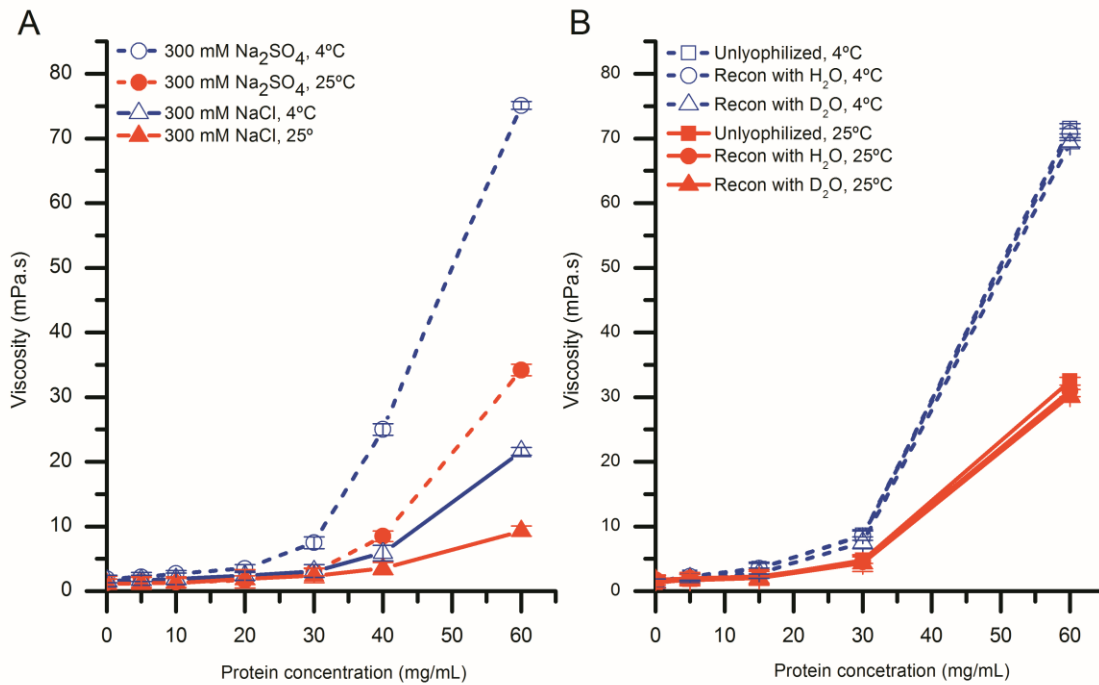


Cross-linking and SDS-PAGE analysis of reversible self-association (RSA) of mAb-C under different solution conditions. The mAb-C samples were prepared in 40 mM potassium phosphate buffer (pH 7) in the presence and absence of 0.3 M Na₂SO₄. The lane in each panel marked “UN” represents a mAb-C control with no added cross-linker. The first and last lane of each gel contains molecular weight standards. The masses are denoted on the left side gels. Subsequent lanes show the extent of mAb-C cross-linking in the presence of increasing concentration of BS²G cross-linker. Top-left panel, non-reduced SDS-PAGE gel showing cross-linking of mAb-C in the absence of Na₂SO₄. Top-right panel, non-reduced gel showing cross-linking of mAb-C in the presence of 300 mM Na₂SO₄. Bottom-left panel, reduced SDS-PAGE gel showing mAb-C in the

absence of Na_2SO_4 . Bottom-right panel, reduced gel of mAb-C in the presence of 300 mM Na_2SO_4 .

Cross-linking reactions were carried out at 4°C.

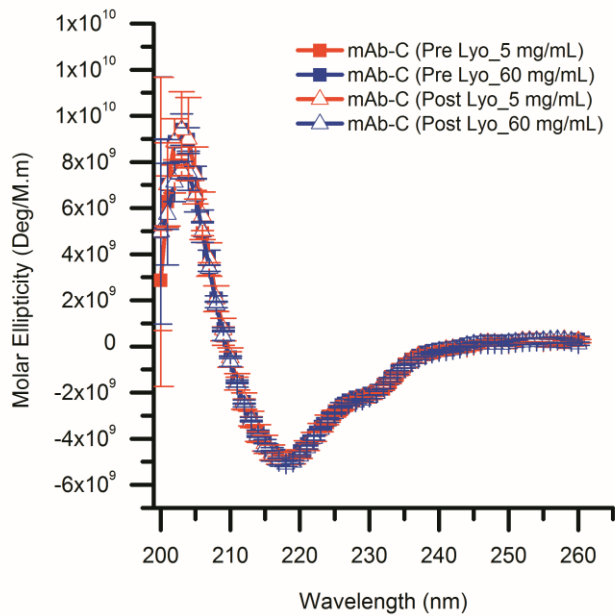
Figure 3.3



The effect of protein concentration, temperature and salt type on solution viscosity of mAb-C samples either before or after lyophilization and reconstitution. (A) Effect of temperature and salt type on viscosity of mAb-C as a function of protein concentration. (B) Effect of lyophilization and reconstitution diluent (with H₂O- and D₂O-based buffers) on the viscosity of mAb-C as a function of protein concentration. Samples of mAb-C for panel A were prepared in 40 mM potassium phosphate buffer (pH 7.0) containing 300 mM salt (NaCl or Na₂SO₄). For panel B, mAb-C samples that were not lyophilized were prepared in 40 mM potassium phosphate buffer (pH 7.0) containing 300 mM Na₂SO₄ and 10% (w/v) trehalose. Lyophilized samples were freeze-dried in 20 mM potassium phosphate buffer (pH 7.0) containing 10% (w/v) trehalose, and then reconstituted with either H₂O or D₂O buffers consisting of 20 mM potassium phosphate buffer (pH 7.0) and 300 mM

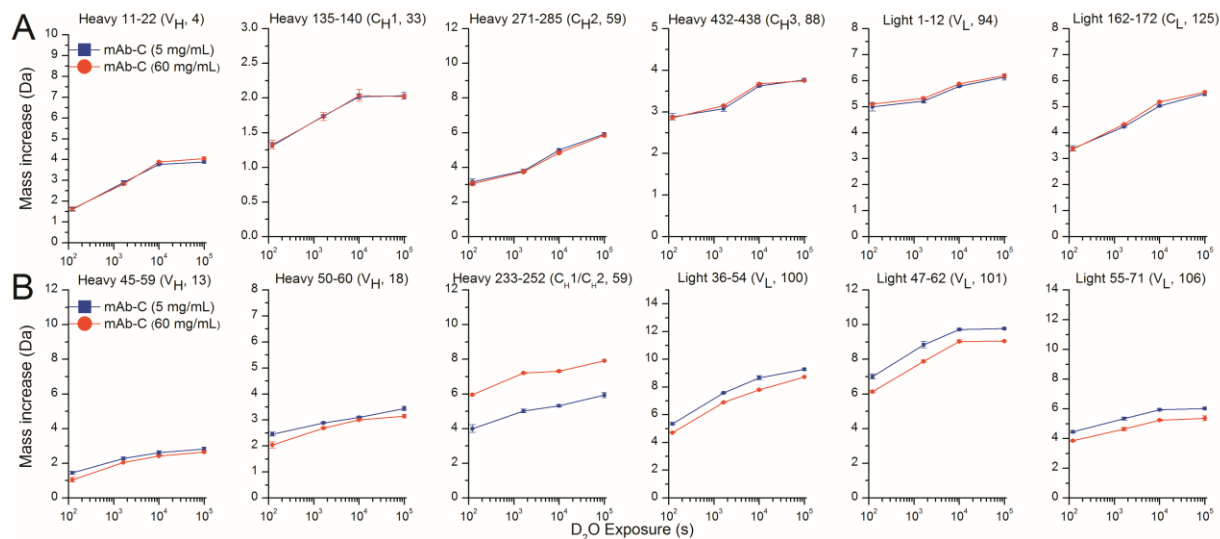
salt Na_2SO_4 . Viscosity measurements were taken either at 4°C or 25°C , as noted. The error bars represent one standard deviation from three independent measurements.

Figure 3.4



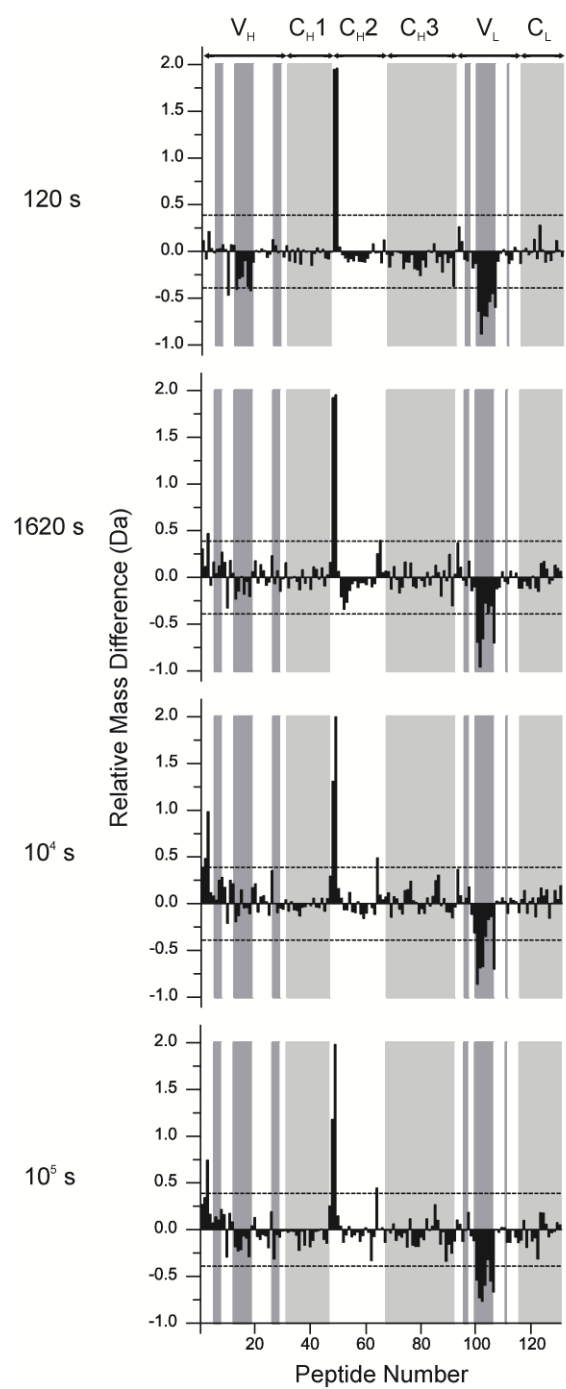
Circular dichroism spectra showing the effect of the lyophilization process on the overall secondary structure of mAb-C. All mAb-C samples (pre and post lyophilization) were diluted to 0.3 mg/mL with 40 mM potassium phosphate buffer (pH 7.0) containing 300 mM Na_2SO_4 and 10% (w/v) trehalose for analysis at 10°C. The error bars represent one standard deviation from three independent measurements.

Figure 3.5



Deuterium uptake by twelve representative peptide segments from mAb-C measured at 5 and 60 mg/mL as determined by HX-MS. (A) Six representative peptides that showed no differences in hydrogen exchange kinetics between low and high protein concentrations. (B) Six representative peptides that showed significant changes in hydrogen exchange kinetics between low and high protein concentrations. Domain location and peptide number of the segment are shown in parentheses. The error bars represent one standard deviation from three independent experiments. Refer to Supplemental Figure S2 for deuterium uptake plots of all 130 peptides in the dataset.

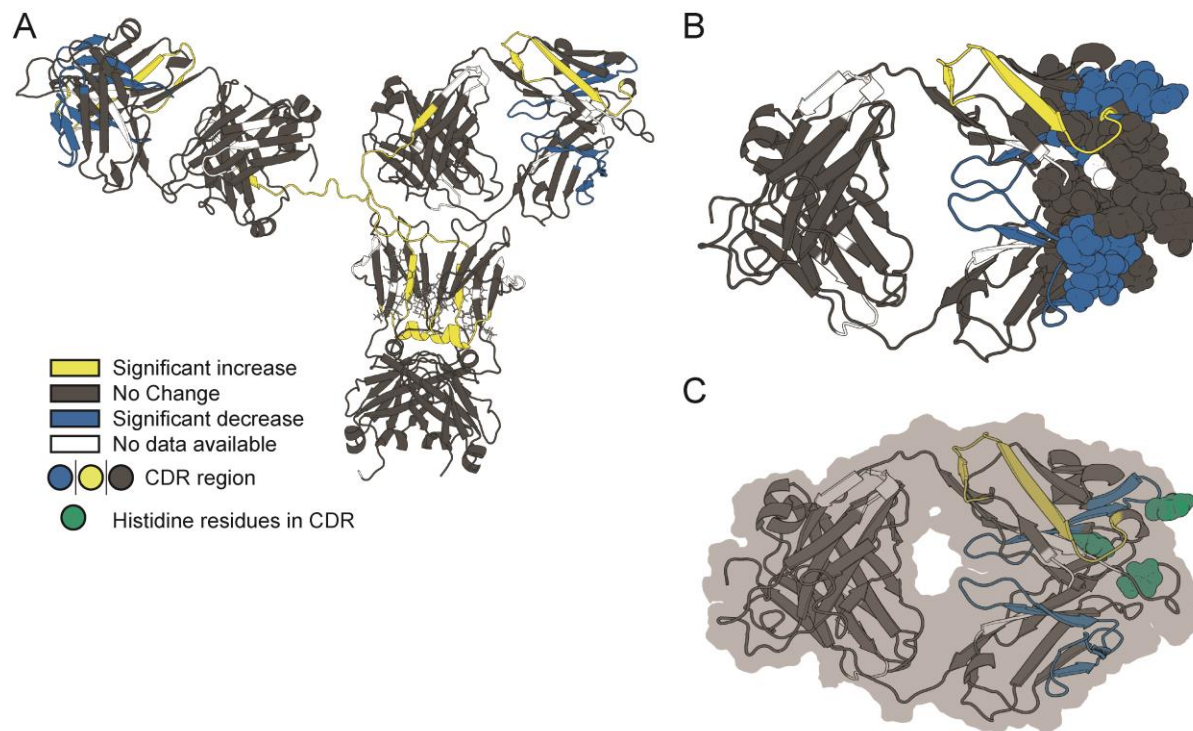
Figure 3.6



Relative differences in deuterium uptake at four exposure times as measured by HX-MS for 130 peptide segments of mAb-C at 60 mg/mL vs. 5 mg/mL at pH 7.0. The individual peptides are

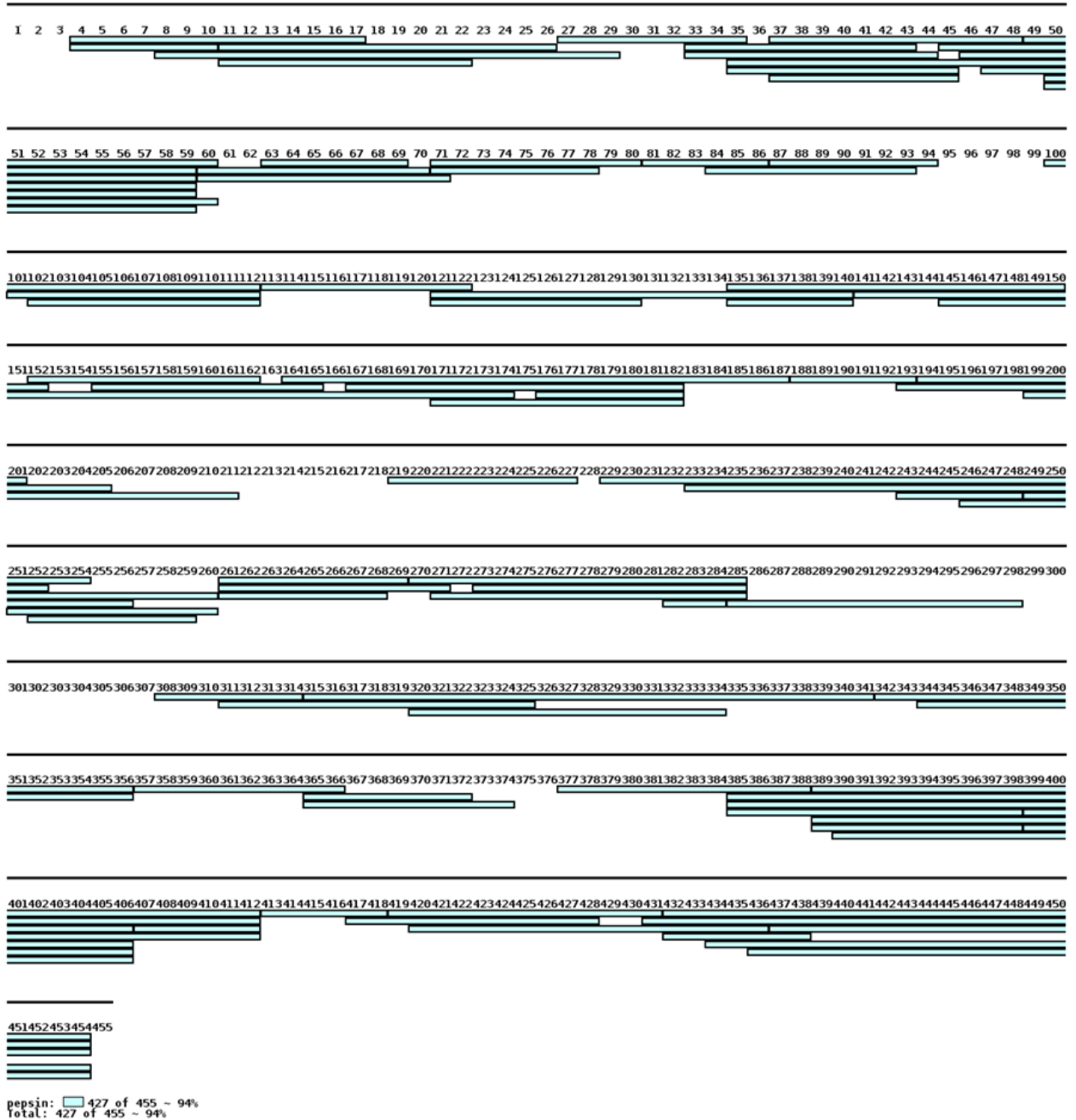
arranged on the horizontal axis starting from the N-terminal of the heavy chain and ending at the C-terminal of the light chain. The peptides are numbered sequentially based on the locations of their middle residues (see Supplemental Table S1 for the identities and locations of the peptides). The horizontal axes of these plots denote the peptide numbers from 1 to 130. The vertical axis is the difference between exchange at 60 mg/mL vs. 5 mg/mL: $\Delta m(t) = m_{60}(t) - m_5(t)$. Positive bars indicate an increase in deuterium uptake for a particular peptide segment at high protein concentration (60 mg/mL) and negative bars indicate decreased deuterium uptake for a peptide segment at 60 mg/mL compared to lower protein concentration (5 mg/mL). The dashed lines at ± 0.4 Da indicate the 99% confidence limits for significant differences. White and grey shades in the background of the figure represent IgG domain boundaries and each domain is labeled at the top of the figure. Shades in blue represent CDR segments on mAb-C. Segment locations in the mAb-C sequence and their corresponding peptide numbers can be found in the Table S1 in the supporting information. An average of three independent mass measurements was used to calculate each mass difference data point corresponding to all the exposure time-points.

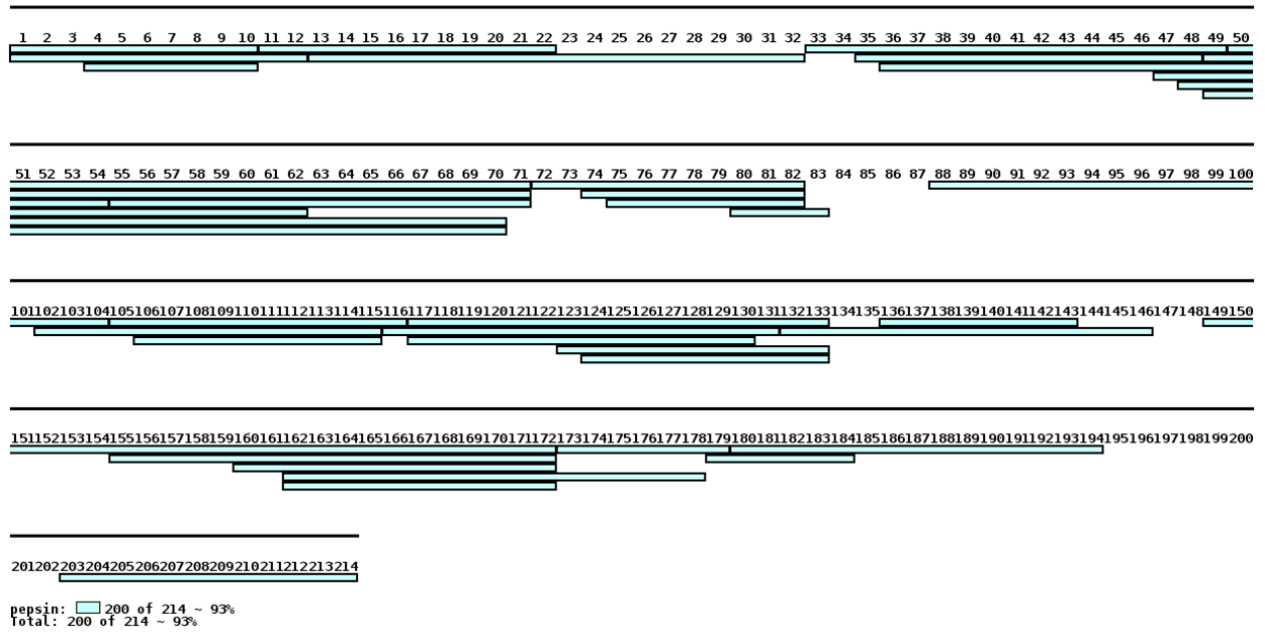
Figure 3.7



Effect of concentration-dependent RSA on deuterium uptake of various segments of mAb-C as measured by HX-MS plotted onto homology models of mAb-C. (A) Entire mAb, (B) view of the Fab domain and (C) view of the Fab domain with histidine residues in the peptide segments containing the CDR2H and CDR3H sequences highlighted in green color. Changes in deuterium uptake of particular peptide segments are colored according to the legend and are derived from the differential exchange data shown in Figure 3.6

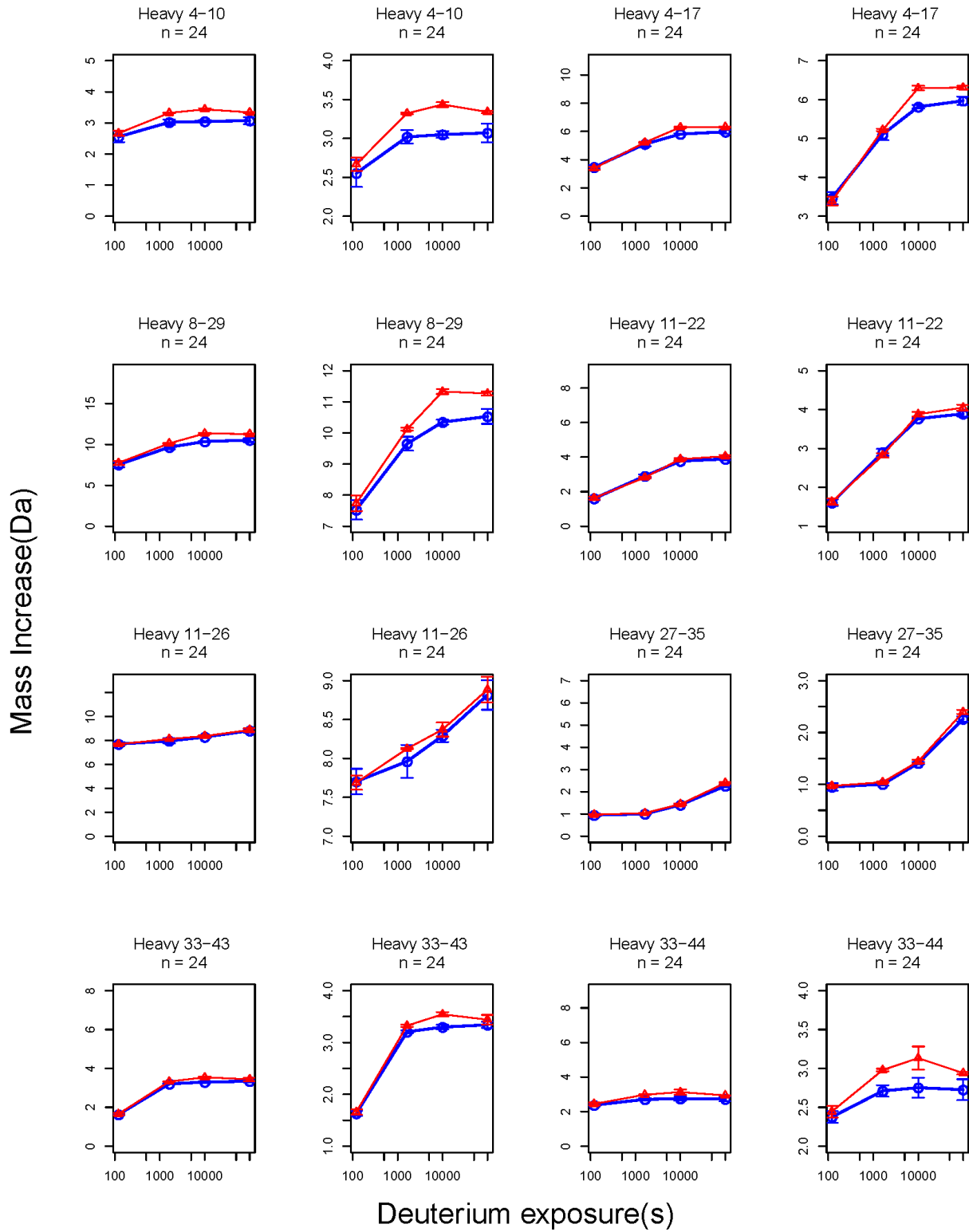
Figure 3.S1



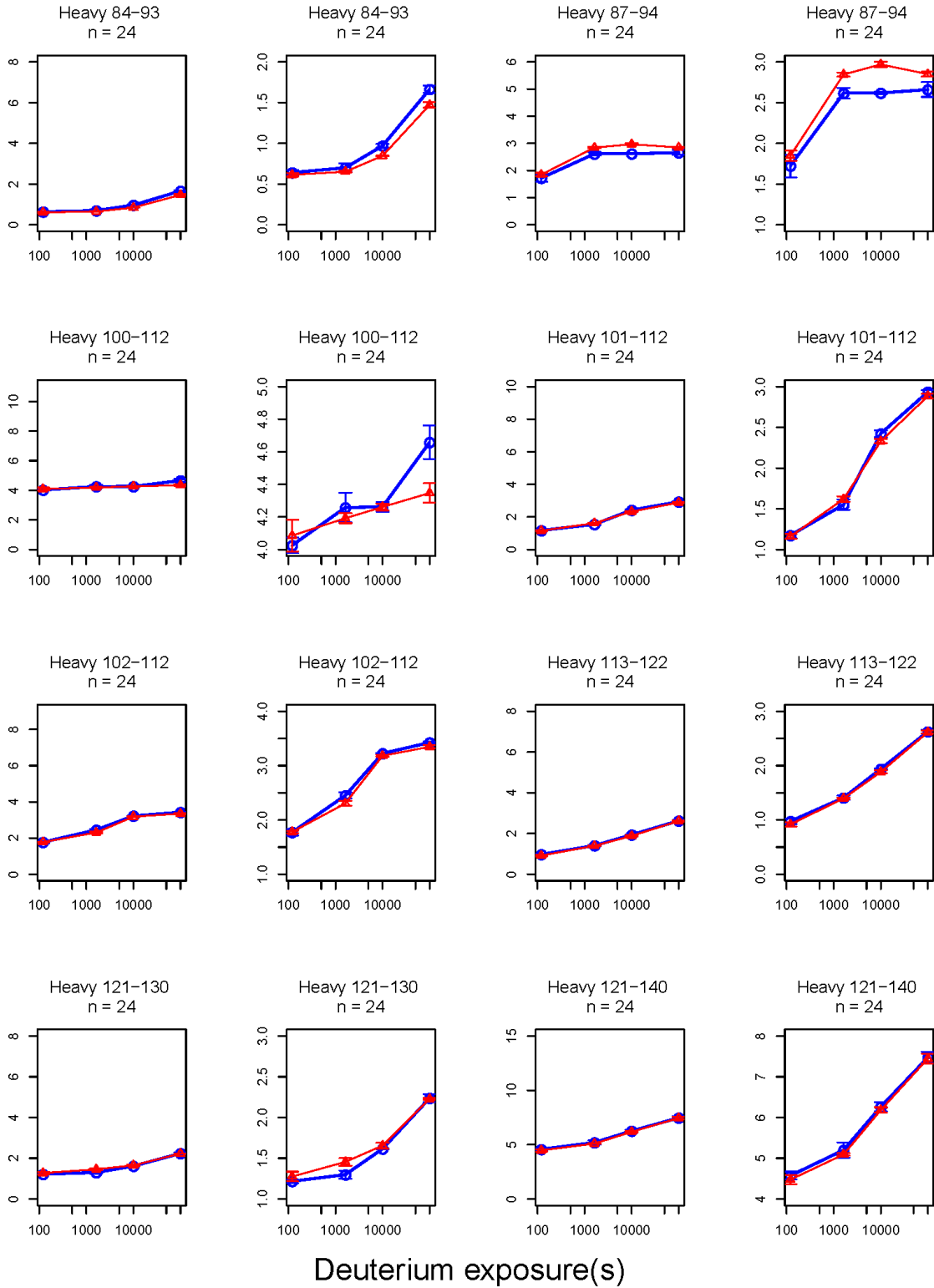


Pepsin peptide map of the (A) heavy chain (HC) and (B) light chain (LC) of mAb-C composed of 130 common peptide segments covering 94% of the HC primary sequence and 93% of the LC primary sequence.

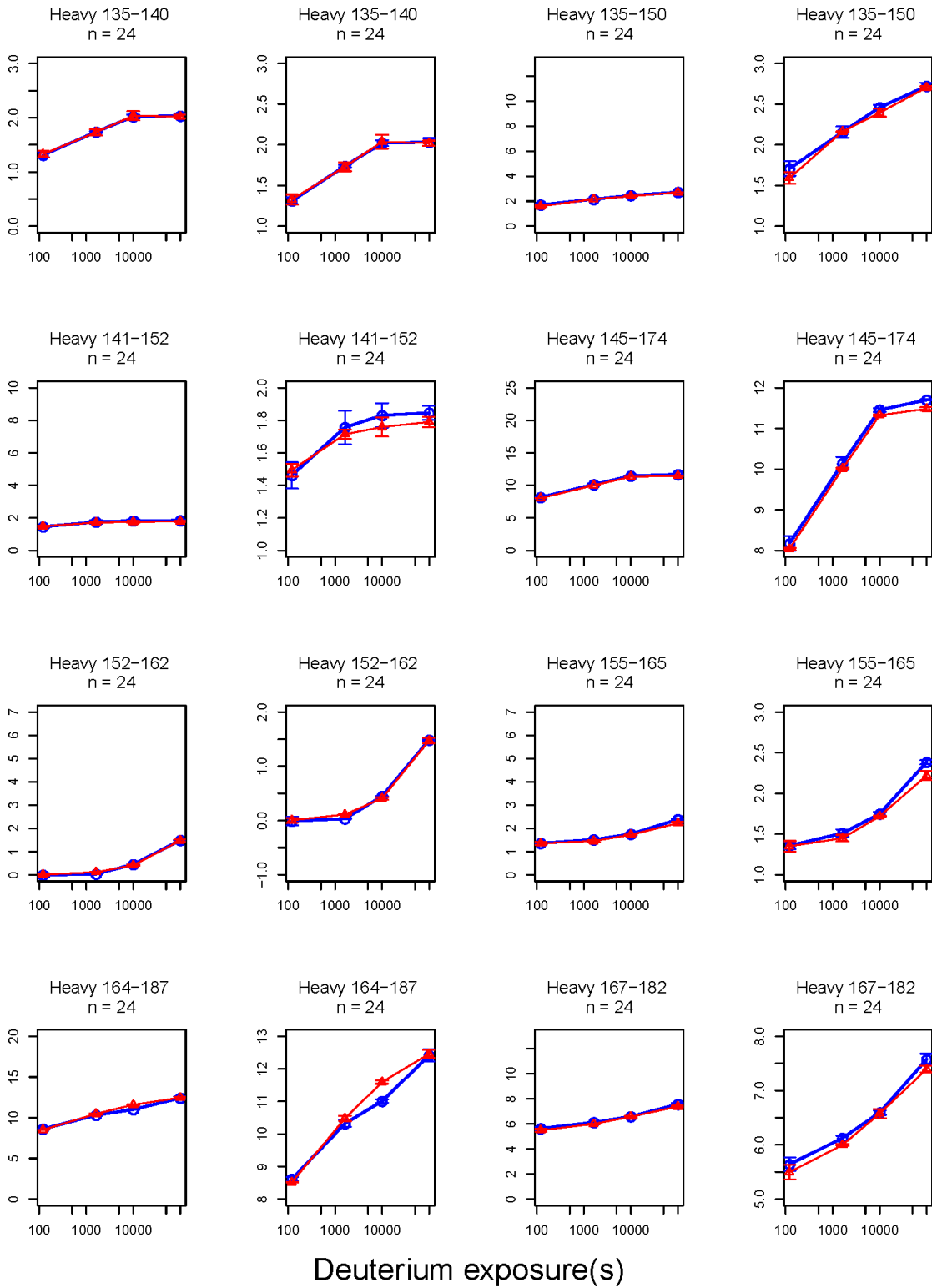
Figure 3.S2



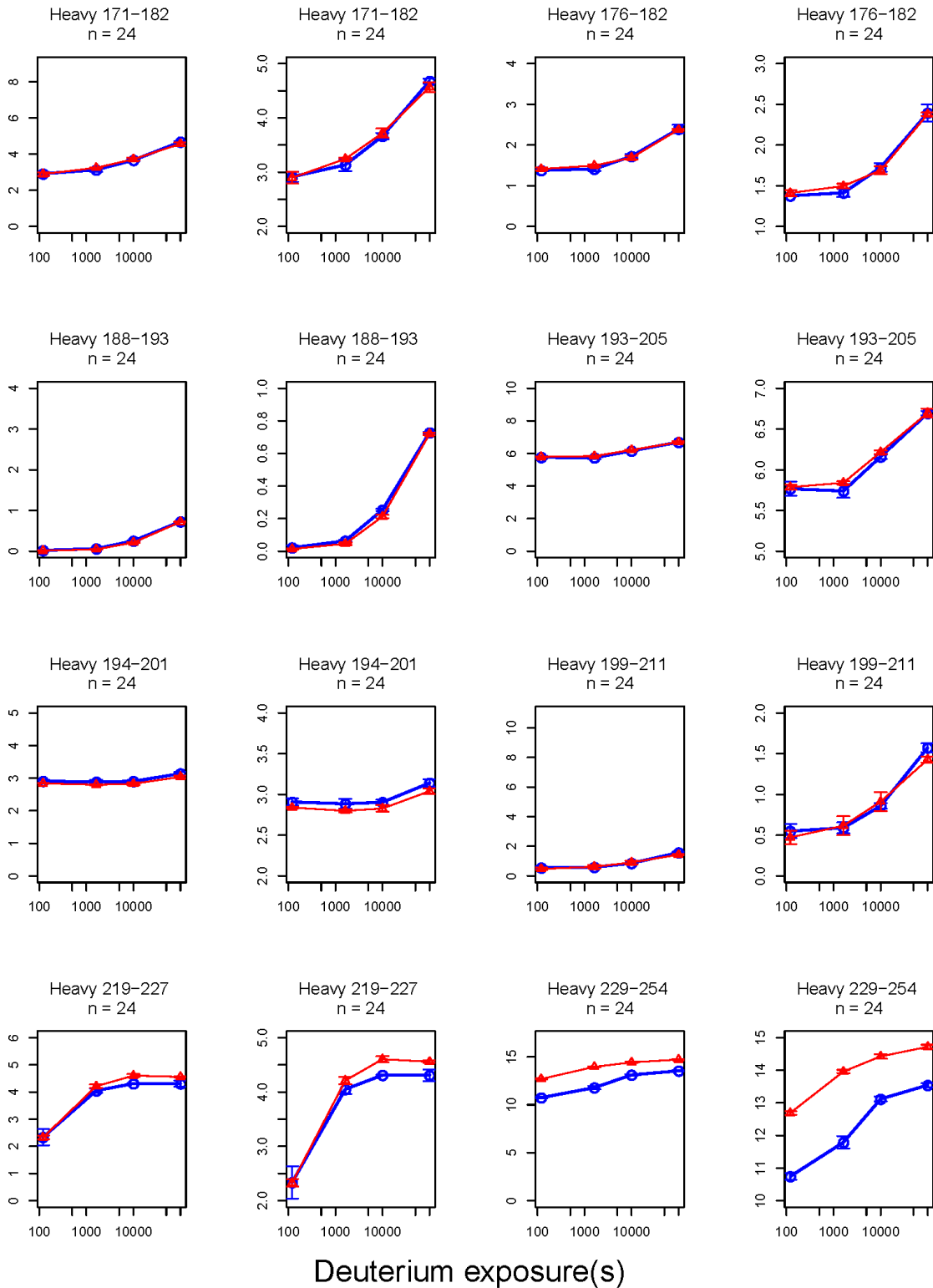
Mass Increase(Da)



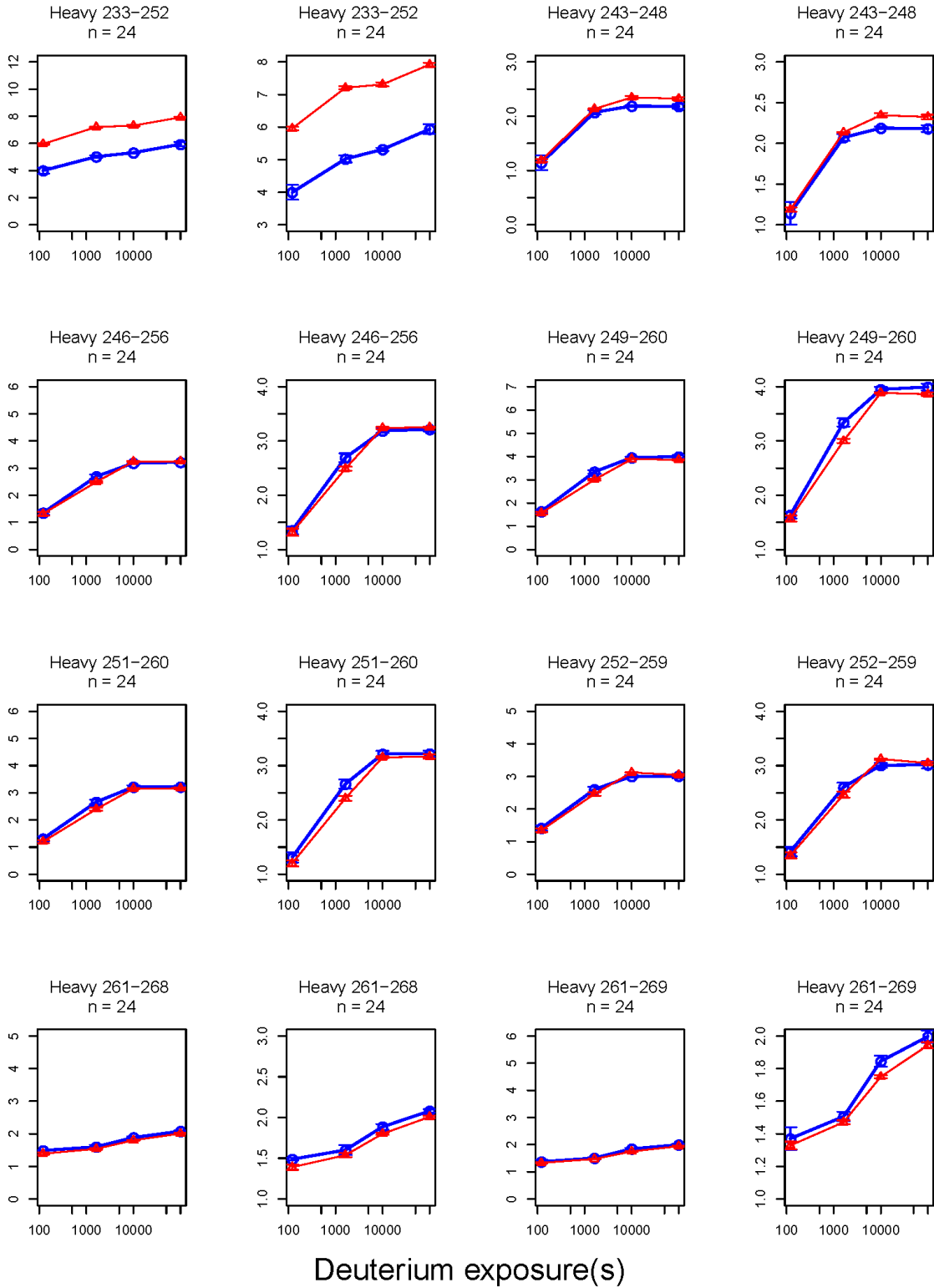
Mass Increase(Da)



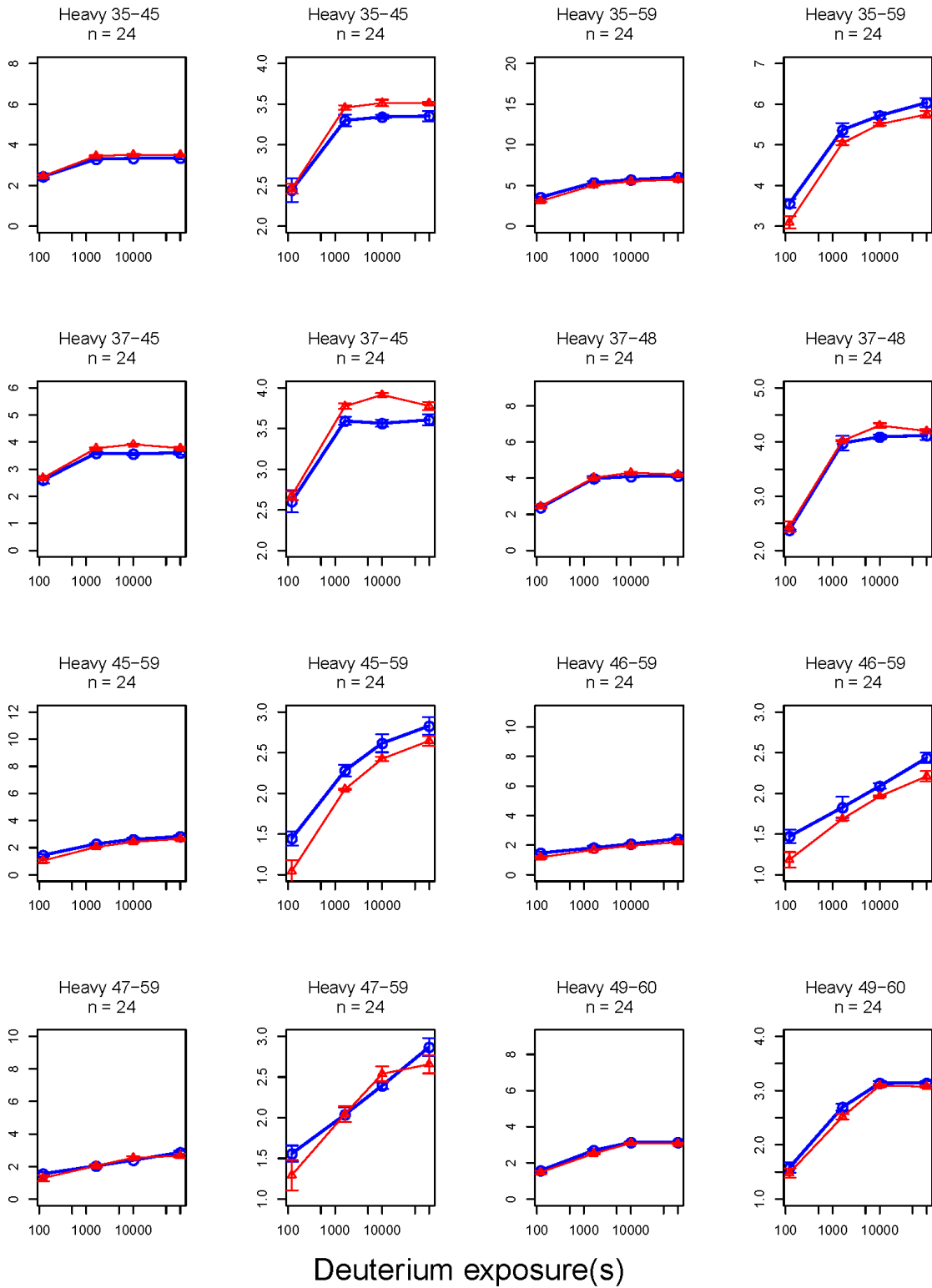
Mass Increase(Da)



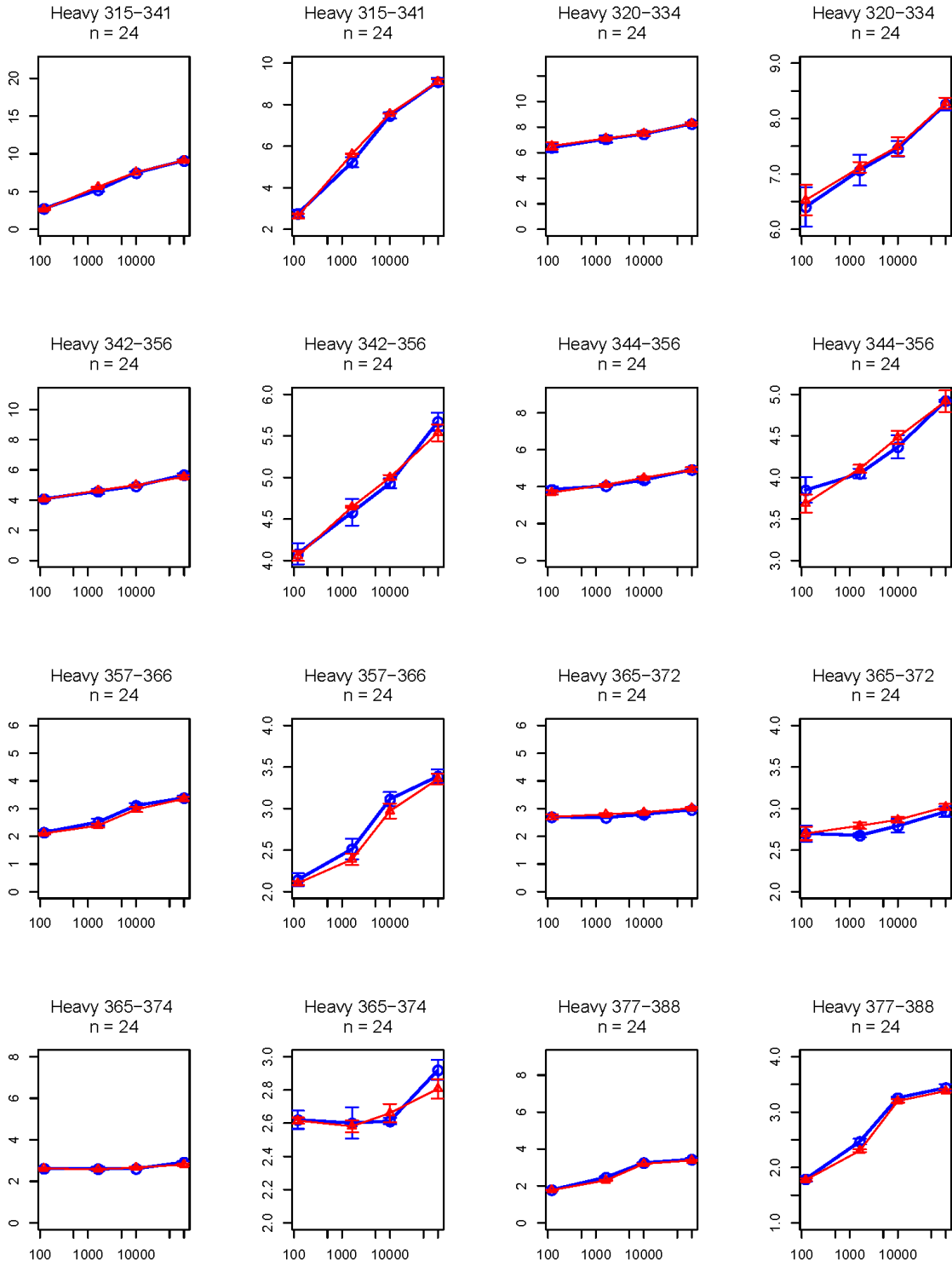
Mass Increase(Da)



Mass Increase(Da)

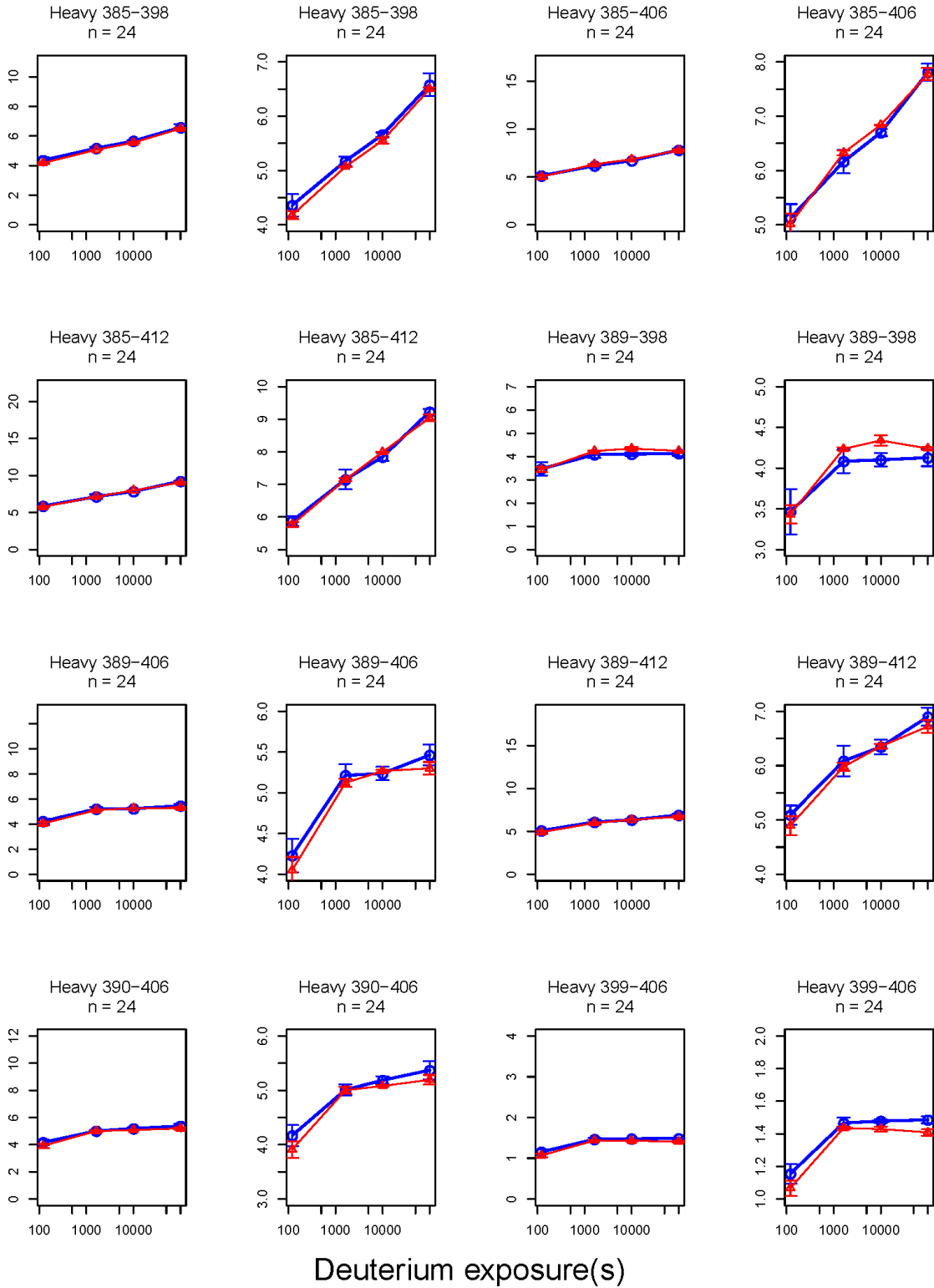


Mass Increase(Da)

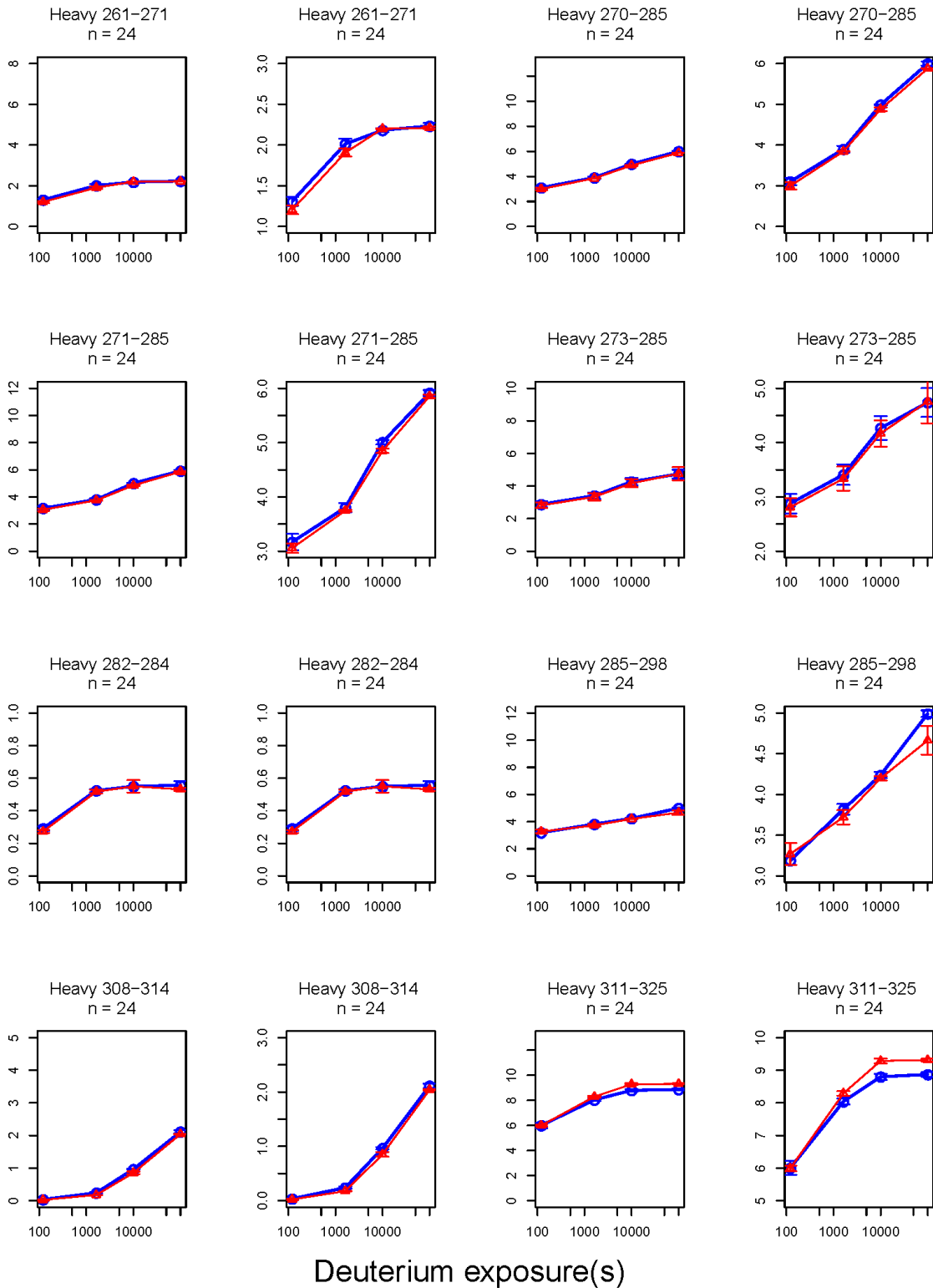


Deuterium exposure(s)

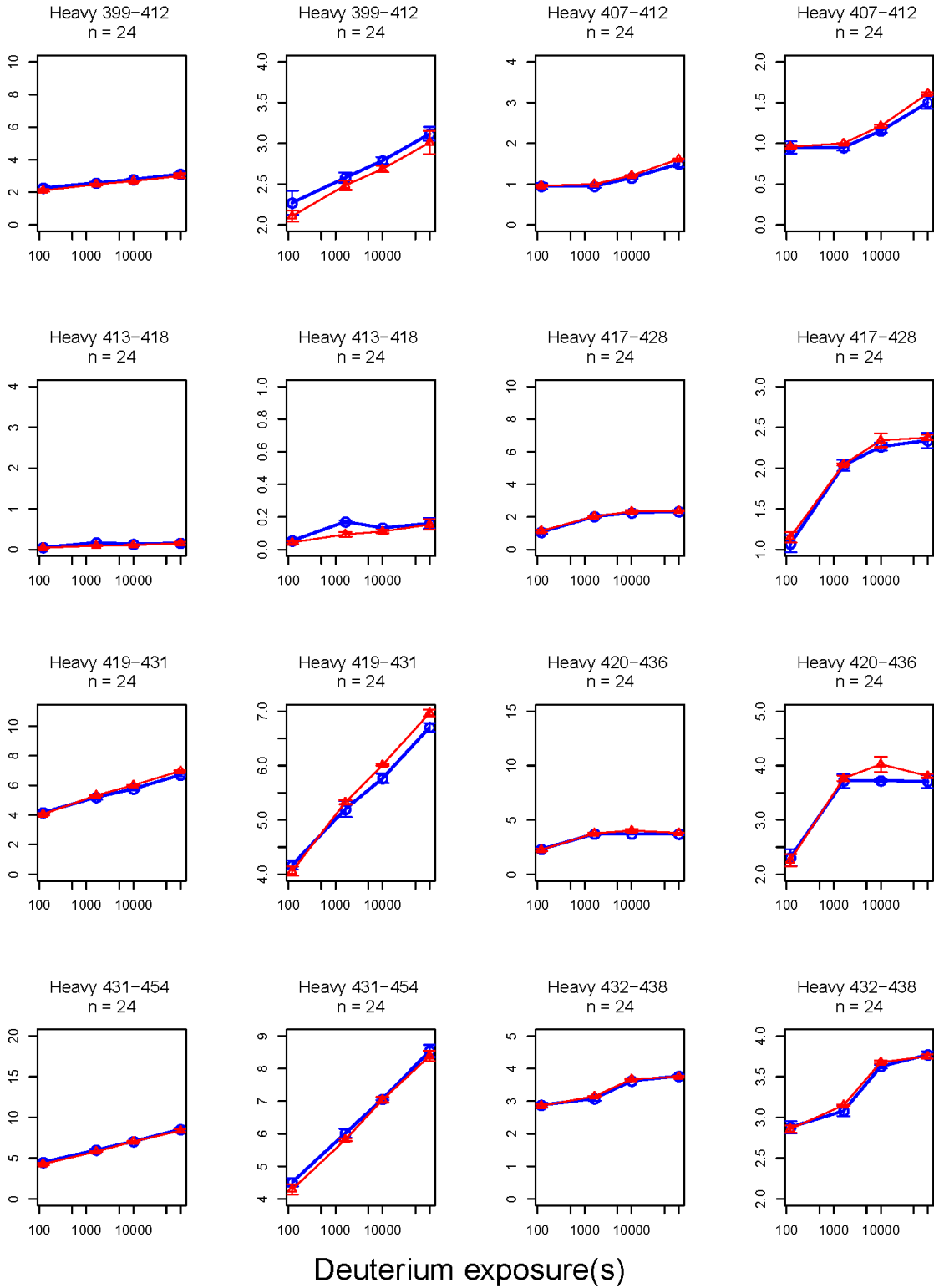
Mass Increase(Da)



Mass Increase(Da)

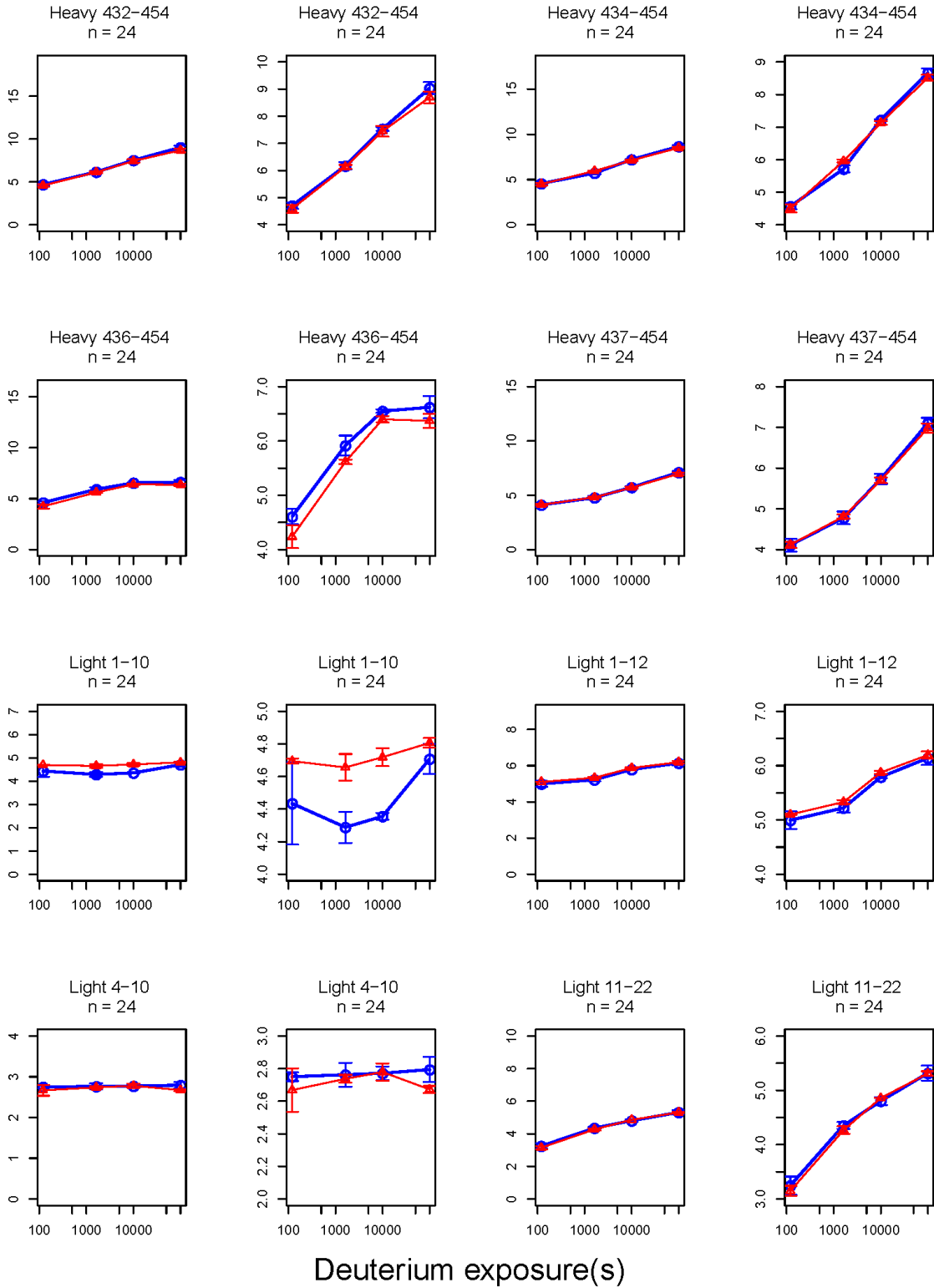


Mass Increase(Da)

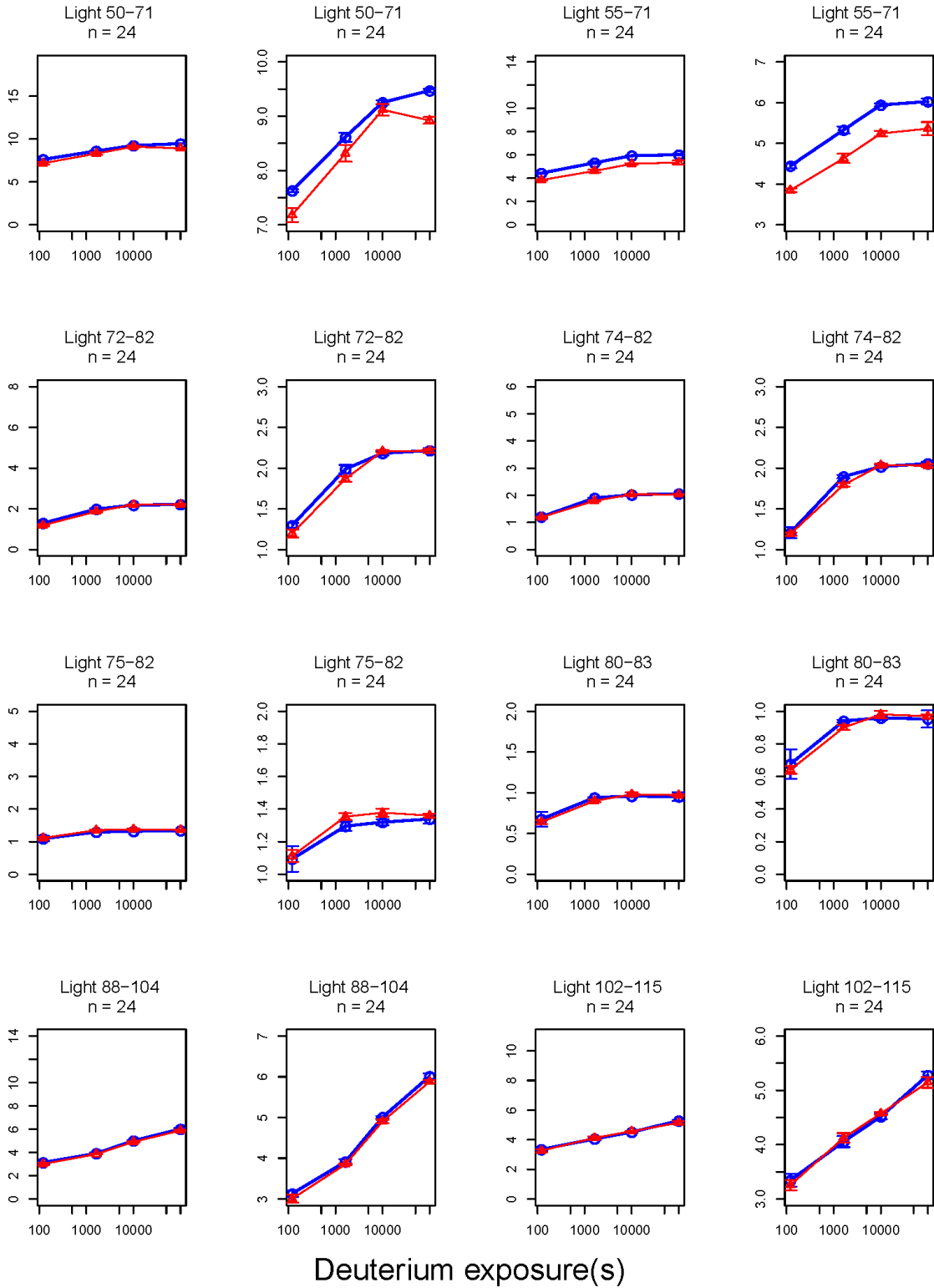


Deuterium exposure(s)

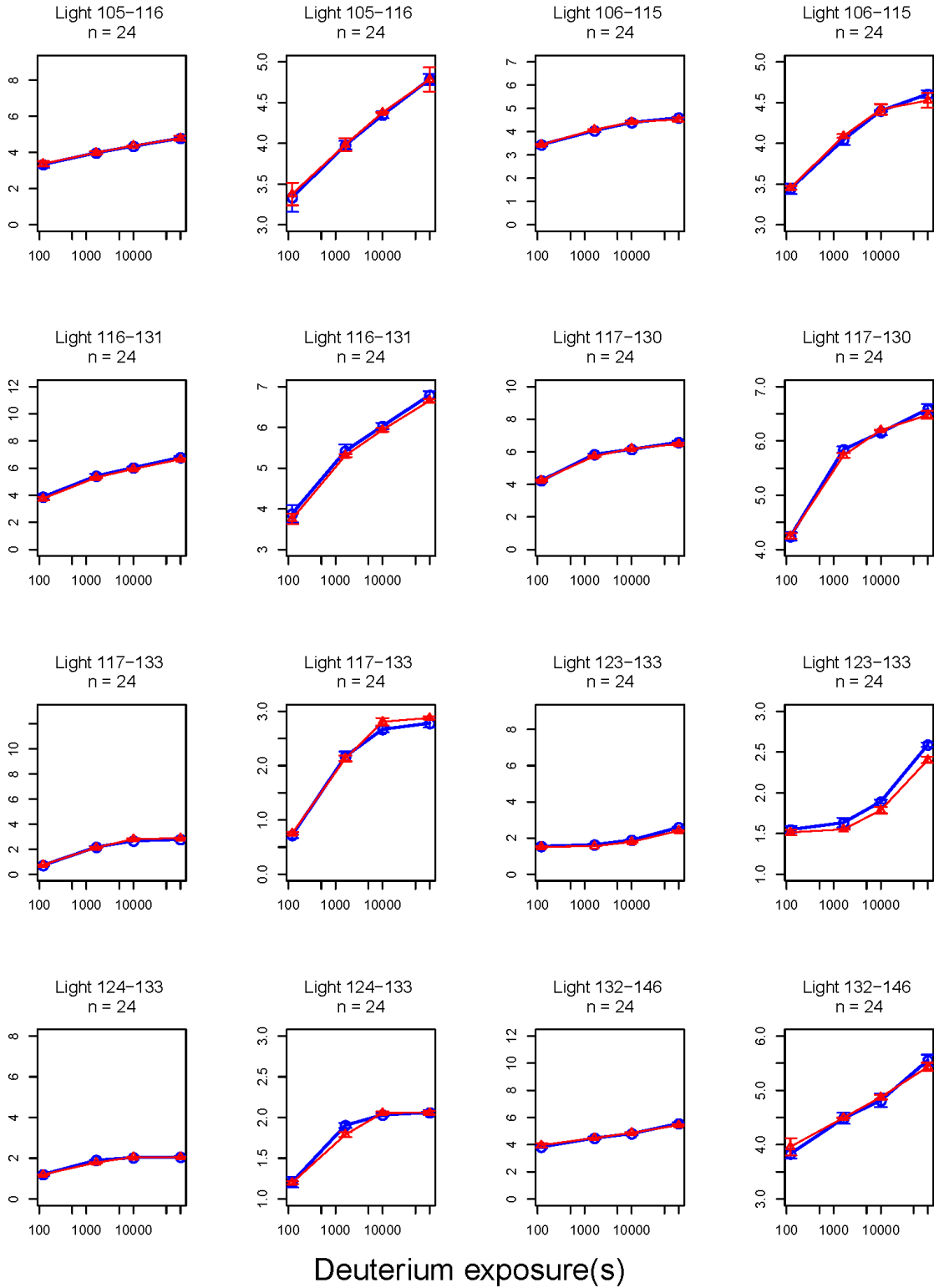
Mass Increase(Da)



Mass Increase(Da)

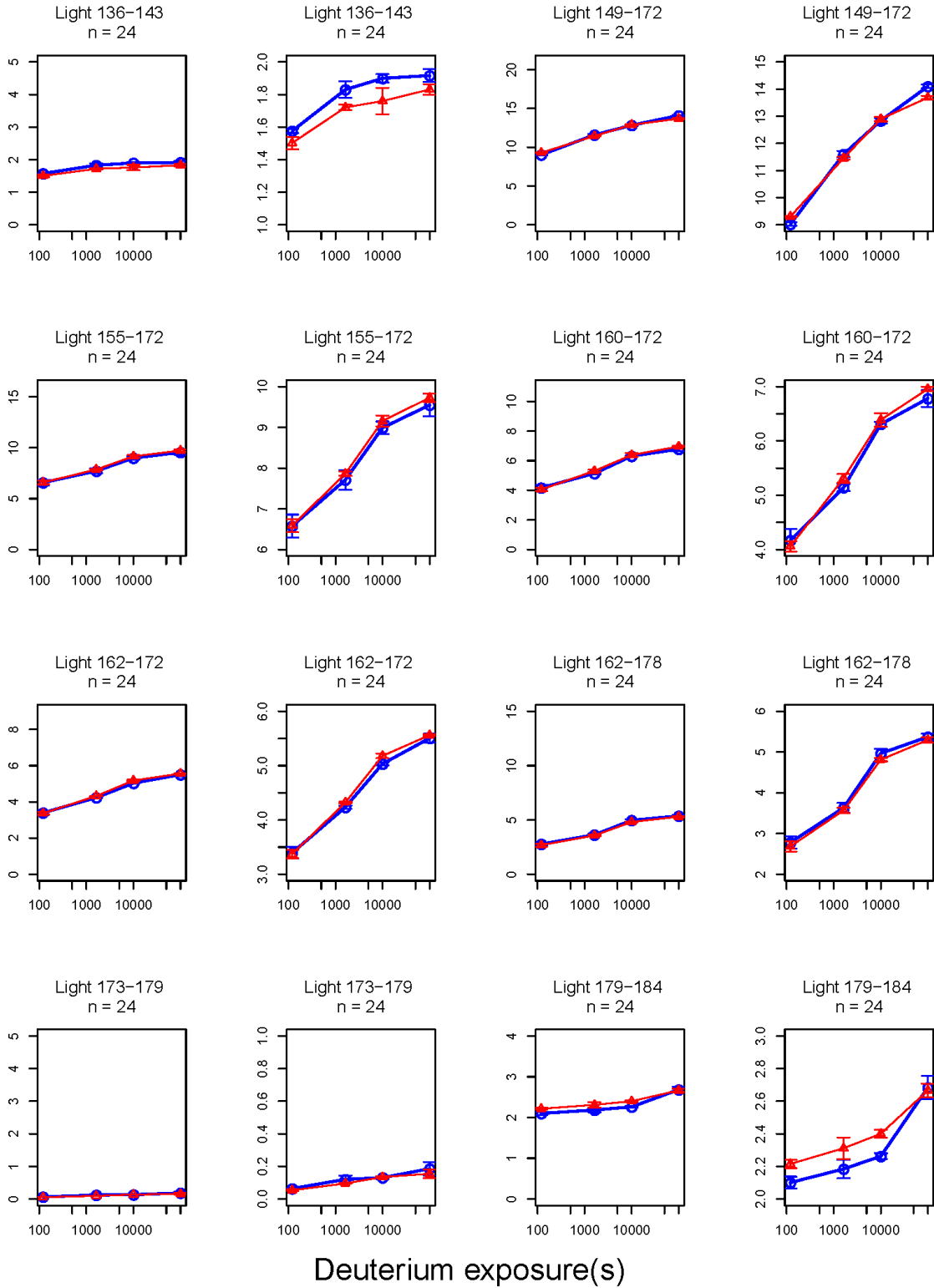


Mass Increase(Da)

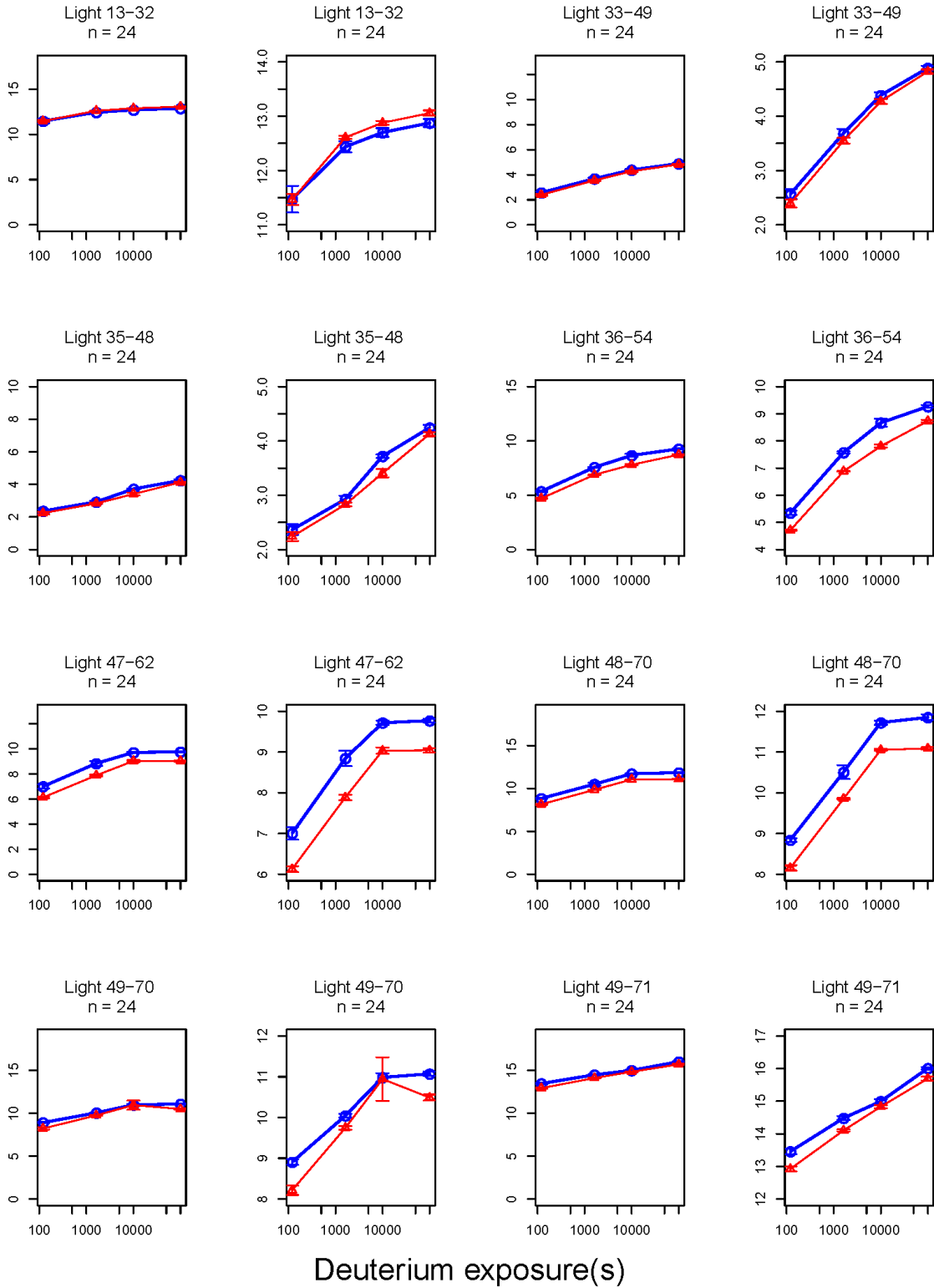


Deuterium exposure(s)

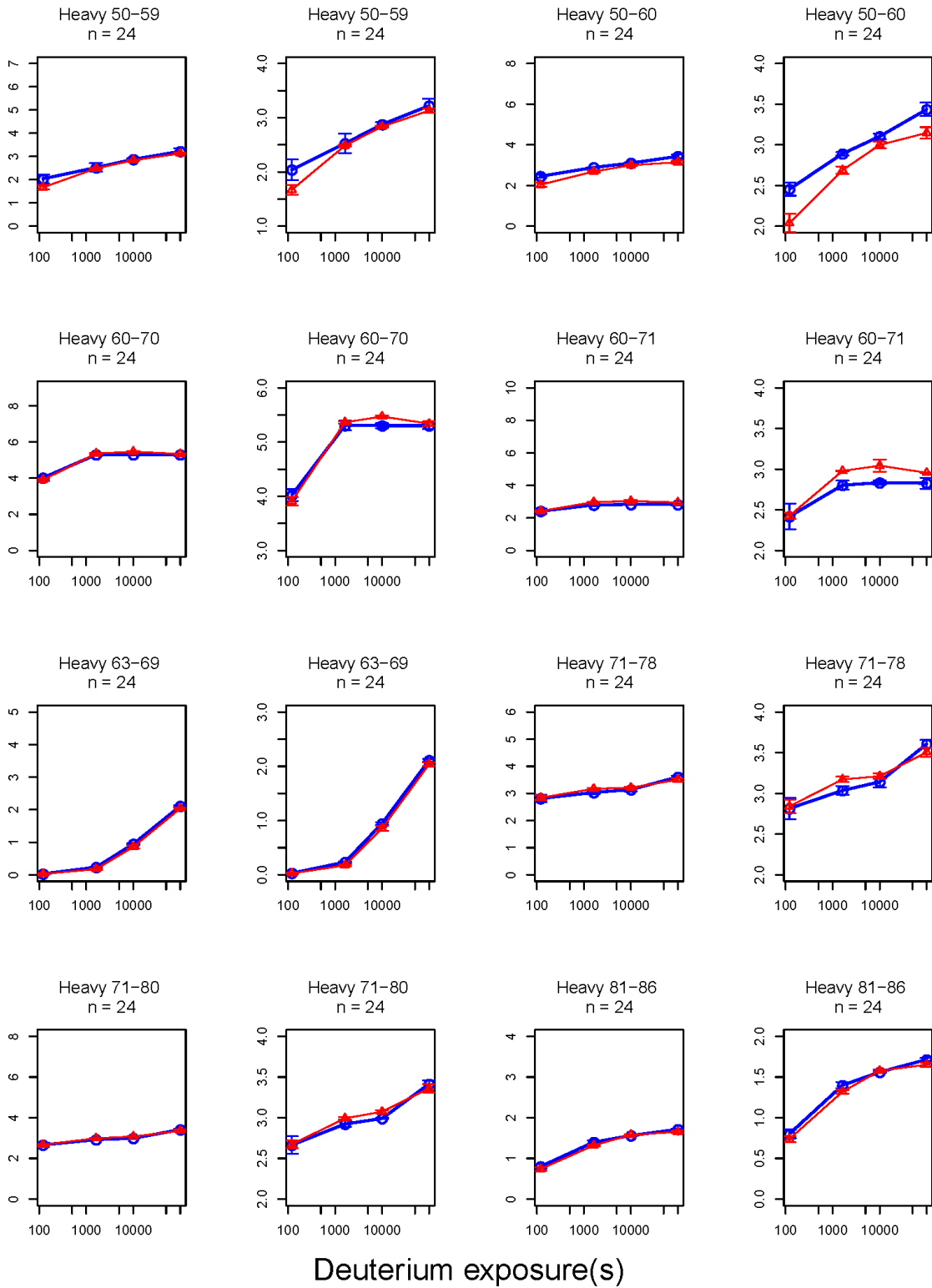
Mass Increase(Da)



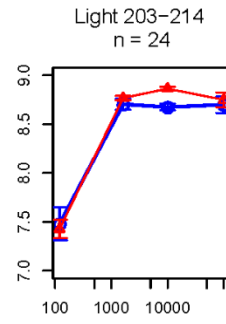
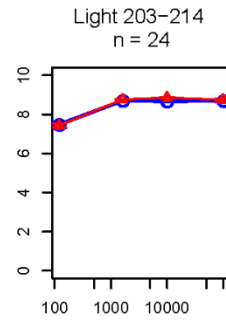
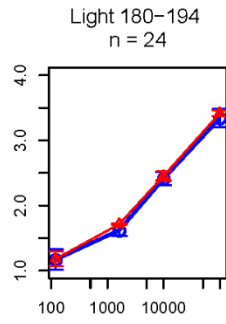
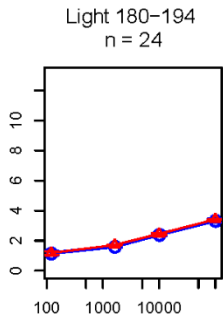
Mass Increase(Da)



Mass Increase(Da)



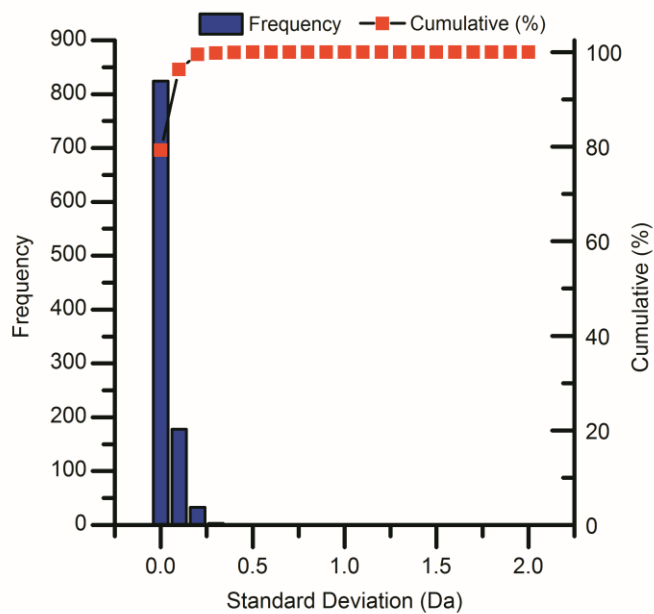
Mass Increase(Da)



Deuterium exposure(s)

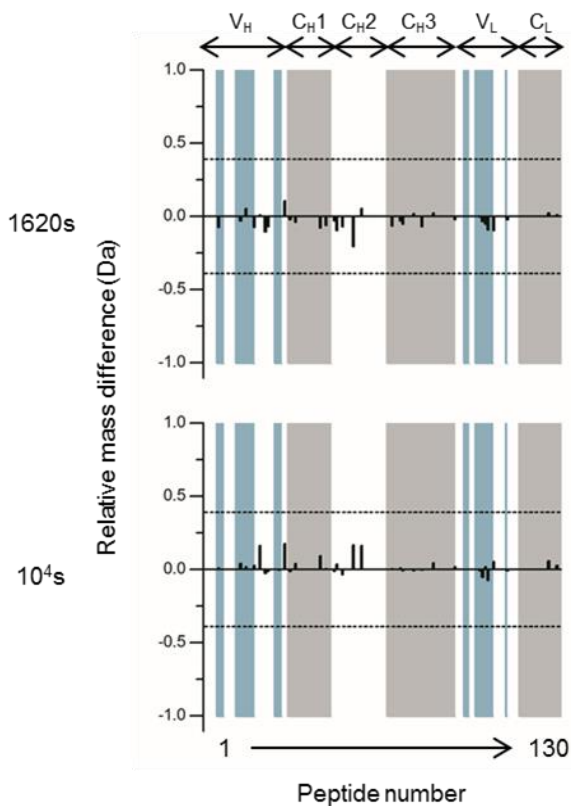
Deuterium uptake plots as measured by HX-MS of 130 peptide segments comparing hydrogen exchange kinetics between 5 and 60 mg/mL mAb-C samples. Domain location and peptide number of the segment are shown in parentheses. The error bars represent one standard deviation from three independent experiments.

Figure 3.S3



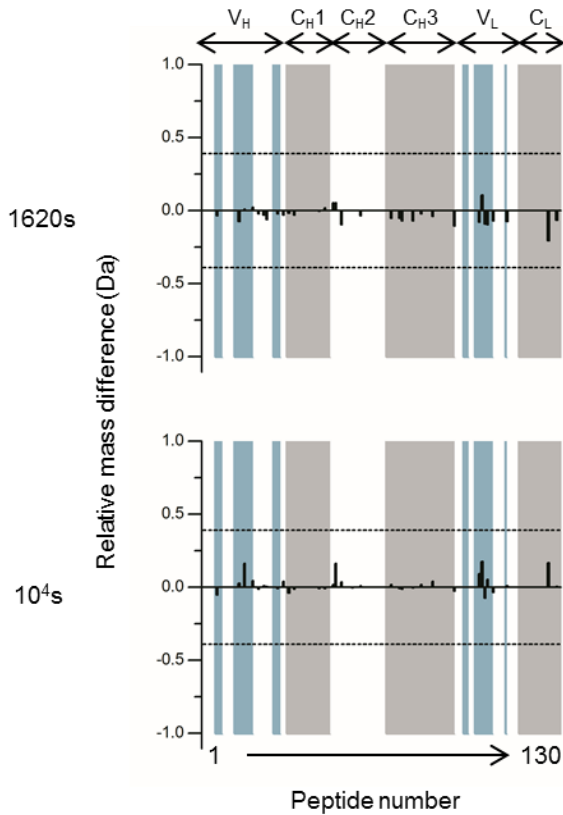
Reproducibility of the HX-MS data represented by the distribution of standard deviations for the mass differences across all time points and segments of mAb-C from the triplicate experiments (N = 1040). The 99th percentile for standard deviations calculated from the dataset is 0.28 Da.

Figure 3.S4



Difference plot showing the relative mass change (Δm) of 35 selected mAb-C peptide segments comparing lyophilized vs. unlyophilized mAb-C samples at 6 mg/mL as measured by HX-MS. The differences in hydrogen exchange between lyophilized and unlyophilized samples of mAb-C at 6 mg/mL [$\Delta m(t) = m_{lyo}(t) - m_{unlyo}(t)$] are plotted on the vertical axis. The positive bars represent peptides that show increased in hydrogen exchange after lyophilization/reconstitution. Negative bars represent peptides that show decreased hydrogen exchange upon lyophilization/reconstitution (refer to Figure 6 for more detailed information about difference plots).

Figure 3.S5



Difference plot showing relative mass change of 35 selected mAb-C peptide segments comparing lyophilized vs. unlyophilized mAb-C samples at 60 mg/mL as measured by HX-MS. The differences in hydrogen exchange between lyophilized and unlyophilized samples of mAb-C at 60 mg/mL $[\Delta m(t) = m_{lyo}(t) - m_{unlyo}(t)]$ are plotted on the vertical axis. The positive bars represent peptides that show increased in hydrogen exchange after lyophilization/reconstitution. Negative bars represent peptides that show decreased hydrogen exchange upon lyophilization/reconstitution (refer to Figure 6 for more detailed information about difference plots).

Chapter 4

Charge-mediated Fab-Fc interactions in an IgG1 antibody induce reversible self-association, cluster formation, and elevated viscosity

4.1 Introduction

Protein-protein interactions play a critical role in many biological and biochemical processes. Like many biological processes however, protein-protein interactions can have negative as well as positive effects.¹⁻⁴ In vivo, cellular proteins are usually present in a very crowded, highly concentrated environment.⁵ At such high protein concentrations, due to increases in molecular crowding and decreases in intermolecular distances between molecules, the extent of specific and non-specific protein-protein interactions driven by exposed charged and apolar regions on the protein surface increase.⁶⁻⁸ Independent of whether a protein is in vivo or in vitro (e.g., a purified protein drug candidate stored in a vial), molecular crowding causes protein solutions to deviate from ideality, thereby affecting macromolecular interactions and potentially protein conformation.⁹ Identification of the interfaces that mediate protein-protein interactions can open new avenues for drug targeting and discovery, and guide protein engineers in the development of macromolecule candidates that are more stable and easier to administer.

Monoclonal antibodies (mAbs) comprise a major class of biotherapeutics used for the treatment of many chronic conditions.¹⁰ The subcutaneous delivery route enables patients to self-administer 1-2 mL of injectable volume per dose. To deliver the amount of drug needed, which is often tens to hundreds of milligrams, in this volume, the mAbs must be formulated at very high protein concentrations.^{2, 10} Due to decreases in intermolecular distances between protein molecules at high protein concentrations, attractive protein-protein interactions may overcome repulsive interactions, thereby favoring the formation of reversibly associating intermolecular protein complexes.^{11, 12} Formation of large protein complexes increases the solution shear modulus, which can result in dramatic increases in viscosity at higher concentration,^{13, 14} leading to formulation and manufacturing-related challenges. In addition, antibody clusters may act as

seeds for the formation of irreversible aggregates at high protein concentration.¹⁵ Moreover, high shear stress during pumping of viscous solutions of self-associated proteins has, in some cases, been shown to also contribute to the formation of irreversible protein aggregates.¹⁶ Such irreversible aggregates can decrease protein activity and stability, and may elicit adverse immunogenic reactions in patients.¹⁷⁻¹⁹ In addition, parenteral administration of highly viscous liquids requires thicker gauge needles that may cause more painful injections.²

Previous work has shown that reversible self-association (RSA) between different IgG1 mAbs can result from different binding interfaces, despite high sequence similarity between the mAbs.²⁰⁻²² Studies of enzymatic fragmentation of IgG1 monomers into Fab and Fc domains,^{21,23,24} site-specific mutations in complementarity-determining region (CDR),²⁵ and coarse-grained simulations of such protein interactions^{26,27} suggest that intermolecular reversible interactions between mAb molecules can be initiated by either Fab-Fab or Fab-Fc associations and to a lesser extent through Fc-Fc interactions. Despite providing experimental insights into how solution conditions modulate the rate and extent of reversible protein-protein interactions, and which major regions of the mAb might be involved in such phenomena, these studies offer an incomplete and low-resolution picture of mAb reversible self-association. A more complete understanding of the specific molecular mechanisms of reversible protein-protein interactions requires site-specific information about the surfaces that mediate such associations.

Hydrogen exchange (HX) is a robust bioanalytical tool used to study protein dynamics and protein-protein interactions.²⁸⁻³³ The rate of hydrogen exchange depends on the higher order structure of the protein: backbone amides that are fully solvated (lacking hydrogen bonding) undergo rapid HX while amides located in structurally protected or strongly hydrogen-bonded regions exchange significantly more slowly.³⁴⁻³⁶ Thus, HX measurements can be used to map

protein interfaces of intermolecular protein-protein interactions because the formation of intermolecular contacts directly affects the solvation and hydrogen bond strengths at the protein interface.³³ Mass spectrometry coupled to HX (HX-MS), extends the HX technique to complex, multi-domain macromolecules like mAbs.³⁷⁻⁴³ Recently, we described a novel HX-MS method to map protein interfaces formed between mAbs undergoing reversible protein-protein interactions directly at up to 60 g/L.³⁹

Here, we applied this technique to investigate the molecular mechanism by which an IgG1 mAb (mAb-J) undergoes reversible self-association, and further probed this mechanism by a variety of other biophysical techniques. We also mapped the interface of the reversible, concentration-dependent intermolecular interactions between mAb-J monomers using hydrogen exchange mass spectrometry (HX-MS). The results of this study augment our knowledge of how proteins interact with each other at high protein concentrations under crowded environments.

4.2 Materials and Methods

4.2.1 Sample preparation

A purified IgG1 mAb, mAb-J, at a concentration of 150 g/L was obtained from MedImmune LLC, Gaithersburg, MD. The stock solution of mAb-J was dialyzed against the “control buffer” (20 mM citrate-phosphate buffer at selected pH values, containing 30 mM NaCl) with or without additional NaCl, arginine hydrochloride, or sugars (sucrose and trehalose) at 4°C using 3500 kDa molecular-weight cutoff membranes (Slide-A-Lyzer, Thermo Scientific, Rockford, IL) for 24 hours. For static light scattering and lyophilization, additional 10% w/v trehalose was added to the samples.

Subsequently, after dialysis stock solutions of mAb-J were diluted using corresponding buffer solutions.

4.2.2 Dynamic light scattering

Samples of mAb-J at 10 g/L prepared in control (pH 5.0-7.0) with or without additional NaCl, arginine hydrochloride or sugars (sucrose and trehalose) were centrifuged at $12,000 \times g$ for 5 minutes before analysis. DLS was measured in triplicate using the DynaPro Plate Reader (Wyatt Technology, Santa Barbara, CA). Scattered light was analyzed using a backscatter detector fixed at an angle of 173° . Fifteen runs of 5 second acquisitions were collected and averaged to determine the hydrodynamic diameter for each sample.

4.2.3 Viscosity Measurements

Samples of mAb-J, ranging from 5 to 60 g/L were prepared by diluting the dialyzed stock with corresponding buffer solutions. Solution dynamic viscosity was measured at 25°C with an m-VROC viscometer (Rheosence, San Ramon, CA) at a rate of $100 \mu\text{L}/\text{min}$ with a shear rate of 1420 s^{-1} . Triplicate viscosity measurements were recorded over a duration of 100 seconds.

4.2.4 Composition-gradient multi-angle light scattering

Dialyzed stock of mAb-J at 150 g/L in control (containing 10% w/v trehalose) with or without additional 100 mM NaCl and arginine was diluted with corresponding buffer solutions to prepare samples of mAb-J at 2 and 20 g/L. Thereafter, these samples were filtered through $0.22 \mu\text{m}$ Millex-GV syringe filter units (EMD Millipore, Billerica, MA). A fully automated CG-MALS instrument with a dual syringe-pump Calypso sample preparation and delivery unit (Wyatt Technology, Santa Barbara, CA) was used to measure light scattering at room temperature. A Dawn Heleos II light scattering instrument (Wyatt Technology, Santa Barbara, CA), equipped with a 661 nm laser and

an Optilab Rex refractive index detector (Wyatt Technology, Santa Barbara, CA), was used to measure both light scattering and protein concentration. Filtered HPLC grade toluene (Fisher Scientific, Fair Lawn, New Jersey) was used to calibrate voltage and light scattering intensities. Rayleigh ratio light scattering intensities were obtained over a protein concentration range of 0.2–20 g/L. The light scattering and concentration data were fit to a set of association models using Calypso software (Wyatt Technology, Santa Barbara, CA).

To obtain a stoichiometric analysis of RSA of mAb-J under different solution conditions, light scattering data were fit to various association models using equation 2, a virial expansion for non-ideal solutions containing associating components;

$$\frac{R_{\theta}}{K} = \frac{\sum_i iMC_i}{1+2A_2MC^{\text{tot}}} \quad (\text{Eq.2})$$

R_{θ} is the excess Rayleigh ratio, M the molecular weight, i is the stoichiometry of the associated species (e.g., $i = 2$ for a dimer), C_i are the concentrations of the individual species, and C^{tot} is the total concentration. A_2 is the osmotic second virial coefficient, left unconstrained during data fitting. A_2 , provides useful insights into intermolecular interactions between protein molecules. A negative value of A_2 indicates that the overall interactions between protein molecules are attractive, while a positive value indicates that the overall interactions are repulsive. K in equation 2 is the optical constant described by equation 3

$$K = \frac{4\pi^2 n_0^2}{N_A \lambda_0^4} / \left(\frac{dn}{dc} \right)^2 \quad (\text{Eq.3})$$

with n_0 as the refractive index of the solvent (1.33), N_A is Avogadro's number (mol^{-1}), dn/dc is the refractive index increment of the protein/solvent pair (0.185 mL/g),^{70, 71} and λ_0 is the wavelength of the incident light in vacuum. Following an iterative procedure, A_2 and C_i values

were optimized to achieve the best fit (based on χ^2) between the light scattering data and various association models (see Table S1 for the χ^2 values). A monomer-dimer-tetramer association equilibrium model best fit the light scattering data for mAb-J (see Table S2 for the A_2 values).

4.2.5 Lyophilization of mAb-J samples

Stock solutions of mAb-J at 150 g/L, dialyzed against the control (containing 10% w/v trehalose), were diluted to 5 and 60 g/L using control buffer, and 500 μ L were dispensed into 3 mL FIOLEX[®] clear Type 1 glass vials (Schott North America, Elmsford, NY) with a fill volume of 500 μ L. The vials were partially stoppered by 2-leg, 13 mm siliconized rubber stoppers (Wheaton Industries Inc., Millville, NJ). The samples were then lyophilized using a LyoStar II lyophilizer (SP Scientific, Warminster, PA) using an optimized lyophilization cycle described previously.³⁹

4.2.6 Circular Dichroism

Lyophilized mAb-J samples at both 5 and 60 g/L were reconstituted with D₂O to a concentration of 0.3 g/L. CD experiments were carried out with a Chirascan Plus Circular Dichroism Spectrometer (Applied Photophysics Ltd., Leatherhead, UK) equipped with a Peltier temperature controller and a four-position cuvette holder. Far-ultraviolet (UV) CD spectra of non-lyophilized control and freeze-dried mAb-J samples (0.3 g/L) were collected from 200 nm to 260 nm using 0.1 cm path length quartz cuvettes. CD scans were collected at 10 °C using a sampling time of 1 second and a bandwidth of 1 nm. Non-lyophilized mAb-J samples were prepared in H₂O-based control buffer. Ellipticity values obtained from the instrument were then converted to molar ellipticity by dividing ellipticity by protein concentration (M) and cuvette path length (m).

4.2.7 Size-Exclusion Chromatography

Freeze-dried mAb-J samples at both 5 and 60 g/L were reconstituted to 0.5 g/L using D₂O and then centrifuged at 14000 x g for 5 minutes to remove any insoluble aggregates prior to SEC analysis. A Shimadzu high performance liquid-chromatography system equipped with a photodiode array detector capable of recording UV absorbance spectra from 200 to 400 nm was used. A 7.8 mm × 30 cm Tosoh TSK-Gel BioAssist G3SW_{xL} (TOSOH Biosciences, King of Prussia, PA) and a corresponding guard column were preconditioned with 0.2 M sodium phosphate, pH 6.8, and then calibrated using gel-filtration molecular weight standards (Bio-Rad, Hercules, CA). mAb-J species were separated at 0.7 mL min⁻¹ based on their size. A dual wavelength quantification method described previously⁷² was used to quantify the amounts of various species of mAb-J in solution. Non-lyophilized samples were prepared in H₂O-based control buffer. To calculate the amount of insoluble aggregates in reconstituted mAb-J samples, the total area of all the species (soluble aggregates, monomer, and fragment) in the chromatogram was calculated. The difference between the total peak areas of the sample and the control was defined as total insoluble aggregates.

4.2.8 Deuteration of arginine

To remove exchangeable ¹H from arginine, arginine hydrochloride was dissolved in D₂O at appropriate concentrations and then dried at 30 °C for 24 hours in a VacufugeTM vacuum concentrator (Eppendorf, Hauppauge, NY). The process was repeated three times. After the third drying cycle, the deuterated arginine powder was reconstituted with D₂O-based 5 mM citrate-phosphate buffer (pH 6.0). The final pH was adjusted with deuterium chloride or deuterium oxide to be within 0.02 pH unit of the desired pH. The pH values were recorded without correction for the deuterium isotope effect.⁷³

4.2.9 Hydrogen-Exchange Mass Spectrometry

Hydrogen exchange was initiated by adding 500 μL of D_2O to vials of lyophilized mAb-J as described in more detail previously.³⁹ Labeling was thermostated to 25 $^\circ\text{C}$ on an Echotherm chilling/heating plate (Torrey Pines Scientific, Inc. Carlsbad, CA). Hydrogen exchange was quenched after 120, 2760, 10^4 and 10^5 seconds by adding 20 μL of the exchange reaction mixture to 180 μL of quench buffer containing 0.5 M tris(2-carboxyethyl) phosphine hydrochloride, 4 M guanidine hydrochloride, and 0.2 M sodium phosphate at pH 2.5 pre-equilibrated at 1 $^\circ\text{C}$. An H/DX PAL robot (LEAP Technologies, Carrboro, NC) was used for sample handling and injection. Subsequent to the quench step, samples were loaded into the sample loop of the refrigerated column compartment containing three valves connected to an Agilent 1260 infinity series LC (Agilent Technologies, Santa Clara, CA), an immobilized pepsin column, a peptide desalting trap, and a C18 column. The level of deuteration in each peptide was measured using an Agilent 6530 quadrupole-time of flight mass spectrometer (Agilent Technologies, Santa Clara, CA), equipped with a standard electrospray ionization source operated in positive mode. A complete description of the hydrogen exchange methodology was previously reported.³⁹

4.2.10 Hydrogen Exchange Mass Spectrometry (HX-MS) with viscosity-decreasing solutes

A D_2O -based 5 mM citrate-phosphate buffer (pH 6.0) was used to make reconstitution solutions containing 100 mM of deuterated arginine and 100 mM NaCl, respectively. Lyophilized mAb-J samples at 5 g/L were reconstituted using 500 μL of D_2O -based 5 mM citrate-phosphate buffer (pH 6.0). Half of the lyophilized mAb-J samples at 60 g/L were reconstituted using 5 mM citrate-phosphate buffer (pH 6.0) containing 100 mM deuterated arginine while the other half was reconstituted using the same buffer containing 100 mM NaCl instead of 100 mM arginine, yielding a final solution composition of 25 mM citrate phosphate buffer (pH 6.0) containing 30 mM sodium chloride, 10 % (w/v) trehalose with or without 100 mM arginine or 100 mM NaCl. The hydrogen

exchange reaction was quenched after 2760 seconds. A full description of the hydrogen exchange process is described elsewhere.³⁹

4.2.11 HX-MS data processing and analysis

mAb-J peptic peptides were identified using accurate mass (± 10 ppm) and tandem MS with collision-induced dissociation on a quadrupole-time of flight mass spectrometer. A total of 182 peptides covering 92% of the primary sequence of mAb-J were identified and used for analysis. HDExaminer (Sierra Analytics, Modesto, CA) was used for initial processing of the HX-MS data. Deuterium uptake plots with average deuterium uptake values and standard deviations from triplicate hydrogen exchange runs for each peptide were generated using an R script, written in-house. A 99% confidence interval of ± 0.40 Da for the differences in our dataset was calculated using a procedure we described previously.³⁹ HX-MS results were mapped onto a homology model of mAb-J created using the method described previously³⁹ based on crystal structures of an isolated Fc⁴⁷ and an in-silico generated KOL/Padlan structure of Fab.⁴⁶ Pymol (Schrödinger LLC, Portland, OR) was used to display the results

4.3 Results

4.3.1 Increases in mAb hydrodynamic diameter suggests reversible self-association

In an initial set of experiments done to better understand the possible mechanism(s) of mAb-J RSA, the effects of solution properties and additives on the magnitude of RSA at relatively low protein concentration (1-10 g/L) were examined. All results are described relative to mAb-J in a control solution (20 mM citrate-phosphate, 30 mM NaCl, pH 6.0). Figure 1 shows the effects of charged co-solutes and sugars and changes in solution pH on the average hydrodynamic

diameter of mAb-J, as determined by dynamic light scattering (DLS). The average hydrodynamic diameter of a full length, monomeric IgG1 mAb molecule is typically 9-12 nm.^{44, 45} At 10 g/L, the hydrodynamic diameter of mAb-J in the control solution was 17.5 nm, significantly higher than a typical monomeric IgG1 mAb. The large hydrodynamic diameter suggests that mAb-J undergoes self-association even at the relatively low concentration of 10 g/L at low ionic strength. The average hydrodynamic diameter of mAb-J in solution decreased (from 17.5 nm at low ionic strength to 12.8 nm) in the presence of an additional 100 mM NaCl. This same hydrodynamic diameter vs. ionic strength trend also was evident in the presence of either sucrose or trehalose (Figure 1A). The average hydrodynamic diameter of mAb-J decreased (from 17.5 nm to 10.8 nm) in the presence of 100 mM arginine. In contrast, the addition of sucrose and trehalose caused increases in the average hydrodynamic diameter (from 17.5 nm to 18.8 and to 19.7 nm, respectively; Figure 1A). Raising the pH from 5.0 to 7.0 also resulted in an increased hydrodynamic diameter (from 13.0 nm to 18.8 nm, Figure 1B). Taken together, these data suggest that the extent of mAb-J RSA, even at 10 g/L, decreases as the ionic strength increases. MAb-J RSA increases, however, in higher pH solutions or upon addition of sugars. Since the experimental limit for DLS is around 10 g/L protein concentration, which limits the investigation of association at higher concentrations, we then used dynamic viscosity to investigate protein-protein interactions at higher mAb-J concentrations.

4.3.2 Effects of solutes on the dynamic viscosity of mAb-J solutions

Highly associated protein will usually cause a dramatic increase in solution viscosity at high protein concentrations.^{20, 21} Trends in mAb-J solution viscosity with increased protein concentration under various solution conditions are shown in Figure 2. The solution viscosity of mAb-J in the control buffer increased exponentially with protein concentration, an effect that can

be attributed to RSA between mAb monomers. Addition of NaCl or arginine to the control solution at concentrations up to 100 mM weakened the effect. Consistent with DLS results, the effect of arginine on the viscosity of mAb-J was stronger than NaCl. The effect of pH and sugars can be seen by comparing the solution viscosity of mAb-J at 60 g/L. As the pH of the control buffer was increased from 5.0 to 7.0, the viscosity of 60 g/L mAb-J increased (Figure 2D). When either trehalose or sucrose was added, the viscosity of the mAb-J solution increased, with the effect of trehalose stronger than sucrose. The solution viscosity of buffer in the absence of protein only increased slightly upon addition of sugars. Taken together, the viscosity results provide further evidence supporting the presence of concentration-dependent transient protein-protein interactions between mAb monomers. An increase in the ionic strength of the solution or addition of arginine decreased solution viscosity, while an increase in pH from 5.0 to 7.0 caused the dynamic viscosity of mAb-J solution to increase. These observations suggest that mAb-J intermolecular interactions are primarily driven by attractive electrostatic interactions.

4.3.3 Reversible self-association of mAb-J involves a monomer-dimer-tetramer equilibrium

The nature of mAb-J intermolecular interactions was further studied using composition-gradient multi-angle light scattering (CG-MALS). Static light scattering quantifies the excess Rayleigh ratio (R), the fractional amount of incident light that is scattered by the macromolecule per unit volume of the solution. Intermolecular interactions affect the magnitude of the Rayleigh ratio. If the relationship between R , as a function of the scattering angle (θ), and protein concentration is known, then the apparent molecular weight, size, and extent of self-association of the molecule can be determined using values of the osmotic second virial coefficient (A_2) combined with stoichiometry estimates based various association models (as described in detail in the Experimental Section of the Supporting Information).

The mole fractions of monomeric, dimeric, and tetrameric forms of mAb-J under the experimental conditions were determined (Figure 3) based on fitting the static light scattering data to a monomer, dimer, tetramer association equilibrium model. First, for mAb-J at 20 g/L in control buffer containing 10% w/v trehalose, the solution had nearly-equal mole fractions of monomeric mAb-J (0.48) and tetrameric mAb-J (0.48) (Figure 3A). This observation suggests extensive protein-protein interactions, supported by an osmotic second virial coefficient (A_2) value of $-9.6 \times 10^{-5} \text{ mol mL g}^{-2}$. In the presence of an additional 100 mM NaCl in the control buffer, the mole fraction of monomeric mAb-J did not decrease as steeply, reaching a value of 0.63 at 20 g/L. Interestingly the mole fraction of dimer was 0.27, whereas tetramer was only 0.1 under these conditions (Figure 3B). The value of A_2 for mAb-J in the presence of additional 100 mM NaCl became positive, $2 \times 10^{-5} \text{ mol mL g}^{-2}$, in contrast to the negative value under low ionic strength solution conditions. The positive A_2 value indicates disruption of protein-protein interactions. In the presence of 100 mM arginine, mAb-J was completely monomeric even at 20 g/L, suggesting complete disruption of attractive intermolecular interaction between mAb-J monomers over the concentration range tested (Figure 3C). Disruption of protein-protein interactions by arginine is further supported by a large, positive value of A_2 ($9 \times 10^{-5} \text{ mol mL g}^{-2}$) for mAb-J in the presence of arginine.

4.3.4 Hydrogen exchange mass spectrometry reveals association between the Fc and Fab

To map the interfaces responsible for protein-protein interactions, the non-associating and associating protein states must be compared. We chose to compare the protein concentrations 5 g/L (~90% monomeric) and 60 g/L (less than 50% monomeric) by HX-MS analysis. To conduct hydrogen exchange at high protein concentration, we followed an approach we recently developed,³⁹ which involves reconstituting lyophilized mAb-J with D₂O-containing buffer rather than diluting

the solution with D₂O. A combination of size-exclusion chromatography (SEC), circular dichroism (CD), and viscosity measurements confirms the structural integrity of mAb-J samples after lyophilization, as described in the Supporting Information (Figure S1, and Table S3). To maintain the high concentration of mAb-J during hydrogen exchange, the lyophilized samples of mAb-J were reconstituted with pure D₂O to yield a final solution composition of 20 mM citrate phosphate buffer (pH 6) containing 10% w/v trehalose and 30 mM NaCl (i.e., control buffer + 10% w/v trehalose in D₂O). To eliminate artifacts that might potentially arise from altered chemical exchange kinetics, the composition of the buffer was held constant while only the mAb-J concentration was changed. Following selected intervals of hydrogen exchange, the reaction was quenched by lowering the pH to 2.5, and the sample was then digested with pepsin, and analyzed by LC-MS (see Supporting Information).

No significant differences were observed in the measured HX between low and high protein concentration for almost 95% of the peptic peptides of mAb-J (see Figure S3). Deuterium uptake plots for some representative peptides in this category are shown in Figure 4A. There were certain peptides, however, that exhibited significant protection against deuterium uptake at 60 g/L mAb-J. Figure 4B shows representative deuterium uptake plots for some of the peptides that became significantly protected. Deuterium uptake plots for all of the peptides from mAb-J are shown in Figure S3 and a list of all the peptides and their sequential numbering is given in Table S4. A global representation of all of the changes in hydrogen exchange between mAb-J at 5 and 60 g/L is shown in Figure 5. Relative mass difference or the differences in deuterium uptake (Δm) between mAb-J peptides from 60 and 5 g/L samples (Eq.4) are plotted on the vertical axis and ordinal peptide number on the horizontal axis of the plot with:

$$\Delta m = m_{60 \text{ g/L}} - m_{5 \text{ g/L}} \quad (\text{Eq.1})$$

These plots show the location of protected ($\Delta m < 0$ Da) and de-protected ($\Delta m > 0$ Da) regions in mAb-J.

Comparison of the level of deuteration revealed various regions within mAb-J that became significantly protected at 60 g/L under conditions where mAb-J was substantially self-associated. The protected regions are located in the variable heavy chain (V_H), variable light chain (V_L), and constant domain of the heavy chain (C_{H3}) of the antibody. In the heavy chain of the antibody, these regions cover HC 92-116 (peptide numbers 42 to 47) located in the third complementarity-determining region of the heavy chain (CDR3H) and HC 381-408 (peptide numbers 105 to 111) that surrounds a region in the C_{H3} domain. In addition, in the light chain, a segment that became significantly protected (LC 39-76), peptide numbers 135 to 140, spans the second CDR of the light chain (CDR2L) located in the V_L domain of the antibody. None of the regions in mAb-J became significantly more flexible (higher HX) at high protein concentration.

Thus, significant decreases in hydrogen exchange (i.e., increased protection against deuterium uptake) were observed upon RSA of mAb-J in two of the six CDR regions (i.e., the CDR2 region of the light and CDR3 region of the heavy chain) and in the C_{H3} domain of mAb-J. Figure 6 shows the protected regions mapped onto a homology model of mAb-J (for details about the homology model, see Materials and Methods in the Supporting Information). The segments that became significantly protected at high protein concentration are highlighted in yellow (Figure 6). A surface representation of the Fab and Fc of mAb-J is also shown in Figure 6 where protected segments, presumably the primary protein interface of RSA, are colored in yellow as in the ribbon representation. In the surface representation, the negatively-charged residues that became protected are colored red, the positively charged residues that became protected are blue, and surface exposed hydrophobic residues are colored in green. The homology model of mAb-J was

constructed with the in silico KOL/Padlan structure of the Fab⁴⁶ and the crystal structure of Fc derived from PDBID:3AVE⁴⁷ after mutations and insertion of missing residues from the mAb-J sequence as described in the Supporting Information. It should be noted that, while the level of confidence in the location and surface exposure of residues in the highly-conserved C_{H3} domain is high, the exact location and surface exposure information of the V_H and V_L domain residues may be less reliable.

To confirm that the changes in hydrogen exchange resulted from specific interactions between mAb-J monomers rather than non-specific interactions arising from non-ideality at high protein concentrations, we compared a mAb-J control at 60 g/L to mAb-J samples at 60 g/L containing control buffer and either 100 mM arginine or 100 mM NaCl (Figure S4). As described above, arginine and sodium chloride both inhibited self-association as indicated both by decreased hydrodynamic diameter (Figure 1A) and reduced solution viscosity (Figure 3). The regions of mAb-J that became significantly protected under control solution conditions were the same regions that became protected at high protein concentration when compared to low concentration non-associating control (Figure 5), confirming the validity of the analysis. Stronger protection in the control mAb-J sample when compared to that with 100 mM arginine reflects arginine's more potent action at disrupting mAb-J RSA in comparison to 100 mM NaCl. Regions in the heavy chain, HC 87-93 (peptide number 41) and LC 35-38 (peptide number 132) became significantly more rigid upon addition of arginine at 60 g/L (see Figure S4A). These regions are at the N-terminal of the RSA interface present in V_H and V_L domains of the antibody. A decrease in local flexibility upon addition of arginine could be attributed to allosteric effects of the arginine-inhibited self-association.⁴⁸

We also compared hydrogen exchange by mAb-J at 60 g/L in control buffers containing

either 100 mM NaCl or 100 mM arginine to a sample of mAb-J at 5 g/L in control buffer without any additional charged solutes. Difference plots comparing HX between these samples are shown in Figure S5. None of the 182 peptides analyzed in this experiment became either protected or de-protected. These observations suggest that a solution of mAb-J containing additional 100 mM NaCl or 100 mM arginine at 60 g/L protein concentration behaves similarly to a dilute solution of mAb-J without any additional charged solutes, indicating the absence of significant specific intermolecular interactions.

4.4 Discussion

MAbs may form intermolecular protein-protein interaction networks at high protein concentration.^{20, 21} These large, associated protein complexes typically cause a dramatic increase in solution viscosity that can introduce a number of challenges to their pharmaceutical use. This work has two primary goals: 1) to determine the macroscopic nature of protein-protein interactions between mAb-J monomers at high protein concentration; and 2) to further delineate the underlying molecular mechanisms that promote RSA by mapping the protein interface of interaction at high protein concentration.

To investigate the nature of reversible non-covalent protein-protein interactions, their extent was measured indirectly by measuring the hydrodynamic diameter and dynamic viscosity of mAb-J solutions at varying pH values, with and without charged and uncharged solutes. The hydrodynamic diameter and the viscosity of mAb-J decreased as ionic strength increased. Based on fitting static light scattering measurements to various association models, we found that a monomer-dimer-tetramer equilibrium provided the best fit for mAb-J self-association. A sharp

decline in monomer mole fraction with increasing protein concentration and a negative A_2 value at low ionic strength was observed. On the contrary, a slower decrease in the monomer mole fraction and positive A_2 values in the presence of additional NaCl or arginine was observed. A decrease in the propensity of mAb-J to form protein-protein complexes with an increase in ionic strength can be attributed to electrostatic attractive interactions being the dominant contributor governing protein-protein interactions between mAb-J monomers.⁴⁹⁻⁵¹ Based on DLVO (Derjaguin-Landau-Verwey-Overbeek) theory, as ionic strength is increased the Debye screening length (the thickness of the electrical double layer surrounding the protein molecule) shortens and the effective charge on the mAb will decrease due to electrostatic charge screening.⁵² Under such conditions, the strength of both repulsive and attractive electrostatic interactions decreases, thereby causing disruption of intermolecular protein interactions between mAb-J molecules.

The predicted isoelectric point for mAb-J is ~7.3. Increasing the pH from 5.0 to 7.0 promoted the extent of protein-protein interactions between mAb-J monomers. This observation contradicts predictions based on the electroviscous effect that describes the viscosity of dilute colloidal solutions as directly proportional to the electrostatic charge on the molecule.⁵³ According to the electroviscous effect, solution viscosity should decrease as the pH is moved towards the pI of the protein where the overall net charge on the molecule approaches its minimum.⁵⁴⁻⁵⁶ However, we observed the opposite. Yadav et al⁴⁹ also observed an increase in the extent of mAb1 association near the pI of the antibody. In another report, Yadav et al⁵⁰ showed that the mutual diffusion coefficient for an antibody decreased as the pH value approached the pI of the protein. This observation was attributed to an increase in the extent of specific protein-protein interactions between mAb-2 molecules near the pI. At a pH value below or above the pI, the overall net charge on a protein will be either positive or negative, respectively. Away from the pI, the electrostatic

repulsive interactions between protein molecules dominate and contributions by attractive dipolar interactions are weakest. At the pI, although the overall net charge on the protein reaches its minimum, thus decreasing global intermolecular repulsions, large numbers of charged amino acids can still be present at the surface. These charged side chains, if present in a specific distribution, can cause formation of localized charged patches on the protein surface. Charged patches on the protein surface can lead to spatial reorientation of protein molecules, which might initiate favorable dipole-dipole and charge-dipole interactions between protein molecules.⁴⁹ At high protein concentrations the intermolecular distances between protein molecules decrease to a few Angstroms. Around the pI, where intermolecular repulsive interactions reach a minimum, short-ranged and non-specific attractive interactions between surface-exposed hydrophobic residues, hydrogen bonding, and van der Waals interactions can also become significant contributors to intermolecular protein-protein interactions. These attractive non-covalent interactions could cause the monomers to form protein-protein associated complexes that further cause a dramatic increase in solution viscosity at high protein concentrations.

The addition of sugars and polyols has been shown to affect protein structure and protein-protein interactions.^{57, 58} Our results (Figures 1B and 2D) showed both sucrose and trehalose enhanced the extent of protein-protein interactions as reflected by increased hydrodynamic diameter and solution viscosity of mAb-J. Sugars are preferentially excluded from the protein surface, causing water molecules to populate around protein domains. Accumulation of water at the surface produces an unfavorable increase in protein chemical potential.^{59, 60} To counter such thermodynamically unfavorable interactions between apolar side-chains and water molecules, the protein structure responds by minimizing the exposed surface area, leading to lower preferential exclusion. Thus, sugars are often added to protein solutions to increase protein conformational

stability. At high protein concentrations, however, where the intermolecular distances between protein monomers are relatively shorter, preferential exclusion can also lead to formation of reversible (or potentially irreversible) protein-protein interactions because the interactions decrease solvent exposure, thereby lowering the extent of unfavorable preferential exclusion. While stabilizing, added sugars can also contribute to the formation of protein-protein complexes that cause an enhanced effect on the exponential increases in solution viscosity at high protein concentrations, as seen here.

To map the protein interfaces of mAb-J self-association at high protein concentration, we used HX-MS to compare associated and non-associated mAb-J. Our results show that the observed reversible protein-protein interactions involve both the Fab and Fc regions of the antibody. Hydrogen exchange in regions covering HC 92-116 in V_H domain spanning CDR3H, LC 39-76 in V_L domain spanning CDR2L and HC 381-408 in the Fc (C_H3) domain of the mAb-J significantly decreased (i.e., increased protection) when the concentration of mAb-J was increased from 5 to 60 g/L. Based on this HX data, we conclude that these protein regions are the primary site of reversible interactions between mAb-J monomers. This is supported by control HX experiments comparing 60 g/L mAb-J with and without viscosity-lowering additives (Figures S4 and S5) where the same regions in mAb-J in control buffer became significantly protected. Based on a lower resolution biophysical analysis, we found that adding NaCl or arginine decreased association, suggesting involvement of electrostatic interactions between oppositely-charged patches at the interface. The regions spanning CDR2L in the V_L domain, LC 39-76 (YQQLPGTAPKLLIYDNFNRPSPDRFSGSKSGTSASL) and the region in the V_H domain of mAb-J that spans the CDR3H, HC 92-116 (AVYYCATVMGKWIKGGYDYWGRGTL) will each have a charge of +2 at pH 6.0. In contrast, the region in the Fc domain of the antibody that became

significantly protected, LC 381-408 (IAVEWESNGQPENNYKTTPPVLDSDGSF) will have a net charge of -4 at pH 6.0.

It should be noted, however, not all of the charged side-chains at the protein interface are expected to be solvent exposed. To correctly predict the net surface charge at the protein interface, only solvent-accessible charged side-chains should be considered. Figure 6A shows a homology model of mAb-J with the HX-protected regions colored in yellow. Here, only the solvent accessible surfaces of Fab and Fc regions of mAb-J are shown in Figures 6B and 6C. Residues containing charged side chains at the Fab and Fc interfaces of mAb-J are colored in blue (positively charged) and red (negatively charged). Among all the charged side-chains, the lysine residue towards the N-terminal of the V_H domain interface (K102) and two arginine and one lysine residues (R507, R514 and K519) in the V_L domain interface are solvent exposed. Only one of the two aspartic acid residues in the V_L domain (D503) has a solvent exposed side chain. In the Fc interface, however, all of the positively and negatively charged side chains are either fully or partially solvent exposed. As mentioned previously, confidence in the homology model is lowest in the variable regions, however, CDR loops are primarily unstructured, dynamic, and solvent exposed⁶¹ thus it is reasonable to expect that the lysine and arginine side-chains will be accessible. The interface on the surfaces of the V_L and V_H domains of the antibody forms a patch with a net positive charge and the interface on the surface of the Fc region has a net negative charge. The presence of charge anisotropy between the protein interfaces of the Fab and Fc regions is consistent with the biophysical characterization of mAb-J RSA that suggests protein association is initiated by long-range electrostatic attractive interactions.

The involvement of the CDR in the Fab region in intermolecular protein-protein interactions has been well documented.^{21, 22, 24, 25, 39} Few reports, however, have implicated the Fc

region in mediating mAb RSA.^{23, 26} Nishi et al. used low resolution biophysical tools to show the involvement of the Fc region in mediating reversible Fc-Fc interactions between mAb monomers. Chaudhri et al. used coarse-grained molecular dynamic simulations to probe the nature of site-site interactions between mAb monomers. Significant intermolecular Fab-Fc interactions were present in one of the two antibodies that they simulated. Ido et al,⁶² using frequency modulation atomic force microscopy (FM-AFM), showed that mAbs self-assemble into rosette-shaped hexamers through lateral Fc-Fc interactions between monomers. Based on our HX measurements, mAb-J monomers could undergo association through Fab-Fab, Fc-Fc or Fab-Fc interactions. However, due to the presence of opposite charges on Fab and Fc domain interfaces of mAb-J, Fab-Fc mediated protein-protein interactions seem most likely.

To the best of our knowledge, this report provides the first direct interfacial mapping of mAb RSA at high protein concentration with protein interfaces in both Fab and Fc region of the antibody. The protein sequence of the mAb-J Fc interface is conserved between all antibodies of IgG1 subclass. Thus, the negatively-charged patch would be present in all IgG1s. In contrast, the corresponding interface in the Fab region spans the CDR2L and CDR3H regions of this specific antibody. Amino acid sequences of the hypervariable regions or the CDR regions differ greatly between different mAbs. A special case of specific orientation and distribution of charged, aliphatic and aromatic amino acids in the Fab region interface of mAb-J might contribute significantly to initiating favorable interactions between Fab and Fc domain interfaces of mAb-J.

Another observation of interest was the more potent action of arginine compared to NaCl on decreasing the size of mAb-J complexes and the viscosity of the mAb-J solutions. Our results showed arginine caused a greater decrease in hydrodynamic diameter and solution viscosity than NaCl, as measured by DLS, viscosity, and CG-MALS (Figures 1A, 2AB, and 3, respectively).

Analysis of the static light scattering data showed that arginine completely disrupts the interactions between mAb-J monomers, and that its effect is stronger than the effect of NaCl, which still allows formation of dimers and tetramers of mAb-J. These results suggest that, although the interactions between mAb-J monomers are dominated by electrostatic attraction, there may also be additional secondary contributions by other short range non-covalent interactions, such as van der Waals interactions, hydrogen bonding, π - π stacking interactions and hydrophobic interactions. These observations collectively suggest that arginine's effect is not limited to only electrostatic charge shielding and disruption of charge-charge attractive interactions.

Arginine's potent effect on protein-protein interactions has been previously reported by other researchers.⁶³⁻⁶⁵ In addition to its charge-charge interactions with the ionizable side-chains of amino-acids, arginine has also been shown to interact favorably with the apolar and aromatic amino-acids.⁶³ Kita et al. and Arakawa et al.^{66, 67} suggested that arginine penetrates the protein solvation shell to interact with specific amino acid side chains in the protein. Shukla et al. performed molecular dynamics simulations that suggested formation of favorable interactions between arginine co-solute and aromatic and charged side-chains present on the protein surface.⁶⁵ Formation of favorable cation- π interactions between the guanidinium side chain of arginine and aromatic side chains of tryptophan, tyrosine, and phenylalanine and formation of salt bridges with charged side-chains of amino acids on the protein surface help to explain the more potent action of arginine in suppression of protein-protein interactions.⁶⁸

In addition to possessing surface-exposed oppositely charged amino acids at protein interfaces in the Fab and Fc regions of the mAb-J, the patches also contain surface-exposed hydrophobic residues. The interaction interfaces in the V_L and V_H domain together contain a tyrosine, a phenylalanine, a valine, and an isoleucine residue that are fully or partially surface-

exposed in the homology model. The protein interface in the Fc domain contains a tyrosine, a tryptophan, and a valine residue that are surface exposed. These surface-exposed aliphatic and aromatic residues at protein interfaces might be involved in mediating short-range non-covalent van der Waals and hydrophobic interactions. The effect of arginine on short-range non-covalent interactions in associating mAb systems is a topic currently being further evaluated in our laboratories.

Our proposed model for mAb-J RSA is shown in Figure 7. Because mAb-J associates through Fab-Fc interactions at high protein concentrations, depending upon the kinetics of association, the associated species might be tetramers or the association could potentially extend to the formation of either linear fibrous complexes or rosette-shaped protein complexes. Higher-order associated complexes formed at high protein concentrations would increase the shear modulus of the mAb solutions, causing a dramatic increase in solution viscosity.

In conclusion, our experiments show that mAb monomers can form reversibly-associated protein complexes mediated through Fab-Fc interactions. We also demonstrated that, although mAb-J intermolecular interactions are primarily driven by electrostatic attractive interactions, other short-ranged non-covalent forces may also play a role in mediating complex formation at high protein concentrations. Our results contribute to a better understanding of the nature of mAb RSA at high protein concentrations. This study further supports the notion that HX-MS can substantially aid protein engineering and candidate selection efforts directed toward the development of improved mAb therapeutics with superior physiochemical properties.⁶⁹

4.5 References

1. Jeong H, Mason SP, Barabási A-L, Oltvai ZN. Lethality and centrality in protein networks. *Nature* 2001; 411:41-2.
2. Shire SJ, Shahrokh Z, Liu J. Challenges in the development of high protein concentration formulations. *J Pharm Sci* 2004; 93:1390-402.
3. Ross CA, Poirier MA. Protein aggregation and neurodegenerative disease. *Nat Med* 2004; 10 Suppl:S10-7.
4. Ballatore C, Lee VM-Y, Trojanowski JQ. Tau-mediated neurodegeneration in Alzheimer's disease and related disorders. *Nat Rev Neurosci* 2007; 8:663-72.
5. Zimmerman SB, Trach SO. Estimation of macromolecule concentrations and excluded volume effects for the cytoplasm of *Escherichia coli*. *J Mol Bio* 1991; 222:599-620.
6. van den Berg B, Ellis RJ, Dobson CM. Effects of macromolecular crowding on protein folding and aggregation. *EMBO J* 1999; 18:6927-33.
7. Simpanya MF, Ansari RR, Suh KI, Leverenz VR, Giblin FJ. Aggregation of lens crystallins in an in vivo hyperbaric oxygen guinea pig model of nuclear cataract: dynamic light-scattering and HPLC analysis. *Invest Ophthalmol Vis Sci* 2005; 46:4641-51.
8. Connolly BD, Petry C, Yadav S, Demeule B, Ciaccio N, Moore JM, Shire SJ, Gokarn YR. Weak interactions govern the viscosity of concentrated antibody solutions: high-throughput analysis using the diffusion interaction parameter. *Biophys J* 2012; 103:69-78.
9. Ellis RJ. Macromolecular crowding: obvious but underappreciated. *Trends Biochem Sci* 2001; 26:597-604.

10. Eisenstein M. Something new under the skin. *Nat Biotechnol* 2011; 29:107-9.
11. Krieger IM, Eguiluz M. The second electroviscous effect in polymer latices. *Trans Soc Rheol (1957-1977)* 1976; 20:29-45.
12. van der Vorst B, van den Ende D, Aelmans NJJ, Mellema J. Shear viscosity of an ordering latex suspension. *Phys Rev E* 1997; 56:3119-26.
13. Graessley WW. The entanglement concept in polymer rheology. *The Entanglement Concept in Polymer Rheology*. Berlin, Heidelberg: Springer Berlin Heidelberg, 1974:1-179.
14. Buscall R, Goodwin JW, Hawkins MW, Ottewill RH. Viscoelastic properties of concentrated latices. Part 1.—Methods of examination. *J Chem Soc, Faraday Transactions 1: Physical Chemistry in Condensed Phases* 1982; 78:2873-87.
15. Cromwell ME, Hilario E, Jacobson F. Protein aggregation and bioprocessing. *AAPS J* 2006; 8:E572-E9.
16. Thomas C, Nienow A, Dunnill P. Action of shear on enzymes: studies with alcohol dehydrogenase. *Biotechnol Bioeng* 1979; 21:2263-78.
17. Braun A, Kwee L, Labow MA, Alsenz J. Protein aggregates seem to play a key role among the parameters influencing the antigenicity of interferon alpha (IFN- α) in normal and transgenic mice. *Pharm Res* 1997; 14:1472-8.
18. Hermeling S, Schellekens H, Maas C, Gebbink MF, Crommelin DJ, Jiskoot W. Antibody response to aggregated human interferon alpha2b in wild-type and transgenic immune tolerant mice depends on type and level of aggregation. *J Pharm Sci* 2006; 95:1084-96.

19. Joubert MK, Hokom M, Eakin C, Zhou L, Deshpande M, Baker MP, Goletz TJ, Kerwin BA, Chirmule N, Narhi LO. Highly aggregated antibody therapeutics can enhance the in vitro innate and late-stage T-cell immune responses. *J Biol Chem* 2012; 287:25266-79.
20. Liu J, Nguyen MD, Andya JD, Shire SJ. Reversible self-association increases the viscosity of a concentrated monoclonal antibody in aqueous solution. *J Pharm Sci* 2005; 94:1928-40.
21. Kanai S, Liu J, Patapoff TW, Shire SJ. Reversible self-association of a concentrated monoclonal antibody solution mediated by Fab–Fab interaction that impacts solution viscosity. *J Pharm Sci* 2008; 97:4219-27.
22. Bethea D, Wu S-J, Luo J, Hyun L, Lacy ER, Teplyakov A, Jacobs SA, O'Neil KT, Gilliland GL, Feng Y. Mechanisms of self-association of a human monoclonal antibody CNTO607. *Protein Eng Des Sel* 2012; 25:531-8.
23. Nishi H, Miyajima M, Wakiyama N, Kubota K, Hasegawa J, Uchiyama S, Fukui K. Fc domain mediated self-association of an IgG1 monoclonal antibody under a low ionic strength condition. *J Biosci Bioeng* 2011; 112:326-32.
24. Esfandiary R, Parupudi A, Casas-Finet J, Gadre D, Sathish H. Mechanism of Reversible Self-Association of a Monoclonal Antibody: Role of Electrostatic and Hydrophobic Interactions. *J Pharm Sci* 2015; 104:577-86.
25. Yadav S, Sreedhara A, Kanai S, Liu J, Lien S, Lowman H, Kalonia DS, Shire SJ. Establishing a link between amino acid sequences and self-associating and viscoelastic behavior of two closely related monoclonal antibodies. *Pharm Res* 2011; 28:1750-64.

26. Chaudhri A, Zarraga IE, Kamerzell TJ, Brandt JP, Patapoff TW, Shire SJ, Voth GA. Coarse-grained modeling of the self-association of therapeutic monoclonal antibodies. *J Phys Chem B* 2012; 116:8045-57.
27. Chaudhri A, Zarraga IE, Yadav S, Patapoff TW, Shire SJ, Voth GA. The role of amino acid sequence in the self-association of therapeutic monoclonal antibodies: insights from coarse-grained modeling. *J Phys Chem B* 2013; 117:1269-79.
28. Hvidt A, Linderstrøm-Lang K. Exchange of hydrogen atoms in insulin with deuterium atoms in aqueous solutions. *Biochim Biophys Acta* 1954; 14:574-5.
29. Hvidt A, Linderstrøm-Lang K. The kinetics of the deuterium exchange of insulin with D₂O. An amendment. *Biochim Biophys Acta* 1955; 16:168-9.
30. Englander SW, Kallenbach NR. Hydrogen exchange and structural dynamics of proteins and nucleic acids. *Q Rev Biophys* 1983; 16:521-655.
31. Zhang Z, Smith DL. Determination of amide hydrogen exchange by mass spectrometry: a new tool for protein structure elucidation. *Protein Sci* 1993; 2:522-31.
32. Bai Y, Sosnick TR, Mayne L, Englander SW. Protein folding intermediates: native-state hydrogen exchange. *Science* 1995; 269:192-7.
33. Wales TE, Engen JR. Hydrogen exchange mass spectrometry for the analysis of protein dynamics. *Mass Spectrom Rev* 2006; 25:158-70.
34. Hvidt A, Nielsen SO. Hydrogen exchange in proteins. *Adv Protein Chem* 1966; 21:287-386.

35. Skinner JJ, Lim WK, Bédard S, Black BE, Englander SW. Protein dynamics viewed by hydrogen exchange. *Protein Sci* 2012; 21:996-1005.
36. Skinner JJ, Lim WK, Bédard S, Black BE, Englander SW. Protein hydrogen exchange: Testing current models. *Protein Sci* 2012; 21:987-95.
37. Houde D, Peng Y, Berkowitz SA, Engen JR. Post-translational modifications differentially affect IgG1 conformation and receptor binding. *Mol Cell Proteomics* 2010; 9:1716-28.
38. Majumdar R, Manikwar P, Hickey JM, Samra HS, Sathish HA, Bishop SM, Middaugh CR, Volkin DB, Weis DD. Effects of salts from the Hofmeister series on the conformational stability, aggregation propensity, and local flexibility of an IgG1 monoclonal antibody. *Biochemistry* 2013; 52:3376-89.
39. Arora J, Hickey JM, Majumdar R, Esfandiary R, Bishop SM, Samra HS, Middaugh CR, Weis DD, Volkin DB. Hydrogen exchange mass spectrometry reveals protein interfaces and distant dynamic coupling effects during the reversible self-association of an IgG1 monoclonal antibody. *mAbs* 2015; 7:525-39.
40. Jensen PF, Larraillet V, Schlothauer T, Kettenberger H, Hilger M, Rand KD. Investigating the interaction between the neonatal Fc receptor and monoclonal antibody variants by hydrogen/deuterium exchange mass spectrometry. *Mol Cell Proteomics* 2015; 14:148-61.
41. Walters BT, Jensen PF, Larraillet V, Lin K, Patapoff T, Schlothauer T, Rand KD, Zhang J. Conformational Destabilization of Immunoglobulin G Increases the Low pH Binding Affinity with the Neonatal Fc Receptor. *J Biol Chem* 2016; 291:1817-25.

42. Fang J, Richardson J, Du Z, Zhang Z. Effect of Fc-Glycan Structure on the Conformational Stability of IgG Revealed by Hydrogen/Deuterium Exchange and Limited Proteolysis. *Biochemistry* 2016; 55:860-8.
43. Houde D, Nazari ZE, Bou-Assaf GM, Weiskopf AS, Rand KD. Conformational Analysis of Proteins in Highly Concentrated Solutions by Dialysis-Coupled Hydrogen/Deuterium Exchange Mass Spectrometry. *J Am Soc Mass Spectrom* 2016; 27:669-76.
44. Armstrong J, Wenby R, Meiselman H, Fisher T. The hydrodynamic radii of macromolecules and their effect on red blood cell aggregation. *Biophys J* 2004; 87:4259-70.
45. Esfandiary R, Hayes DB, Parupudi A, Casas-Finet J, Bai S, Samra HS, Shah AU, Sathish HA. A systematic multitechnique approach for detection and characterization of reversible self-association during formulation development of therapeutic antibodies. *J Pharm Sci* 2013; 102:3089-99.
46. Padlan EA. Anatomy of the antibody molecule. *Mol Immunol* 1994; 31:169-217.
47. Matsumiya S, Yamaguchi Y, Saito J-i, Nagano M, Sasakawa H, Otaki S, Satoh M, Shitara K, Kato K. Structural comparison of fucosylated and nonfucosylated Fc fragments of human immunoglobulin G1. *J mol biol* 2007; 368:767-79.
48. Fischer G, Rossmann M, Hyvönen M. Alternative modulation of protein–protein interactions by small molecules. *Curr Opin Biotechnol* 2015; 35:78-85.
49. Yadav S, Liu J, Shire SJ, Kalonia DS. Specific interactions in high concentration antibody solutions resulting in high viscosity. *J Pharm Sci* 2010; 99:1152-68.

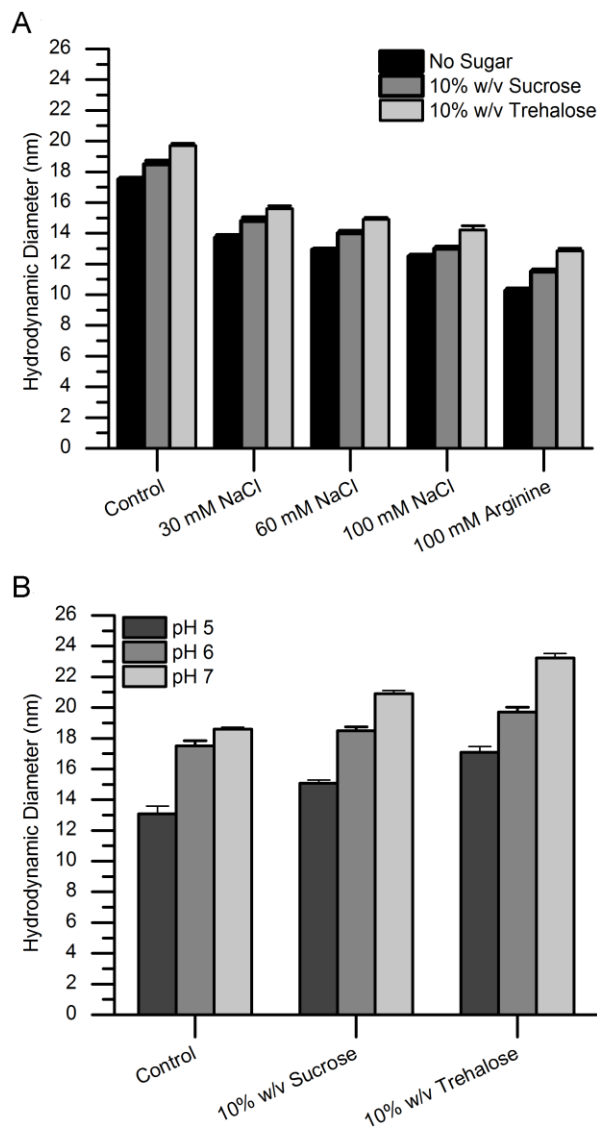
50. Yadav S, Shire SJ, Kalonia DS. Viscosity behavior of high-concentration monoclonal antibody solutions: Correlation with interaction parameter and electroviscous effects. *J Pharm Sci* 2012; 101:998-1011.
51. Yadav S, Laue TM, Kalonia DS, Singh SN, Shire SJ. The influence of charge distribution on self-association and viscosity behavior of monoclonal antibody solutions. *Mol Pharm* 2012; 9:791-802.
52. Zhang J. Protein-protein interactions in salt solutions. INTECH Open Access Publisher, 2012.
53. Smoluchowski Mv. Theoretische Bemerkungen über die Viskosität der Kolloide. *Kolloid Z* 1916; 18:190-5.
54. Buzzell JG, Tanford C. The effect of charge and ionic strength on the viscosity of ribonuclease. *J Phys Chem* 1956; 60:1204-7.
55. Komatsubara M, Suzuki K, Nakajima H, Wada Y. Electroviscous effect of lysozyme in aqueous solutions. *Biopolymers* 1973; 12:1741-6.
56. Bull HB. The electroviscous effect in egg albumin solutions. *Trans Faraday Soc* 1940; 35:80-4.
57. Arakawa T, Timasheff SN. Stabilization of protein structure by sugars. *Biochemistry* 1982; 21:6536-44.
58. Chi EY, Krishnan S, Randolph TW, Carpenter JF. Physical stability of proteins in aqueous solution: mechanism and driving forces in nonnative protein aggregation. *Pharm Res* 2003; 20:1325-36.

59. Lee JC, Timasheff SN. The stabilization of proteins by sucrose. *J Biol Chem* 1981; 256:7193-201.
60. Kendrick BS, Chang BS, Arakawa T, Peterson B, Randolph TW, Manning MC, Carpenter JF. Preferential exclusion of sucrose from recombinant interleukin-1 receptor antagonist: role in restricted conformational mobility and compaction of native state. *Proc Natl Acad Sci* 1997; 94:11917-22.
61. Chothia C, Gelfand I, Kister A. Structural determinants in the sequences of immunoglobulin variable domain. *J Mol Biol* 1998; 278:457-79.
62. Ido S, Kimiya H, Kobayashi K, Kominami H, Matsushige K, Yamada H. Immunoactive two-dimensional self-assembly of monoclonal antibodies in aqueous solution revealed by atomic force microscopy. *Nat Mater* 2014; 13:264-70.
63. Arakawa T, Ejima D, Tsumoto K, Obeyama N, Tanaka Y, Kita Y, Timasheff SN. Suppression of protein interactions by arginine: A proposed mechanism of the arginine effects. *Biophys Chem* 2007; 127:1-8.
64. Baynes BM, Wang DI, Trout BL. Role of arginine in the stabilization of proteins against aggregation. *Biochemistry* 2005; 44:4919-25.
65. Shukla D, Trout BL. Interaction of arginine with proteins and the mechanism by which it inhibits aggregation. *J Phys Chem B* 2010; 114:13426-38.
66. Kita Y, Arakawa T, Lin T-Y, Timasheff SN. Contribution of the surface free energy perturbation to protein-solvent interactions. *Biochemistry* 1994; 33:15178-89.

67. Arakawa T, Timasheff S. The mechanism of action of Na glutamate, lysine HCl, and piperazine-N, N'-bis (2-ethanesulfonic acid) in the stabilization of tubulin and microtubule formation. *J Biol Chem* 1984; 259:4979-86.
68. Gallivan JP, Dougherty DA. Cation- π interactions in structural biology. *Proc Natl Acad Sci* 1999; 96:9459-64.
69. Geoghegan JC, Fleming R, Damschroder M, Bishop SM, Sathish HA, Esfandiary R. Mitigation of reversible self-association and viscosity in a human IgG1 monoclonal antibody by rational, structure-guided Fv engineering. *mAbs* 2016:00-.
70. Van Holde KE, Johnson WC, Ho PS. *Principles of physical biochemistry*. 2006.
71. Barer R, Joseph S. Refractometry of living cells. *J Cell Sci* 1955; 3:423-47.
72. Bond MD, Panek ME, Zhang Z, Wang D, Mehndiratta P, Zhao H, Gunton K, Ni A, Nedved ML, Burman S. Evaluation of a dual-wavelength size exclusion HPLC method with improved sensitivity to detect protein aggregates and its use to better characterize degradation pathways of an IgG1 monoclonal antibody. *J Pharm Sci* 2010; 99:2582-97.
73. Glasoe PK, Long F. Use of glass electrodes to measure acidities in deuterium oxide¹, ². *J Phys Chem* 1960; 64:188-90.

4.6 Tables and Figures

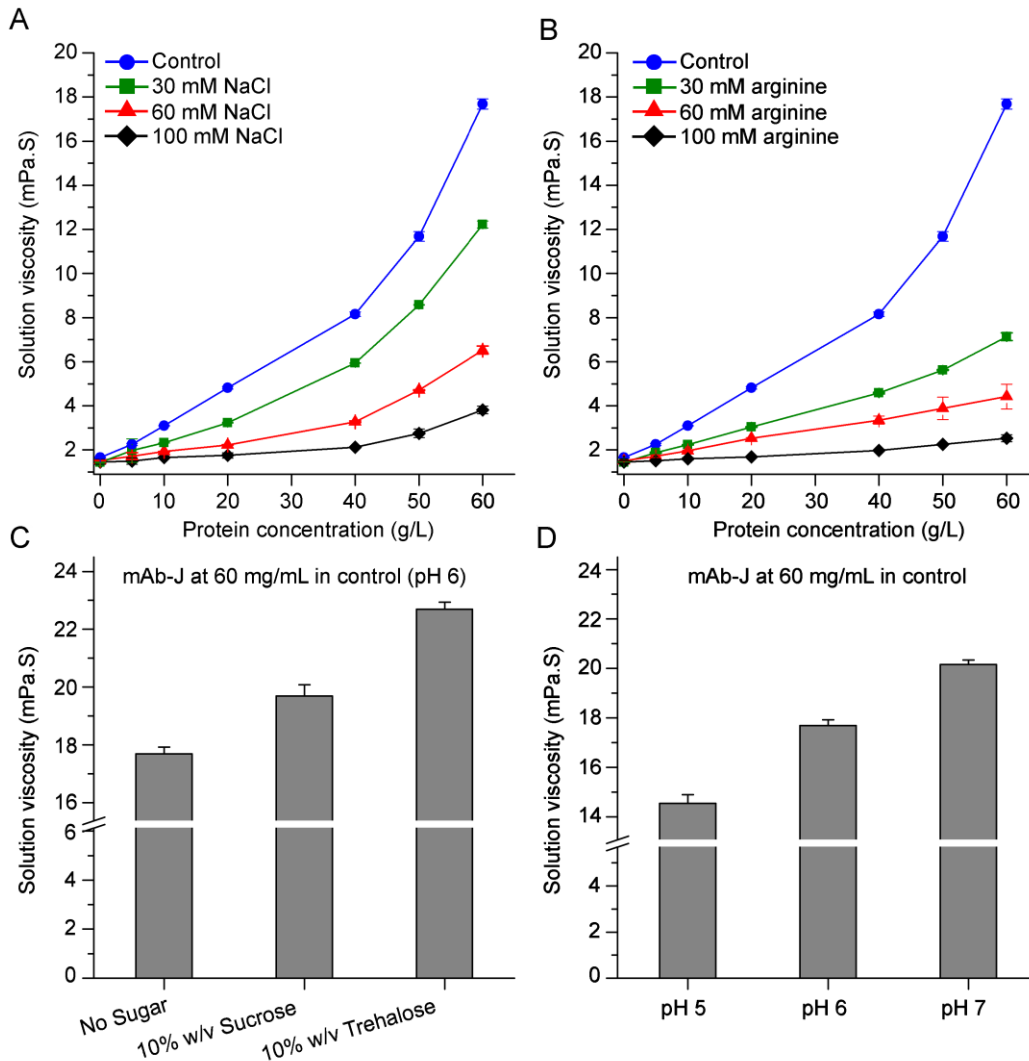
Figure 4.1



Effects of additives and pH on the hydrodynamic diameter of mAb-J as measured by dynamic light scattering. (A) Addition of incremental amounts of NaCl and 100 mM arginine to the control buffer and (B) addition of sugars and the effect of pH on the hydrodynamic diameter of mAb-J. All measurements were taken at 25°C. For panel A, mAb-J was prepared at 10 g/L in control solution (20 mM citrate-phosphate buffer containing 30 mM NaCl at pH 6.0) containing either additional

NaCl (30, 60 and 100 mM) or 100 mM arginine. For panel B, additional 10% (w/v) sucrose and trehalose were added to the control solution with the pH adjusted to (5.0, 6.0 and 7.0). The error bars represent one standard deviation from three independent DLS measurements.

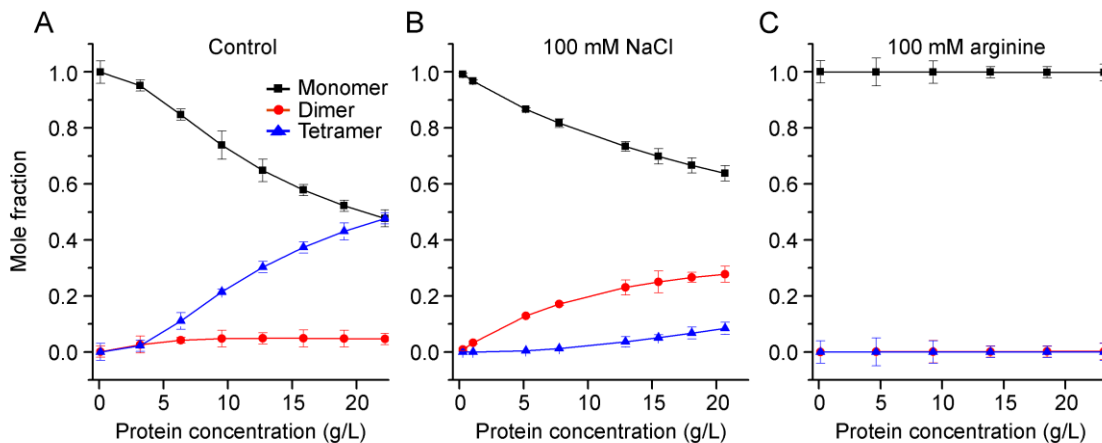
Figure 4.2



Concentration-dependent effects of additives and pH on the dynamic viscosity of mAb-J solutions. Effects of (A) NaCl and (B) arginine on solution viscosity as a function of mAb-J concentration. Effects of (C) 10% (w/v) sucrose and trehalose and (D) pH on solution viscosity of mAb-J solutions at 60 g/L protein concentration. All measurements of solution viscosity were taken at 25°C. In panels A, B and C, all samples of mAb-J were prepared in the control solution containing additional amounts of NaCl, arginine, or sugars. In panel D, mAb-J samples were prepared in the

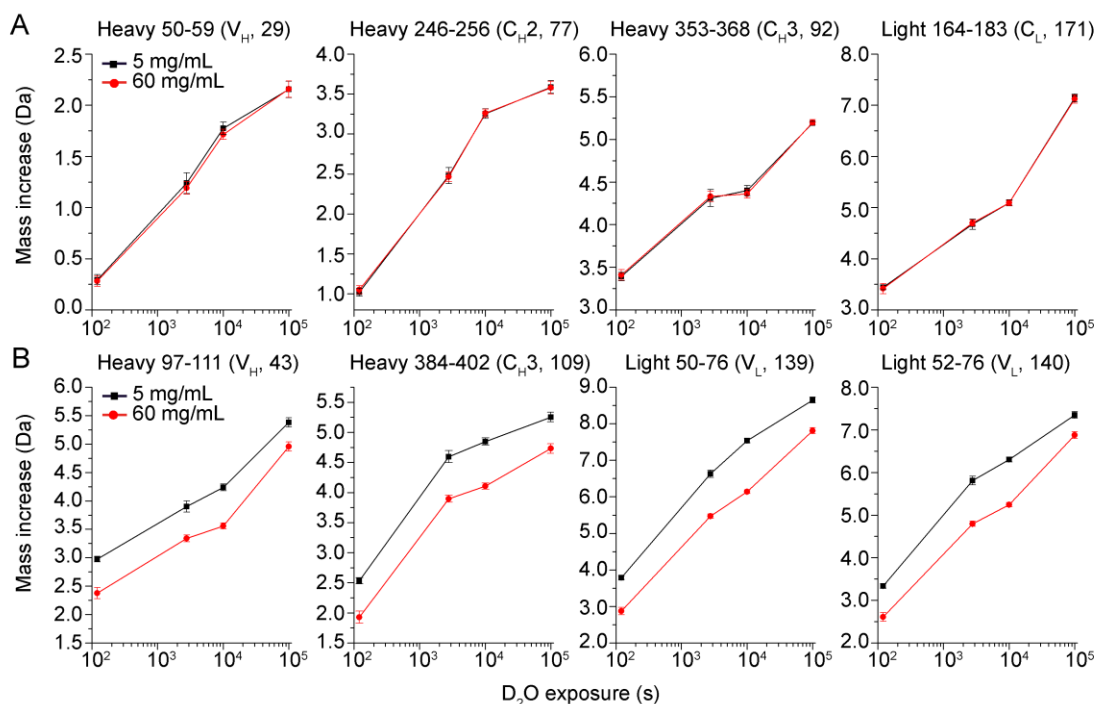
control with pH adjusted to (5.0, 6.0 and 7.0). The error bars represent one standard deviation from a set of three independent measurements in A and B the error bars are smaller than the symbols.

Figure 4.3



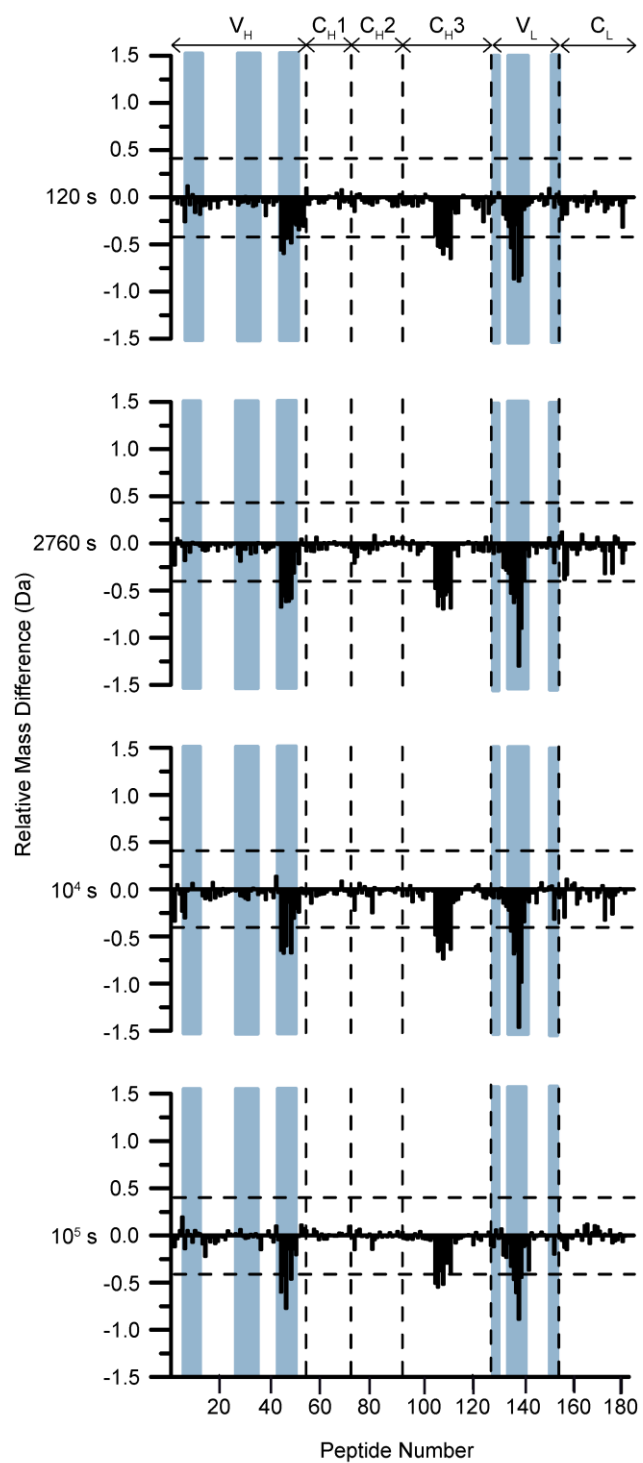
Effects of additives on the reversible self-association of mAb-J monomers based on analysis of static light scattering showing the mole fractions of monomeric (black squares), dimeric (red circles), and tetrameric (blue triangles) mAb-J species over a protein concentration range of 0.2-20 g/L in (A) control solution, (B) control solution + NaCl, and (C) control solution + arginine. In Panel C, the mole fractions of both dimer and tetramer are superimposed at zero. Samples of mAb-J were prepared in the control solution containing 20 mM citrate-phosphate buffer, 30 mM NaCl, 10% (w/v) trehalose at pH 6.0 with or without additional 100 mM NaCl or arginine. Panel A, B and C show mean of triplicate measurements at 25°C and error bars represent one standard deviation from the calculated mean.

Figure 4.4



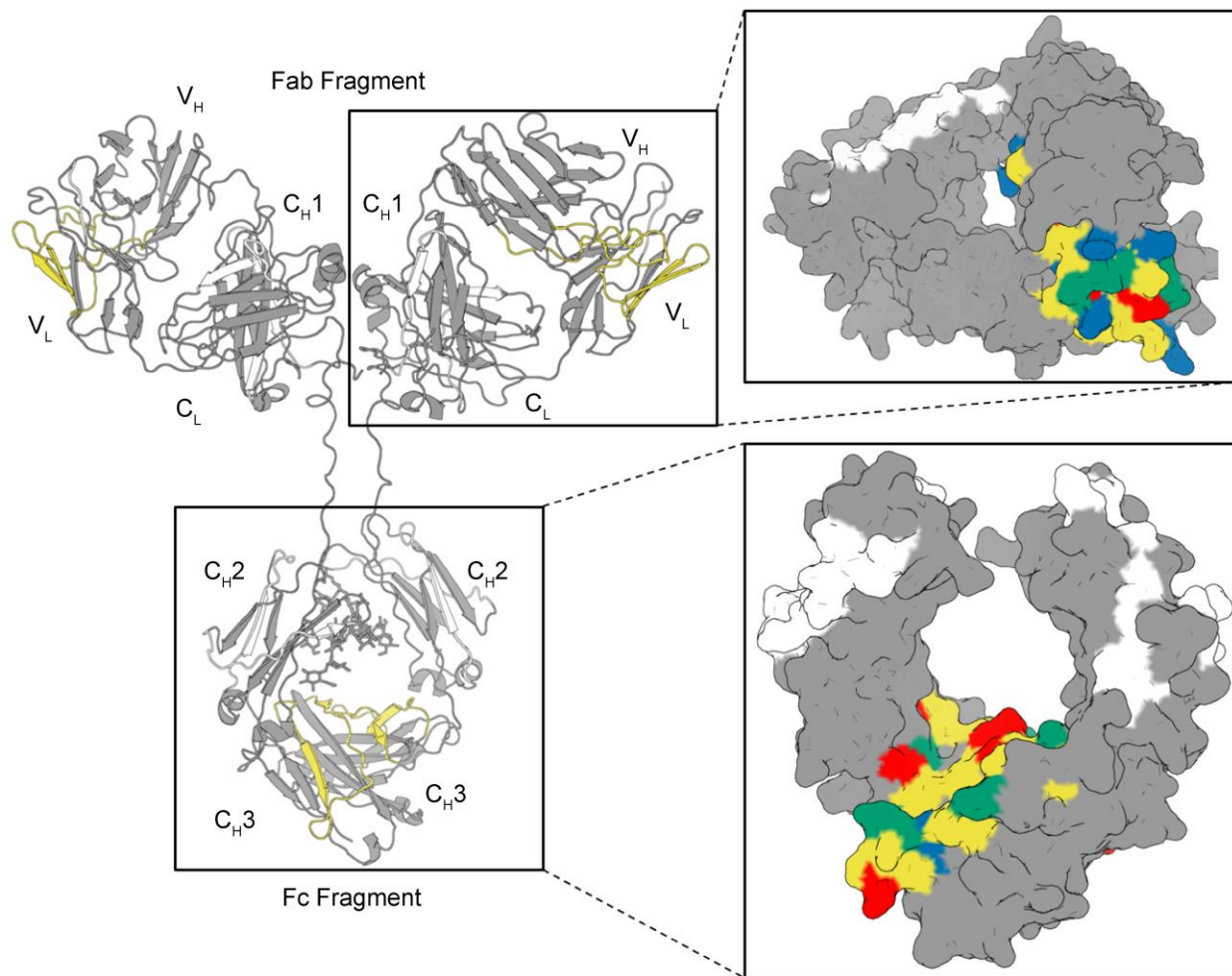
Representative deuterium uptake plots for 8 peptide segments of mAb-J. Black squares and red circles represent HX-MS experiments at low (5 g/L) and high (60 g/L) protein concentrations, respectively. The data in panel A are representative of peptides that showed no significant differences in hydrogen exchange kinetics between the two concentrations of mAb-J. Peptide segments shown in panel B are representative of peptide segments that showed significant protection (slowed HX) at high protein concentration. The domain location and peptide index number are shown in parenthesis at the top of each plot. Error bars represent one standard deviation from three independent HX measurements. (For deuterium uptake plots of all peptide segments of mAb-J, refer to Figure S3).

Figure 4.5



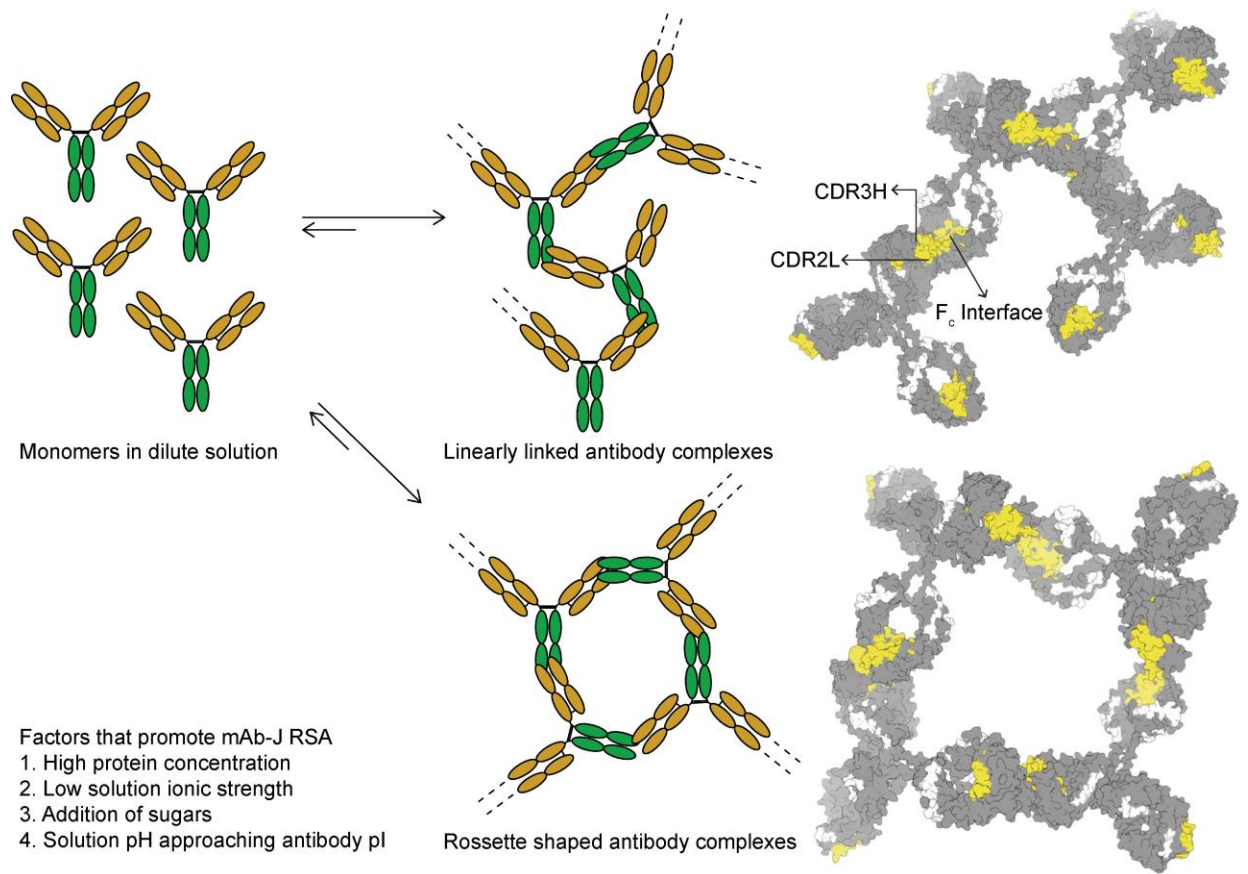
Differential deuterium uptake by 182 peptides at 4 different hydrogen exchange times comparing high (60 g/L) and low (5 g/L) concentrations of mAb-J at pH 6.0. Peptides are numbered in order from N terminus of the heavy chain to the C terminus of the light chain on the horizontal axis of the plots (see Table S4 for exact locations). The vertical axis is difference in HX between high vs. low protein concentrations, $\Delta m(t) = m_{60}(t) - m_5(t)$. Positive bars show peptide segments with faster HX at high protein concentration and negative bars indicate peptide segments with slower HX at high protein concentration. The dashed horizontal bars at ± 0.40 Da are the 99% confidence intervals. Vertical dashed lines separate boundaries of different domains of mAb-J (domains are listed on the top of the plot). The locations of the CDR segments are shaded in blue. Some peptides span more than one domain thus the boundaries are approximate. An average of three independent HX measurements was used to calculate each mass difference.

Figure 4.6



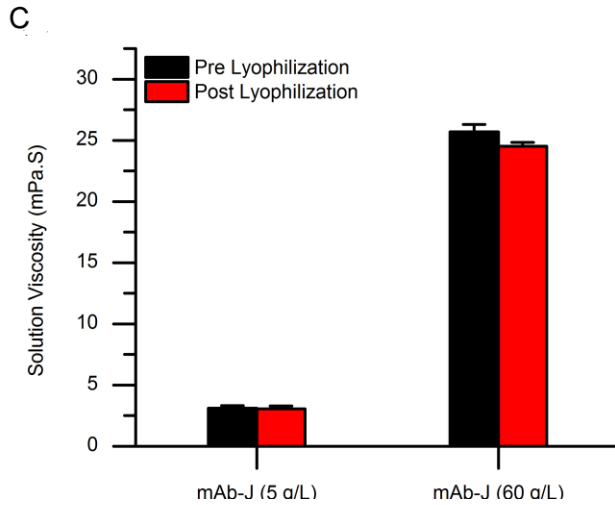
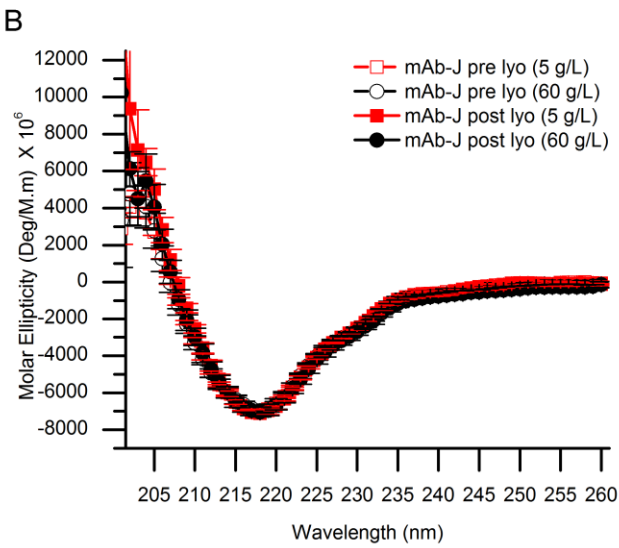
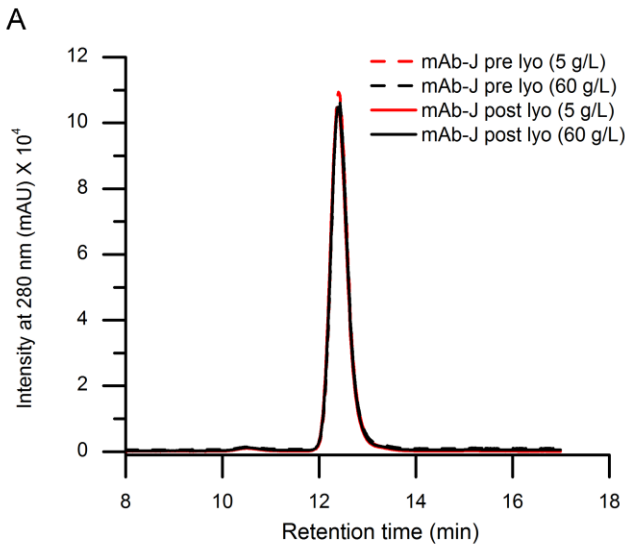
Locations of significant protection at high protein concentration mapped onto a homology model of mAb-J. The protected regions are colored yellow. A zoomed in surface representation of Fab and Fc domains of mAb-J is presented in the inset panels to the right. Surface exposed, positively and negatively charged residues are highlighted in blue and red, respectively, surface exposed hydrophobic residues are colored in green. Segments with no significant difference in HX between high and low protein concentrations of mAb-J are grey; regions with no mass spectrometry data are white.

Figure 4.7



A model of mAb-J reversible self-association illustrating two possible morphologies that an associated mAb network could form at high protein concentrations resulting in elevated solution viscosity. On the left, the Fab domain of the antibody is shown in orange and the Fc is green. On the right homology model of mAb-J with protein interfaces of RSA colored in yellow are arranged to show contact points between mAb-J monomers and possible arrangement of associated complexes.

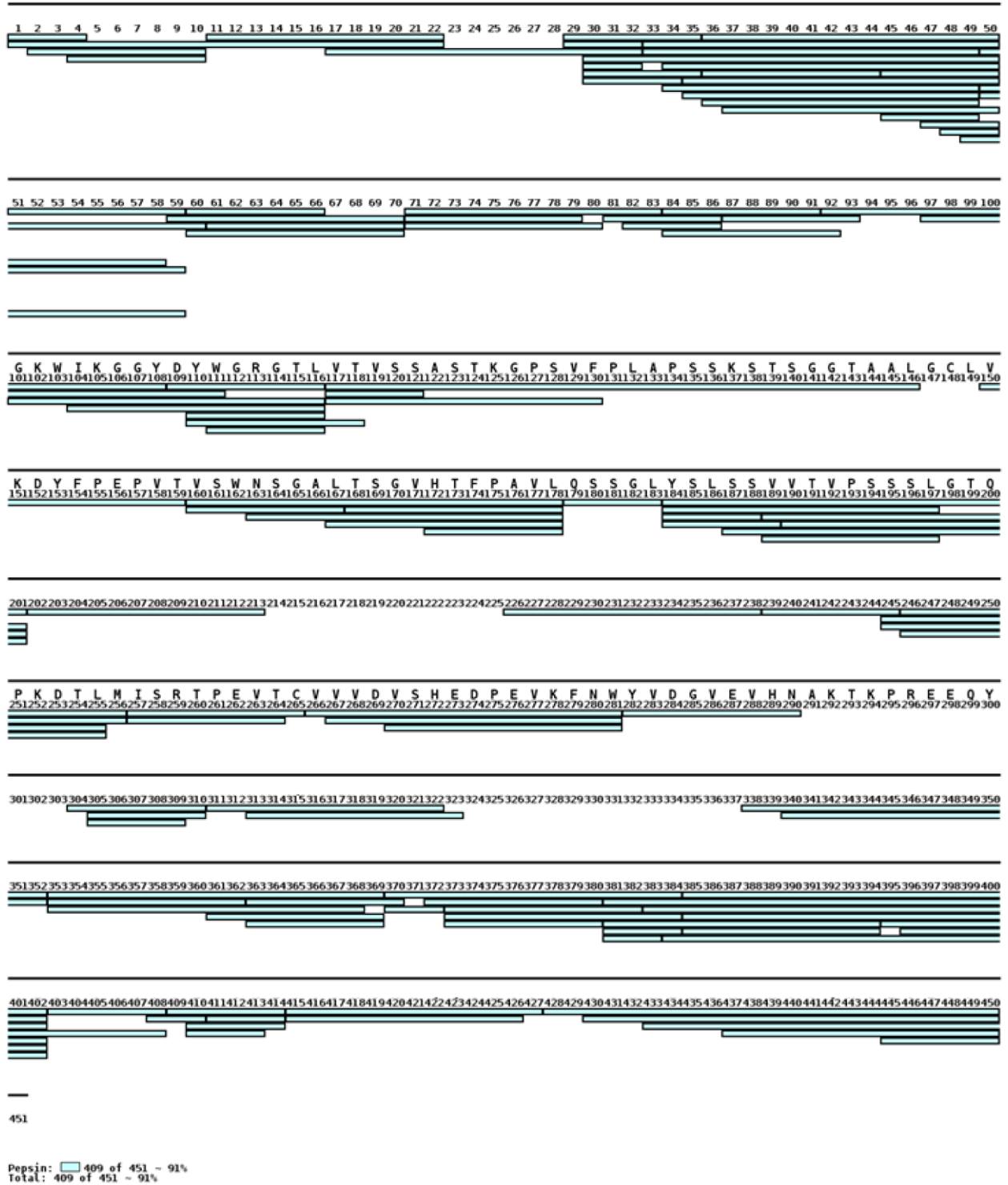
Figure 4.S1



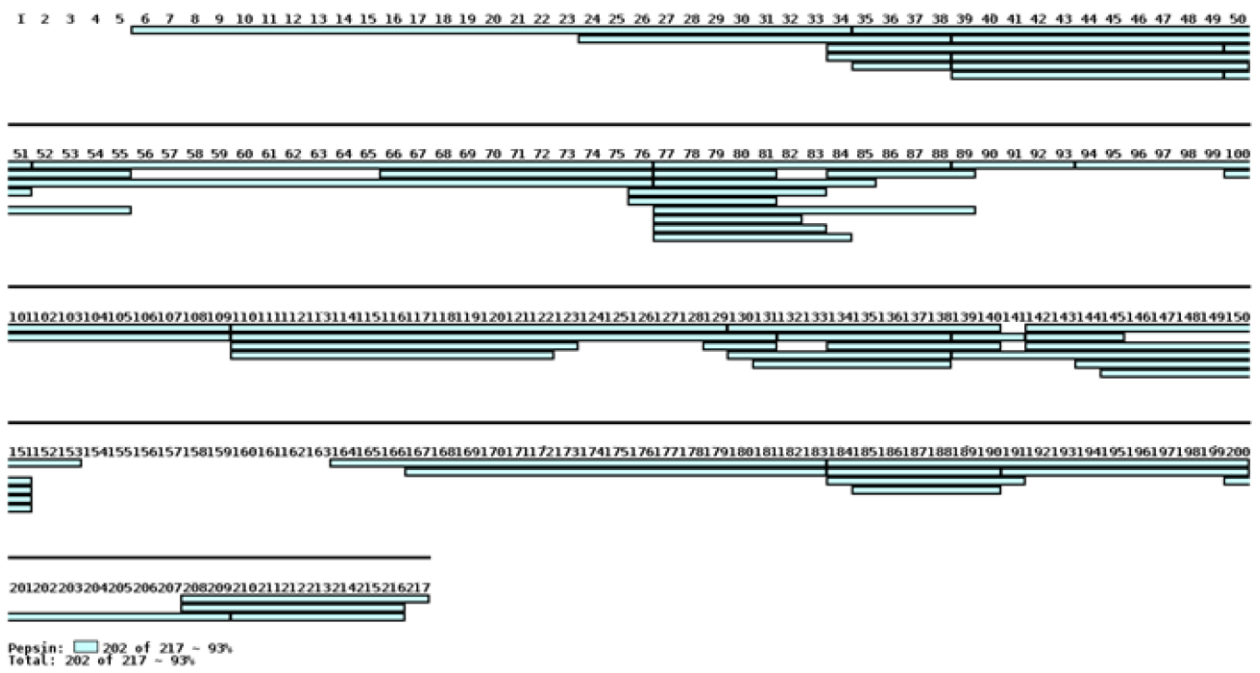
Post-lyophilization biophysical characterization of mAb-J. (A) Circular dichroism (CD) spectra showing the effect of lyophilization process on secondary structure of mAb-J. (B) Size exclusion chromatography (SEC) chromatograms comparing pre and post lyophilization mAb-J samples. (C) Solution dynamic viscosity measurements comparing pre- and post-lyophilization mAb-J samples to test the effect of lyophilization on mAb-J protein-protein interactions. Samples of mAb-J were prepared in control buffer containing 10% (w/v) trehalose. Error bars in panel B and C represent one standard deviation from three independent measurements.

Figure 4.S2

A

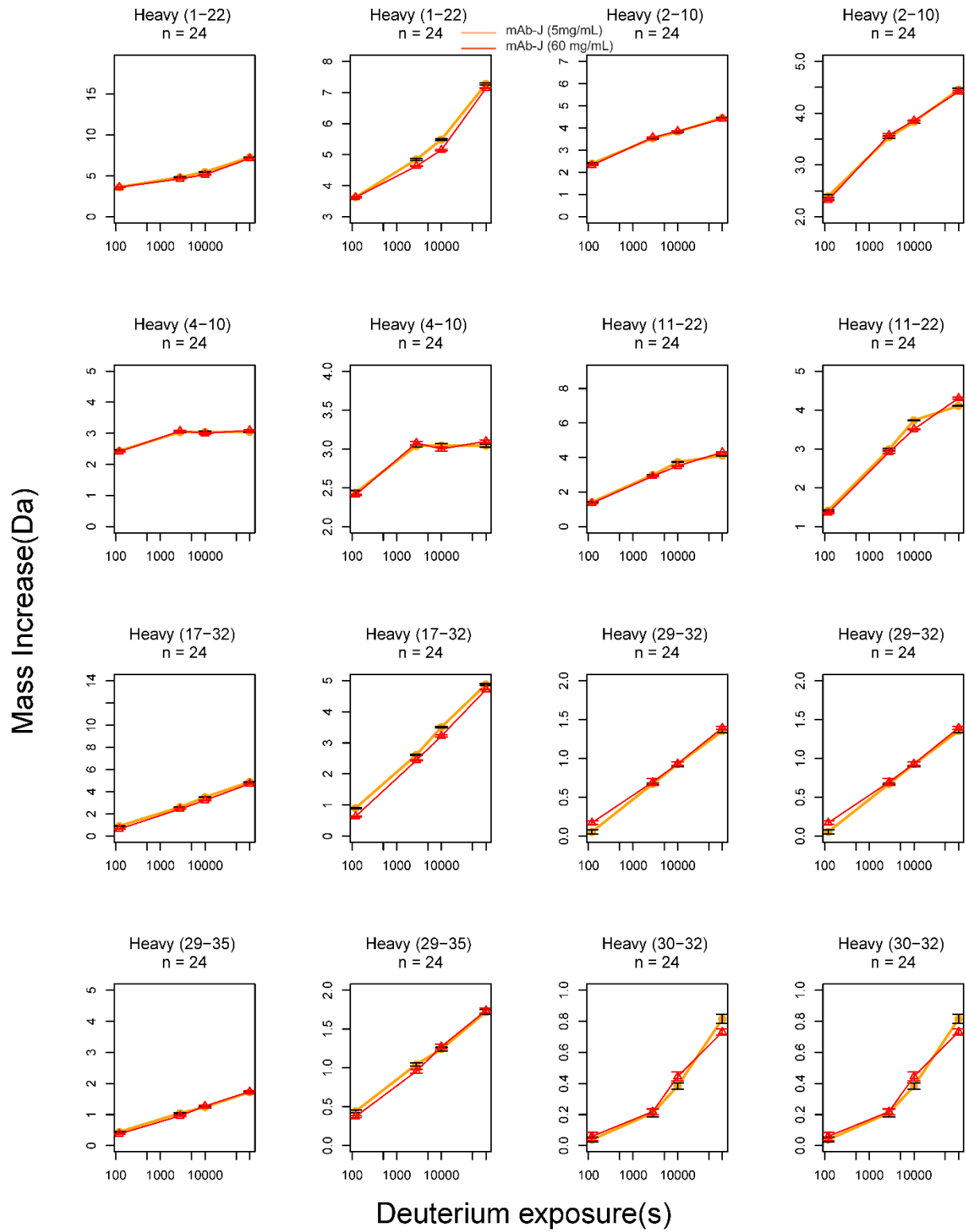


B

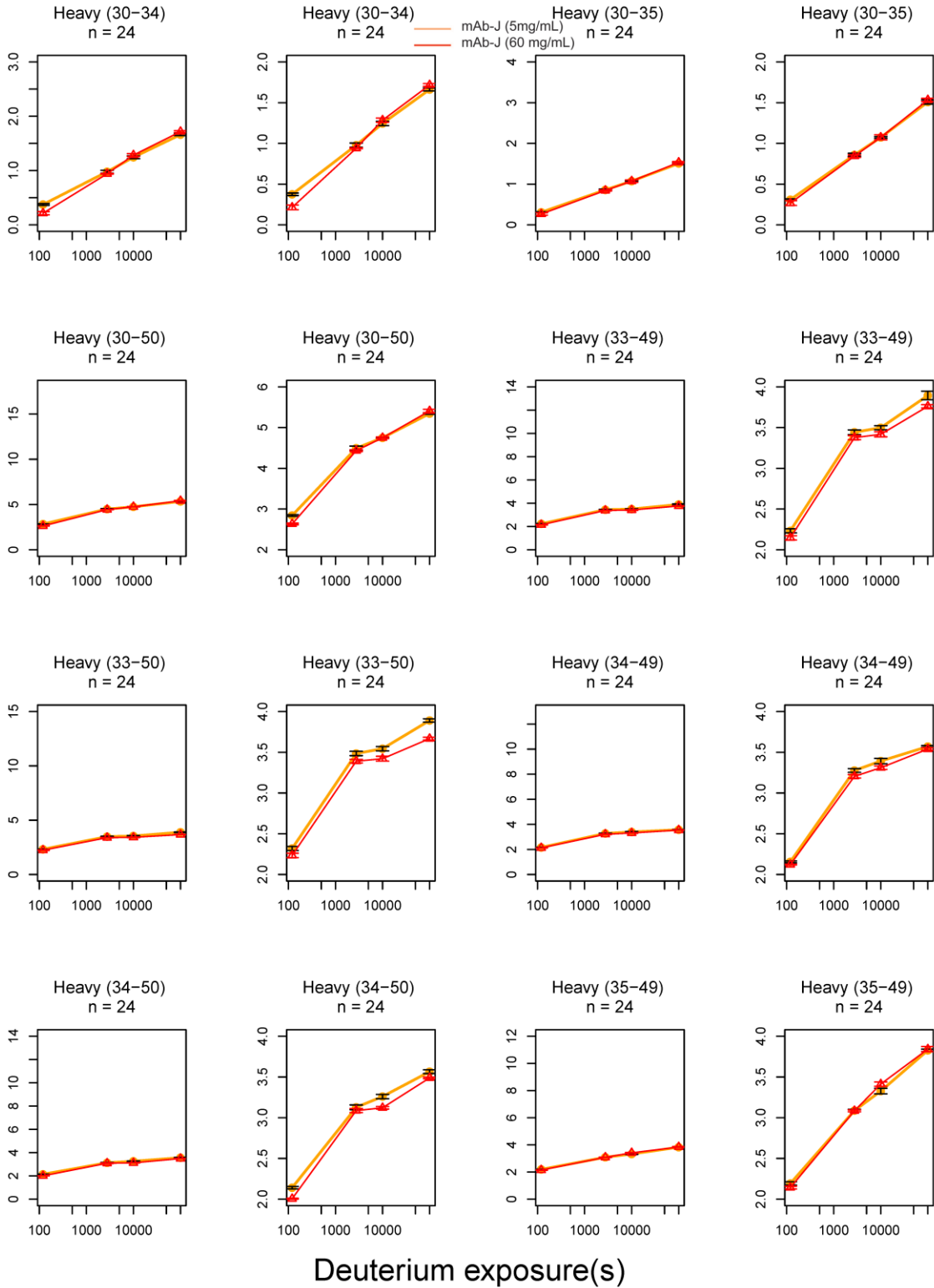


Peptic peptide coverage map of mAb-J (A) heavy chain and (B) light chain. 182 peptide segments of mAb-J covered 91% of heavy chain and 93% of light chain primary sequence.

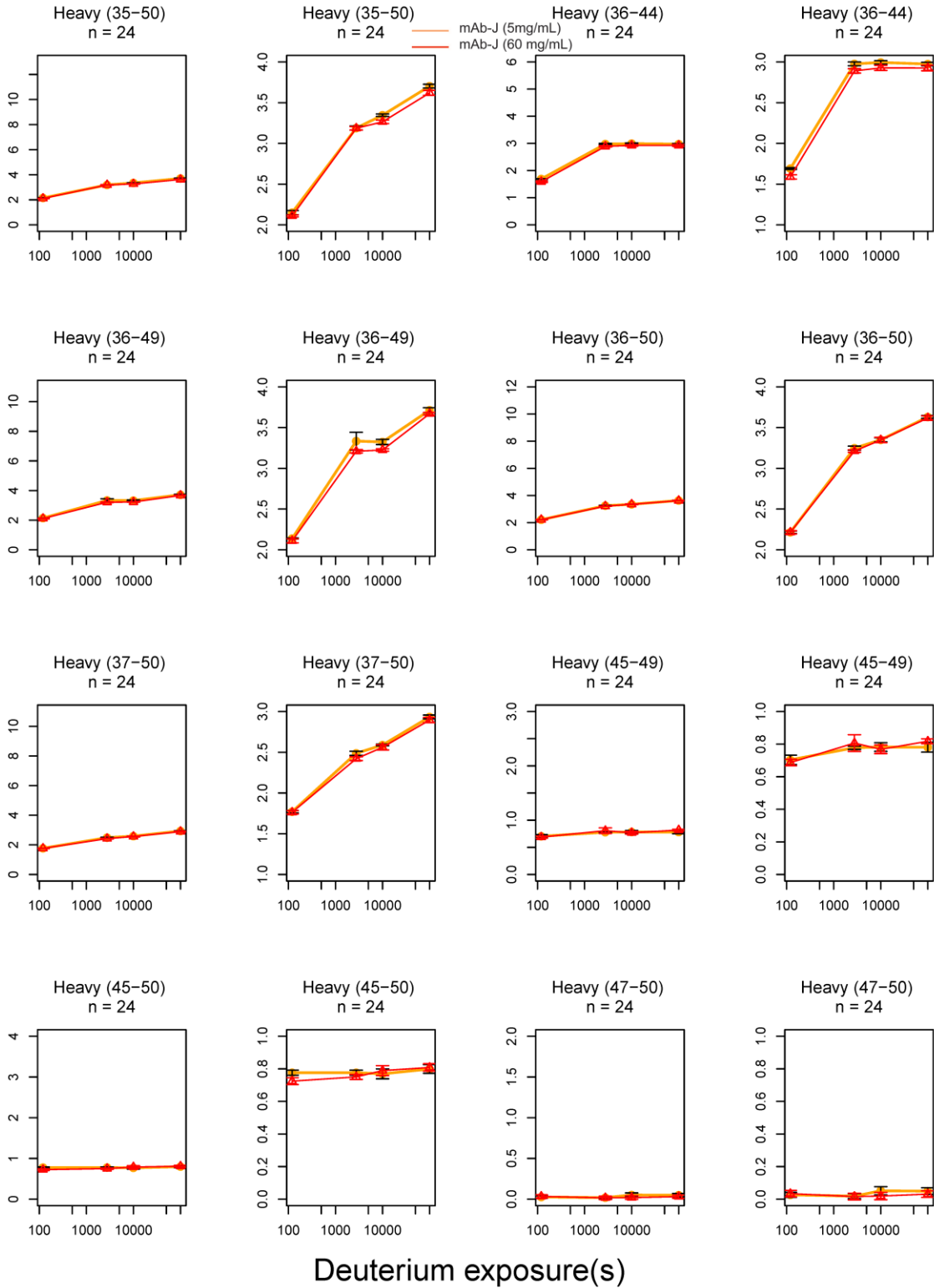
Figure 4.S3



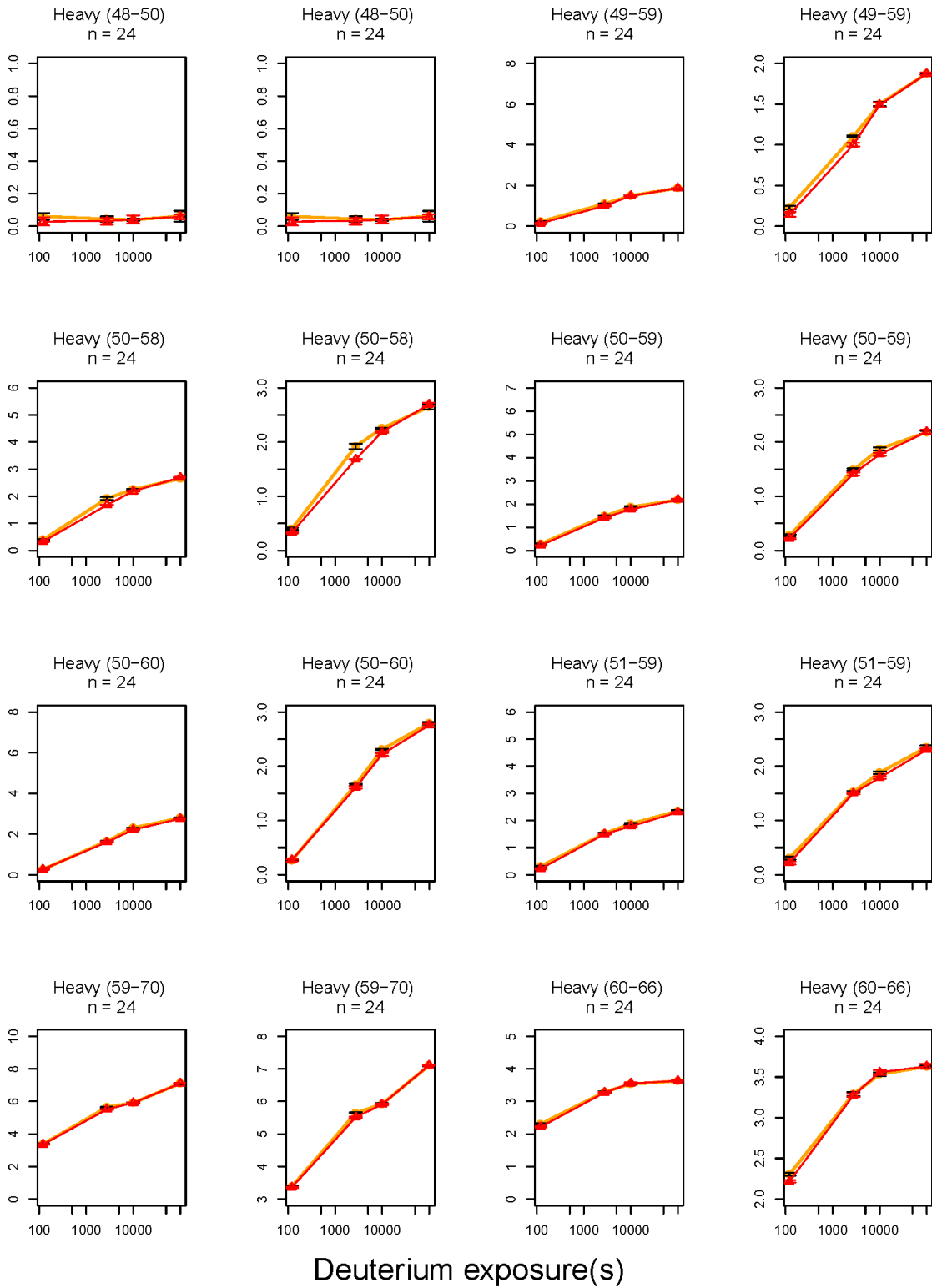
Mass Increase(Da)



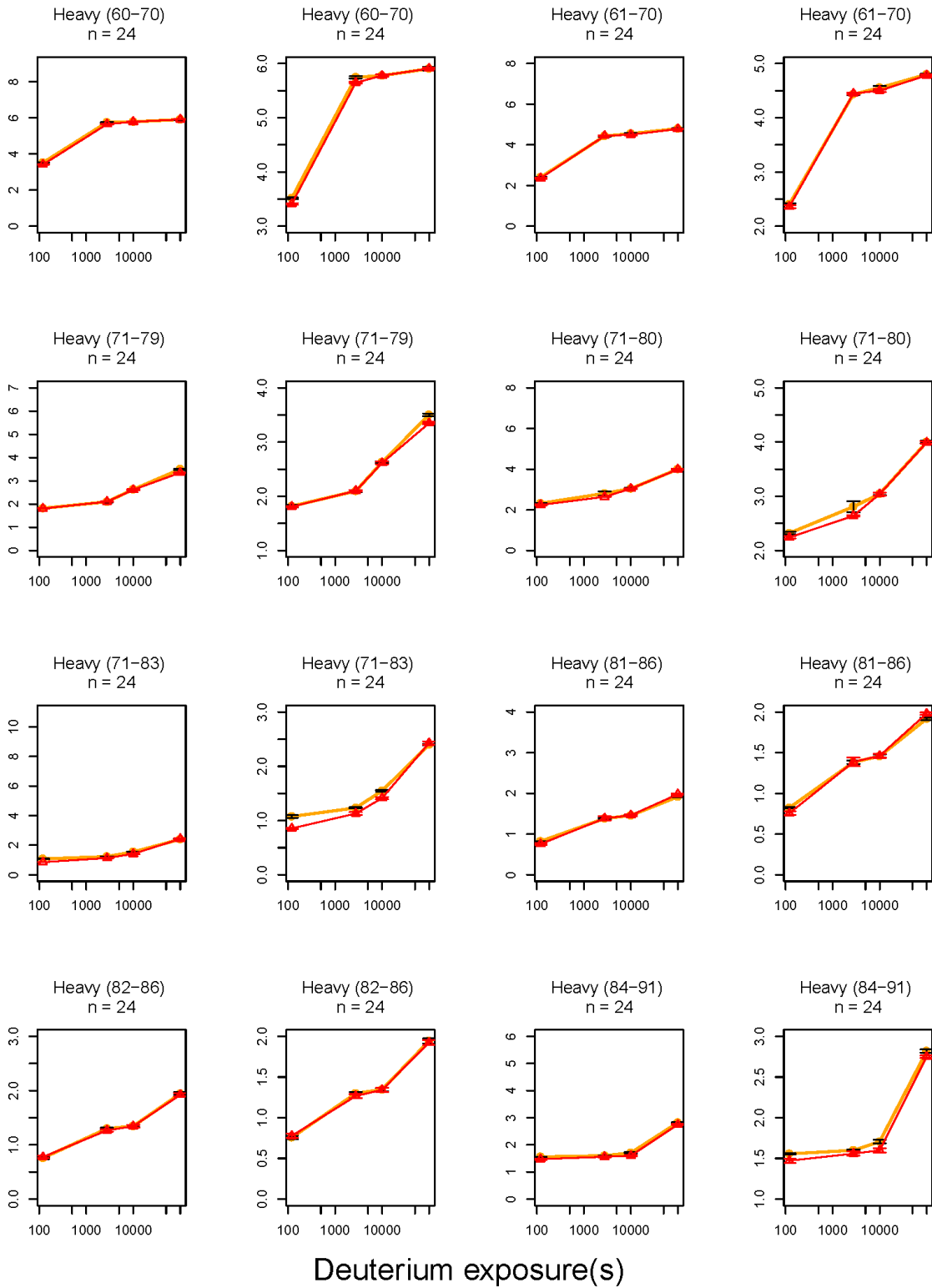
Mass Increase(Da)



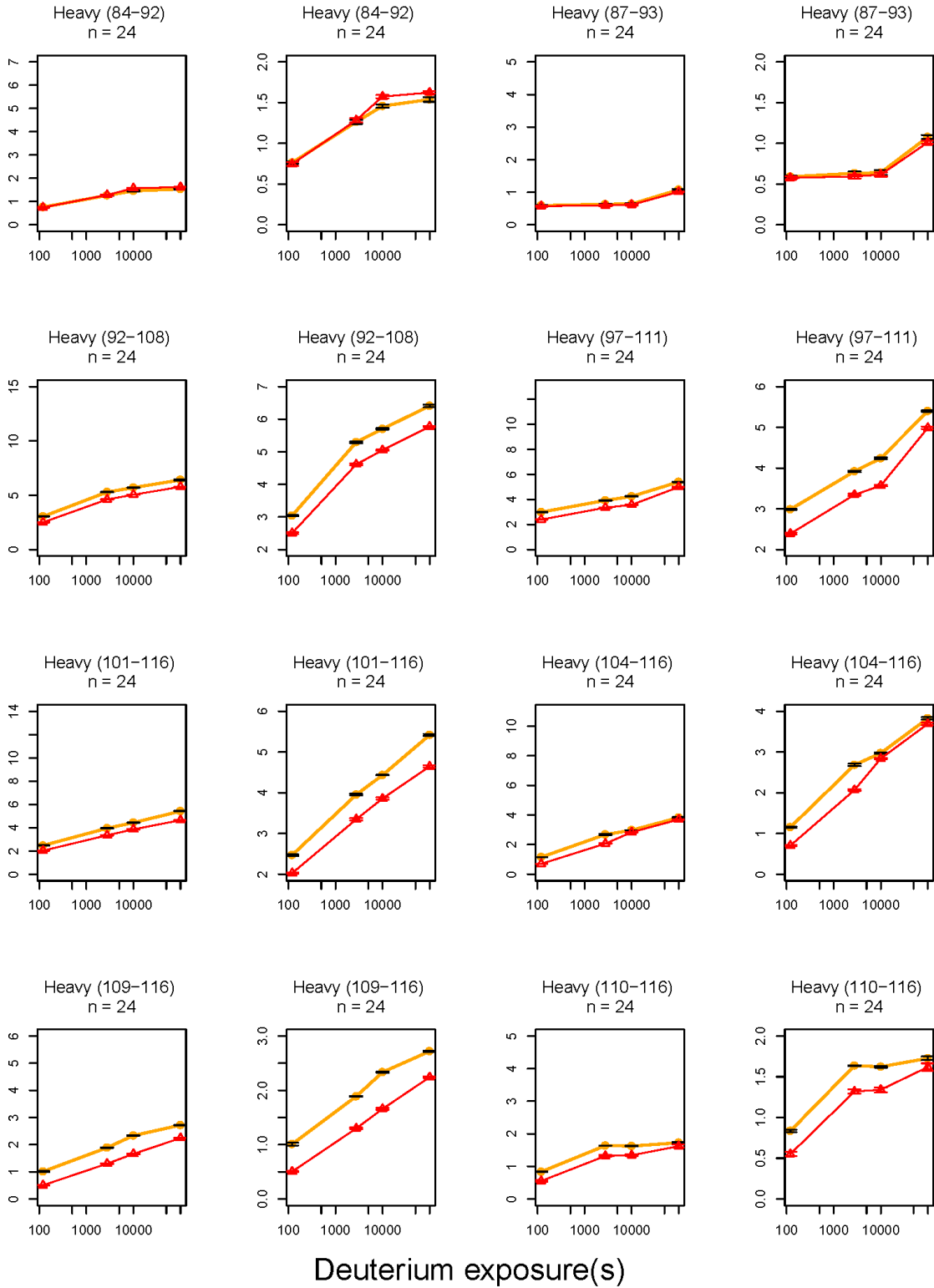
Mass Increase(Da)



Mass Increase(Da)

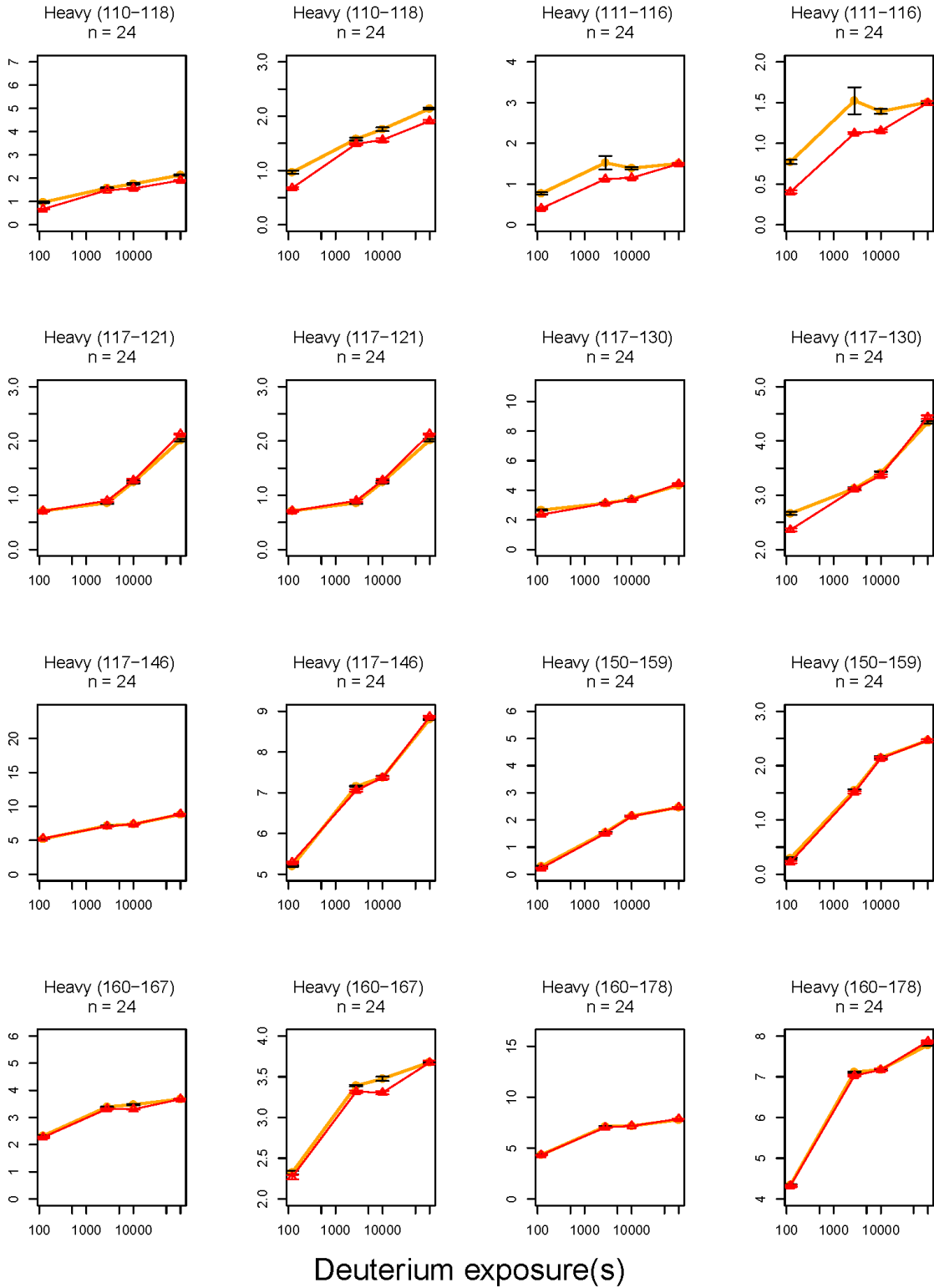


Mass Increase(Da)



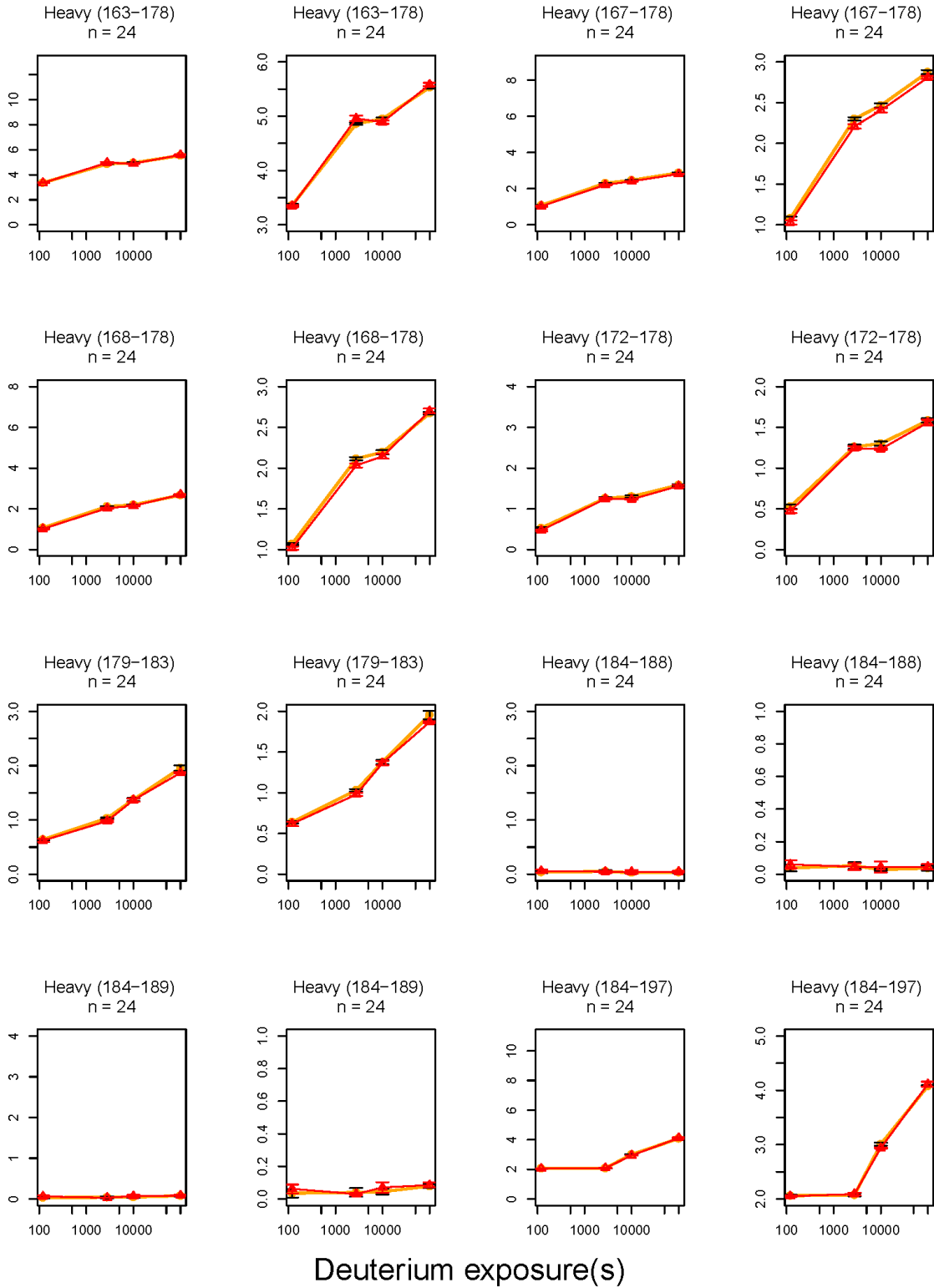
Deuterium exposure(s)

Mass Increase(Da)

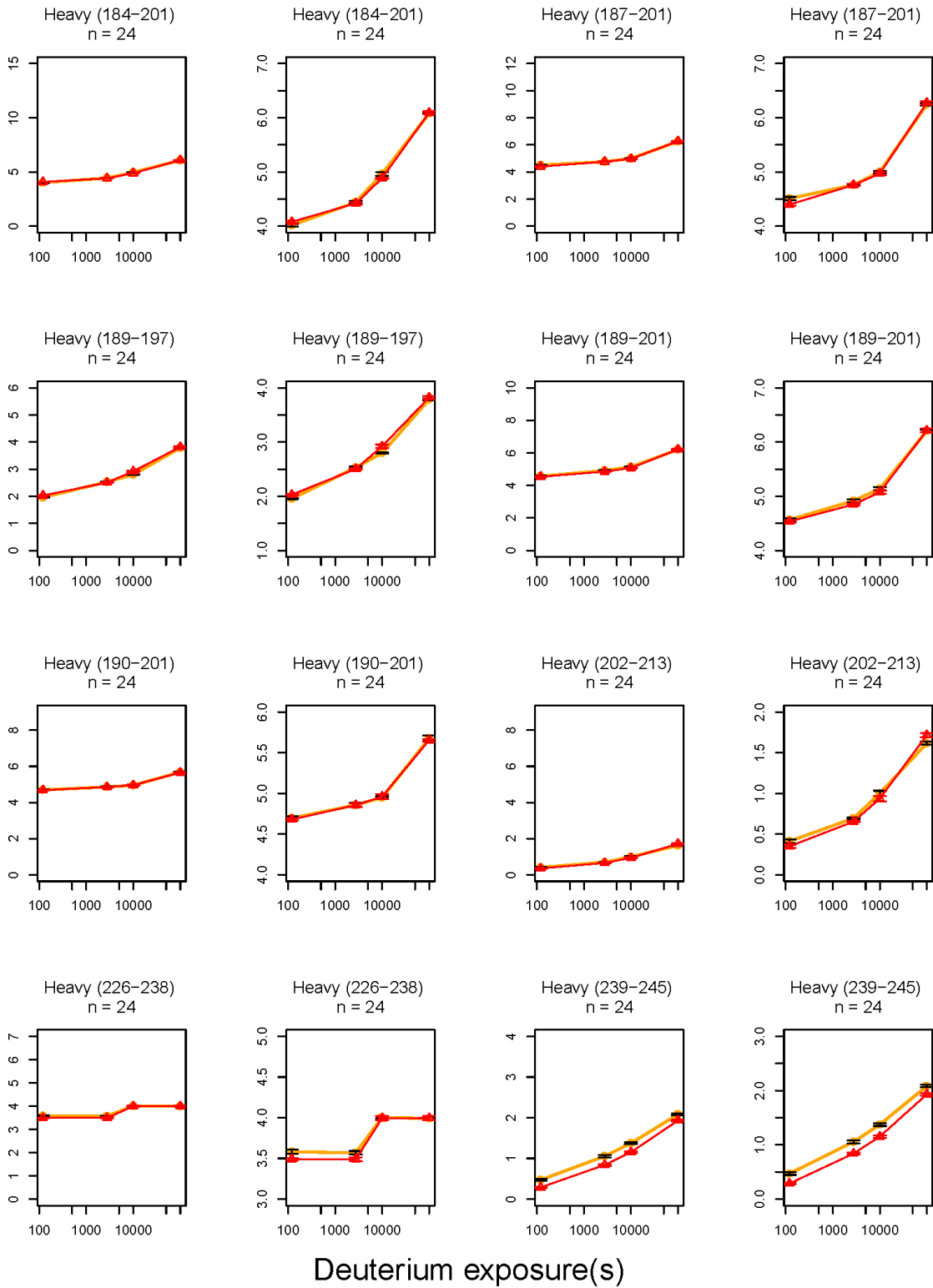


Deuterium exposure(s)

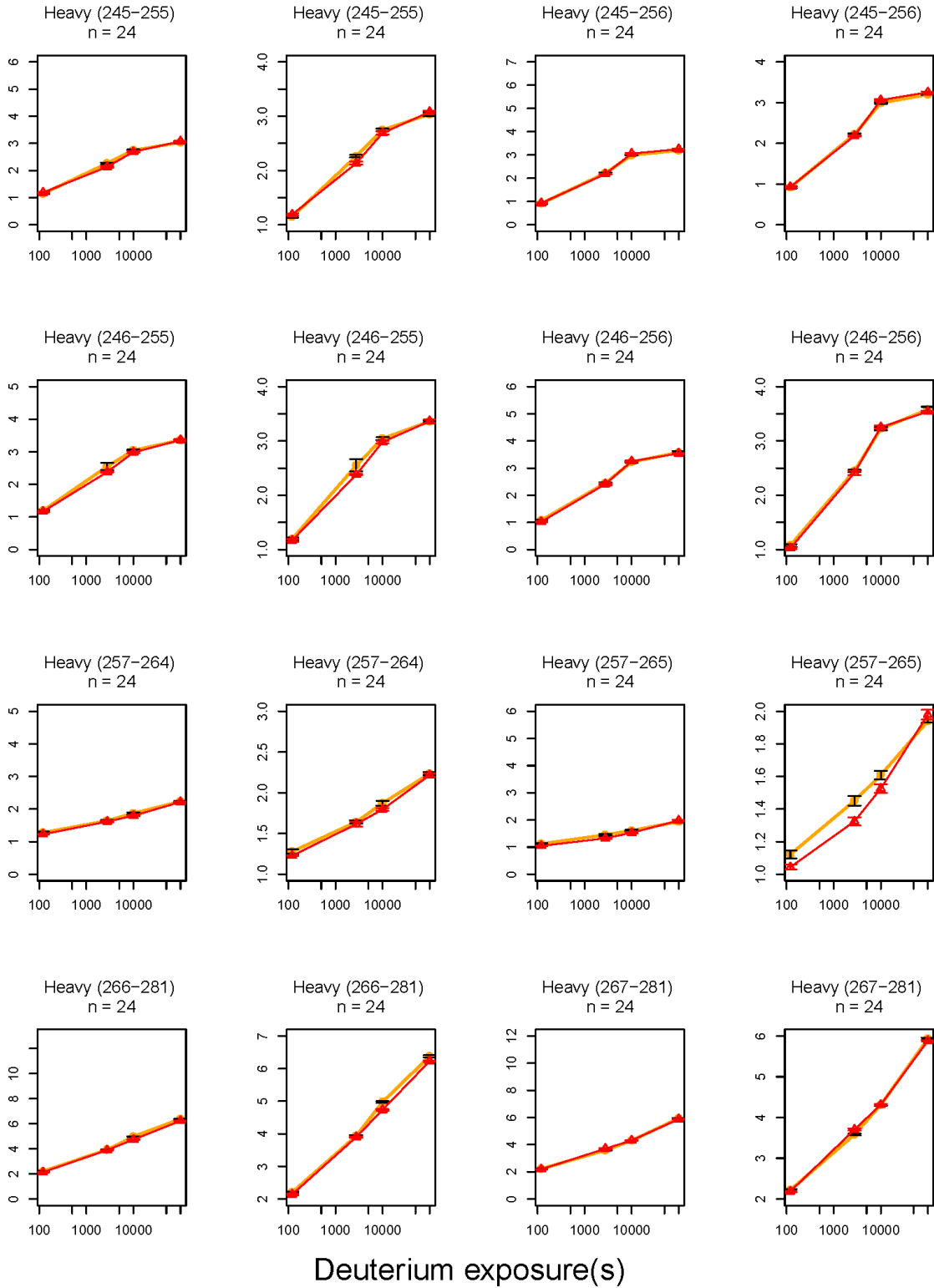
Mass Increase(Da)



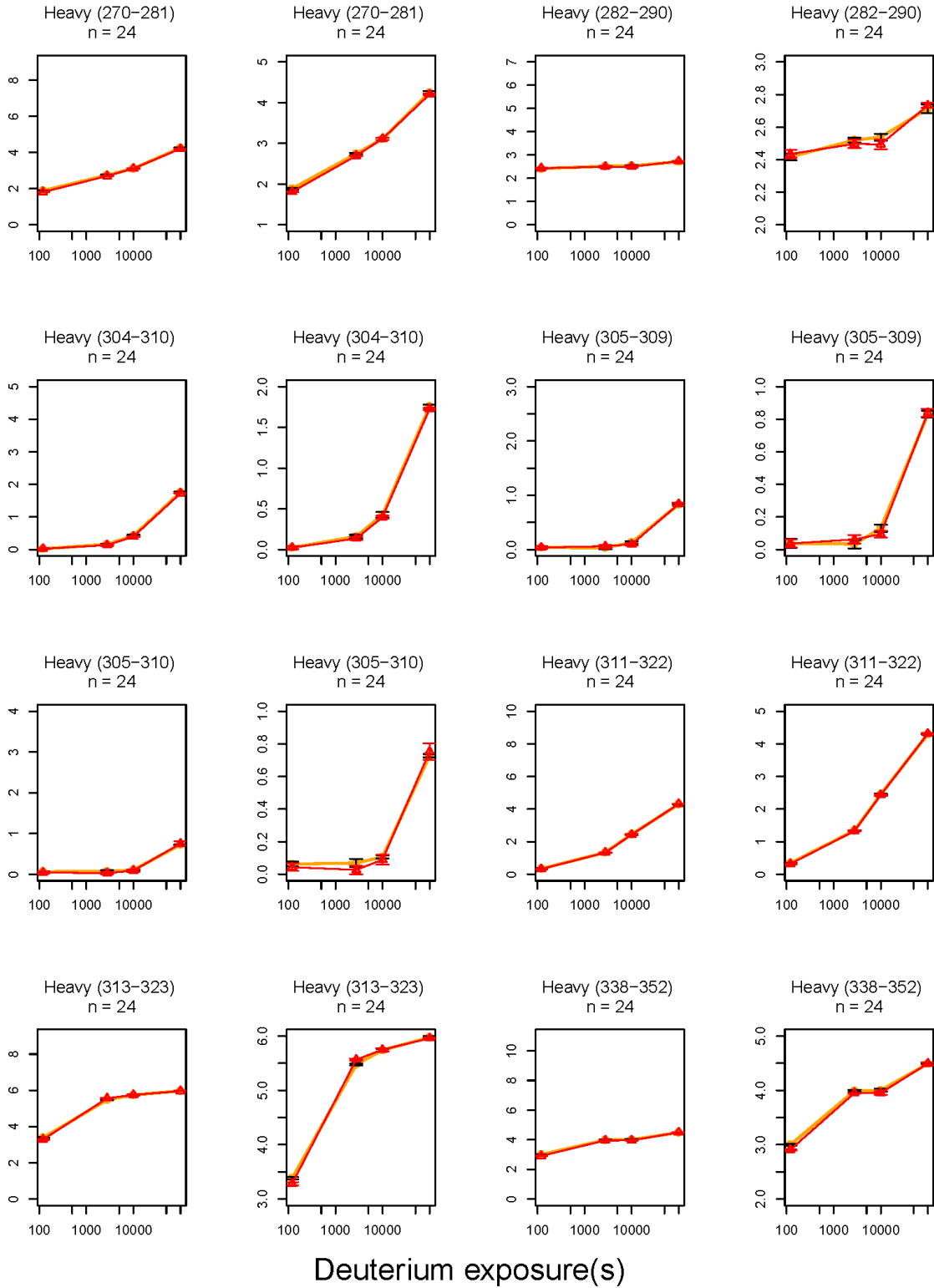
Mass Increase(Da)



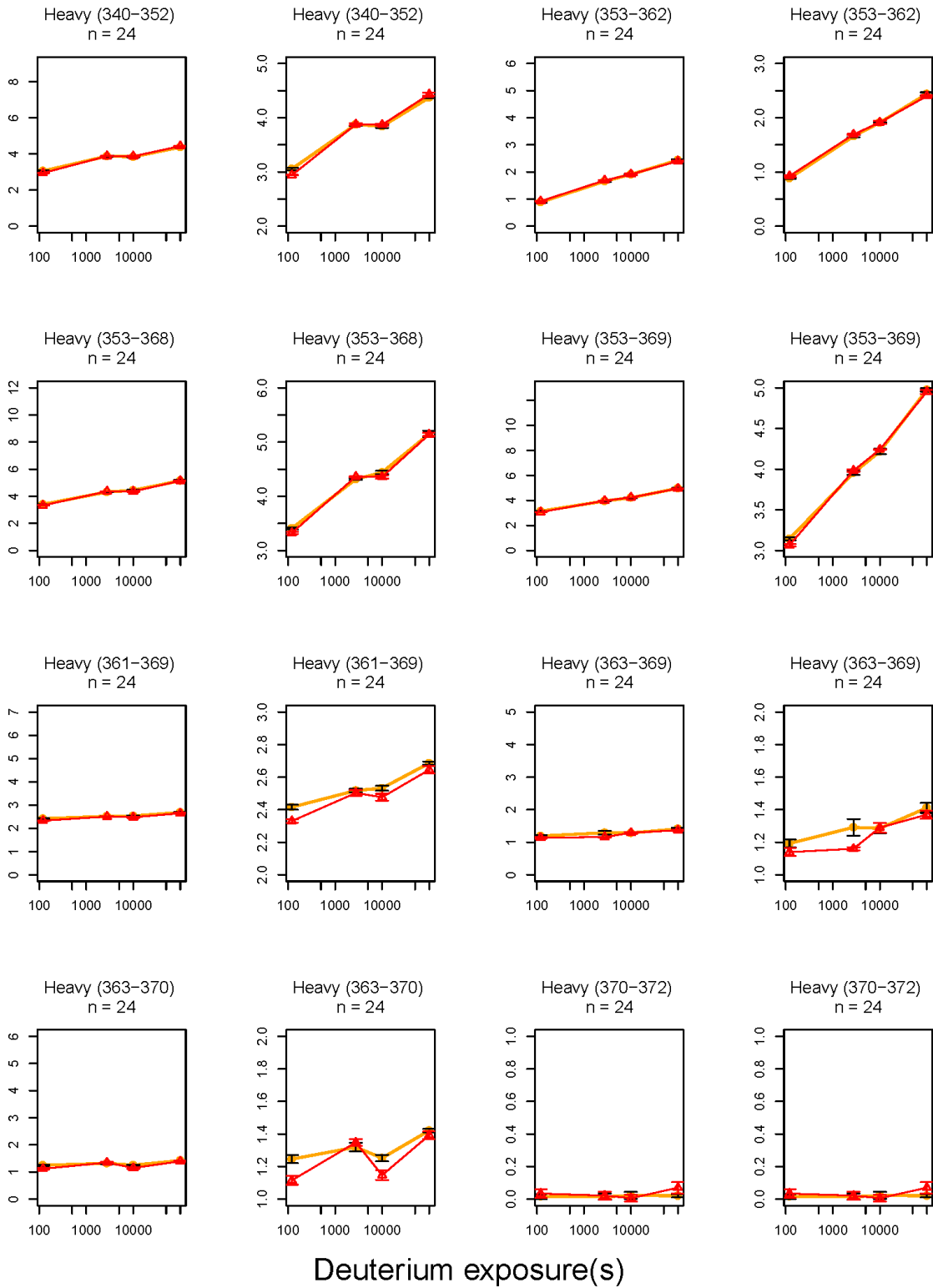
Mass Increase(Da)



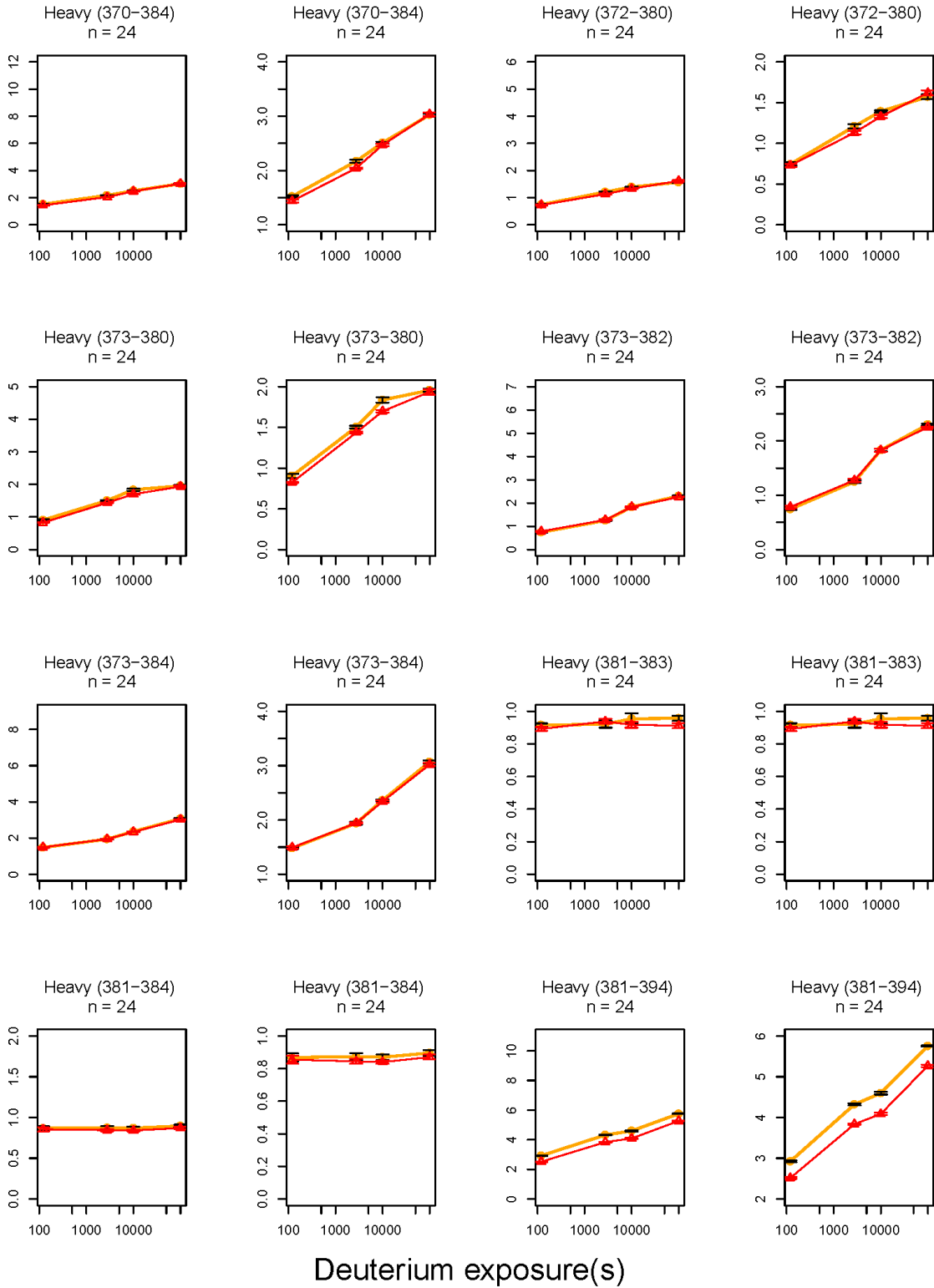
Mass Increase(Da)



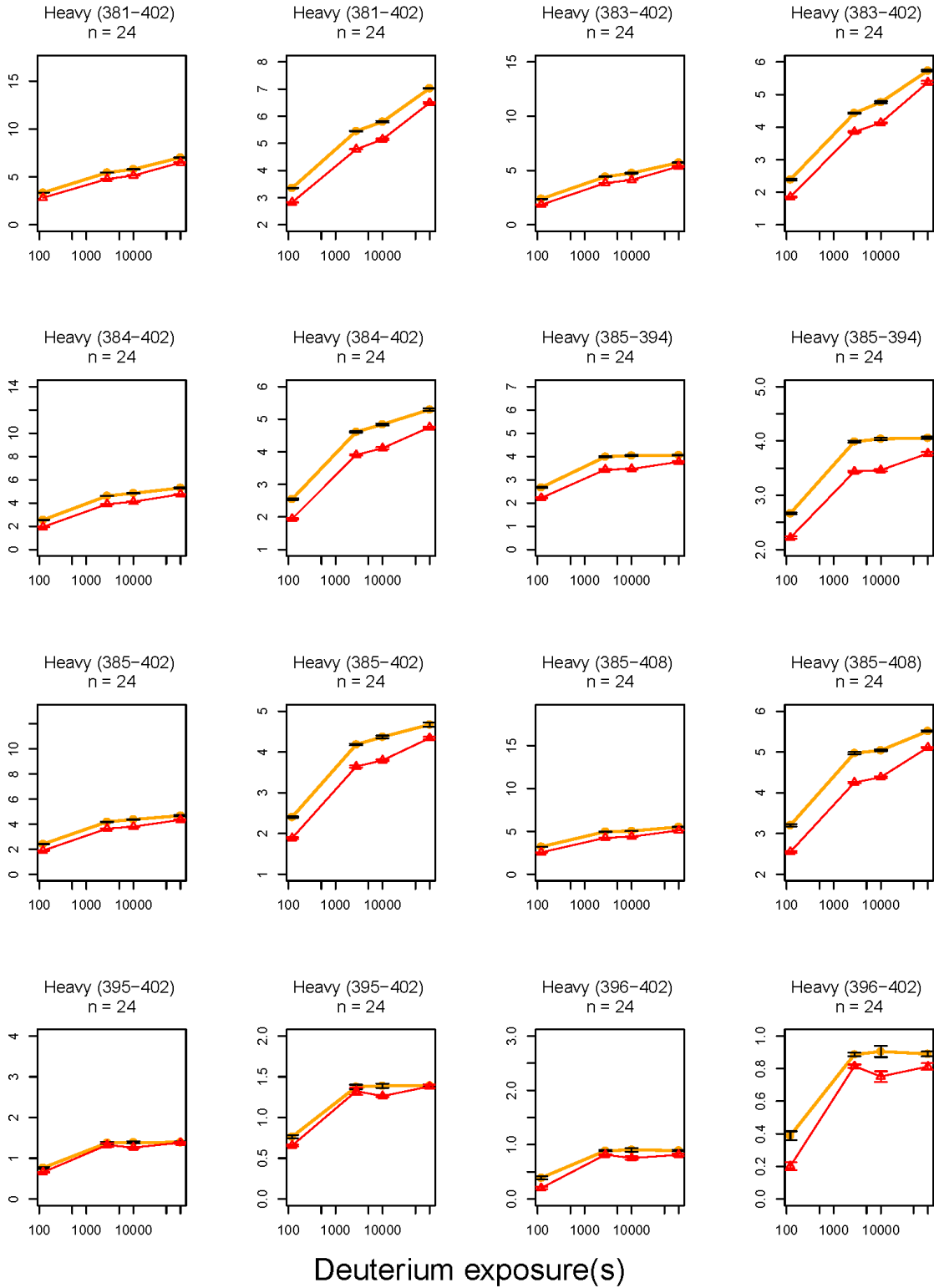
Mass Increase(Da)



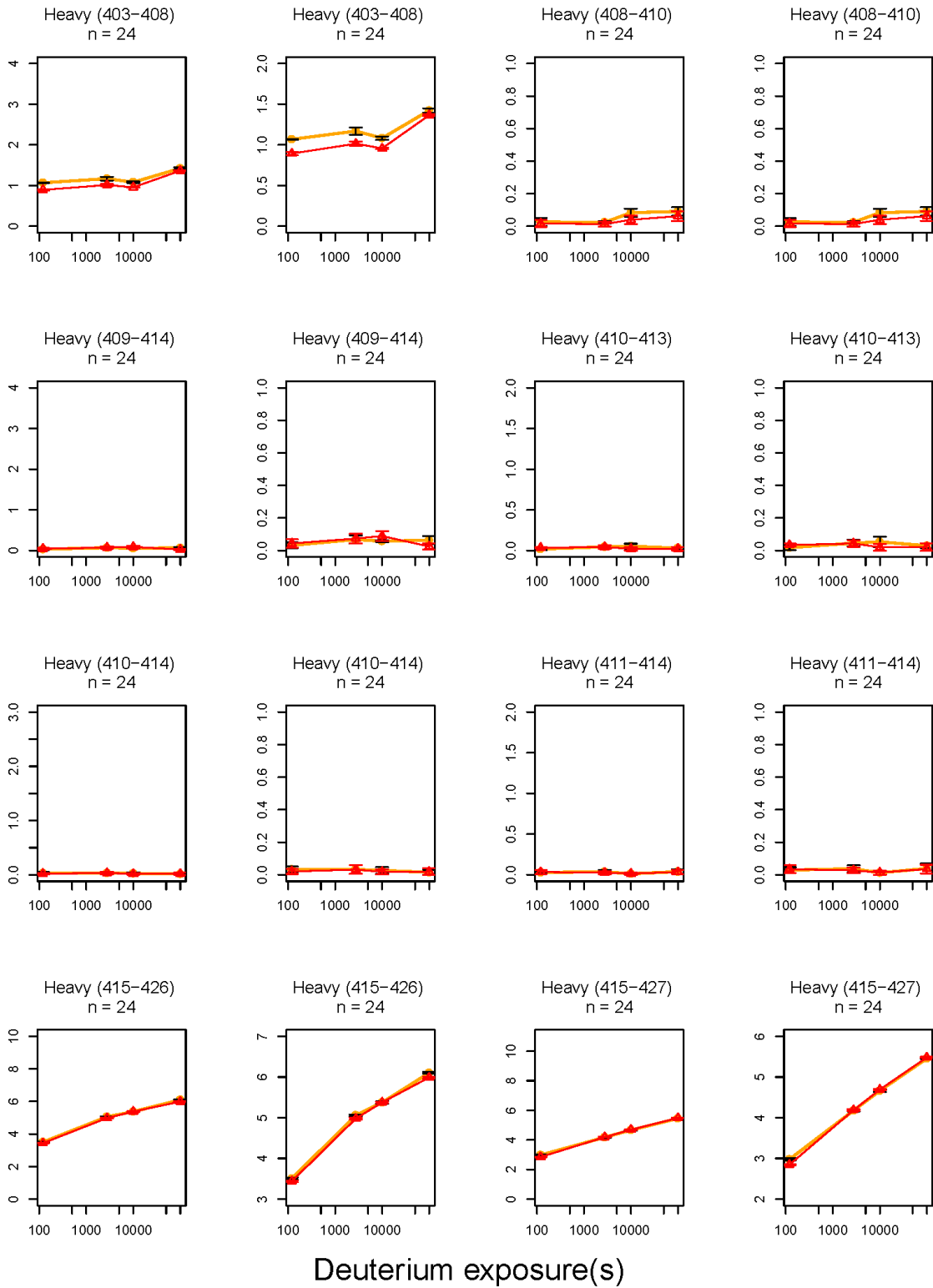
Mass Increase(Da)



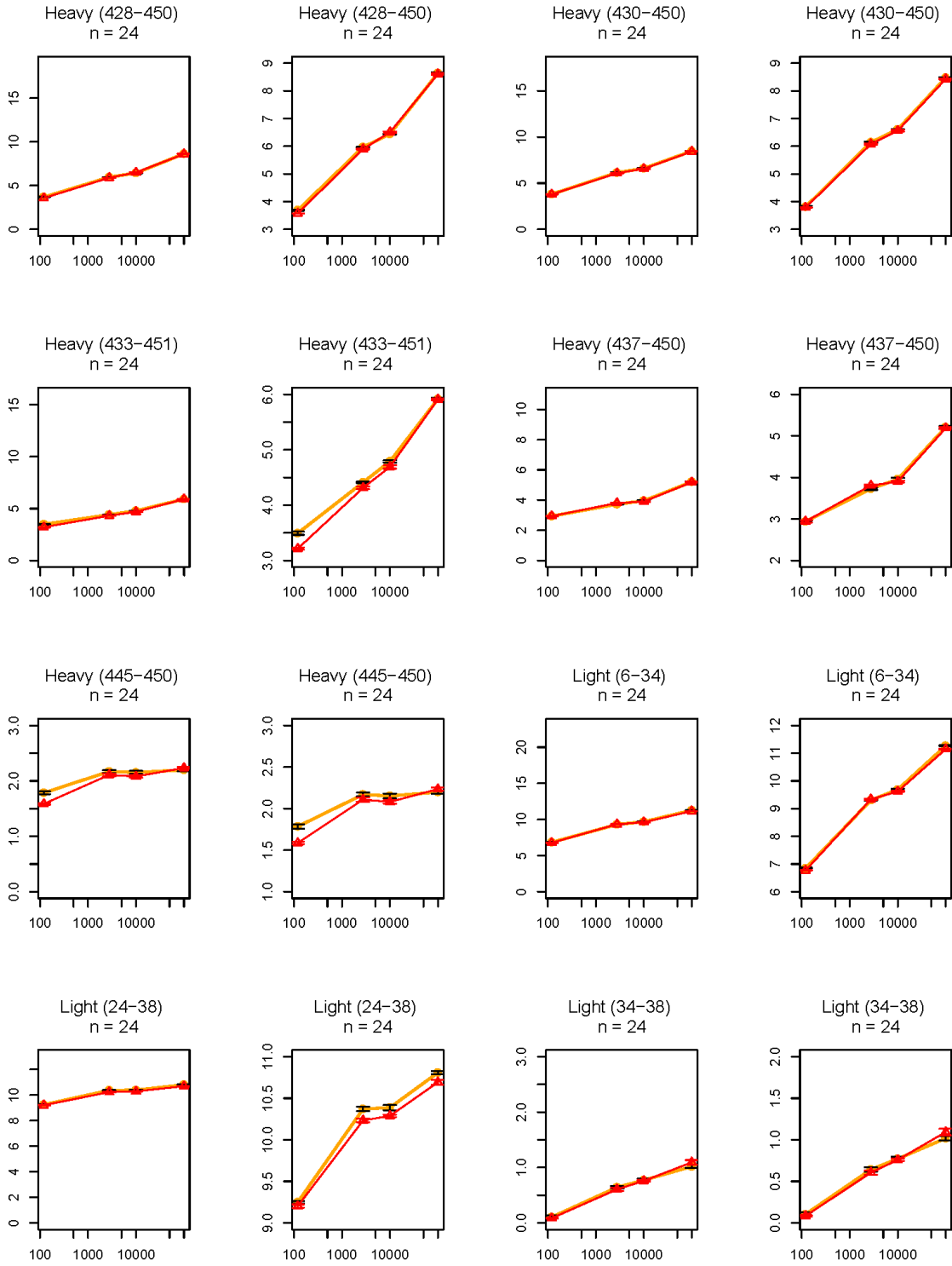
Mass Increase(Da)



Mass Increase(Da)

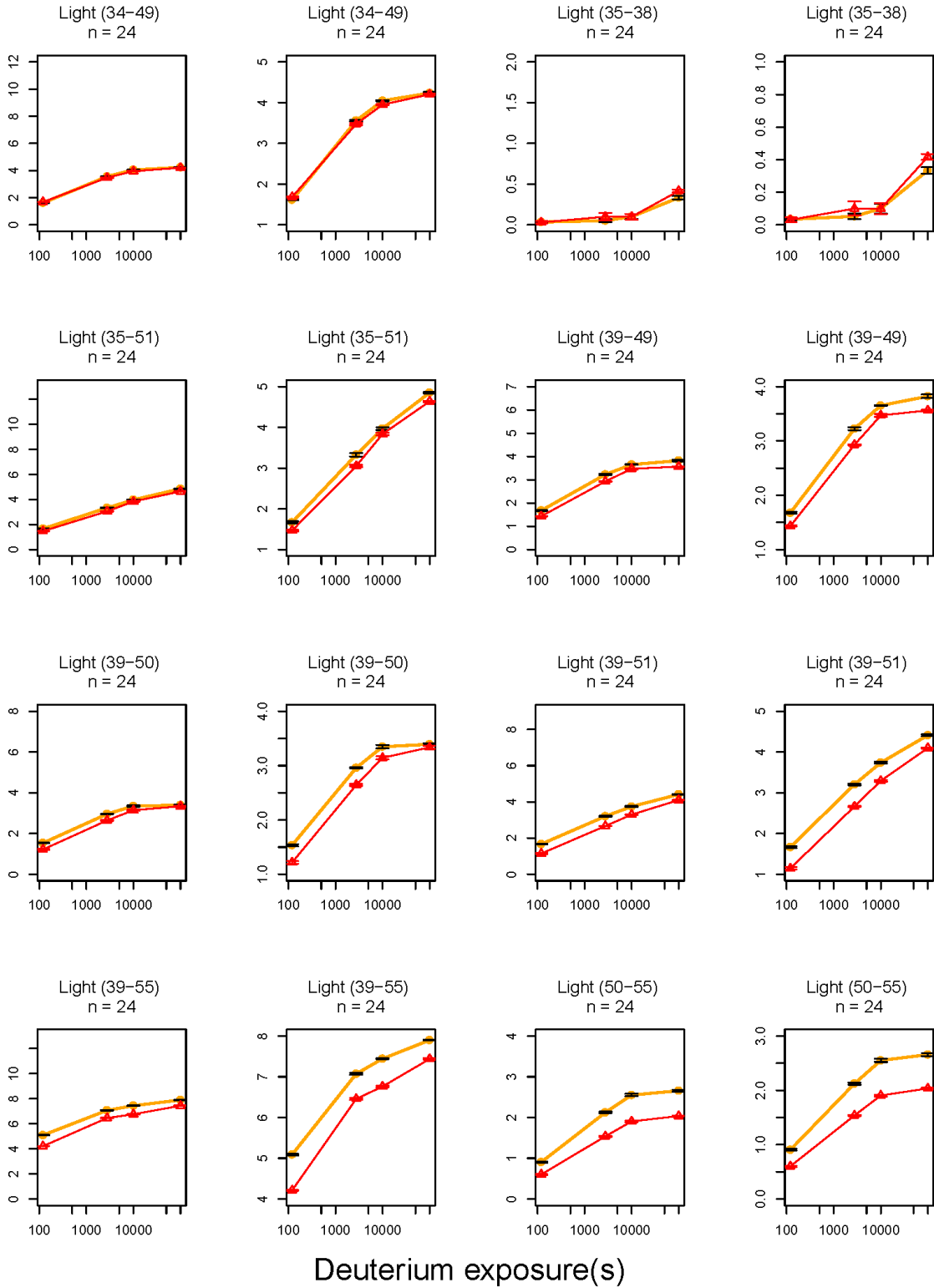


Mass Increase(Da)

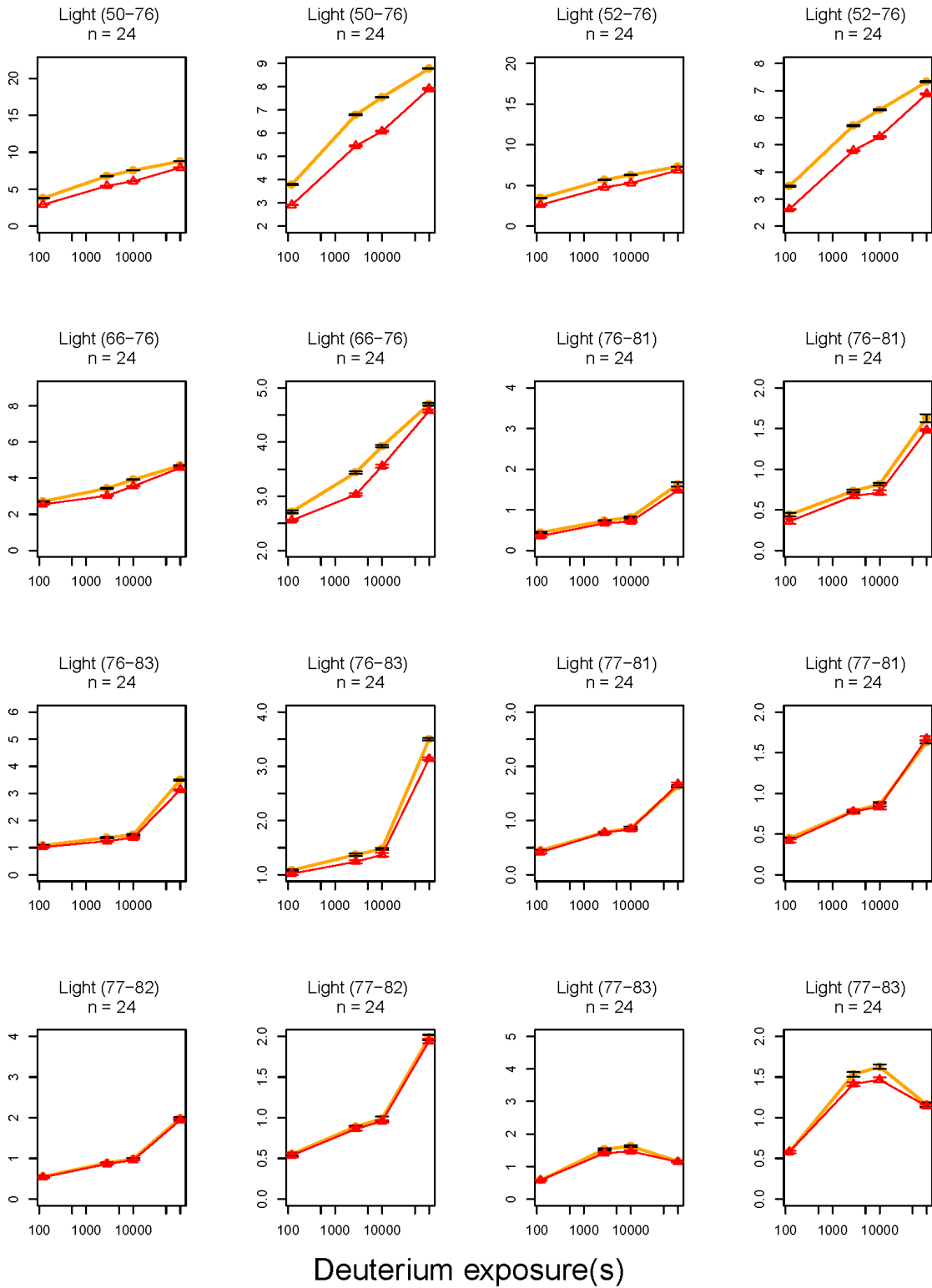


Deuterium exposure(s)

Mass Increase(Da)

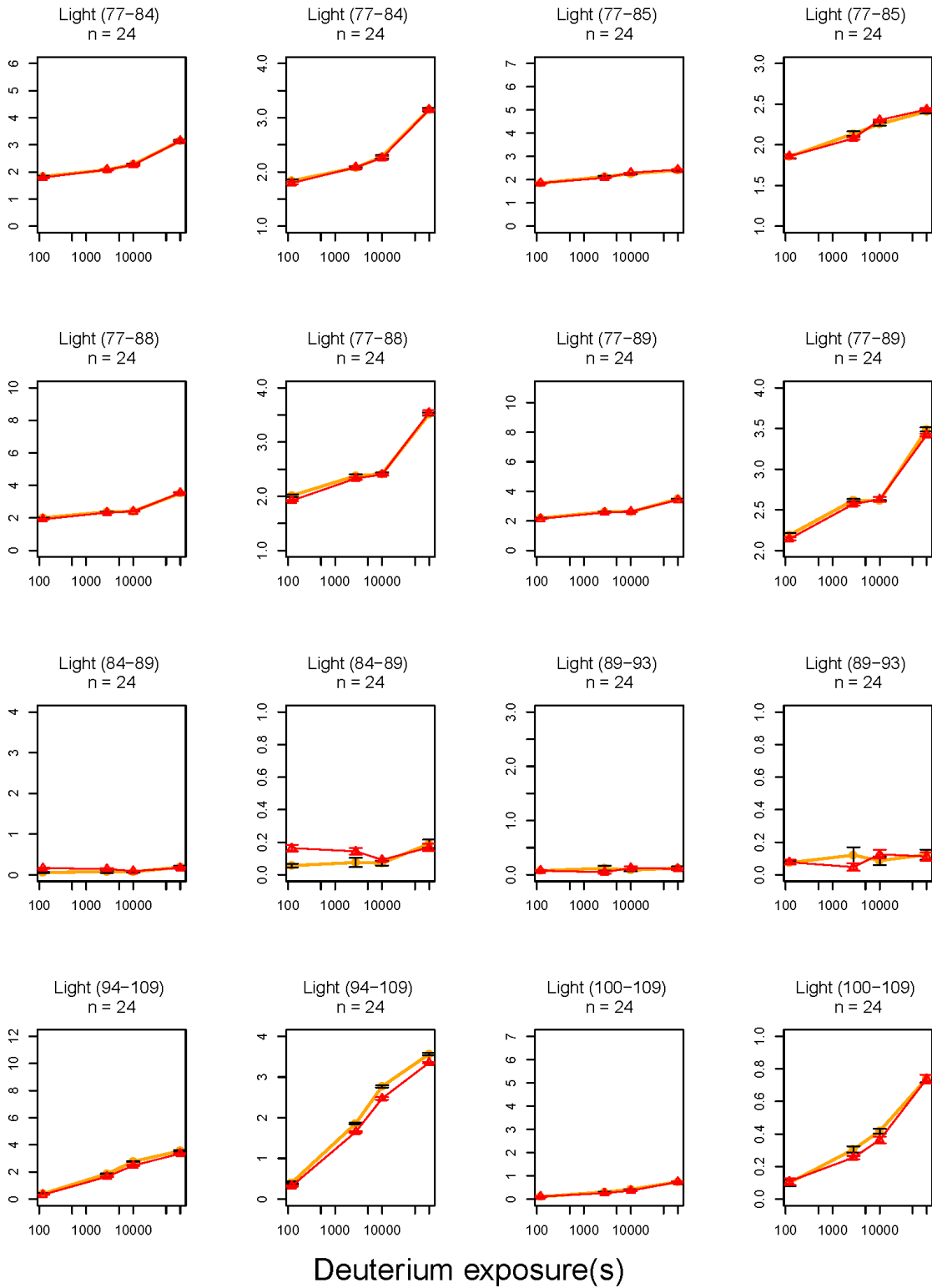


Mass Increase(Da)

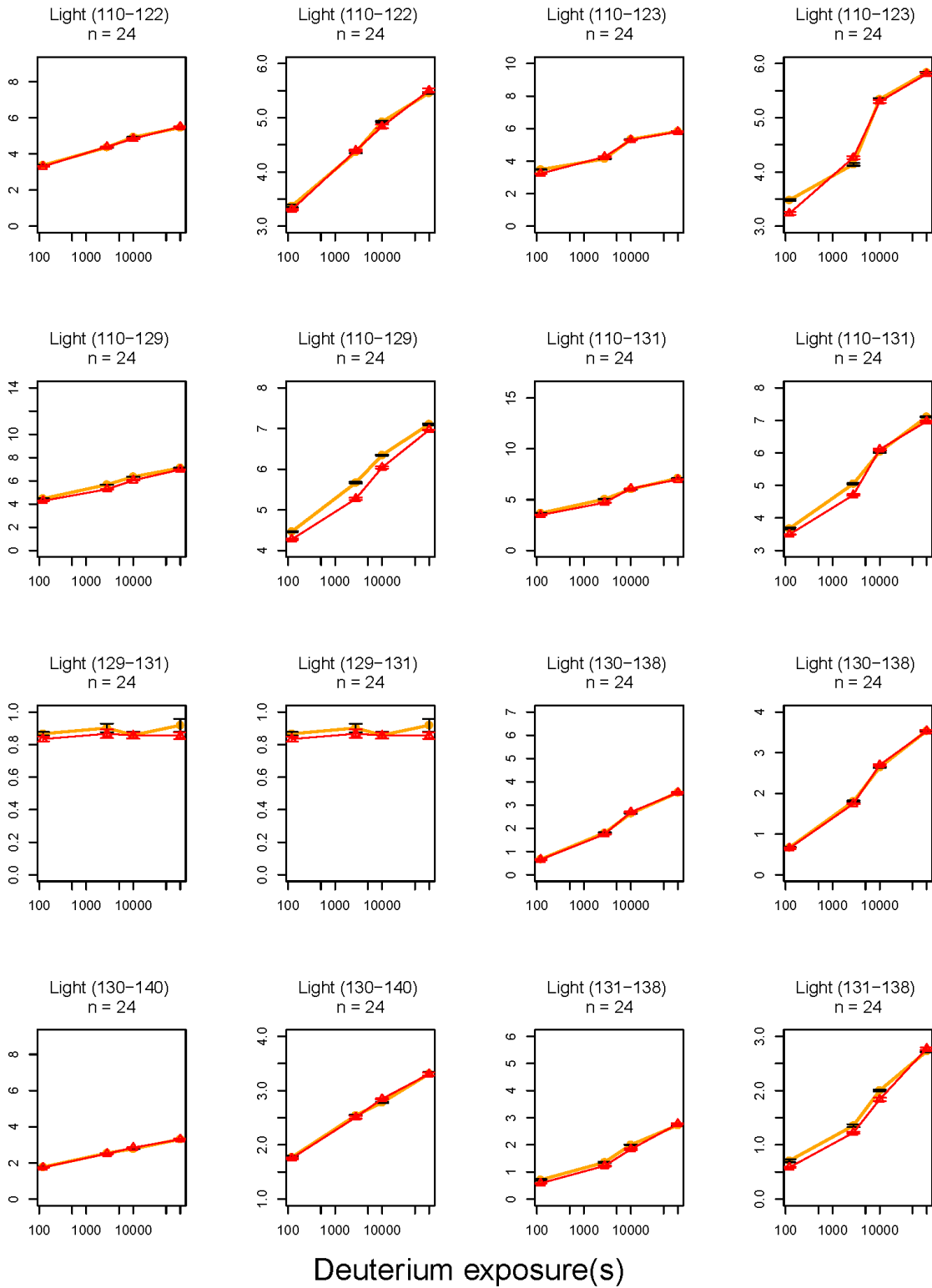


Deuterium exposure(s)

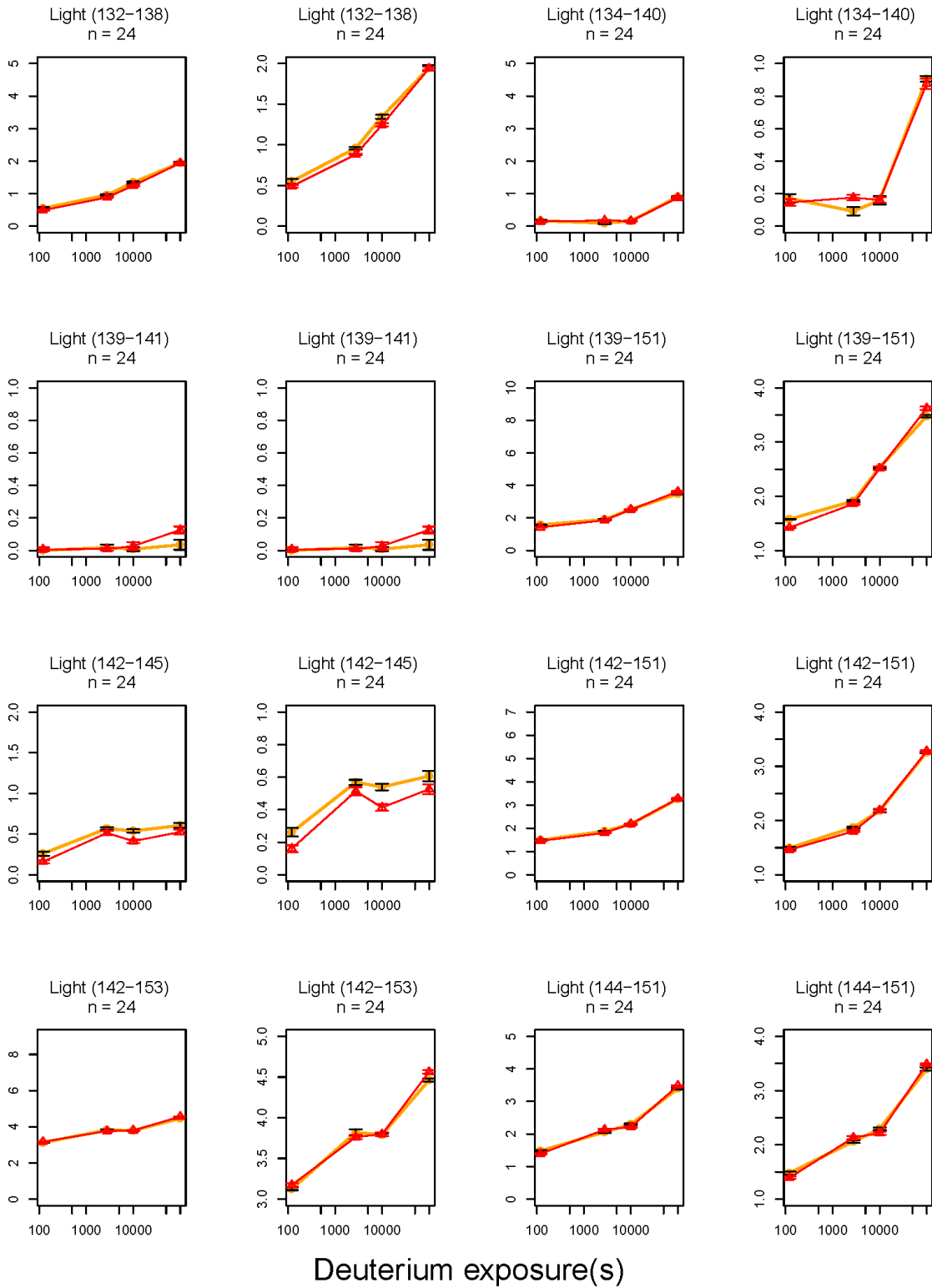
Mass Increase(Da)



Mass Increase(Da)

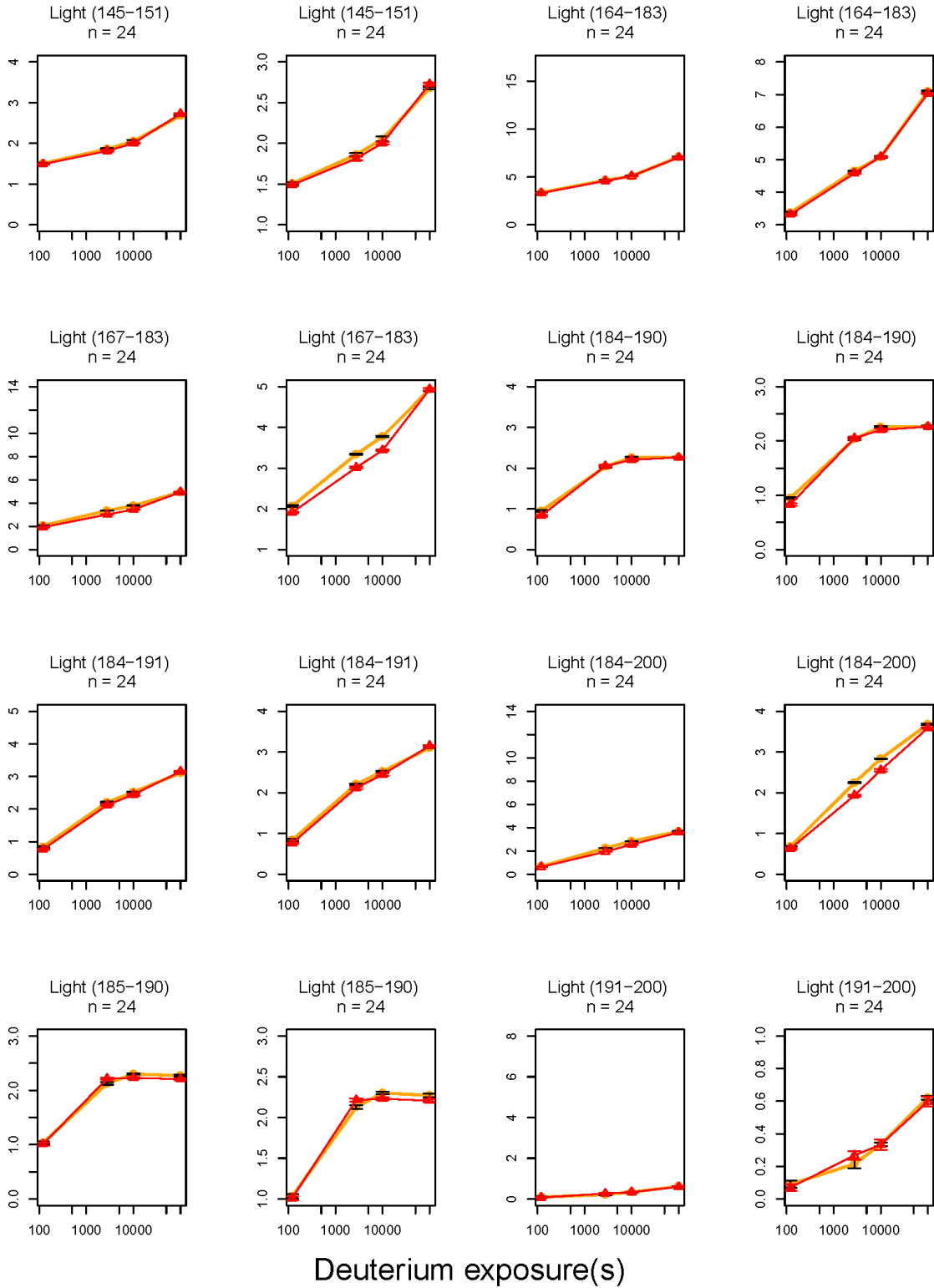


Mass Increase(Da)

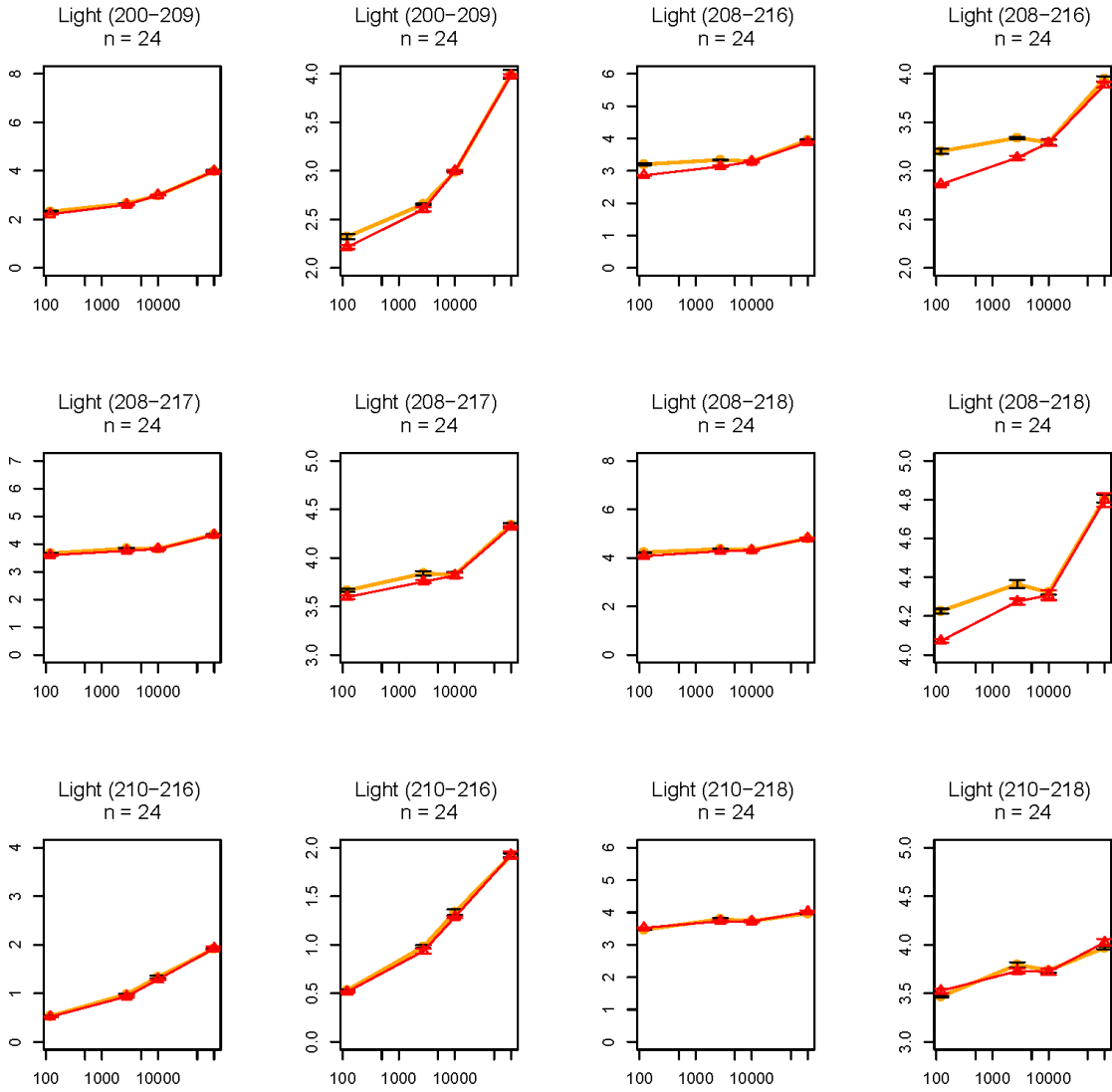


Deuterium exposure(s)

Mass Increase(Da)



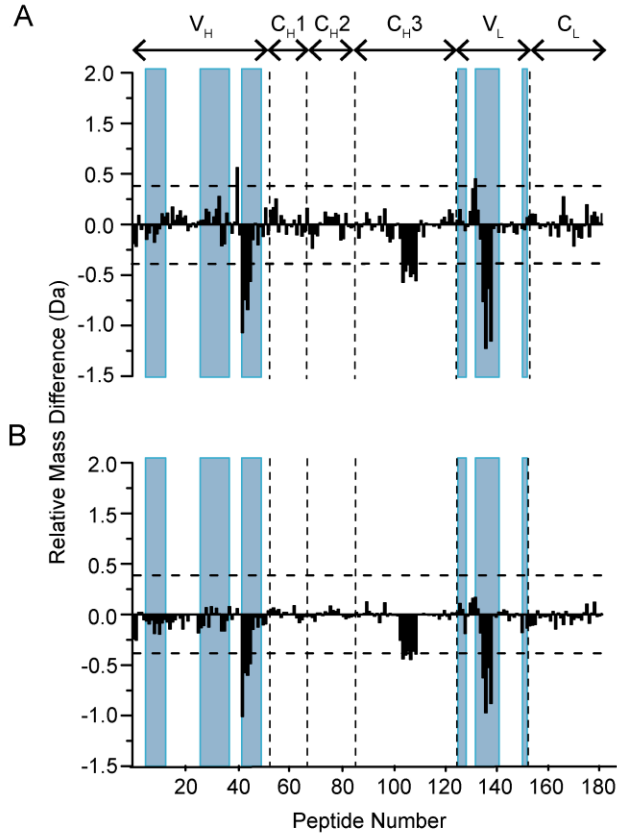
Mass Increase(Da)



Deuterium exposure(s)

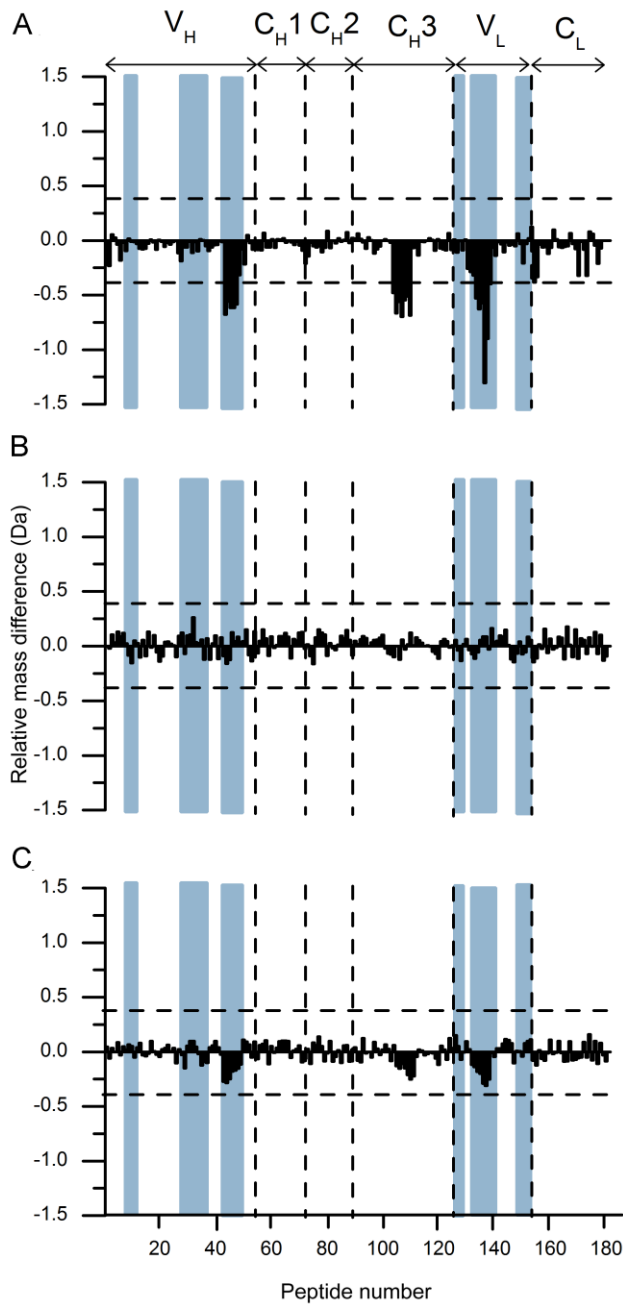
Deuterium uptake plots for 182 peptide segments of mAb-J comparing HX kinetics between 5 and 60 g/L mAb-J samples (orange and red, respectively). Domain location of the peptide is given in parentheses. Error bars represent one standard deviation from three independent HX experiments. The number of independent measurements for each peptide is denoted by n.

Figure 4.S4



Difference plots showing HX differences after 2760 seconds of hydrogen exchange for 182 peptides. The plots compare mAb-J samples at 60 g/L in control containing 10% (w/v) trehalose with mAb-J samples at 60 g/L containing additional (A) 100 mM arginine and (B) 100 mM NaCl, $\Delta m(t) = m_{60, \text{no additive}}(t) - m_{60, \text{arginine/NaCl}}(t)$. (Refer to the caption for Figure 5 for a more detailed description of difference plots).

Figure 4.S5



Difference plots showing relative mass differences at 2760 second exchange time-point for 182 peptides. The plots compare mAb-J samples at 60 g/L in control containing (A) no additional charged additives, (B) 100 mM arginine and (C) 100 mM NaCl with mAb-J samples at 5 g/L

containing no additional charged additives, $\Delta m(t) = m_{60, \text{arginine/NaCl}}(t) - m_{5, \text{no additives}}(t)$.

(Refer to the caption for Figure 5 for a more detailed description of difference plots).

Chapter 5

Conclusions and Future Work

5.1 Overview

Monoclonal antibodies (mAbs) are one of the major classes of biopharmaceutical agents. However, like other protein drugs, antibodies are also prone to physical and chemical degradation. During their manufacture, storage and transport, antibodies encounter various external stresses such as heat stress, shaking, various different kinds of interfaces, administration devices, etc. These stresses affect both conformational and colloidal stability of antibodies and make them predisposed to undesirable degradation like protein aggregation, fragmentation, loss of potency and increased potential for immunogenicity upon administration in patients. With the recent trend of formulating antibodies at high protein concentrations for subcutaneous administration by patients at home, physical phenomenon such as reversible self-association and high viscosity have also become significant challenges. Transient protein-protein interactions at high protein concentrations not only may cause issues related to process engineering and drug delivery (e.g., high solution viscosity), but also have been shown to lead to increased levels of protein aggregation over time. Analytical tools that can provide reliable and high resolution data at high protein concentrations can greatly help protein engineers and protein formulators to design mutant antibodies with enhanced physiochemical properties that remain stable and pharmaceutically well behaved at high protein concentrations.

Hydrogen-exchange mass spectrometry (HX-MS) provides an excellent opportunity to study protein-protein interactions at residue level resolution. Other physical phenomena such as solution non-ideality, viscosity, multiple-scattering etc. do not affect mass spectrometry operations and results, therefore, mass spectrometry can prove as an excellent partner for hydrogen exchange (HX) to study protein interactions at high protein concentrations. Recent work has also shown applicability of HX-MS to probe possible interactions between protein local flexibility and long

term physical stability. Majumdar et al¹ and Manikwar et al² tested the effect of certain destabilizing and stabilizing excipients on the local flexibility of a reporter peptide region in the C_{H2} domain of an IgG1 mAb that showed correlations with accelerated and longer term physical stability profile of that mAb.

This dissertation further explored the utility of HX-MS as an analytical tool for potentially predicting mAb physical stability by drawing strong correlations between the local flexibility of the reporter peptide region in the C_{H2} domain and mAb aggregation propensity and thermal stability. We also developed a novel HX-MS methodology to study transient protein-protein interactions between mAb monomers at high protein concentrations (i.e., reversible self-association). In this pursuit, we studied two different IgG1 mAbs (mAb-C and mAb-J) and mapped the protein interfaces of their reversible self-interactions.

5.2 Chapter summaries and future work

5.2.1 Chapter 2

Chapter 2 of this dissertation examines the effect of various phenolic antimicrobial preservatives on an IgG1 class of monoclonal antibody (mAb). The pharmaceutically relevant antimicrobial preservatives (APs) m-cresol, phenol, phenoxyethanol and benzyl alcohol were chosen. They all are relatively hydrophobic molecules, and the extent of hydrophobicity, with m-cresol being the most hydrophobic followed by phenol, phenoxyethanol and the least hydrophobic being benzyl alcohol. The thermal stability of the mAb was measured using DSC and extrinsic fluorescence spectroscopy. SEC was used to study the effect of APs on mAbs aggregation

propensity under thermal stress conditions over time. Local dynamics of mAb were then measured using HX-MS.

The criteria behind choosing the APs tested in this study was their degree of hydrophobicity. All the APs that were tested in this study showed a destabilizing effect on the mAb. The most hydrophobic AP, m-cresol, showed the biggest effect on mAb physical stability of as well as aggregation propensity, followed by phenol, phenoxyethanol and the least destabilizing AP, benzyl alcohol. Each of these APs also caused changes in the local flexibility of the mAb. A trend of small increases in flexibility was observed with all of the APs, however, majority of such changes were not significant. Deuterium uptake values for all mAb-4 peptides at all four time-points were normalized to their peptide lengths and added to get a global deuterium uptake value for each AP. The difference between the global deuterium uptake values of the APs and control strongly correlated with the physical stability data and hydrophobicity of the APs. These global increases in flexibility could indicate towards a mechanism of mAb destabilization that is not centralized to any one domain. However, a peptide segment in the C_{H2} domain (HC 237-254) showed significant increase in local flexibility upon addition of APs and this increase in local flexibility showed an excellent correlation to the mAb physical stability and aggregation propensity trends in the presence of APs. Interestingly, increase in mAb local flexibility in HC 237-254 also correlated with the level of hydrophobicity of the tested phenolic APs.

The utility of tracking the flexibility differences in the C_{H2} region hotspot peptide segment (HC 237-254) using HX-MS has been demonstrated previously¹⁻⁴. This study in addition to strengthening this argument also showed that increasing levels of physical destabilization induced by excipients correlated with flexibility trends in the aggregation hot-spot peptide segment which further demonstrates the utility of HX-MS in conducting quantitative analysis of physical

destabilization in the presence of excipients for mAbs. Pharmaceutical excipients are usually categorized into various categories and experiments using various excipients to further explore the utility of HX-MS to predict long term stability in their presence are currently being conducted in our laboratories. A high-throughput HX-MS method to screen various formulation combinations or pharmaceutical excipients involving global deuterium uptake as well as the aggregation hot-spot regions in the antibody structure may be a promising addition to the formulation development toolkit. In addition to physical stability, mAbs can also undergo degradation through chemical destabilization. Investigation of local flexibility shifts within the antibody structure upon chemical modification of specific amino-acids, and correlations to differences in conformation stability and changes in the aggregation propensity upon long term storage of the mAb, will help to develop a better understanding of mAb degradation pathways and mechanisms.

5.2.2 Chapter 3

Protein-protein interactions can have serious implications towards the pharmaceutical product stability and immunogenicity profile of therapeutic protein products^{5,6}. High protein concentration formulations are necessary to develop for subcutaneous delivery of mAbs. At high protein concentrations, however, due to the presence of solvent exposed patches of hydrophobic residues or asymmetrically charged residues on protein surfaces, certain mAbs molecules undergo transient protein-protein interactions and form oligomeric networks. Transient protein networks at high protein concentrations can cause significant increases in protein solution viscosity which in turn causes challenges related to process development, drug delivery and protein aggregation overtime. High-resolution characterization and mapping of such transient antibody reversible self-interactions can be a significant challenge as most of the classical techniques like NMR and X-ray

crystallography fail to provide reliable data for antibodies in pharmaceutical dosage forms due to various analytical limitations. This chapter describes a novel HX-MS methodology to study local flexibility and protein reversible self-associations at high protein concentrations. The extent of antibody reversible self-interactions was measured using low-resolution biophysical tools such as DLS, chemical-crosslinking and cross-linking. The IgG1 mAb tested in this study showed increase in self-association propensity with increase in pH (i.e., solution pH approaching the pI value of the mAb), ionic strength and with decrease in temperature. These observations collectively indicated towards a reversible self-associating system initiated by hydrophobic interactions.

To map the protein interface of mAb self-association, mAb-C at 60 mg/mL was compared to 5 mg/mL (associating sample vs non-associating sample) using HX-MS. Significant protection in deuterium uptake was observed in certain peptides segments in the V_H and V_L domain, primarily within sequences spanning the CDR2L and CDR2H regions of the antibody. Both of these regions were found to be rich in hydrophobic amino-acids upon closer examination of the primary sequence of the antibody. Three histidine amino-acids were also a part of the interface of sequence adjacent to the interface. These observations showed good correlations with the biophysical characterization studies of the mAb reversible self-association and its dependence on solution pH. Interestingly, certain peptide segments showed significant increase in local flexibility under self-associating conditions. Increase in the local flexibility of peptide sequences in the V_H and C_H2 domains of the antibody at high protein concentration was regarded as distant dynamic coupling effects of antibody reversible self-association.

The data presented in this study was later used as a guide for designing mutant versions of mAb-C by other researchers where they were able to design molecules with enhanced physiochemical properties, decreased association potential and lower viscosity at high protein

concentrations⁷. Molecular dynamics (MD) docking studies and computer simulations of protein self-associations to understand how certain protein primary sequences influence the extent of protein-protein interactions will further extend our knowledge concerning such phenomenon. Correlations between HX-MS observations and MD simulations will help in explaining correlations between local flexibility of the interfaces, nature of amino-acid makeup and affinities of associations.

5.2.3 Chapter 4

The work presented in chapter 3 was extended in chapter 4 to explore the reversible self-association behavior of a monoclonal antibody that showed a completely distinct mechanism of transient protein associations. The IgG1 mAb, “mAb-J”, showed increased propensity of self-association and reversible oligomerization upon decrease in solution ionic strength and at solution pH near the pI of the mAb (~7.4), indicating an electrostatic attractive interactions driven self-association. Previous studies have experimentally shown that mAbs reversibly-self associate through either Fab-Fab or Fc-Fc contacts points between patches of exposed charged or hydrophobic amino-acids⁸⁻¹². Similarly to chapter 3, low and high protein concentrations of mAb-J were identified (5 and 60 mg/mL) using DLS, CG-MALS and viscosity measurements. Both low and high protein concentration samples were then subjected to HX-MS analysis and the protein interface of association was mapped at a residue level resolution. Significant protection in deuterium uptake was observed in two continuous interfaces in the V_H and V_L domains (spanning CDR3H and CDR2L loops) and C_H3 domain in the Fc fragment of mAb-J. Both, CDR3H and CDR2L interfaces in the Fab domain contained several exposed positively charged amino-acids and the overall charge on the interface was positive, however, the Fc domain interface was

negatively charged with several exposed negatively charged amino-acids. This observation correlated very well with the low-resolution characterization of mAb-J self-association and indicated towards an association even involving Fab-Fc interactions driven by electrostatic attractive interactions. Interestingly, no distant dynamic coupling effects, where certain regions of mAb-J showed increased local flexibility under association promoting conditions, were observed which may potentially be related to the more extensive network of interactions via the Fab-Fc mechanism of RSA of this mAb.

The results from this chapter, experimentally present the first case of Fab-Fc interactions driven reversible self-association of an IgG1-mAb. This also was the first example of experimental mapping of Fab-Fc interactions at a peptide level resolution. Site-specific mutagenesis studies geared towards mutating residues in the interface to develop stable mutants of mAb-J with superior physicochemical and rheological properties at high protein concentrations should be planned for the future. Similarly, to chapter 3, MD simulations and docking studies can strengthen the correlations between HX-MS studies and low-resolution biophysical characterization studies of transient self-association events. More user-friendly and easy to use HX-MS methodologies to study mAb local flexibility and protein-protein interactions will be a great addition and advancement for the field, development of such methods is currently being tested in our laboratories.

5.2.4 References

1. Majumdar R, Manikwar P, Hickey JM, Samra HS, Sathish HA, Bishop SM, Middaugh CR, Volkin DB, Weis DD 2013. Effects of salts from the Hofmeister series on the conformational stability, aggregation propensity, and local flexibility of an IgG1 monoclonal antibody. *Biochemistry* 52(19):3376-3389.
2. Manikwar P, Majumdar R, Hickey JM, Thakkar SV, Samra HS, Sathish HA, Bishop SM, Middaugh CR, Weis DD, Volkin DB 2013. Correlating excipient effects on conformational and storage stability of an IgG1 monoclonal antibody with local dynamics as measured by hydrogen/deuterium-exchange mass spectrometry. *Journal of pharmaceutical sciences* 102(7):2136-2151.
3. Houde D, Peng Y, Berkowitz SA, Engen JR 2010. Post-translational modifications differentially affect IgG1 conformation and receptor binding. *Molecular & Cellular Proteomics* 9(8):1716-1728.
4. Zhang A, Singh SK, Shirts MR, Kumar S, Fernandez EJ 2012. Distinct aggregation mechanisms of monoclonal antibody under thermal and freeze-thaw stresses revealed by hydrogen exchange. *Pharmaceutical research* 29(1):236-250.
5. Wang W, Singh S, Zeng DL, King K, Nema S 2007. Antibody structure, instability, and formulation. *Journal of pharmaceutical sciences* 96(1):1-26.
6. Joubert MK, Hokom M, Eakin C, Zhou L, Deshpande M, Baker MP, Goletz TJ, Kerwin BA, Chirmule N, Narhi LO 2012. Highly aggregated antibody therapeutics can enhance the in vitro innate and late-stage T-cell immune responses. *Journal of Biological Chemistry* 287(30):25266-25279.

7. Geoghegan JC, Fleming R, Damschroder M, Bishop SM, Sathish HA, Esfandiary R 2016. Mitigation of reversible self-association and viscosity in a human IgG1 monoclonal antibody by rational, structure-guided Fv engineering. *mAbs*:00-00.
8. Kanai S, Liu J, Patapoff TW, Shire SJ 2008. Reversible self-association of a concentrated monoclonal antibody solution mediated by Fab–Fab interaction that impacts solution viscosity. *Journal of pharmaceutical sciences* 97(10):4219-4227.
9. Yadav S, Liu J, Shire SJ, Kalonia DS 2010. Specific interactions in high concentration antibody solutions resulting in high viscosity. *Journal of pharmaceutical sciences* 99(3):1152-1168.
10. Nishi H, Miyajima M, Wakiyama N, Kubota K, Hasegawa J, Uchiyama S, Fukui K 2011. Fc domain mediated self-association of an IgG1 monoclonal antibody under a low ionic strength condition. *Journal of bioscience and bioengineering* 112(4):326-332.
11. Yadav S, Sreedhara A, Kanai S, Liu J, Lien S, Lowman H, Kalonia DS, Shire SJ 2011. Establishing a link between amino acid sequences and self-associating and viscoelastic behavior of two closely related monoclonal antibodies. *Pharmaceutical research* 28(7):1750-1764.
12. Arora J, Hickey JM, Majumdar R, Esfandiary R, Bishop SM, Samra HS, Middaugh CR, Weis DD, Volkin DB 2015. Hydrogen exchange mass spectrometry reveals protein interfaces and distant dynamic coupling effects during the reversible self-association of an IgG1 monoclonal antibody. *mAbs* 7(3):525-539.